The Electrochemical Characterisation of Carbon-based Nanomaterials and their Application in the Detection of Heavy Metal Ions

NUI MAYNOOTH

Ollscoil na hÉireann Má Nuad

Lynn M. Garry

Department of Chemistry

National University of Ireland Maynooth

2013

Thesis Submitted to the National University of Ireland in Fulfilment of the Requirements for the Degree of

Doctor of Philosophy

Supervisors: Dr Bernadette E. Alcock-Earley and Prof. Carmel B. Breslin

Head of Department: Dr John C. Stephens

TABLE OF CONTENTS

CHAPTER 4: THE ELECTROCHEMICAL DETECTION OF CR(VI) USING ELECTRODES MODIFIED WITH MULTIWALLED CARBON NANOTUBES 118

Declaration

I hereby certify that this thesis, which I now submit for assessment on the programme of study leading to the award of PhD, has not been submitted, in whole or part, to this or any other university for any degree, and is, except where otherwise stated, the original work of the author.

Signed:_____ Date:_____

Abbreviations

μ	micro
AuNPs	gold nanoparticles
BET	Brunauer–Emmett–Teller theory
CPA	constant potential amperometry
CV	cyclic voltammetry
DDC	diethyl dithiocarbamate
DMF	dimethyl formamide
DOS	density of states
DPV	differential pulse voltammetry
e^-	electron
$E_{1/2}$	half-wave potential
EDX	electron dispersive X-ray
E_p	peak potential
E_{pa}	anodic peak potential
E_{pc}	cathodic peak potential
EtOH	ethanol
F	faraday unit
FTIR	fourier transform infrared spectroscopy
GCE	glassy carbon electrode
HOMO	highest occupied molecular orbital
HOPG	highly orientated pyrolytic graphite
Ip	peak current
Ip_a	anodic peak current
Ip_c	cathodic peak current
k_s	heterogeneous rate constant
LOD	limit of detection
LUMO	lowest unoccupied molecular orbital
M	moles per litre
MWCNTs	multiwalled carbon nanotubes

MWCNTsOx	oxidised multiwalled carbon nanotubes
NHE	standard hydrogen electrode
Ppy	polypyrrole
Py	pyrrole
RDE	rotating disc electrode
SCE	saturated calomel electrode
SEM	scanning electron microscopy
SWCNT	single-walled carbon nanotube
TEM	transmission electron microscopy
UV-vis	ultraviolet-visible
V	volts
WE	working electrode
α	alpha
β	beta
ΔE_p	peak potential separation
ν	scan rate

Acknowledgement

Firstly I would like to thank my supervisors Ber and Carmel, for giving me this opportunity, for answering my millions of questions through the past 5 years and giving me the freedom to become an independent researcher. I am very grateful to the EPA also, who funded my research. I would like to say a special thanks to Dr Denise Rooney for her help on this thesis and for everything she has taught me over the past 9 months especially. My thesis would be very different without your input, as would my training and for that I am exceptionally grateful. Thanks also to the current head of Department, Dr John Stephens, and his predecessor: Prof. John Lowry, and to the staff and technicians at NUIM, for all of their hard work to keep the department running smoothly- especially Mr Noel Williams. A kind word of gratitude must go to Prof. J. Justin Gooding in UNSW, Sydney, Australia for allowing me to visit for 6 months. I learned a lot about the fundamental basics of electrochemistry from my experience and would like to thank all of the staff, especially Dr John Stride for letting me use his graphene samples. I would also like to acknowledge the help of Prof. Alan Bond in Melbourne for allowing me to visit shortly and learn some graphite related techniques.

Special thanks are owed to one of my oldest friends Roisin for her support through undergrad and postgrad years especially. Who would have known all those years ago, Irish Dancing in Brenda's kitchen that we would end up doing PhDs in Chemistry together? A huge thanks is due to my original lab-buddy John, for also being a great friend over the years. You have both made the past 9 years very memorable. I would also like to thank my partner-in-crime Conor, for accompanying me through the 5 years of our PhDs. I couldn't have picked a better lab partner had I tried, thanks for the much-needed coffee breaks and random chats, pranks and music choices that broke up the long days. Thanks of course to Niall (Joey) for joining us in our lab towards the end, your "Dear Mr Google" searches were a great help. A big shout out to all of the chemistry gang, for the well-needed department nights out, coffee breaks and lunch time banter also. I'll definitely miss Thursday night harmonies, "ping"-pong games,

all of the Halloween, Christmas and summer parties. You all made Maynooth a great place to study and I doubt I will ever find colleagues like you, so thanks for everything. A special word of thanks is owed to David for his help over the last few months. A kind word of thanks is definitely owed to my Aussie lab friends, from allowing me to take part in group meetings to tasting my version of beef and Guinness pie and introducing me to some exotic new foods.

Huge thanks are owed to the girls, Carla, Cailín, Rachel, Cherry, Emma and Elaine. Thanks for being great friends over the years, for all the things I can't write down on paper and for all the things I shouldn't. Thanks for reminding me that "all my studying will be worth while" (I hope you were right) and for keeping my feet on the ground, not letting me forget how ditsy I can be sometimes. I've greatly appreciated you all helping me wind down from the tough weeks and understanding my distance over the last few hurdles. Thanks to all of my extended family and friends for always "seeming" interested in my college work and wishing me well the whole way through. To answer the most asked question: Yes, I am finished college ☺.

My PhD would not have been possible without my parents, Maureen and Brendan, for always encouraging me to achieve whatever I want, for giving me so many opportunities and for supporting me in every way throughout the past 9 years (well, 27 years, really). You are both wonderful parents and I am truly blessed to have you, so thank you. A huge thanks to my siblings; Amy, Katie and Conor; for putting up with me over the years and especially over the past few months – I'm sure I was a bit highly strung whilst writing my thesis, so thank you all for not killing me. I don't think many siblings are as close as we are, so I would like to take this opportunity to thank you for all of the fun we have, you are three extremely talented people and your music and singing have been a welcomed distraction from Chemistry and great comfort after long days spent in college. I most definitely would like to thank my boyfriend Stephen, for encouraging and supporting me through the past 9 years of University. I couldn't have done any of this without your love and support.

Abstract

In the work described in this thesis, electrochemical sensors are designed and investigated for their potential use in the detection of metal ions in aqueous solutions. Firstly, the use of carbon-based nanomaterials commonly used in the construction of electrochemical sensors; multiwalled carbon nanotubes (MWCNTs) and graphene, were characterised using a potassium ferricyanide probe. The carbon nanomaterials were constructed using pencil style electrodes which were modified *via* drop-casting. Both carbon nanomaterials were used in their pristine form, simply cast from a DMF suspension. It was found that the electrode modified with sonicated MWCNTs possessed a greater electroactive surface area (0.377 cm^2) and larger rate constant for electron transfer (2.579×10^{-3} cm s^{-1}) than the electrode modified with graphene (0.092 cm^2 and 8.160×10^{-4} cm s^{-1}) therefore the MWCNTs modified electrode was further investigated for its use in the detection of Cr(VI). The electrode modified simply with pristine MWCNTs gave a limit of detection of 1.95×10^{-4} M with reasonable selectivity in the detection of Cr(VI) using cyclic voltammetry. To further enhance the sensitivity of detection, various alterations were made to the construction of the electrode including the use of gold nanoparticles to modify oxidised MWCNTs. A lower limit of detection of Cr(VI) (1.20×10^{-6} M) was achieved at this modified electrode using constant potential amperometry and a rotating disk electrode, which is close to the mandatory limits set by the EPA (9.61×10^{-7} M). The detection of Cu(II) was also studied in this thesis. The construction of this sensor involved the modification of an electrode with a ligand, diethyldithiocarbamate (DDC) *via* its incorporation into a Nafion film. The electrochemical detection of Cu(II) at this sensor was based on its complexation to DDC and the cycling of Cu(II) to Cu(I). The detection mechanism was investigated using UV-vis spectroscopy and cyclic voltammetry. The limit of detection achieved in this preliminary sensor study was 5.40×10^{-5} M which is close to the mandatory limit set by the EPA of 3.20×10^{-5} M.

Chapter 1:

Introduction and Literature Review

1.1 Introduction

The aim of this research was to produce new electrochemical sensors for the potential detection of two specific metal ion pollutants; chromium, in the form of Cr(VI), and copper in the form of Cu(II). In this thesis, the use of carbon-based nanomaterials in electrochemical sensors is investigated; namely multiwalled carbon nanotubes (MWCNTs) and graphene. The use of MWCNTs in the detection of both Cr(VI) and Cu(II) is explored and they are electrochemically characterised using a potassium ferricyanide probe. Many variations of a MWCNTs-based electrochemical sensor are explored in the detection of Cr(VI); namely the use of polymers and nanoparticles. In the detection of Cu(II), the use of ligand-metal complexation is investigated as a means of electrochemical detection and the use of MWCNTs to enhance the sensitivity of detection is explored.

The experimental techniques used throughout this thesis are discussed in Chapter 2, with details on the preparation of each electrode and the analytical techniques used. This chapter provides a brief introduction to electrochemical sensors and their importance in metal ion detection with a brief review of the advances reported in the field to date. The nature of each material used is also discussed with reference to their use in electrochemical sensors.

1.1.1 Metal Pollution

In the 21st century, one of the most important challenges is still to supply clean, potable water worldwide. Although in Ireland, the water supply is of relatively good quality, in 2009 the EPA listed heavy metal pollutants, among others such as nitrates and PCPs, as a major threat to our drinking water supply.[1] It is therefore crucial to develop sensitive, cheap and easy methods of monitoring water quality. Metal pollution in aquatic systems mostly occurs in areas of past mining or Industrial plants, however the natural geographical composition of the soil can also contribute to high levels of some metal ions in

some areas. Chromium is a metal pollutant that occurs naturally in the environment and is found in both its trivalent and hexavalent oxidation states in aquatic systems. It can be found naturally in soil in moderate concentrations, however, it is also a dangerous pollutant, which can be leached into groundwater from industries such as tanning, stainless steel production and metal finishing.[2] The speciation of Cr(VI) in aqueous solutions can be seen in Figure 1.1, which illustrates that Cr(VI) primarily exists as H_2CrO_4 in acidic solutions (pH < 1.0). In solutions of approximately pH 1.0 to 6.0, the predominant species is $HCrO_4^-$, and at significantly high concentrations (> 10^{-2} g L^{-1}), the $Cr_2O_7^{2-}$ species prevails. In alkaline solutions (pH > 6.0) the CrO_4^{2-} species is the predominant anion.

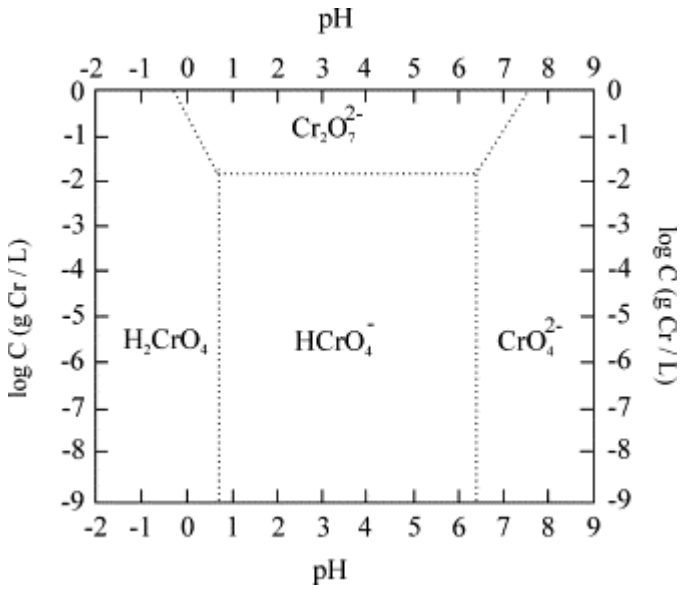

Figure 1.1: Chromium speciation diagram showing the relative predominant species of Cr(VI) with respect to the pH of the solution. Diagram is adapted from the Atlas of Electrochemical Equilibria.[3]

Chromium(VI) exists as highly toxic metal complexes that are well known for their contribution to a variety of health problems such as cancers,[4] mucosal ulcerations[5] and chronic dermatitis.[6] The complexes are weakly adsorbed onto inorganic surfaces, therefore, they can readily be transported in soil and leached into water bodies far from the original sites of contamination.[7] In acidic solutions, Cr(VI) complexes are very strong oxidising agents due to the

high redox potential of Cr(VI) at 1.33 V (vs. NHE), therefore, there is a need to ensure complete removal of chromium from industrial waste with sensitive monitoring of Cr(VI) in water sources.

Copper is another naturally occurring metal that in high concentrations can cause serious health defects. It is found in its monovalent and divalent forms mostly and is an essential dietary requirement. In relatively high concentrations or with prolonged exposure, copper is known to cause organoleptic (taste) problems, can induce symptoms of severe food poisoning,[8] and is linked to cognitive impairment and Alzheimer's disease.[9, 10] Copper is often used in electrical and plumbing systems, and is known to corrode under certain circumstances, resulting in its leaching into soils and water sources.[11, 12] There are also areas with high concentrations of copper due to mining waste,[13] and the production of pigments and ceramics.[14] As it is more toxic to fish and aquatic life with high levels of bioaccumulation, there is a strong need for its sensitive detection in aqueous systems.

The need for metal ions such as Cr(VI) and Cu(II) to be monitored in Irish water was clearly outlined in The Water Quality (Dangerous Substances) Regulations by the EPA.[15] The EPA has set a recommended limit of 9.6×10^{-7} M (50 μg L^{-1}) chromium and 3.2×10^{-5} M (2 mg L^{-1}) copper in Irish waters. The most common techniques used currently for detection of chromium and copper metal ions involve the ionisation of the sample by inductively coupled plasma (ICP) and detection of the analyte using mass spectrometry (ICP-MS) or optical emission spectrometry (ICP-OES).[1] Another method used to qualitatively monitor the presence of metal ions is x-ray fluorescence (XRF) combined with ICP-MS.[16, 17] Unfortunately, these techniques are carried out off-site, are relatively expensive and cannot distinguish between the oxidation states of the metal, unless coupled with a chromatographic technique. The use of electrochemical sensors for the detection of metal ions in aqueous environments would potentially allow for on-site, real time monitoring of samples at a relatively low cost.

1.1.2 *Electrochemical Sensors*

A sensor can be defined as a device that continuously provides information about the sample being analysed and an electrochemical sensor is a device that does so using the interaction of electricity with chemistry.[18] There are many classifications of electrochemical sensors, such as; potentiometric sensors, which measure the difference between two potentials and amperometric sensors, which measure a current response. The first reported potentiometric sensor was the pH meter, which selectively detected the concentration of H^+ ions using a glass electrode.[19] Amperometric sensors are generally based on the sensitive detection of a species with the concentration of the species represented by a current response. One of the most common techniques used in electrochemical detection is voltammetry, where the current response is studied as a function of applied potential. This allows for good control over both the sensitivity and selectivity of the detection.

Cyclic voltammetry is one of the most commonly used voltammetric techniques and is explained in great detail in Chapter 2. Briefly, it involves cycling the applied potential between two limits, allowing for the oxidation and reduction steps to be observed as peaks in the current. This technique is relatively simple and useful for the characterisation of the sample solution as well as the characterisation of the electrode itself. In the sensitive monitoring of an oxidation or reduction process, techniques such as constant potential amperometry (CPA) and differential pulse voltammetry (DPV) are often used. CPA involves the application of a potential suitable to complete the electron transfer reaction required, which is generally determined from cyclic voltammetry experiments. The oxidation or reduction reaction in this case is observed as a peak or trough in the amperogram. The sensitivity of this technique is often enhanced by the use of rotating disc electrodes (RDEs), which are also further detailed in Chapter 2. Briefly, they provide a constant flow of fresh analyte to the electrode surface from the bulk solution, thus removing the time-consuming restraint of diffusion. DPV is a technique that

operates by applying the potential in pulses (illustrated in Chapter 2) which removes the capacitive effect of current build up at the electrode surface. This allows for a more clear observation of faradaic processes, thus enhancing the sensitivity of detection.

Many electrochemical sensors used in the detection of metal ions are based on stripping voltammetry. This involves the pre-concentration of the electrode with the target ion, and its subsequent deposition onto the electrode surface. The metal is then "stripped" from the electrode which is monitored using a sensitive technique such as DPV. Another common class of electrochemical sensor used in the detection of metal ions are ion selective electrodes (ISEs), which are potentiometric in nature. ISEs generally consist of a membrane that is tailored specifically to the individual analyte and the activity of the analyte is related to the changes measured in the potential.

The most recent advancements in sensor applications have been the design of wearable sensors,[20] for example where the sensor has been directly attached to the epidermis for the non-invasive monitoring of physiological responses such as the heart rate, developed by Kim *et al*.[21] Other interesting advancements in this field include the production of flexible screen-printed sensors such as those reported by Chuang *et al*.[22] for the detection of glucose, which were prepared using Nafion. The development of ultra light aerogel materials consisting of MWCNTs has also been reported by Zou *et al*.,[23] with potential uses in pressure and chemical vapour sensing.

One of the major advantages of electrochemical sensors is their ability to provide real-time, on-site information which is particularly useful for environmental monitoring.[24, 25] Current research in the area of electrochemical sensing in aquatic environments involves the use of flow-systems to enable remote sensing with automatic, controllable measurements and simple data collection. In recent years, advancements have been made in this area, such as in the development of microfluidic systems; in particular the work by Prof

Diamond's group[26, 27, 28] in the construction of on-site detection systems for environmental monitoring has introduced a means of employing electrochemical sensors in this field. The benefits of these systems are highlighted by Feier *et al.*,[29] for example, who have developed a flow-analysis sensor for the detection of zinc at a graphite-felt electrode. The authors have stated that the flow system allowed for increased mass transport to the electrode surface. Impressively, Noyhouzer *et al.*[30] recently described a system designed to implement the use of most commercially available sensors. They designed a light-weight system consisting of less than 10 parts (half that of standard systems), including an 11.45 µL measuring chamber, making it easy to clean with minimal sealing and contamination issues.

1.2 Materials used in the Detection of Heavy Metal Ions

The detection of metal ions at bare substrates is generally avoided due to bio fouling and corrosion issues. To avoid such problems, and to improve the selectivity and sensitivity at some electrodes, a wide range of materials have been studied for their ability to detect metal ions in aquatic systems. These materials include coatings such as polymers, membranes as well as nanomaterials and chelating agents.

1.2.1 Carbon based Nanomaterials

Carbon has long been known to form various stable structures such as diamond and graphite however, the interest of scientists in carbon based nanomaterials is said to originate from the synthesis of the buckminsterfullerene, C_{60}, in 1985.[31] This spherical fullerene molecule consists of twenty hexagons and twelve pentagons, taking the shape of a soccer ball. C_{60} is extremely stable and it is known to behave similarly to an electron-deficient alkene, and reacts readily with electron-rich molecules. In 2001, Csiszar *et al.*[32] used C_{60} in the modification of an electrochemical sensor showing its potential use in the detection of Cytochrome-C. The development

of C_{60} fuelled the interest in finding other allotropes of carbon,[33] and lead to the use of arc vapour deposition to produce C_{60}, a technique similar to that later used by Iijima in 1991[34] in his discovery of carbon nanotubes. Although graphene had been long discussed by theoretical physicists, it was not discovered until 2004 by Andre Geim and Konstantin Novoselov using the scotch-tape method.[35] Both materials have since been the subject of many advances in synthetic and physical chemistry. The electrochemical properties of pristine MWCNTs and graphene, drop-cast on an electrode, are compared in Chapter 3 of this thesis, and the MWCNTs are used in the sensing of Cr(VI) in Chapter 4.

1.2.1.1 Carbon Nanotubes

1.2.1.1.1 Structural and Electronic/Electrochemical Properties of Carbon Nanotubes

Carbon nanotubes are rolled up sheets of graphene, or sp^2 hybridised carbon sheets with a helical structure that provides a length to diameter ratio greater than any other material. They are produced using various methods such as the electric arc discharge process which involves the sublimation of carbon under inert atmospheres or chemical vapour deposition (CVD) with the use of metal catalysts.[36, 37] They are produced as either single or multi walled nanotubes, both with a large aspect ratio, which is illustrated in Figure 1.2. For the purpose of this thesis, only multiwalled carbon nanotubes will be discussed herein.

(a) (b)

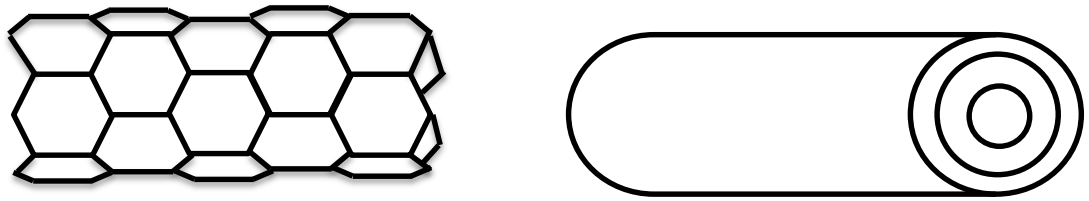

Figure 1.2: Schematic representation of (a) the sp^2 hybridised structure of carbon nanotubes and (b) a simplified structure of a MWCNT, highlighting its length to diameter ratio.

Multiwalled carbon nanotubes (MWCNTs) have been shown to exhibit extraordinary properties such as immense surface area, great mechanical strength,[38] large capacitance[39, 40] and high conductivity.[41] Most importantly for their use in electrochemical sensors are the ballistic transport properties giving rise to fast electron transfer of the material.[42, 43] Recently, Borowiec *et al.*[44] have shown the sensitive detection of ketoconazole at a MWCNTs sensor, with impressive enhancements in the current response owed to the increase active surface area provided by the MWCNTs and thermodynamically improved electron transfer which they attributed to the inherent properties of the MWCNTs. These fast electron transfer properties of carbon nanotubes have been much studied with many reports that the defects in the nanotube structure and oxygenated ends of the nanotubes are responsible for the observed properties.[45, 46] In 2003, Wu *et al.*[47] showed the detection of dopamine and serotonin at a MWCNTs modified electrode with increased current responses and a decrease in the over-potentials. This resulted in their simultaneous detection, as the peaks for both neurotransmitters were well separated. The large surface area, fast electron transport and electrocatalytic activity of the edge planes of MWCNTs were also acknowledged by Liu *et al.*[48] in the detection of thiocholine at a MWCNTs modified electrode.

MWCNTs are also known to have a mesoporous structure that is of particular benefit in the formation of composites, such as the MWCNTs/Polysulfone film reported by Sanches *et al.*[49] that showed a significant increase in the porosity of the film which in turn decreased its elasticity and hardness. The mesoporous structure of the MWCNTs describes pores of 2 to 50 nm in diameter which are inherent to MWCNTs (intraparticle mesopores) and also that arise between networked tubes (interparticle mesopores).The mesoporous structure of MWCNTs has also been shown to influence the wettability of its composites and of electrodes modified directly with MWCNTs. In particular, studies by Kwok-Siong *et al.*[50] have shown a decrease in contact angle with increasing thickness of a PpyMWCNTs film. They attribute this increased hydrophilicity to an increase in the surface roughness of the film caused by the presence of MWCNTs. Similarly, Choi *et al.*[51] have reported the increase in hydrophilicity of a MWCNTs/Polysulfone membrane with increasing MWCNTs content.

1.2.1.1.2 The use of MWCNTs in Electrochemical Sensors

Although they have the ability to adsorb large amounts of water, all graphitic carbon nanostructures are inherently hydrophobic in nature. [52] The utilisation of MWCNTs in electrochemical applications therefore, requires the production of homogenously dispersed solutions in water or polar organic solvents as nanotubes are known to aggregate and readily form clusters.[53, 54] The interactions between nanotubes are described as "soft" forces and are described in the well established Derjaguin, Landau, Verwey and Overbeek (DLVO) theory.[55, 56] This theory is based on the stability of lyophobic dispersions (dispersions of particles that are not surrounded by solvent layers) and assumes a balance between the repulsive and attractive potential energies of interaction of the dispersed particles. Repulsive energies are proposed to be due to particle-solvent interactions whereas attractive energies are believed to be caused by van der Waal forces between the particles. To disperse the particles, these attractive energies must be overcome. There are three main

methods to form carbon nanotube dispersions: (i) the use of aqueous surfactant solutions, (ii) the use of polar organic solvents and (iii) the modification of carbon nanotubes to make the surface more hydrophilic and then their dispersion in aqueous solutions.

The use of surfactants to disperse carbon nanotubes has therefore been widely studied over the past decade or so.[57, 58, 59, 60, 61] Islam *et al.*[59] compared the use of various surfactants such as sodium dodecyl benzene sulfonate (NaDDBS), Triton X-100 (TX100) and sodium dodecyl sulfate (SDS) at various weight fractions of single walled carbon nanotubes. They postulated that the stabilisation of nanotubes occurred in their solutions as hemi micelles sheathed the surface of the tubes. Results found by this group indicated that NaDDBS provided the most reliable nanotube dispersion, i.e. the solution remained free of aggregate bundles for over 2 months. This was explained by the benzyl component of the surfactant improving the dispersion of the nanotubes as π-stacking interactions increases the binding and surface coverage of the surfactants on the nanotubes. The mode of adsorption of surfactant molecules on the surface of carbon nanotubes has not yet been confirmed however, models have been proposed for a vertical monolayer of adsorbed molecules with the anionic head groups extended to the aqueous phase.[60] The researchers also suggest that surfactant molecules may block off charge transport through MWCNT networks and recommend minimal use of such molecules for electronic applications.

Organic solvents such as N,N-dimethylformamide (DMF) and N-methylpyrrolidine (NMP) have consequently been used in the dispersion of nanotubes, providing well dispersed, clean nanotubes.[62, 63] Stable, homogenous samples of nanotubes are provided in solutions such as DMF by industrial suppliers such as NanoLab[64] and are widely used in the current literature.[65, 66, 67, 68] In particular, Nguyen *et al.*[69] showed the beneficial effects of dispersing MWCNTs in DMF, using UV-vis, FT-IR and Raman spectroscopy.

The modification of carbon nanotubes is generally carried out using acid treatment, with further modification also performed in some cases.[70] Acid treatment of carbon nanotubes is performed by refluxing the pristine nanotubes in a mixture of concentrated acids, such as HNO_3 and H_2SO_4 and is known to result in the oxidation of the carbon nanotubes resulting in carboxylate and carbonyl functional groups at the edge-plane defects of the cylindrical structures.[64] This method of functionalisation generally results in great improvement to the dispersion of carbon nanotubes in aqueous solutions. The harshness of this treatment however, has been shown to result in severe damage to their structure, for example drastically decreasing their length to diameter ratio.[71, 72]

The use of MWCNTs in electrochemical sensors ranges widely from the use of pristine nanotubes to those that have been highly functionalised. Recently, Han et al.[73] have reported on the growth of well-aligned MWCNTs on patterned Si substrates and the subsequent electrochemical functionalisation produced oxygen containing groups. The antibodies of microcystin LR (MC-LR) were added to the surface. The resulting electrode was highly effective at detecting the toxin MC-LR in the range of 0.05 to 20 μg L^{-1}. Moreover, Chebil *et al.*[74] have demonstrated the use of MWCNTs functionalised with an nitro-triacetic acid Cu(II) complex and a His-tag D-dimer antibody to electrochemically monitor D-dimers (products of a fibrin degradation). Both of these biosensor papers accredited the electronic properties and large surface area of MWCNTs for the efficiency of detection achieved.

The use of metal nanoparticles and nanostructures in electrochemical sensing has also been receiving a lot of attention. Recently, Wang *et al.*[75] reported the detection of 1 μg L^{-1} Cu(II) and Pb(II) at a micro-sensor using square wave voltammetry. They utilised gold nanoparticles to increase the electroactive surface area of the modified electrode by 1.5 fold. The sensitive detection of the metal ions in this work was based on their complexation to cross-linked L-cysteine and L-aspartic acid which also showed good selectivity in the

presence of common interferants such as Ni(II), Co(II) and Cd(II). Advancements in the electrochemical detection of Cr(VI) include those from Ouyang *et al.*[76] who have fabricated gold nano-particles in a flower-like assembly, modified with pyridinium achieving detection of 2.9 ng L^{-1} Cr(VI).

Much advancement in the use of MWCNTs has exploited their large surface area by decorating them with such metal nanoparticles to further enhance the surface are of the modified material and its conductivity.[77] [78] Lu *et al.*,[79] for example, have demonstrated sensitive and selective detection of Hg(II) using a MWCNTs modified electrode containing gold nanoparticles and DNA. They have attributed the amplitude of the signal for the detection of Hg(II) to the large surface area of the MWCNTs. Zhang *et al.*[80] have also shown the use of MWCNTs and gold nanoparticles to be beneficial in electrochemical sensing. This group found enhanced sensitivity and good selectivity in the detection of Nitrite.

1.2.1.2 Graphene

1.2.1.2.1 The Structural and Electronic/Electrochemical Properties of Graphene

Graphene was discovered in 2004 by Andre Geim and Konstantin Novoselov[81] who won a Nobel Prize in 2010 for their work on the two dimensional sheet of carbon. In Figure 1.3 (a), the general structure of a graphene sheet is illustrated, showing the irregular curves which are known to form folds in the graphene sheets. The structure of the molecule can be seen in Figure 1.3 (b) showing the sp^2 hybridized carbon atoms arranged in a hexagonal form.

It is reported that the partially filled π-orbitals of graphene provide phenomenal electronic properties making it a zero-gap semiconductor whose charge carriers are mass less Dirac fermions and whose mobilities can exceed 15,000 cm^2 V^{-1} s^{-1}.[82,35] Gooding *et al.*[83] published a review in 2010 comparing

carbon nanotubes to graphene for their use as a biosensor material, with some of the advantages of graphene over carbon nanotubes being the ease of assembly and low noise levels.

(a)

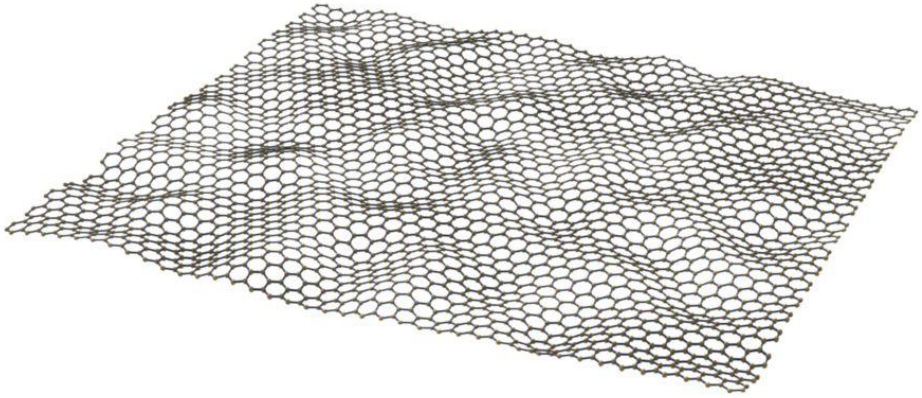

(b)

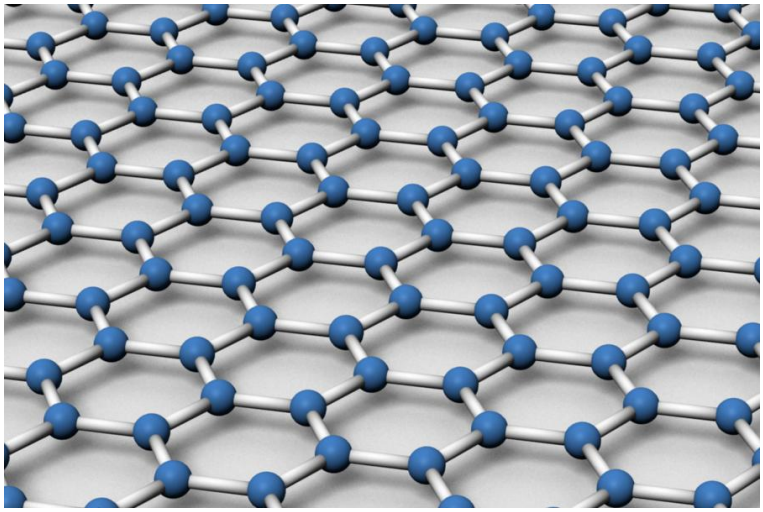

Figure 1.3: Schematic representation of graphene highlighting (a) a single graphene sheet[84] and (b) its basic sp^2 hybridised structure.[84]

In 2009, Ohno *et al.* [85] were the first to propose a sensing device using single layer graphene for pH detection and protein adsorption, making use of its electronic properties. Also in 2009 Pumera[86] published a report on the electrochemistry of graphene, suggesting it as a competitor for carbon nanotubes due to its large surface area, high conductivity and low levels of impurities. In 2010, Kang *et al.*[87] described a sensor modified with functionalised graphene, by the drop-cast method, for the sensitive detection of paracetamol. Reports by Wang *et al.*[88] have attributed the selective detection of dopamine in the presence of ascorbic acid at a graphene-modified sensor, to the π-π interactions between dopamine and graphene. The authors suggest the better performance of graphene to that seen at a CNT modified electrode is due, in this case to its unique planar structure and high quality sp^2 hybridised carbon.

1.2.1.2.2 The use of Graphene in Electrochemical Sensors

The use of graphene in electronic devices requires the formation of well dispersed suspensions, however, similarly to carbon nanotubes, graphene sheets are known to aggregate, forming stacks via the π-orbitals, as illustrated in Figure 1.4. This leads to the formation of bi-layer and multi-layer graphene and at a certain level of stacking (100 layers according to Pumera *et al.*[86]) it becomes graphite, which does not possess the impressive properties of single-layer graphene, such as the enormous surface area with respect to its weight. To overcome stacking, similarly to MWCNTs, graphene is often treated with surfactants and sonication is often employed to disperse the suspensions. In particular, work by Keeley *et al.*[61] has shown the production of nano-graphene sheets using sonication in DMF for use in the electrochemical detection of ascorbic acid. They have shown the electrochemical surface area of the modified electrode to be 0.15 cm^2 using a hexaammineruthenium(III) chloride redox probe. They estimated that the sheets consisted of 5 layers (or fewer) of carbon atoms.

Si and Samulski[89] have used a more elaborate method of separating individual graphene sheets by their modification with platinum nanoparticles. The authors describe the mechanical exfoliation of graphene suspensions by introducing nanoparticles to a dispersed solution, which inhibits the re-stacking of the graphene sheets upon drying. Using this method, they found an increase in the surface area (calculated using the BET theory) of the modified electrode by approximately 20 fold, and calculated that the samples were limited to approximately 3 layers of graphene re-stacked in comparison to 60 layers in samples without the Pt nanoparticles. In 2012, Wang *et al.*[90] showed a further improvement of this method by the modification of graphene oxide sheets with carbon nanoparticles. They found excellent separation with this method that they calculated limited only two layers of graphene to re-stack in comparison to 40 layers in their non-modified sample.

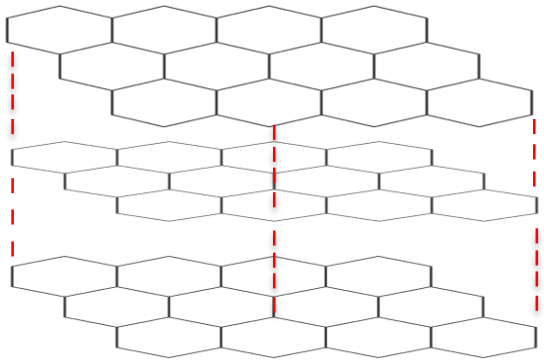

Figure 1.4: Illustration of the stacking of graphene sheets.

Current investigations into the material include its adsorption and desorption characteristics,[91] and the formation of composite materials from graphene such as hydrogels.[92] Most recently, Rajesh *et al.*[93] have reported on the formation of hybrid materials of graphene with nanostructured platinum and carbon nanotubes for the oxidation of methanol. They characterise their material vertically grown carbon nanotubes from a single layer of graphene, resulting in a three-dimensional material that they modify with the electrochemical deposition of platinum nanoparticles.

1.2.2 Metal Chelators

Metal chelation is a term that refers to the coordination of a metal ion to a binding molecule known as a chelator, to form a stable, insoluble product. Chelators are generally either macro-cyclic or non-macro-cyclic. The macro-cyclic class of chelators includes crown ethers and cyclodextrins, among others, which have been reported to coordinate to a species via the formation of a host-guest complex. This requires the guest molecule (e.g. metal ion) to become localised to the "cavity" of the host molecule or macro-cycle.[94, 95] This makes the complex formation selective for analytes of a specific size. El Shal *et al.*,[96] for example have recently reported on the fabrication of carbon paste electrode modified with β-cyclodextrin for the sensitive detection of Gemifloxacin and Nadifloxacin. The authors reported limits of detection of 1.2 × 10^{-8} and 1.0 × 10^{-8} M respectively for the anti-bacterial agents using DPV stripping voltammetry with an accumulation time of 2 min. Recent reports on the use of crown ethers include that from Cheraghi *et al.*[97] who describe the use of carbon paste electrode modified with dicyclohexyl-18-crown-6 for the detection of Tl(I). These authors reported a limit of detection of 0.86 ng mL^{-1} also using DPV stripping voltammetry and a deposition time of 5 min.

In the case of non macro-cyclic chelators, some of the most commonly studied agents are thiols,[98] neutral pyridines[99] and Schiff bases.[100] Recent reports on the use of Schiff bases in electrochemical sensing of metal ions include that by Kucukkollbasi *et al.*[101] who synthesised chitosan nanoparticles which they modified with a Schiff base. The resulting material was incorporated into a carbon paste electrode and DPV with stripping voltammetry was used for the detection of Pb(II). The limit of detection achieved was 7.24 × 10^{-7} M. Jahandari *et al.*[102] similarly showed sensitive detection of Ag(I) using DPV stripping voltammetry at a carbon paste electrode modified with carbon nanotubes, graphite powder and a silver selective Schiff base. The authors reported sensitivity of 0.08 ng mL^{-1} in this case.

Other well known metal ion ligands are a class derived from dithiocarbamates, such as dimethyl dithiocarbamate, which generally contain two sulfur atoms which coordinate to the metal ion.[103, 104] Kanchi *et al.*[105] for example, have shown the detection of Co(II) using ammonium piperidine dithiocarbamate and ammonium morpholine dithiocarbamate ligands with detection limits of up to 0.001 ppm using differential pulse polarography.

1.2.2.1 Diethyl dithiocarbamate (DDC)

Diethyl dithiocarbamate (DDC), illustrated in Figure 1.5, is one of the more basic dithiocarbamate molecules and has been studied since the 1950s for its ability to chelate metal ions.[106, 107] It is used to form insoluble metal-dithio salts, used in the precipitation of various metals in waste-water treatment.[108] The chelation generally involves the coordination of the metal ion via the sulfur atoms between two DDC molecules, resulting in a square planar complex.[109] This complex has been fully characterised throughout the literature,[110, 111, 112, 113, 114] and importantly has shown good affinity for the Cu(II) ion with a stability constant of approximately 5.44×10^{27}.[113] DDC has been used in Chapter 5 for the detection of Cu(II) at a modified electrode.

The formation of the $Cu(DDC)_2$ complex has shown promise as a means of removing copper from water sources.[115, 116] Li *et al.*[117] have described the use of diethyl dithiocarbamate in flocculation process for the removal of copper from electroplating waste water with good results. Furthermore, Fu *et al.*[118] have reported a method of removing copper complexes from aqueous solutions using a dithiocarbamate compound using simple precipitation and filtration. Dithiocarbamate ligands have also been used for the detection of various metal ions, such as that reported by Weldegebriel *et al.*[119] whereby vegetables, water and soil samples were treated with ammonium pyrrolidine dithiocarbamate, and flame atomic absorption spectrophotometry was used to detect Co(II), Cr(III) and Cu(II) metal ions. The $Cu(DDC)_2$ complex has shown promise in

many biological applications,[120] with anti-tumour activity reported by Burkitt *et al.*[121] among others.

(a) (b)

N,N-diethyl-dithiocarbamate (DDC)

$Cu(DDC)_2$

Figure 1.5: Structure of diethyl dithiocarbamate (DDC) and (b) the square planar complex of DDC to Cu(II).

1.2.2.1.1 The use of DDC in Electrochemistry

The electrochemical detection of metal ions using DDC is generally carried out in organic solvents as the metal complexes are insoluble in water. For example, Hendrickson *et al.*[111] reported electrochemical data in 1976 regarding various metal ion chelates with the DDC ligand, showing quasi-reversible electrochemistry of the $Cu(DDC)_2$ complex in acetone-based solutions. In 1981, Bond and Wallace[122] used DDC in reverse phase liquid chromatography where they added Cu(II), and detected the formation of $Cu(DDC)_2$ electrochemically at bare electrodes in acetonitrile/water mixed solutions. The authors reported a limit of detection of 2.0×10^{-7} M Cu(II) in this publication which they enhanced to 3.1×10^{-8} M Cu(II) in 1982,[123] with the use of a thin layer cell.

The analysis of such complexes in aqueous solutions generally involves the anchoring of the complex to a solid substrate. This has led to the development of sensors such as that reported by Chen *et al.*[124] who have shown the use of DDC immobilised in a Nafion film cast on a GCE for the detection of Cu(II). The authors obtained a limit of detection of 1.0×10^{-8} M Cu(II) using stripping voltammetry. More recent reports on the use of DDC in electrochemical sensing includes work by de Carvalho *et al.*[125] in the detection of As(III) and

As(V) at a hanging mercury drop electrode using stripping voltammetry. Most recently, Dong *et al.* have shown the production of Bismuth-DDC nanorods which they have drop-cast on a GCE for the sensitive detection of ascorbic acid (8.3×10^{-7} M) [126] and H_2O_2 (2.0×10^{-7} M).[127]

1.2.3 Polymer and Polymer Composites

Polymers are macromolecules that consist of small repeating units known as monomers. They are generally associated with plastics and insulating substances, used frequently in packaging materials and for the protection of electronic wires and devices as they are characteristically insulating.[128] Conductive polymers or ICPs (intrinsically conducting polymers) however, are a class of polymer that consist of carbon, hydrogen and simple heteroatoms (e.g. sulfur, nitrogen etc.) with a π-conjugated backbone providing the basis for conductivity. They are widely used in sensors, batteries and as corrosion protection materials amongst many other applications, mainly due to the fact that they retain the mechanical properties of traditional polymers in combination with their specific electronic properties. Their development has been accredited to A.J. Heeger, A.G. MacDiarmid and H. Shirakawa and they were awarded the Noble Prize in Chemistry in 2000 for their work in the advancement of the materials.[129] Frequently used ICPs include polyaniline, polythiophene, and polypyrrole.[130] Polypyrrole (Ppy) is used in Chapter 4 of this thesis in the development of a Cr(VI) sensor and its repeating unit structure is illustrated in Figure 1.6.

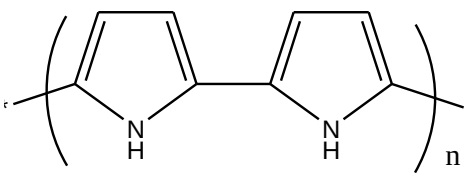

Figure 1.6: Structure of polypyrrole (Ppy) in its neutral form.

1.2.3.1 Polypyrrole

Polypyrrole (Ppy) is one of the most studied conducting polymers in electrochemistry, since its first electrochemical synthesis in 1968 by Dall'Ollio *et al.*[131] it has been implemented in a wide range of applications such as sensors, batteries, and corrosion inhibitors.[132, 133, 134, 135] The extensive use of Ppy can be attributed to its biocompatibility, ease of preparation, stability and conductivity.[132] There has been much research on the various factors affecting the growth and properties of Ppy films,[136, 137, 138, 139] with the more recent publications focussing on the formation of nano and microstructures of the polymer.[140] There has also been a lot of attention paid to the incorporation of nano materials in Ppy films, in particular carbon nanotubes.[141, 142, 143]

The use of Ppy in metal ion detection has been well studied, for example, by Zanganeh *et al.*[144] who polymerised Ppy on a GCE for the sensitive and selective detection of Ag(I). The authors achieved good selectivity of the polymer towards Ag(I) using a pre-treatment step of cycling the Ppy film in $AgNO_3$ and observed a sensitive response of 6.3×10^{-9} M Ag(I) using potentiometry. More recent advancements in the use of Ppy for the detection of metal ions include that by Wang et al.[145] who used a nanowire morphology of Ppy in the detection of Fe(III). The authors described the modification of Ppy nanowires with 2-guanidinobenzimidazole which coordinated to Fe(III), as confirmed by UV-vis and FTIR spectroscopy. The limit of detection achieved at the modified Ppy nanowires was 5×10^{-6} M Fe(III).

1.2.3.1.1 Polypyrrole/ Carbon Nanotube based composites

The incorporation of carbon nanotubes into Ppy matrices has gained a lot of attention over the past decade, as the resulting composites retain the electronic properties of the nanotubes and the polymer provides good stability and process-ability as a support matrix, in addition to its inherent properties.[146, 147, 148] Recent advances in Ppy-carbon nanotube (Ppy/CNT) composites include those described by Mi *et al.*[149] who functionalised the nanotubes with an organometallic compound which was used to oxidise pyrrole in the creation of a Ppy/CNT composite which showed high capacitance. Ionita *et al.*[150] have also recently described the enhanced mechanical properties, morphology and anti-corrosion properties of Ppy/CNT composites containing functionalised carbon nanotubes.

Some studies have focussed on the use of functionalised MWCNTs as dopant anions during polymerisation,[151, 152] where MWCNTs are generally refluxed in sulfuric and nitric acids for the attachment of carboxylate groups prior to their use. Tsai *et al.*[152] highlight this functionality as being useful for the reduction of Van der Waals forces between the nanotubes, thus aiding in their dispersion in solution. The researchers also displayed the use of these acid-treated MWCNTs as dopant anions during polymerisation performed in the absence of a supporting electrolyte. As Snook *et al.*[151] have explained, the incorporation of MWCNTs into the polymer structure can increase the conductivity of the material, as they provide the ion and electron conducting paths that would saturate with increasingly thicker polymers in their absence.

1.2.3.2 Nafion

Nafion is an ionic polymer (ionomer), consisting of a tetrafluoraethylene backbone with perfluorovinyl ether branches, terminated with sulfonate ends, developed by Dr Walther Grot[153] for DuPont in the 1960s. This material has been used extensively in forming modified electrodes, and in Chapter 5 of this thesis, it is used in the detection of Cu(II). There has been great interest in the structure of Nafion over the years, with a general agreement that it consists of ionic clusters that are arranged differently depending on its level of hydration.[154, 155, 156, 157] The molecular structure is illustrated in Figure 1.7.

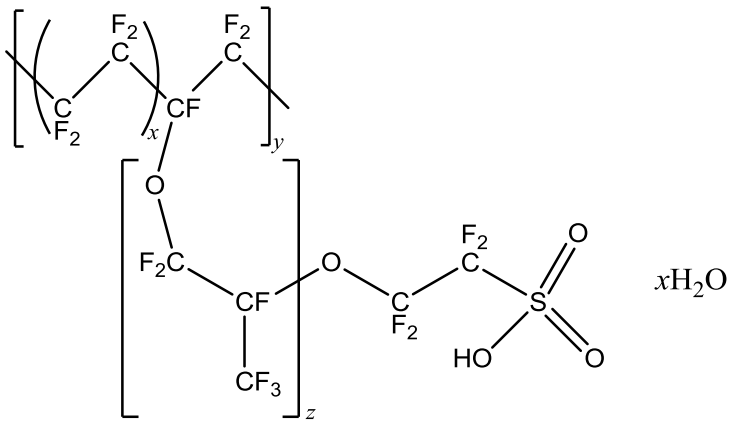

Figure 1.7: Structure of Nafion.

Nafion thin films are mainly used in electrochemical sensors to provide selectivity[158] and increase the sensitivity of detection,[159] however, they have also been used as support systems in the fabrication of electrodes, as shown by Thangavel,[160] for example, who used the thin film as a reaction vessel and template in the preparation of multi branched gold nanostructures. The conductivity of Nafion films has shown to be relatively good but dependent on swelling which reduces the contact of the film to its substrate.[161] Chen *et al.*[162] displayed the stability of Nafion during heat treatment in the investigation of a Pt/WO_3 electrode, where the Nafion coating prevented the dissolution of tungsten from the electrode.

The use of Nafion is often employed in electrochemical sensors for *in-vivo* use. For example, Brown *et al.*[163] have shown the use of a Nafion coated Pt wire for the detection of nitrous oxide in the brain. The authors have reported a sensitivity of 1.67 nA mM^{-1} at this sensor with a limit of detection of 5.0×10^{-9} M achieved using constant potential amperometry.

1.2.3.2.1 Nafion based composites

The incorporation of chelators into Nafion films has been developed mainly to enhance the selectivity and sensitivity of electrodes modified with Nafion composites. Recently, Yusof *et al.*[164] showed the use of Nafion to support MWCNTs and aspartic acid in the detection of Pb(II). The authors describe a sensitivity of 5.22 μA μM^{-1} using cyclic voltammetry for the modified screen printed electrode. Chen *et al.* [124] have also shown good detection of metal ions using a Nafion composite modified electrode. This group performed stripping voltammetry on electrodes modified with neutral chelating agents in a Nafion film to detect Pb(II), Hg(II) and Cu(II). They achieved a limit of detection of 1.0×10^{-9} M using stripping voltammetry with 5 min accumulation time for all of the metals. Other developments of MWCNTs composites include a MWCNT/Nafion film produced by Kumar *et al.*,[165] showing good sensitivity in the detection of ascorbic acid. They used square wave voltammetry to achieve a limit of detection of 1.4×10^{-6} M ascorbic acid and found it comparable to HPLC methods.

Chapter 2:

Experimental

2.1 Introduction

Electrochemistry is the area of chemistry that uses electricity to create a chemical change, providing a means of monitoring the transfer of electrons. An electrochemical sensor, therefore, is a device that provides constant information of the transfer of electrons, using the interaction of electricity with a solution.[18] This chapter outlines the electrochemical experimental procedures used in this thesis. Firstly the materials, instruments and chemicals that have been used are illustrated, including the construction of the electrochemical sensors themselves. The specific techniques performed in this work are also detailed. Analytical methods and equations applied to the experimental data throughout this thesis are also described in this chapter.

2.1.1 Sensor Materials

The nature of the electrochemical sensors varies slightly throughout this work. In the preparation of the MWCNTs modified electrodes (Chapters 3 & 4), pencil-type working electrodes (WE) were prepared, with working surfaces of 0.1257 cm^2. In the construction of these electrodes the conducting substrates, glassy carbon (GC) and gold (Au) were encased in Teflon tubing (60 x 5 mm), using an epoxy resin as a sealant and a conducting wire was used as an electrical connection (illustrated in Figure 2.1). The GC and Au rods were purchased from Goodfellow and were of 99.50 and 99.95 % purity. Pristine working surfaces were prepared before each experiment by polishing the exposed material with diamond pastes (Beuhler) of successively decreasing particle size and sonicating in both ethanol and water for 5 mins each. Intermittently, the working surface was completely refreshed by grinding the top layer using SiC grinding paper (Beuhler), revealing a new surface.

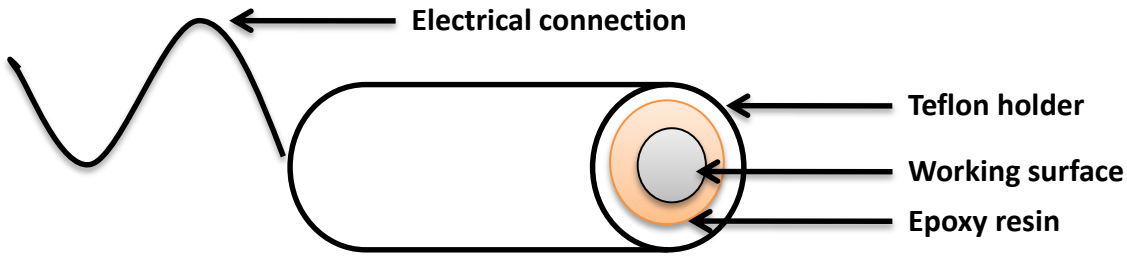

Figure 2.1: Schematic diagram of the pencil-type working electrode.

For the work involving the detection of copper (Chapter 5), platinum mesh was utilised as the WE with a conducting wire attached to one end providing the electrical connection via a silver epoxy resin, which is shown in Figure 2.2. Platinum mesh was purchased from Goodfellow with 99.9% purity and a nominal aperture of 0.25 mm. The mesh was cut to a size suitable for use in both electrochemical and spectroscopic instruments from a large sheet, giving measurements of 0.5 × 20.0 mm and the silver epoxy was sealed with a coating of non-conducting epoxy resin to avoid interference from silver in the analytical measurements.

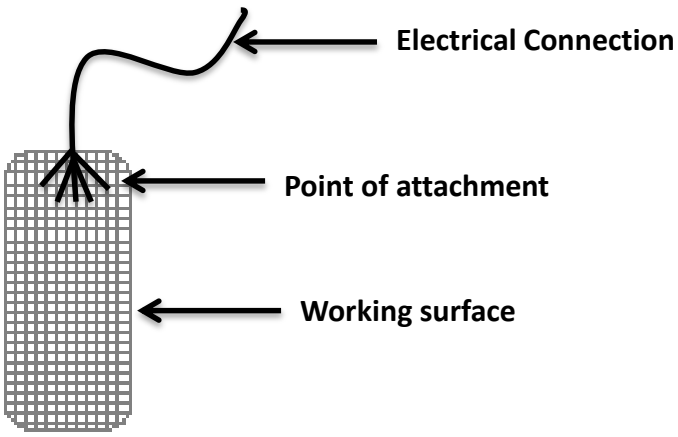

Figure 2.2: Schematic of a Pt mesh working electrode

In Chapter 3, highly orientated pyrolytic graphite (HOPG) was used as an electrode substrate. HOPG is a semi metallic allotrope of carbon, consisting of stacked layers of graphite sheets. As graphite sheets are made up of carbon atoms arranged in a hexagonal lattice, the properties of HOPG are highly anisotropic, and either the edge-plane of the material or its basal plane can be utilised (Figure 2.3).

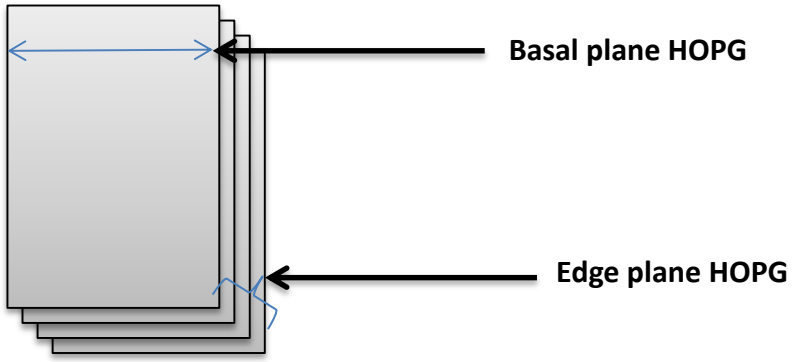

Figure 2.3: Schematic of HOPG block illustrating its basal and edge planes.

The basal plane of the material was primarily used as a working surface and, as defects are undesirable in the delicate top layer, polishing and sonication were avoided in its regeneration. The HOPG working surface was therefore regenerated between experiments by stripping the top layer away with scotch tape, until an even surface was revealed underneath without visible defects. The use of a non-conducting epoxy resin was also avoided in its construction, which is normally used to achieve a reliable seal around the working surface of the substrate. As the resin is generally loaded over the entire surface and the working surface revealed by grinding the epoxy down, the top layer of the typical electrodes are damaged and therefore require extensive polishing to remove any imposed defects. In the use of basal plane HOPG, this method would destroy the basal plane structure making it very difficult to remove the defects, and resulting in the loss of a large quantity of the substrate. Therefore, to accommodate the HOPG as a WE, another method was established to

construct the electrode, which in turn required an alternative cell set-up (illustrated in Figure 2.4). HOPG was received as a block and the WE was constructed to specifically expose the basal plane of the material. The HOPG substrate was fixed to a conducting foil (aluminium) using a silver epoxy resin, to provide an electrical contact to the potentiostat. The electrode was mounted on an insulating block, wooden in this case, and was held in place using adhesive tape, as shown in Figure 2.4 (a). This required the glass cell to be mounted on top of the electrode, which is detailed in Section 2.3, and briefly illustrated in Figure 2.4 (b).

(a)

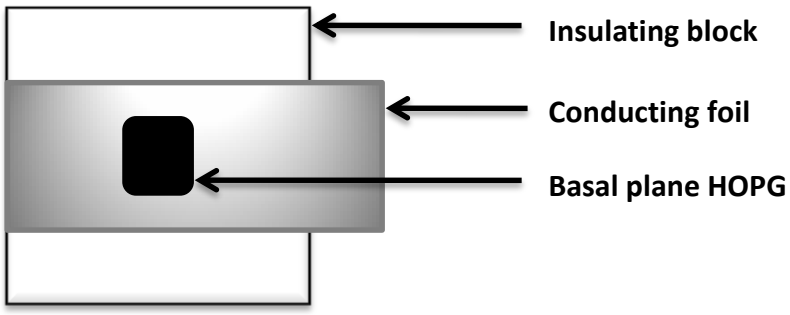

(b)

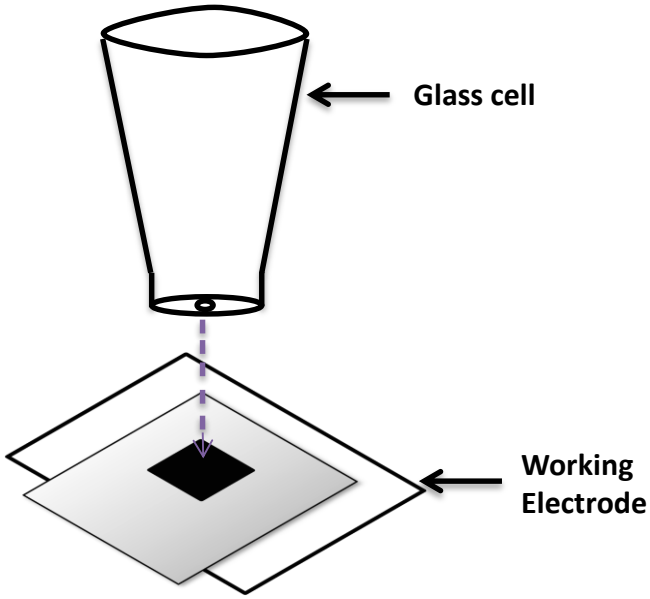

Figure 2.4: Schematic of (a) the HOPG working electrode and (b) visualisation of the alternative cell set-up.

2.1.2 The Electrochemical Cell

Electrochemical experiments for potentiostatic measurements and techniques such as cyclic voltammetry (CV) and differential pulse voltammetry (DPV) were performed using a standard three electrode cell. This involves the use of a working electrode (WE), reference electrode (RE) and counter electrode (CE) which are connected to a potentiostat. The WE served as the electrochemical sensor in this work and consisted of a conducting substrate which had been modified to improve the sensing of a particular metal ion. A standard saturated calomel electrode (SCE) was utilised as the reference electrode which provided a reference point to aid in the identification of oxidation and reduction peaks. A platinum wire of large surface area was used as a CE in all experiments, balancing the current generated at the working electrode, for example if an oxidation reaction occurred at the WE, the opposing reduction reaction occurred at the CE. In general, the potential was measured between the WE and RE and the current was measured between the WE and CE.

The conventional and modified electrochemical cell set-ups used in this work are illustrated in Figure 2.5 (a) and (b) respectively. The former involves the use of electrodes that are submerged in a cylindrical soda-glass cell containing the sample solution, however the use of highly orientated pyrolytic graphite (HOPG) as a WE required the used of a different cell set up. As the HOPG surface was attached to a base (Figure 2.4) rather than the tip of a pencil-style electrode, the cylindrical cuvette holding all three electrodes was replaced by a conical-shaped cell holding both the CE and RE, mounted on the WE base. A hole in the bottom of the cell revealed the working surface and the solution was contained in the vessel with the use of a clamp and O-ring. In both cases the submerged electrodes were held in place using a PTFE lid.

(a)

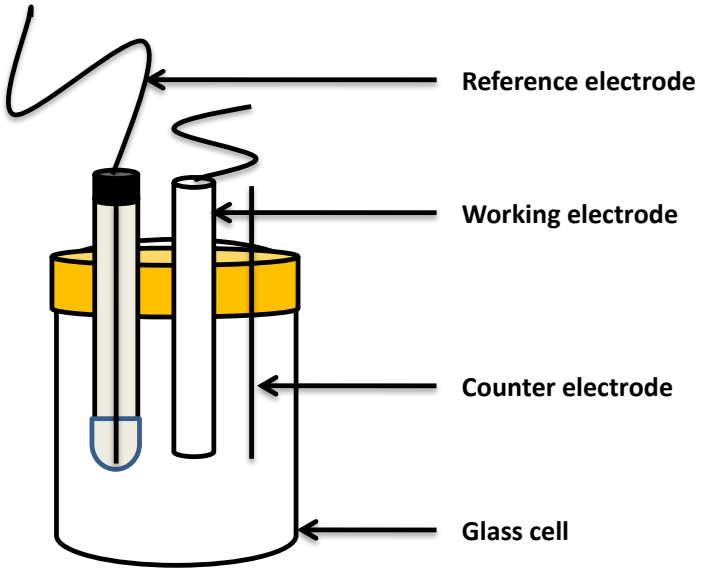

(b)

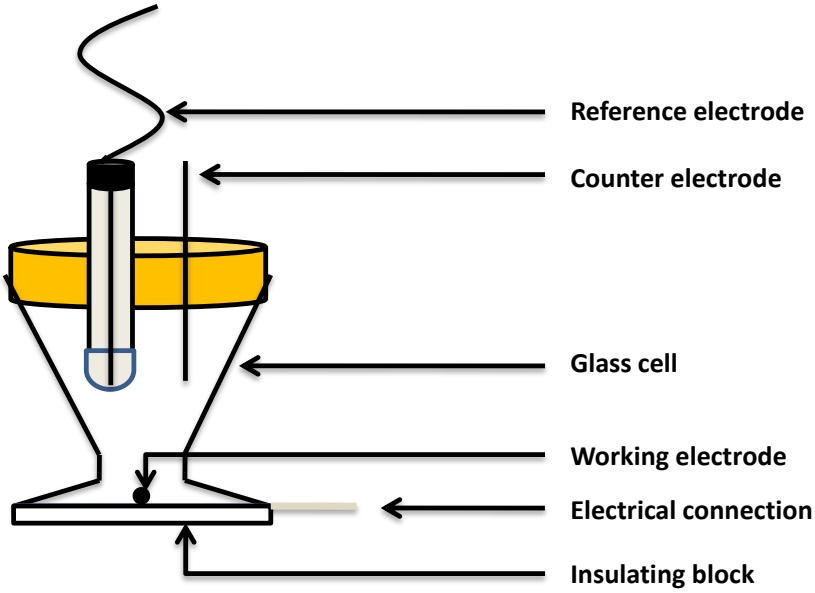

Figure 2.5: Schematic representation of (a) a conventional electrochemical cell set-up and (b) the modified cell set-up of the three electrode cell.

2.1.3 Instruments

Electrochemical experiments were carried out primarily using a Solartron Potentiostat Model 1285A and an Autolab M101, and a CH1760C Potentiostat was used to carry out DPV analysis. Scribner Associates Corrware, GPES and CH900i software packages were used respectively to perform and analyse the electrochemical experiments. UV-Vis spectroscopy was performed using a Varian Cary series spectrophotometer which comprises of a Xenon lamp. SEM and EDX characterisations were carried out with the help of Ms. Bakul Gupta at UNSW and more extensively by Dr Conor McCarthy at NUIM, who's assistance is greatly appreciated in this work. All experimental instruments and the models used are listed in Table 2.1. Precise analysis of experimental data was carried out using EC-Lab Software and Microsoft Excel.

Table 2.1 : List of instruments used in experimental procedures with relevant model details.

Instrument	Model
Potentiostat	Solartron 1285A / AutoLab M101 / CH1760
UV-Vis Spectrometer	Varian Cary 50 UV-Vis Spectrometer
SEM	Hitachi S400 / S900
EDX	Inca-X Energy
pH meter	Eutech Cyberscan pH 510
Conductivity meter	Jenway 4510
Sonicator	Fisher Scientific Fb 15048

2.1.4 Chemicals

In this body of work, electrochemical sensors were constructed by modifying WEs, i.e. gold, glassy carbon and basal plane HOPG, with various materials. The materials; multiwalled carbon nanotubes (MWCNTs), graphene and diethyldithiocarbamate (DDC), were chosen based on their specific individual properties, and various methods to modify the electrodes were carried out to cater for the individual materials. Aqueous solutions were prepared from Millipore distilled water and stored under cool, dark conditions to ensure maximum stability.

2.1.4.1 Pyrrole

Pyrrole was purchased from Sigma-Aldrich as a 98% pure solution, however purification was carried out before its use by simple distillation under vacuum to remove any dimeric or oligomeric impurities. The purified monomer was stored at -20.0 °C before use.

2.1.4.2 Multiwalled Carbon Nanotubes (MWCNTs)

In chapter 1, multiwalled carbon nanotubes (MWCNTs) are reviewed and their unique physical and electronic properties are discussed in depth. Briefly, they are rolled up sheets of graphene, or sp^2 hybridised carbon sheets with a helical structure that provides a length to diameter ratio greater than any other material.[34] The MWCNTs used in this work were obtained from Sigma Aldrich, of 6-13 nm in open diameter and 2.5-20 μm in length and were used as received, unless stated otherwise.[166] They were produced by a chemical vapour deposition (CVD) method followed by HCl demineralisation to obtain >99% purity and the reported surface area (by BET method) is approximately 220 $m^2\ g^{-1}$.

2.1.4.3 Graphene

Graphene is a two dimensional sheet of sp^2 hybridized carbon. The graphene used in this body of work was provided by Dr Mohammad Choucair who published his "top-down" synthesis in 2010 which involved the low-temperature flash pyrolysis of a solvothermal product of sodium and ethanol, followed by gentle sonication of the nano-porous carbon product.[167] The reported surface area, calculated by the BET method, of this graphene was 1692 $m^2 g^{-1}$ and it was used without further modification in this work.

2.1.4.4 Diethyl Dithiocarbamate (DDC)

Dithiocarbamic acid or diethyl dithiocarbamate (DDC) is an amino formic acid containing two sulfur atoms in place of the oxygen atoms. It is a well known ligand, as discussed in Chapter 1 that is generally used in its salt form. In this work, the diethyl ammonium salt of DDC was purchased from Sigma Aldrich and was of 97 % purity.

2.1.4.5 Nafion

Nafion is an ionic polymer, or ionomer, consisting of a tetrafluoraethylene backbone with perfluorovinyl ether branches, terminated with sulfonate ends. Although Nafion membranes are commonly used, for the purpose of this work, its acidic ionomer which is prepared in low aliphatic alcohols was solely used. It is available in various concentrations, however in this work only the 5% wt. solution was utilised, which was purchased from Sigma Aldrich and contained 15-20% water.

2.2 Methods

The methods used in the modification of electrodes varied throughout this body of work. The use of MWCNTs and graphene required good dispersion of the materials prior to surface modification. The use of polypyrrole as a supporting scaffold involved the electrochemical polymerisation of pyrrole and the use of Nafion as a support material involved its electrodeposition. The methods implemented for modifying the individual electrodes are detailed in this section.

2.2.1 Dispersion

To prepare dispersed solutions of MWCNTs and graphene, ultrasonic agitation was implemented. This technique is widely used in the preparation of dispersed solutions and briefly, involves the transmittance of ultrasound by waves that alter the molecular spacing of the sample. Ultra sonication is unique in that it uses solid disruption to decrease the size of solid particles in solution which increases the total solid surface in contact with the solution.[168] Ultra sonication can be applied either directly to a sample, using an ultrasonic probe or indirectly using an ultra sonication bath. As the use of probes is very costly and can potentially introduce sample contamination,[169] a sonication bath (Table 2.1) was utilised in this work to disperse solutions of MWCNTs and graphene.

2.2.2 Adsorption

The modification of electrodes using physical adsorption was predominantly carried out with MWCNTs and graphene. To modify the electrodes by this method, specific volumes of the dispersions were drop-cast on the electrode surface. An IR lamp (approx. 500 °C) was utilised to evaporate the solvent from the electrode surface leaving the modification material adsorbed on the surface.

2.2.3 Polymerisation

In this work, polymerisation of pyrrole to form polypyrrole (Figure 2.6) was carried out electrochemically. Electrochemical polymerisation is defined as a process of polymer synthesis, initiated by particles which are the product of electrode reaction.[170] This is performed with the application of a suitable potential to a conducting substrate which is immersed in a solution containing the monomer and required doping electrolyte. This is generally carried out using galvinostatic, potentiostatic or potentiodynamic methods. Potentiostatic deposition of polypyrrole was carried out in this work as it generally produces polymers with the most consistent morphologies.[171]

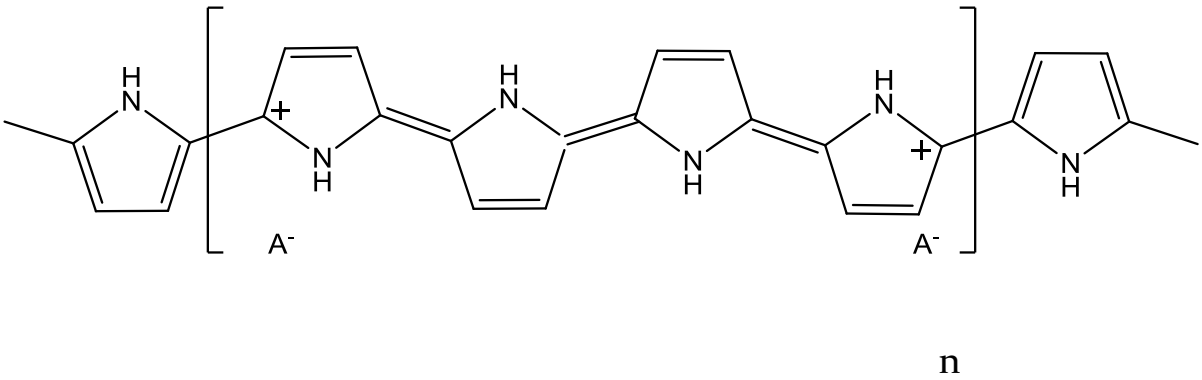

Figure 2.6: Structure of polypyrrole in the oxidised form, where A^- are the anionic dopants required to balance the charge.

The role of the dopant anion in polymerisation is to balance the charge formed on the polymer backbone. Dopants are generally introduced to a polymer as the electrolyte salt, such as Cl^- or SO_4^{2-} in the polymerisation solution during electropolymerisation and the level of doping can largely effect the conductivity of the polymer by creating more mobile charges.[171]

2.2.4 *Electrodeposition of Nafion*

The method of coating a material by electrodeposition is widely used in industries such as paints and plastics[172] to achieve reliable, cost-effective coverage of all varieties of materials. It is based on the electrostatic interactions of the substrate with the coating. In this case, the Pt mesh electrode substrate was positively charged using constant potential amperometry, whilst submerged in a solution of Nafion for a specific time. The electrostatic interactions between the electrode and the solution ensured each aperture of the mesh was evenly coated with the ionomer.

2.3 Theory of Electrochemical Techniques

The various electrochemical techniques employed in the characterisation of the electrochemical sensors and used in the detection of metal ions in this work are detailed in this section. Specifically they include cyclic voltammetry, differential pulse voltammetry and rotating disk voltammetry.

2.3.1 *Cyclic voltammetry*

As mentioned in Section 2.1, electrochemical measurements are based on Ohm's Law, in that they measure the effects of potential (E) and resistance (R) on current (I). Cyclic voltammetry is an electrochemical technique that measures changes in current as the cell potential is cycled between two specific limits. The changes in current can represent either a faradaic process i.e., the oxidation or reduction of a species in the sample solution, or a non-faradaic process such as capacitance. The faradaic processes occur at the interfacial region of the WE, and the CE balances the electron transfer with the opposing reaction. The working electrode can thus act as an electrochemical reductant or oxidant depending on the potential applied to the surface. The application of a negative potential creates a reducing electrode and as the potential applied becomes more positive, the WE becomes more oxidising.

The rate at which the potential is cycled (the scan rate) and the number of cycles recorded can both be varied to provide various information on the electroactive species which is generally displayed as a voltammogram which is a plot of current (*I*) vs. potential (*E*), illustrated in Figure 2.7.

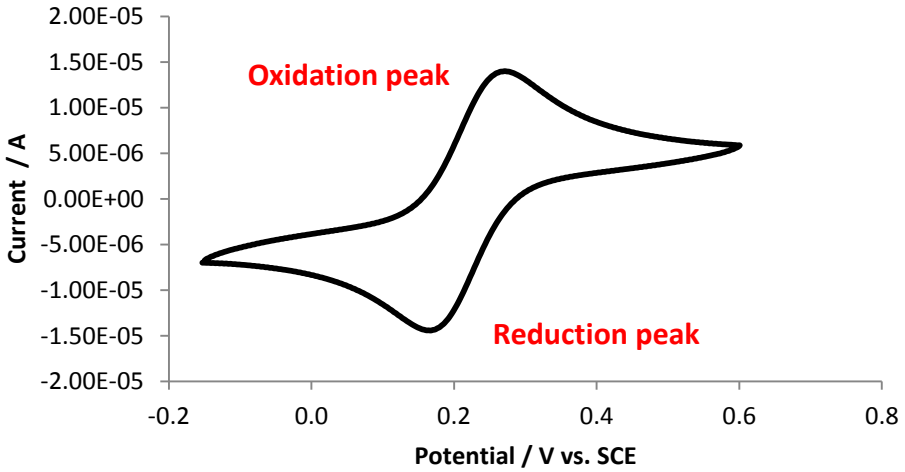

Figure 2.7: Typical voltammogram of a reversible redox couple.

In the case of simple redox couples, both the oxidation and reduction of the species are represented by waves or peaks in the voltammogram. The potential at which the peak exhibits a maximum current can be used to identify the electron transfer that is occurring, and the process can be quantified by the amplitude of this peak current. The increase in peak current as the potential is scanned forward is representative of the analyte being oxidised, and its decrease is representative of the concentration of the original analyte in the diffusion layer decreasing due to its oxidation. In the reverse sweep the same process occurs, whereby the reduction peak current increases as there is a high concentration of the oxidised species. As this species is reduced, there is a decrease in the oxidised species in the diffuse layer and the current approaches zero.[173]

Cyclic voltammetry was used extensively in this thesis as it provides a wide range of information on electroactive species and conducting surfaces. It can be used without the observation of a solution based redox couple, in a background supporting electrolyte solution to provide information such as the anion/cation exchange properties of a material (e.g. a conducting polymer) or by measuring a region of the voltammogram where no known redox processes occur, as an indication of its capacitive properties (e.g. for carbon nanotubes).

Capacitance is defined as the ability of a material to store charge, and in capacitive electrode materials, when a potential is applied to the electrode surface, the charge from solution builds up at the electrode surface which is identified by a charging current. The combination of the charge on the electrode surface and the build up of charge at the electrode-solution interface is known as the electrical double layer, and the double layer capacitance is used to characterise the electrode-solution interface, which can therefore be used to characterise an electrode material. The double layer is made up of (i) an inner layer or Helmholtz plane (IHP), which contains solvent molecules and any adsorbed species and (ii) a diffuse layer which extends from the outer Helmholtz plane (OHP), where solvated ions interact with the inner layer, to the bulk solution.[174] The proposed model of the electrical double layer is illustrated in Figure 2.8.

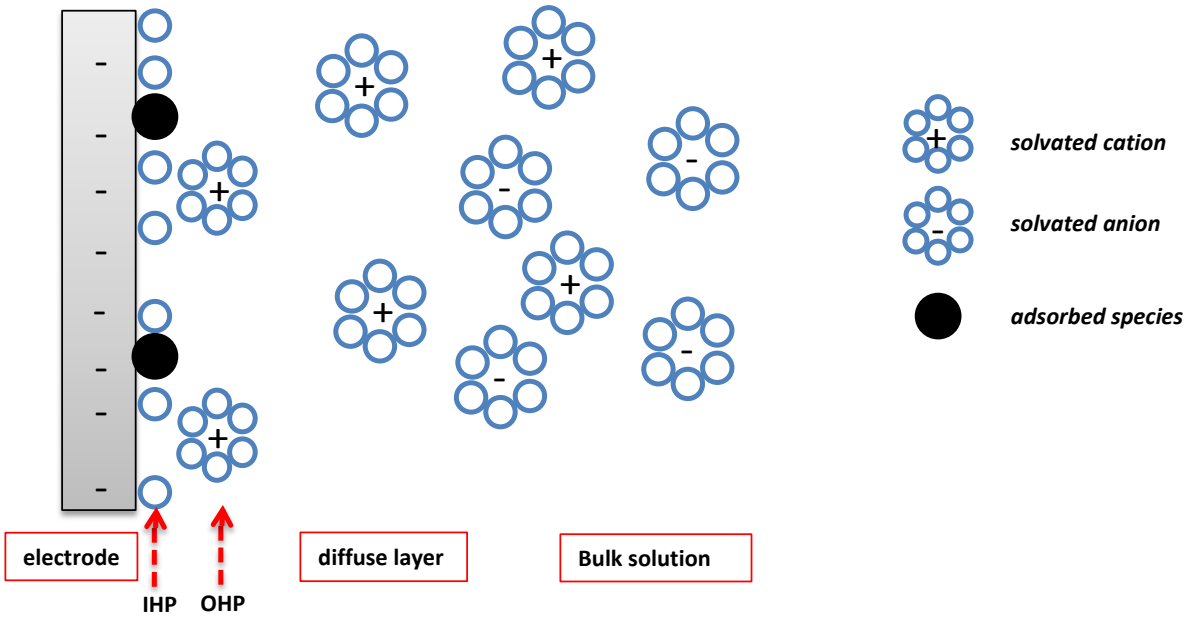

Figure 2.8: Illustrated model of the electrical double layer.[174]

The capacitance of an electrode is often measured by electrical impedance spectroscopy however it can also be calculated using cyclic voltammetry. In the latter case, the current is measured in a region of the voltammogram where no faradaic processes are evident and the voltammogram is rectangular in shape.[40] This current (I / A) can be related to the scan rate (v / V s^{-1}) according to the linear Equation 2.1. To calculate the capacitance (C / F), a plot of the currents against the scan rate is generated and the slope is therefore equal to the capacitance. If the currents have been normalised to the mass of the material on the electrode, the units of capacitance then relate to the mass (F g^{-1}).

$$C = \frac{I}{v} \qquad 2.1$$

Cyclic voltammetry was the primary technique used in the detection of metal ions in this thesis, with attention paid mainly to the peak position (E_p) and the peak currents (I_p) recorded. In general E_p gave information on the thermodynamic properties of the reactions and I_p gave information regarding their kinetics. Relevant parameters were varied within this technique, specifically scan rate and potential window, to achieve the optimum

conditions for each sensor. The electron transfer properties of the working electrodes modified with carbon-based nanomaterials were studied using this technique. This involves analysis of the redox behaviour of an electrochemical probe, i.e. a well established redox couple that exhibits efficient electron transfer. In this work, the redox behaviour of $[Fe(CN)_6]^{3-}$ / $[Fe(CN)_6]^{4-}$ was studied, as it is a commonly used example of an outer sphere reaction, however, it is known to be sensitive to surface conditions.[175] The electron transfer of an outer sphere reaction therefore occurs in the outer Helmholtz layer, and the couple is not chemically bound to the substrate. Outer sphere reactions are said to be highly thermodynamically dependent, that is they are predominantly effected by the potential difference in the redox exchanging sites. Analysis of such reactions provides information on the electron transfer abilities of modified surfaces when compared to the bare substrate.

The ratio of peak currents (I_{pc}/I_{pa}) is often used to describe the reversibility of a redox reaction according to Equations 2.2, 2.3 and 2.4. Here, unity (Equation 2.2) signifies a fully reversible reaction and the observation of one process shows irreversibility (Equation 2.3). In the case where the currents recorded for the reduction reaction are lower than those recorded for the oxidation reaction, (Equation 2.4) it is said that the reaction is partially reversible and is expected to depend greatly on scan rate.[176] Partial irreversibility can be due to many factors such as chemical instability or the occurrence of a chemical process.

$$I_{pc} = I_{pa} \qquad 2.2$$

$$I_{pc} = 0 \qquad 2.3$$

$$I_{pc} < I_{pa} \qquad 2.4$$

2.3.1.1 Diffusional Models

The diffusion of analytes to and from the electrode surface also has an important role in the thermodynamics of a redox reaction. Electrochemical experiments are therefore performed in solutions containing an electrolyte of sufficient concentration to overcome any mass transport limitations. For simplicity in this section, simple solvated anionic and cationic species are considered in their diffusion to an electrode. It is illustrated in Figure 2.9 (a) that when a negative potential is applied to the electrode, positively charged species from the bulk solution are attracted to the electrode surface. Here they are reduced and diffuse back to the bulk solution. This is known as semi-infinite planar diffusion as there is, theoretically, a semi-infinite amount of cations diffusing from the bulk solution. A second diffusional process must be considered however in the modification of electrodes with MWCNTs, thin layer diffusion.[177, 178] This model assumes the formation of "solvent pockets" within an entangled network of MWCNTS where anions and cations are essentially trapped, as illustrated in Figure 2.9 (b). When a cathodic potential is applied to an electrode in this case, the cation is already at the electrode surface and is therefore reduced without the limitation of diffusion from the bulk solution. When the potential is switched (as in cyclic voltammetry) this reduced species is still at the surface and thus is oxidised promptly, reducing the ΔE_p of the redox couple. [174] It should be noted however that such effects tend to rely on slow scan rates to allow for the initial diffusion of the analyte into the thin layer cavities.[174, 177]

(a)

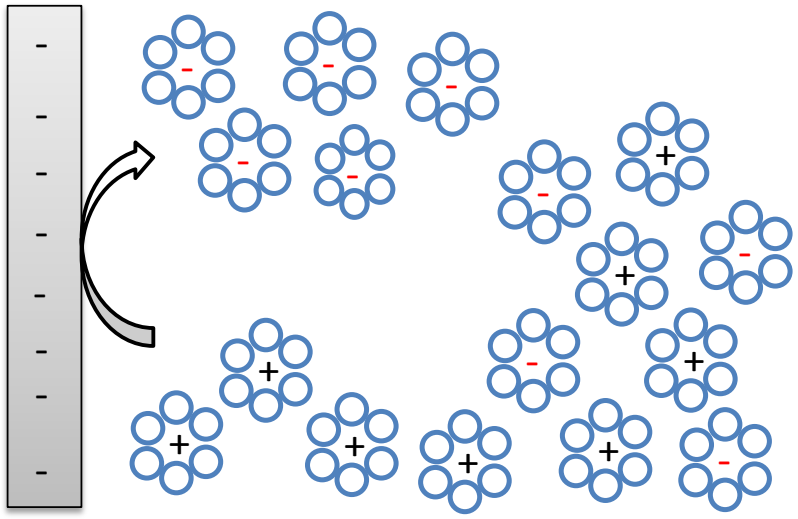

Semi-Infinite Planar Diffusion

(b)

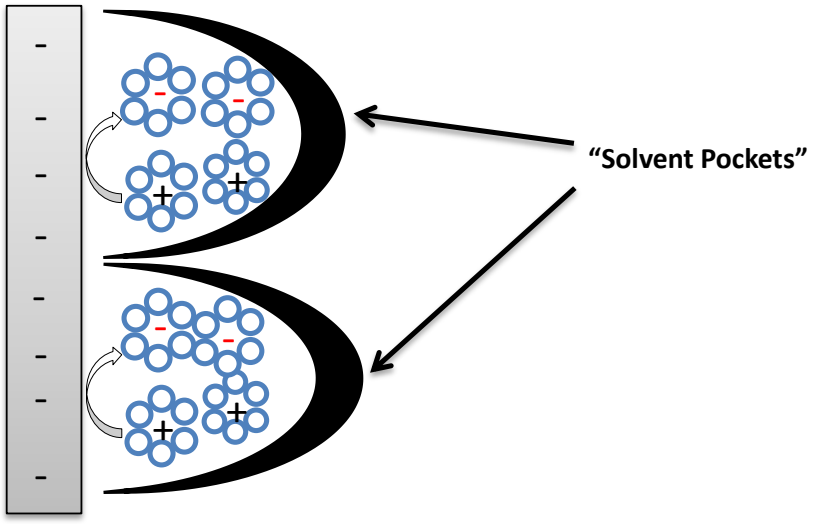

Thin Layer Diffusion

Figure 2.9: Schematic illustration depicting the relationship between an electrode and the sample solution (a) when a cathodic potential is applied, causing semi-infinite planar diffusion and (c) the formation of "solvent pockets" at an electrode modified with MWCNTs is illustrated where the application of a cathodic potential causes thin layer diffusion.

2.3.1.2 Analytical measurements

Analysis of the results obtained in the electrochemical characterisation of the sensors and detection of the metal ions are discussed in this section. The information gained from cyclic voltammetry was applied to kinetic equations to gain further knowledge about the electron transfer occurring at the working electrode. In particular, the separation between the oxidation and reduction peak potentials can give details on the reversibility of the reaction. Equation 2.5 shows the ideal peak separation for a reversible redox couple which is independent of scan rate and can be used to determine the number of electrons (*n*) transferred in the reaction.

$$\Delta E_p = E_{pa} - E_{pc} = \frac{57}{n}\ mV \qquad 2.5$$

Poor reversibility can be identified by a large *ΔEp*, and refers to the kinetics of the electrode, which can be affected by the limitations imposed by mass transport at the electrode surface. In the case of *quasi*-reversible systems, an intermediate case of reversibility, the peak separation is generally used to calculate the rate of electron transfer of an electrochemical reaction and it is dependant on the scan rate. In this work, two methods were employed to calculate rate constants at the various unmodified and modified electrodes for the redox of $[Fe(CN)_6]^{3-}$ / $[Fe(CN)_6]^{4-}$, namely the theory published by Nicholson[179] in 1965 and the equation derived by Kochi and Klingler[180] in 1981. The peak currents (I_p) are also very useful in the electrochemical characterisation of the detection process. In the case of a reversible redox couple, the magnitudes of I_p for the forward and reverse sweeps are the same and regardless of reversibility, the I_p height is dependant on scan rate. In this work particularly, the Randles-Sevcik equation has been used in two ways to present information gained from monitoring I_p; namely the calculation of the diffusion coefficient of the probe at the bare electrode, and the

electrochemically available surface area of the modified electrode. The use of these Equations is detailed herein.

2.3.1.3 Nicholson Theory

Nicholson used the absolute rate equation to construct a rate equation which overcame the problems of concentration polarisation, and allowed him to calculate theoretical values for the constant Ψ, based on specific peak separations, ΔEp. The peak separations were limited to those larger than 60 mV to ensure a *quasi*-reversible reaction and lower than 212 mV to maintain agreement of the equation with the transfer coefficient, α. The transfer coefficient or "symmetry factor" describes the change in the energy barrier for the transition of an electrochemical reaction, with respect to the electrode potential.[181, 182] Typical values of α are between 0.3 and 0.7, and represent the efficiency of the transition between oxidation states of an electrochemical reaction. They are also indicative of the position of the reaction with respect to the outer Hemlholtz layer.[183] The term "symmetry factor" refers to the effect of β on the shape of the energy-potential plot, i.e. how symmetrical the redox peaks appear.[173]

The theoretical values of the peak separations, proposed by Nicholson, are listed in Table 2.2, and were used to construct Figure 2.12, a plot of $1/\Psi$ vs. $1/\Delta E_p$. The trend of this plot (Figure 2.10) was utilised to deduce a polynomial equation. This was used to calculate Ψ values based on experimental ΔE_p values at each scan rate. The standard rate of the reaction was then calculated, k_s, according to Equation 2.6 at each scan rate.

$$k_s = \Psi (\pi a D_O)^{1\ 2} \qquad 2.6$$

In the equation constructed by Nicholson (2.6), k_s is the standard rate constant, Ψ is the dimensionless constant calculated based on the theoretical

plot in Figure 2.10, π is 3.14159, D_o is the diffusion coefficient ($cm^2\ s^{-1}$) and a is calculated from Equation 2.7.

$$a = nF\nu RT \qquad 2.7$$

Where n is the number of electrons transferred, F is Faradays Constant (96485.3 C mol^{-1}), ν is the scan rate (V), R is the gas constant (8.3145 J $K^{-1}mol^{-1}$) and T is the temperature (K).

Table 2.2: Variation of peak potential separations with kinetic parameters for cyclic voltammetry[179].

Ψ	**ΔE_p x n / mV**
20.00	61
7.00	63
6.00	64
5.00	65
4.00	66
3.00	68
2.00	72
1.00	84
0.75	92
0.50	105
0.35	121
0.25	141
0.10	212

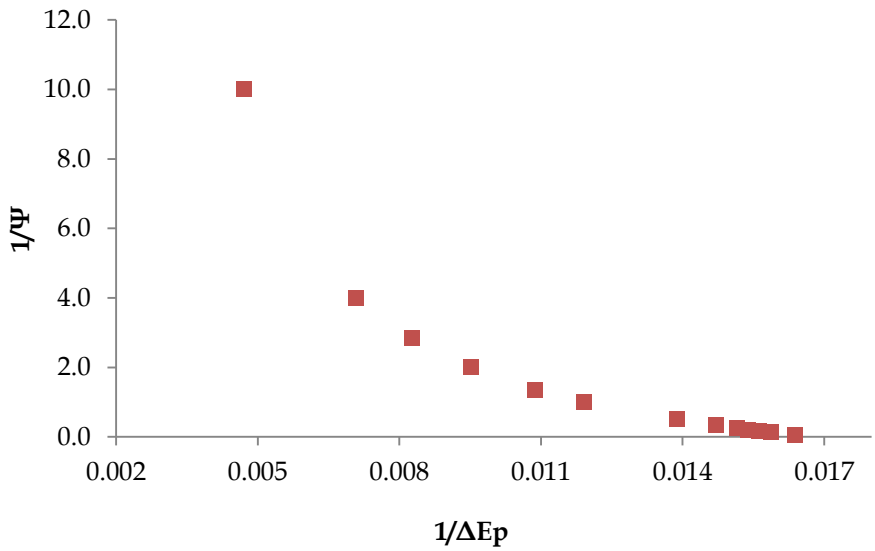

Figure 2.10: A plot of the inversed theoretical values for Ψ as a function of the inversed peak separations given by Nicholson. The polynomial equation for the trend is $y = 4 \times 10^{13} x^6 - 3 \times 10^{12} x^5 + 8 \times 10^{10} x^4 - 1 \times 10^9 x^3 + 1 \times 10^7 x^2 - 49703 x + 105.32$, which was used to calculate Ψ values for the experimental ΔE_p values. Here, y is $1 / \Psi$ and x is $1 / \Delta E_p$.

2.3.1.4 Kochi and Klingler Equation

In 1981 Kochi and Klingler devised an equation to calculate the rate of a reaction, similar to that of the Nicholson Theory, but without the use of theoretical data, and including the calculation of the transfer coefficient β, where $\beta = 1-\alpha$. This method uses the rearrangement of Equation 2.8, and a linear equation can be deduced, Equation 2.9.

$$k_s = 2.18 \left(\frac{\beta DnFv}{RT}\right)^{\frac{1}{2}} exp\left(-\frac{\beta^2 nF}{RT}\left(E_p^a - E_p^c\right)\right) \qquad 2.8$$

$$lnv = \frac{2\beta^2 nF}{RT}\Delta E_p + 2lnk - 2ln(2.18) - ln\frac{\beta DnF}{RT} \qquad 2.9$$

Here, k is the rate constant (cm s^{-1}), D is the diffusion coefficient (cm^2 s^{-1}), n is the number of electrons transferred, F is Faraday's constant (96,485.3415 C mol^{-1}), v is the scan rate (V s^{-1}), R is the gas constant (8.314 J K^{-1} mol^{-1}) and T is

the temperature (K). If a linear correlation between the natural logarithm of the scan rate, v, and ΔE_p can be achieved experimentally, the slope of this equation can be used to calculate β. A typically constructed plot of this data can be seen in Figure 2.11 with good linear correlation. The calculated β value can then be used to calculate the average rate constant for electron transfer for the observed electrochemical process, over the range of scan rates tested.

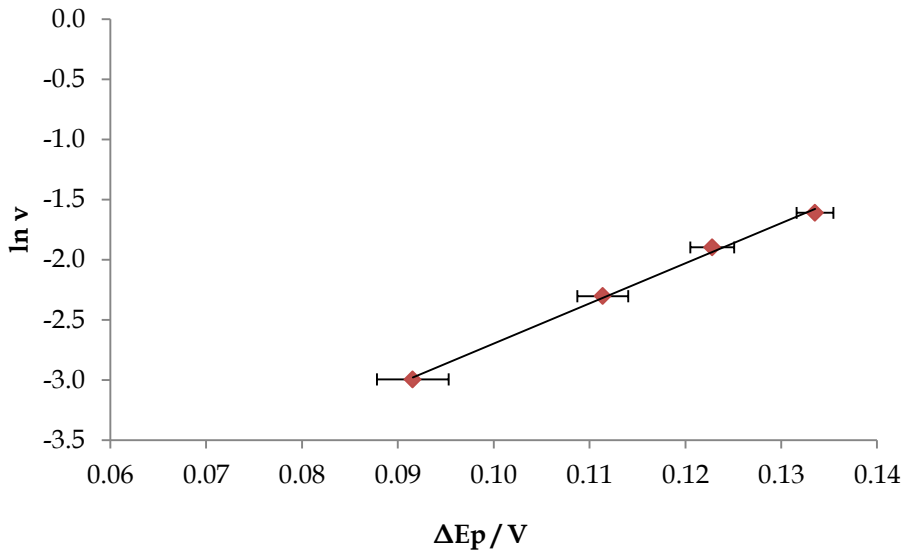

Figure 2.11: Typical plot monitoring the change in electron transfer (ΔE_p) with the natural log of the scan rate (ln v) used to determine the rate of reaction.

2.3.1.5 Randles Sevcik Equation

The Randles Sevcik Equation utilises the current response (I_p) of an electrochemical redox reaction at various scan rates to analyse an electrochemical process. In this work particularly, the Randles Sevcik equation (Equation 2.10) has been used in two ways to present information gained from monitoring I_p. Experimentally, the scan rate was varied between 10 and 200 mV s^{-1} and the peak currents were monitored. In the first application, a plot of the square root of the scan rate as a function of the peak current was generated, and as a linear relationship was established (Figure 2.12), the Randles-Sevcik equation was used to determine the diffusion coefficient, D, of a particular analyte at a bare electrode, based on Equation 2.7. In Chapter 3

this equation was used to calculate the diffusion coefficient for $[Fe(CN)_6]^{3-}$ / $[Fe(CN)_6]^{4-}$.

$$I_p = K\, n^{3/2}\, A\, D^{1/2}\, c\, v^{1/2} \qquad 2.10$$

Here I_p is the peak current (A), K is a constant (2.69 x 10^5), A is the surface area (cm^2), c is the concentration of the redox species (mol cm^{-3}), D is the diffusion coefficient ($cm^2\ s^{-1}$) and v is the scan rate ($V\ s^{-1}$). By rearranging Equation 2.10 to give Equation 2.11, and utilising the diffusion coefficient calculated at the bare electrode, the electroactive surface area of the modified working electrodes were calculated. The ferricyanide couple was chosen for this study as it has highly reproducible electrochemistry and has been studied extensively in the literature.

$$A = \frac{I_p}{(v^{1/2} K\, n^{3/2} D^{1/2} c)} \qquad 2.11$$

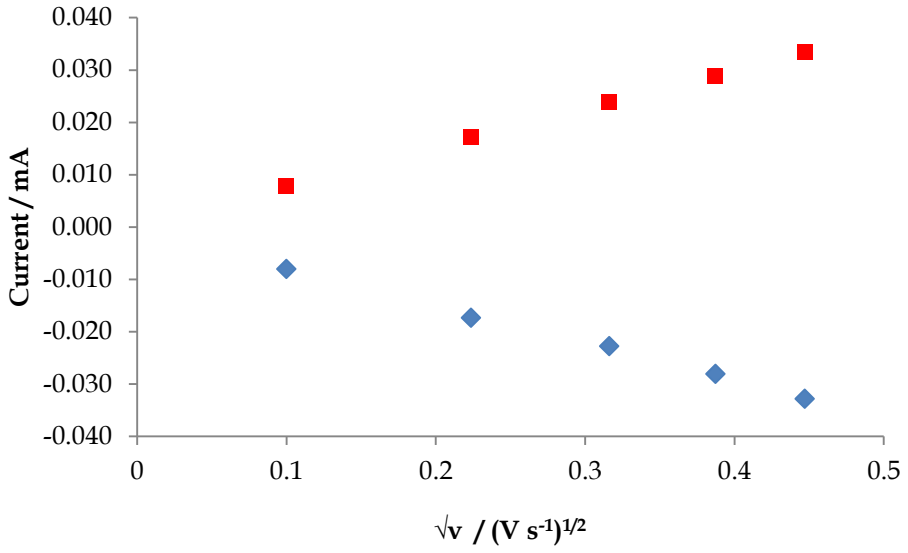

Figure 2.12: Typical plot monitoring change in oxidative ■ and reductive ■ peak currents (I_p) with the square root of the scan rate ($\sqrt{v}$) used to calculate the electroactive surface area.

2.3.2 Differential Pulse Voltammetry (DPV)

Although cyclic voltammetry can provide a broad spectrum of information on electrochemical sensors, it is not the most sensitive technique accessible, however pulse voltammetry is a sensitive electrochemical technique used widely in ion detection. In contrast to cyclic voltammetry, where there is a constant application of potential to the WE, in pulse voltammetry the potential is applied in pulses which can be tightly controlled. As potential is applied to the electrode surface, a charge builds up known as a "double layer" and creates large background signals due to its capacitance. Pulsing the applied potential allows this current to decay, preventing a build up of background capacitive current, thus enhancing the redox signals. Generally, either normal pulse voltammetry or differential pulse voltammetry are used, which are illustrated in Figure 2.13. In normal pulse voltammetry, the base potential applied is constant; however with DPV, the base potential is incremented at a fixed rate. The pulses applied are of the same magnitude each time and the pulse period, which comprises the pulse duration as well as the lapse between pulses, is set to be repeated identically each time also. Unlike normal pulse voltammetry, in DPV the current is sampled twice, just prior to each pulse and then again at the end of the pulse, as shown in Figure 2.13. The difference between the two values is calculated and a plot is generated of the resulting current values (ΔI), as a function of the applied potential, V. In this work, DPV was utilised to reduce the large background current caused by the capacitance of MWCNTs, in order to increase the sensitivity and the detection properties of the electrode surface modified with MWCNTs. The specific parameters used are outlined in the relevant sections.

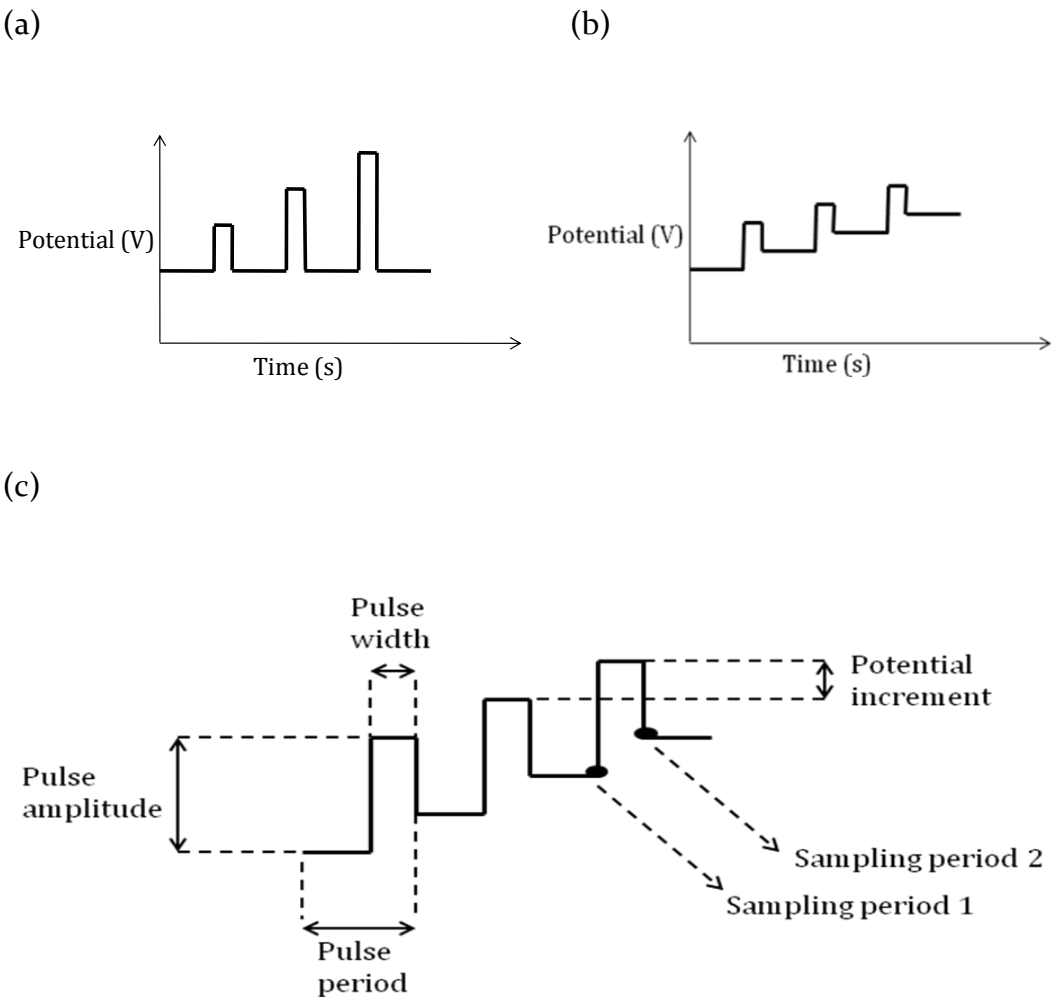

Figure 2.13: Schematic of (a) normal pulse voltammetry, (b) differential pulse voltammetry and (c) the variable parameters for DPV.[184]

2.3.3 Rotating Disc Voltammetry

Rotating Disc Voltammetry (RDV) is a mechanical alteration to the cell set up to increase the rate of mass transport to the electrode surface. In combination with constant potential amperometry, RDV was employed in the sensitive detection of Cr(VI) in Chapter 4. A rotating disc electrode, similar to the pencil-style electrode shown in Figure 2.1, was used for these studies. The RDV set-up consists of an electrode attached to a rotor spindle *via* a suitable

electrical contact which is illustrated in Figure 2.14. When the electrode is rotated at a particular rotation speed in solution, fresh reactant is brought to the working surface. A well-defined flow pattern as shown in Figure 2.14 (b), is obtained where the rotating electrode acts as a 'pump', dragging the solution perpendicular to the electrode surface which is subsequently thrown out in a radial direction on contact with the electrode surface.[185]

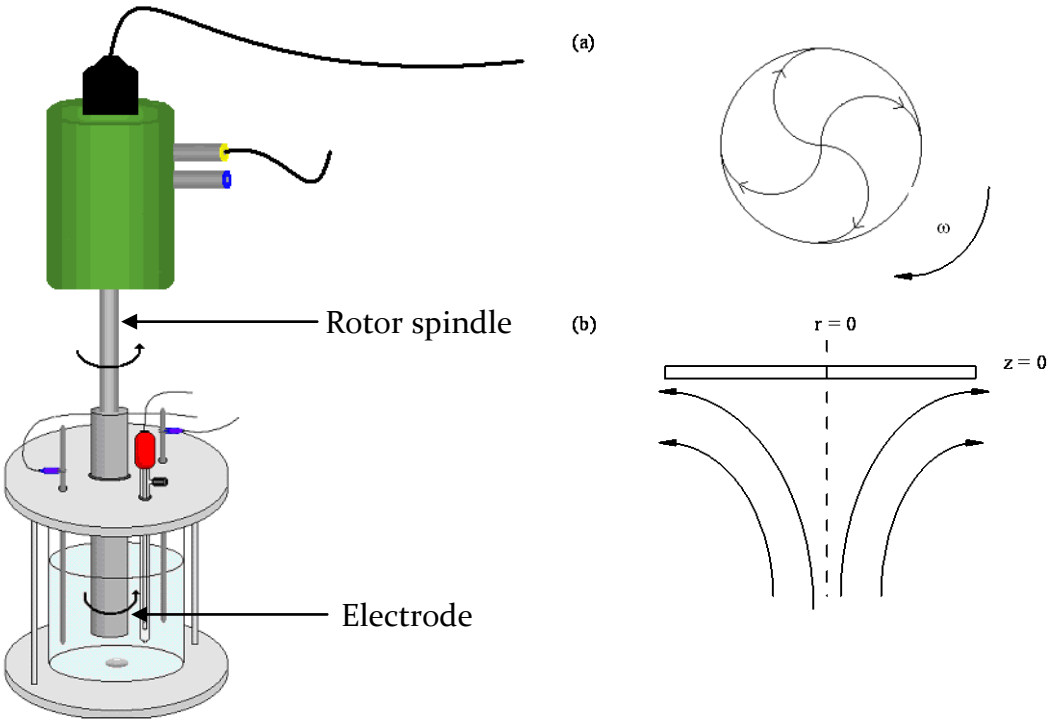

Figure 2.14: Schematic diagram of electrode in the RDV set-up. The patterns of flow to a rotating disc electrode (a) viewed from below the electrode face and (b) across its surface as viewed from the side.[184]

This technique is generally more sensitive than a traditional cell set up, where the diffusion layer is time dependent. The thickness of the diffusion layer using RDV can be controlled by changing the rotation speed of the electrode. This technique theoretically leads to higher currents, greater sensitivity and improved reproducibility due to the increased transport of electroactive

species to the electrode surface. The electrode is rotated at a known frequency, *f*, where the angular velocity, ω, is described by Equation 2.12:

$$\omega = \frac{2\pi f}{60} \qquad 2.12$$

The rotation of the electrode must be controlled to avoid turbulence in the sample solution, therefore ensuring laminar flow of the substrate to the electrode surface.[186] Two rotation speeds were compared in this work; 900 and 1900 rpm for their effect on enhancing the sensitivity of the Cr(VI) detection.

2.4 Physical Characterisation Techniques

Further characterisation of the materials and sensors were carried out using the following methods.

2.4.1 UV-vis Spectroscopy

Ultraviolet-visible (UV-vis) spectroscopy is an analytical technique that measures the amount of ultraviolet and visible light transmitted or absorbed by a sample. The absorption of light gives rise to electronic transitions, from the highest occupied molecular orbital (HOMO) to the lowest unoccupied molecular orbital (LUMO) which are quantitatively measured simply on a scale of 0 to 1, dependent on concentration. The radiation source has wavelengths from 200 to 800 nm. The absorption of UV light (by seemingly colourless species) occurs between 200 and 400 nm whereas the visible region of the spectra, i.e. the absorption by visibly coloured species, is from 400 to 800 nm (Figure 2.15). Absorptions occur at a frequency that is characteristic of the electronic structure of a particular species, therefore changes in the absorption wavelength can signify changes in the electronic structure of the species. Simply, the wavelength at which a chemical absorbs light is dependent on its structure and the intensity of the light absorption is related to its

concentration. A UV-vis spectrum can be used to identify specific chemical species and to monitor processes where either the structure or concentration of that species changes. In this work UV-vis spectroscopy was used to analyse the complexation of copper to DDC in Chapter 5.

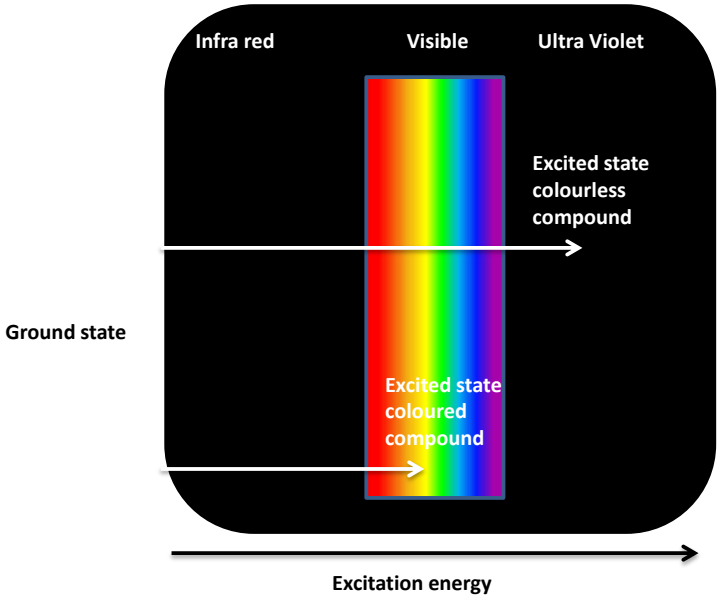

Figure 2.15: Illustration of UV-Vis theory depicting the excitation of electrons from the ground state and where the resultant compounds absorb light.

2.4.2 Physical characterisation of solutions

The physical properties of each solution were documented and used in the analysis of experimental data where appropriate. In all cases, the pH of the solution was tested using a pH meter. This was specifically important in Chapter 4, where the pH of the sample solution was varied and its effects were analysed in depth. The acidity of solutions was increased by addition of concentrated acid, e.g. H_2SO_4 or decreased by addition of a base, e.g. Na_2SO_4 as outlined in the respective sections.

When required, the conductivity of solutions was measured using a conductivity meter and used within comparative studies. Solutions were

prepared in the same manor as for the relevant experimental procedures and digital measurements were recorded for analysis.

2.4.3 Scanning Electron Microscopy and Energy Dispersive X-ray Analysis

Scanning Electron Microscopy (SEM) allows the observation and characterisation of samples on a micrometre (μm) to a nanometre (nm) scale. The technique uses electron beams to capture images of conducting solid surfaces. The electrons are applied to the surface using an electron gun under vacuum (at 20 kV), and electrons emitted from the sample (as well as backscattered electrons) construct an image at the detector. EDX is a technique that is often coupled with SEM, and is used to identify the elemental composition of the surface. In the same chamber as for SEM, when the surface is bombarded with electrons from the electron gun, X-rays are emitted from the sample, which are used to identify elements present on the surface according to the energy required to remove the outer electrons from their respective orbitals.

SEM images were obtained from an Avalon 8000, Princeton Gamma Technology and a Hitachi S3400. A shorter version of the pencil-style electrode of 5 mm in diameter was used as a support for each substrate. This electrode was specifically designed for use in the SEM chamber, in order to fit on the stage where the samples were placed.

2.4.4 Transmission Electron Microscopy

Transmission electron microscopy (TEM) is a surface analysis technique similar to SEM, however the electrons in this case are accelerated at a much higher speed (300 kV in this case) and are focused on a much smaller area. The benefit to this technique is that the resolution is far superior to SEM due to the speed of the electrons, allowing for imaging predominantly on the nano scale.

The TEM images in this work were carried out by Clive Downing at CRANN in TCD, using an FEI Titan TEM.

2.4.5 Fourier Transform Infra-red Spectroscopy (FT-IR)

Fourier transform infra-red spectroscopy (FT-IR) is a physical characterisation technique used to identify the bonding within a sample. It is based on the vibration of molecules when infrared radiation is passed through a sample. "Fourier transform" refers to the mathematical modification made to the raw data for a spectrum to be obtained.[187] The bonds in the sample are identified by the wavelength at which they absorb light, indicated by their vibrational modes. The position of the infra-red band is specified by its wavelength measured in microns or its reciprocal value called wavenumber (cm^{-1}). The frequency of the vibrations between two atoms is governed by Hooke's law as the frequency of the vibration depends on both the masses of the atoms and the rigidity of the bond. Heavier atoms vibrate slower than light ones and stronger bonds are generally stiffer. In order for a vibrational mode to be IR active the vibration must alter the dipole moment in the molecule.[188] The vibrational bands of many functional groups occur at characteristic wavenumbers which helps aid interpretation of a spectrum and the entire IR spectrum may be used as an unique fingerprint of a compound. In this research infrared spectra (cm-1) were recorded as KBR disc using a Perkin Elmer 2000 FT-IR spectrometer.

Chapter 3:

The Electrochemical Characterisation of Multiwalled Carbon Nanotubes and Graphene

3.1 Introduction

The use of nanomaterials in electrochemical devices has excelled in recent years due to the improved sensitivity achieved with large surface to volume ratios. Both graphene[81, 189] and multiwalled carbon nanotubes (MWCNTs)[34] in particular have been at the forefront of research in nanomaterials over the past decade and many advances have been made in recent years which are discussed in Chapter 1, in their applications due to their unique, impressive properties. Briefly, graphene is a two dimensional sheet of sp^2 hybridized carbon,[81] and MWCNTs are helical structures of graphene sheets, consisting of multiple concentric nanotubes. Carbon nanotubes have attracted much interest in electrochemical sensing due to their immense aspect ratio which provides an impressive surface area (approximately 2200 $m^2\ g^{-1}$)[190] and reports of their catalytic ability to promote electron transfer.[43, 191] Similar to MWCNTs, literature reports of graphene boast properties of fast electron mobility[82] and immense surface area (approximately 2630 $m^2\ g^{-1}$)[192], amongst other electronic properties.

Carbon nanotubes are known to agglomerate in solution, a process which is attributed to high van der Waals interactions between individual tubes.[54] This hinders their use in electronic applications and has thus required the development of various methodologies to achieve dispersed solutions.[53, 63] Similarly, graphene is also known to undergo agglomeration in solution, due to Van der Waals and π-stacking interactions between the individual sheets.[86] To overcome this agglomeration or stacking, both materials are often chemically modified which generally involves introducing oxygen-containing species to the surface. This modification involves the use of strong acids which can shorten the nanotubes and can be time consuming. As the oxygenated species are often accredited with a large influence on the electrochemistry of the materials,[86, 193] it is often unclear if the reported electrocatalytic properties are a property of the material itself or simply due to the modification. The use of sonication to disperse agglomerates of MWCNTs and of graphene has been

proven to be very successful, as discussed in Chapter 1, improving the electrical and mechanical properties of materials made from the suspensions.[57, 70, 194]

The electron transfer properties of materials such as MWCNTs and graphene are of particular interest in electrochemical sensing and are generally described in terms of their density of states (DOS), which refers to a large amount of energy states at the Fermi level. A higher DOS therefore increases the possibility that an electron will be of the appropriate energy state for electron transfer with an electroactive species.[195] The high DOS of carbon nanotubes and graphene are known to be enhanced by defect areas which can be described as either intrinsic or extrinsic. Intrinsic defects refer to structural anomalies, e.g. sp^3 hybridised carbons, and extrinsic defects refer to edge plane defects and their associated functionalities, e.g. oxygenated species. These defects can affect the electrochemical activity observed at a material differently depending on the nature of the electrochemical species. The mechanism by which a species is oxidised or reduced can be described as either outer sphere or inner sphere. In the case of inner sphere reactions, bond breakage or formation occurs which allows for the oxidation or reduction of the species. Such reactions are therefore largely affected by extrinsic defects of the electrode material. In the case of outer sphere reactions, the species remain in close proximity to the material and charge is transferred without the breaking of bonds. Outer sphere reactions are therefore largely affected by intrinsic defects of a material.

The amount of material used to modify the electrode surface varies significantly throughout literature reports, with very little reasoning given to the amounts used.[196] Kang *et al.*[87] for example have shown the increase in I_p for the detection of paracetamol with increasing cast volume of graphene from 5.0 to 8.0 µL, from a 1 mg mL^{-1} suspension in EtOH, with a decrease observed when volumes exceeded 10 µL. Borowiec *et al.*[44] have seen an increase in I_p with increasing the casting of MWCNTs in the range of 1.5 to 2.5 µL with respect to the detection of ketoconazole. They noted a decrease in the I_p with a

casting volume of 8.5 µL which they ascribe to the instability of the cast film, which in this case was also cast from a 1 mg mL^{-1} suspension, however, using DMF as a dispersant. The ratio of materials used and the nature of the dispersant used in the suspensions is also known to vary significantly throughout reports, making them difficult to compare. The aim of this chapter is therefore to investigate the basic electrochemical properties of an electrode modified with MWCNTs and graphene to further support observations thus far of fast electron transfer and increased surface area. In this chapter, the effect of sonication is investigated on samples of MWCNTs and graphene with respect to the electrochemical properties of the resulting modified electrodes. The volume cast is also varied for both sonicated and non-sonicated samples, and its effect is analysed with respect to the electrochemical properties of the resulting modified electrodes.

The electrochemistry of the materials is evaluated using a potassium ferricyanide ($K_3Fe(CN)_6$) probe. It is known that the kinetics of this probe can be significantly influenced by the surface properties of the electrode such as functional groups or defects although its redox activity is generally considered an outer sphere reaction.[197] The redox properties of this probe therefore provide an indication of the level of defects in a material, both extrinsic and intrinsic. For porous materials, such as MWCNTs, it is known that the electrochemical response recorded can be influenced by three predominant factors; diffusion from the bulk solution, thin layer diffusion and adsorption.[177] The contribution from each factor greatly depends on the electrode material and its treatment, as well as the probe used and will be considered throughout this work.

An important property of MWCNTs is their mesoporous structure, which describes pores of 2 to 50 nm in diameter which are inherent to MWCNTs (intraparticle mesopores) and also that arise between networked tubes (interparticle mesopores). This structure prevails in cast films of dispersed MWCNTs as larger agglomerates are diminished and networking between

smaller agglomerates is enhanced. This mesoporosity has recently been highlighted for its impact on the diffusion of analytes to the active sites of electrodes modified with carbon nanotubes. Streeter *et al.*[178] in particular have noted the importance of considering thin layer diffusion in such systems to avoid the misinterpretation of electrocatalytic responses of electron transfer. As the MWCNTs in this work were not functionalised or treated harshly enough to cause significant defects to the structure of the nanotubes, it can be assumed that the major contributors to the electrochemical properties evaluated with $K_3Fe(CN)_6$ are characteristic of the inherent properties of the MWCNTs purchased commercially. The planar structure of graphene is not known to form mesopores, but moreover to re-stack, decreasing its relative surface area and electronic properties.[198] The graphene in this work also is not functionalised; therefore its properties are examined relative to its mild treatment herein.

The electrochemical responses of the MWCNTs and graphene modified electrodes are measured in this chapter using cyclic voltammetry which is discussed fully in Chapter 2. Specifically in this work, the magnitude of the peak currents, I_p, and the observed symmetry of the peaks provide information on the electroactive surface area and kinetic properties of the modified electrodes. The peak positions, E_p, are used to characterise the thermodynamics of the reaction, and the distance between the oxidation and reduction peak potentials, ΔE_p, is utilised to calculate the rate constants at the modified surfaces. The Randles-Sevcik Equation, the Kochi and Klingler Equation and the Nicholson Theory are all implemented in this electrochemical characterisation of the modified electrodes. The materials are thus directly compared in their pristine state for use in the simple modification of electrodes. Some results from this chapter have been published in ECS Transactions.[199]

3.2 Results and Discussion

3.2.1 Electrodes Modified with Multiwalled Carbon Nanotubes

3.2.1.1 Physical Characterisation of Electrodes Modified with MWCNTs

The MWCNTs used in this work were purchased from Sigma-Aldrich (>99% purity) and as they were not modified prior to their use, they did not require extensive physical characterisation. The MWCNTs samples were therefore characterised using Fourier transform infrared spectroscopy (FTIR) and electron dispersive X-ray (EDX) analysis, as described in Chapter 2 to assess the effects of sonication in DMF on the properties of the MWCNTs. The use of FTIR spectroscopy allowed for the identification of any oxygen-containing groups on the MWCNTs and the EDX analysis was utilised to identify any impurities in the MWCNTs sample.

In the preparation of the modified electrodes, a GC pencil-style WE was prepared as illustrated in Chapter 2, and pristine working surfaces were prepared before each experiment by polishing with diamond paste. The MWCNT samples were prepared by adding 10 mg MWCNTs to 1 mL DMF. The non-sonicated samples were inverted several times to mix the suspension and the sonicated samples were subjected to 30 min sonication to disperse the nanotubes. The glassy carbon electrode (GCE) was modified by drop casting a specific volume of the MWCNT sample on the polished surface and the electrode was dried at room temperature or with the aid of an IR lamp. Scanning electron microscope (SEM) imaging was carried out on the electrode surfaces to highlight the effect of sonication on the morphology of the resultant castings.

3.2.1.1.1 FTIR Spectroscopy of MWCNTs

The FTIR spectra of MWCNTs sonicated for 30 min in DMF and non-sonicated (pristine) MWCNTs are compared in Figure 3.1. Both samples were prepared as KBr disks and exhibit large O-H stretches with bands at 3433 cm^{-1} and 1632 cm^{-1} due to the absorbance of water, and a less intense peak at 1385 cm^{-1} that can be identified as a standard impurity in the KBr used in preparing the samples.[200] The presence of DMF in both sonicated and unsonicated samples was apparent by the absorbance bands representing C-H_2 between 2849 and 2959 cm^{-1},[201, 202] and by the band representing an N-H vibration at 805 cm^{-1}.[203] Surprisingly however, the absorbance of the C=O component of DMF at 1680 cm^{-1} was absent. The DMF is known to adsorb on the nanotube surface via hydrophobic or π-π interactions,[69] which could have caused this bond to weaken, leading it to be shifted and masked by the water absorbance in the same region. The bands between 2849 and 2959 cm^{-1} and at 805 cm^{-1} however provide an indication that some DMF had adsorbed onto the MWCNTs in both the sonicated and non-sonicated samples.

The increase in oxygenated species on MWCNTs with sonication was identified by a small C=O band at 1723 cm^{-1}, which was not visible in the non-sonicated sample.[69] This analysis further supports the reports that oxygenated species can be introduced at defect sites or edge planes of MWCNTs from the air.[204] However, as the band was of low intensity, it shows that sonication in DMF does not drastically increase the content of oxygenated moieties in the MWCNTs sample in comparison to modification of MWCNTs surfaces, for example, with -COOH groups using acid treatment.[69] The MWCNTs used herein can therefore be described as pristine MWCNTs.

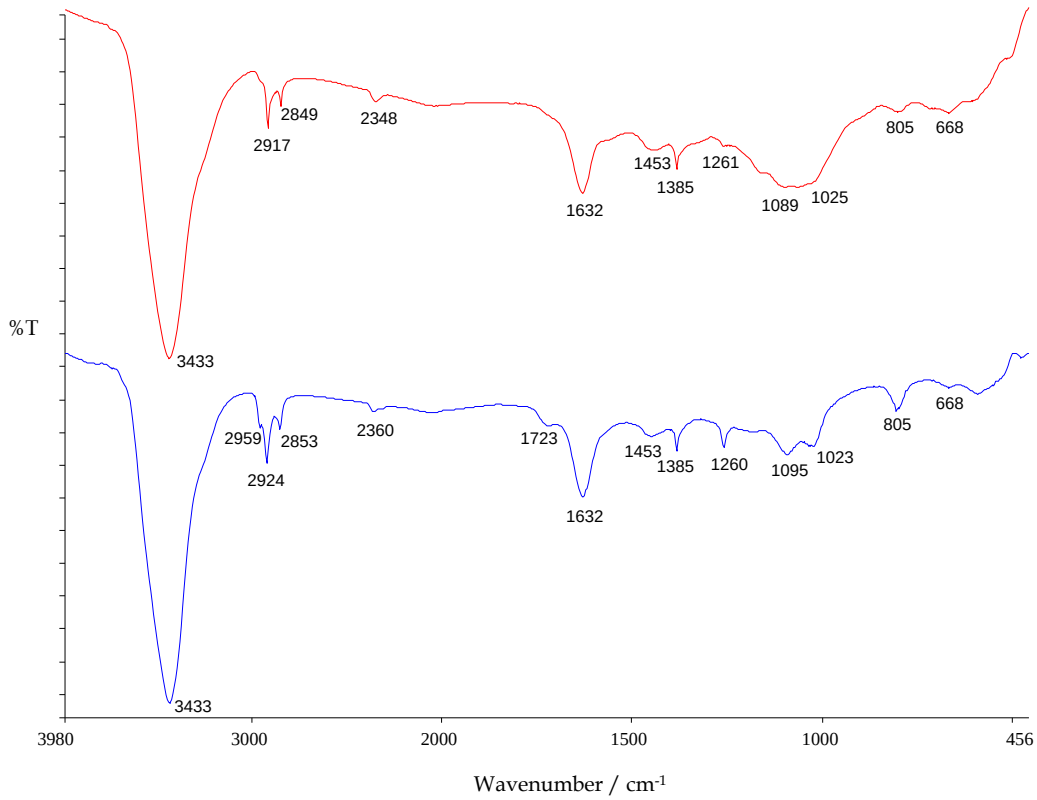

Figure 3.1: FT-IR spectra of — non-sonicated MWCNTs and — MWCNTs sonicated for 30 min in DMF.

3.2.1.1.2 SEM and EDX Analysis of MWCNTs

Scanning electron imaging of the modified surfaces was used to highlight the effect of sonication on the morphology of the resultant castings. The images in Figure 3.2 (a) and (b) compare the morphologies of GCEs modified with 20 µL non-sonicated and sonicated MWCNTs at a low magnification showing the overall increased coverage obtained by sonication of the MWCNTs. The non-sonicated sample exhibited large agglomerations of MWCNTs on the GCE surface whereas the sonicated sample showed more evidence of networking between the smaller agglomerations of MWCNTs. Images of increased magnification seen in Figure 3.2 (c) and (d) show the compact structure of the non-sonicated sample in comparison to the loosely entangled sonicated MWCNTs. The highly magnified images in Figure 3.2 (e) and (f) highlight the

structure of the sonicated MWCNTs with individual MWCNTs visible in both samples indicating that reasonable dispersion was achieved with gentle shaking of the sample in DMF. The images suggest an increased surface area of the sonicated MWCNTs due to the separation of the large agglomerations, in comparison to the slightly more dense packed structure of the non-sonicated MWCNTs. Similar surface morphologies have been observed by Lawrence *et al.*[68] for 20 μL casting of 2 mg mL^{-1} suspensions in DMF.

EDX analysis was carried out on the modified electrode surface (Figure 3.3 (a) and (b)) as described in Chapter 2. The recorded spectra showed evidence of cobalt and chlorine impurities which can arise from the metal catalysts used in the production of MWCNTs. Giri *et al.*[205] have recently used Co(II) in doping polymer/MWCNTs composites for application in super capacitors. The Co-doped composites showed improved capacitance and electrical conductivity in comparison to the un-doped composites, which is attributed to the charge accumulation property of the transition metal ion. There is no evidence however that the presence of Co(II) would enhance the electron transport properties of MWCNTs, and as the amount of Co(II) in the MWCNTs present in this study were lower, at 0.2 wt.% in comparison to the 4.0 wt.% used by Giri *et al.*, it is highly unlikely that it significantly contributed to any observations in this work. The Au peaks observed in the spectra are due to the pre-treatment of the electrodes with Au sputter-coating to prevent charging of the surface. No differences were seen in comparing the non-sonicated sample to the sonicated sample.

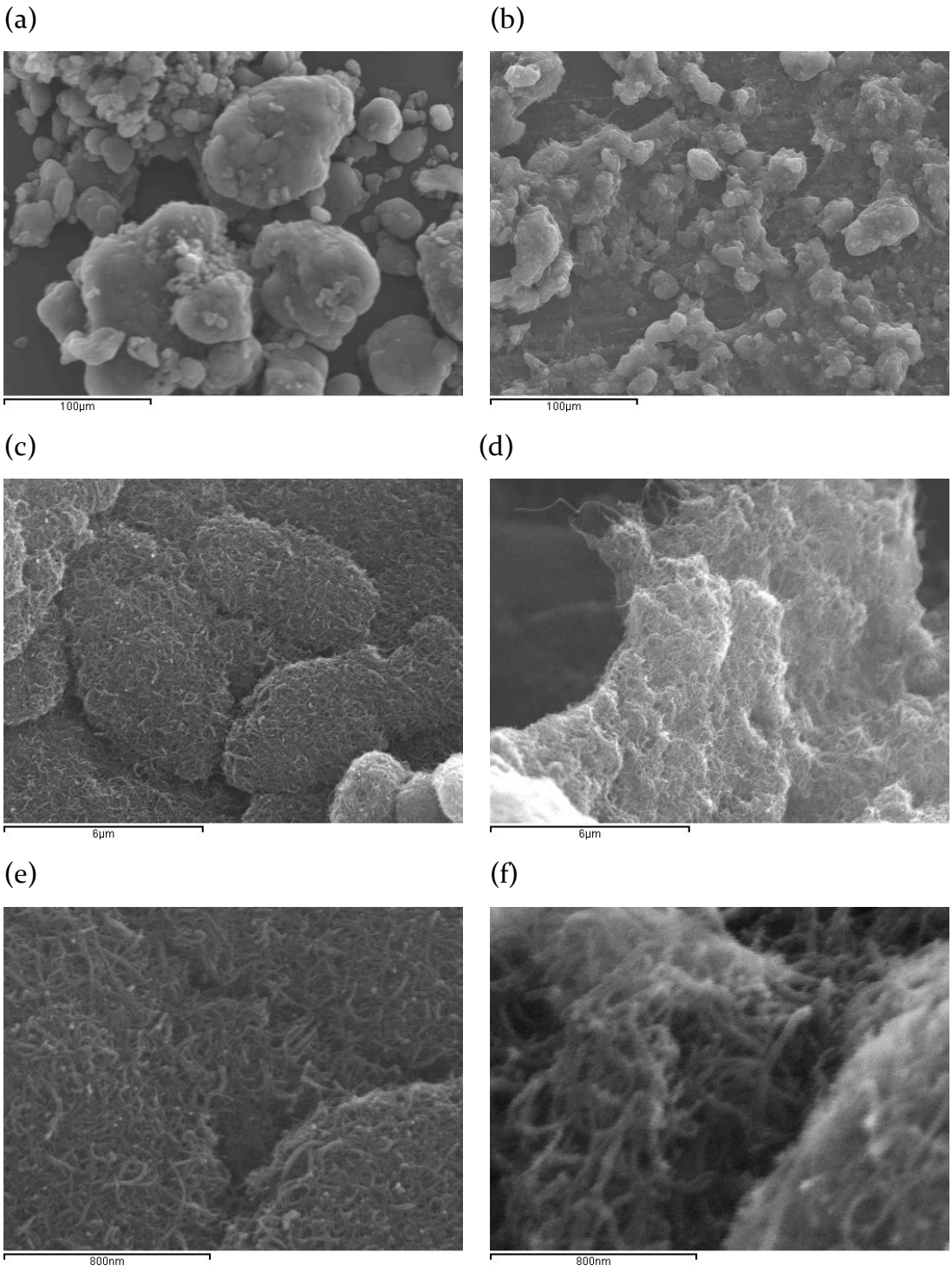

Figure 3.2: SEM micrographs of GCE modified with 20 µL 10 mg mL^{-1} MWCNTs in DMF. (a), (c) and (e) show varying magnifications of non-sonicated MWCNTs and (b), (d) and (f) show the corresponding sonicated samples.

(a)

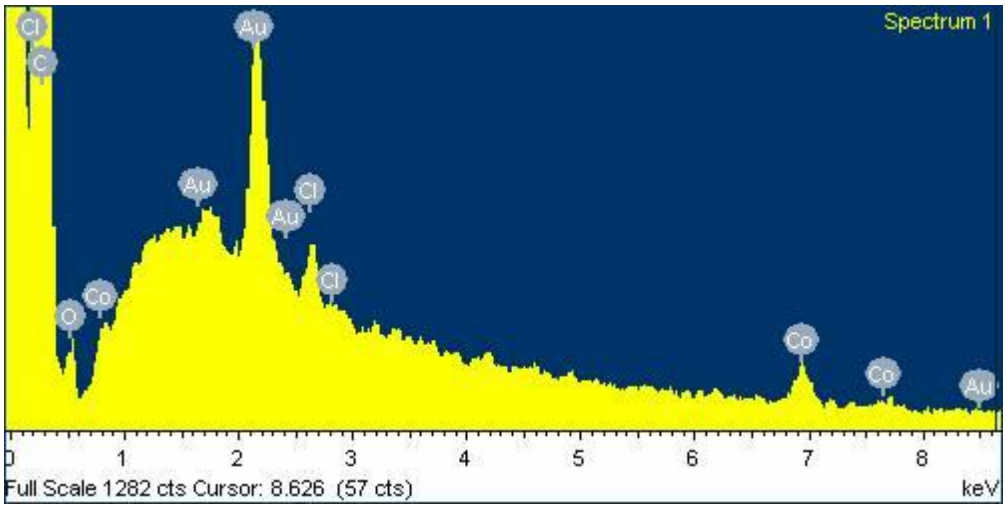

(b)

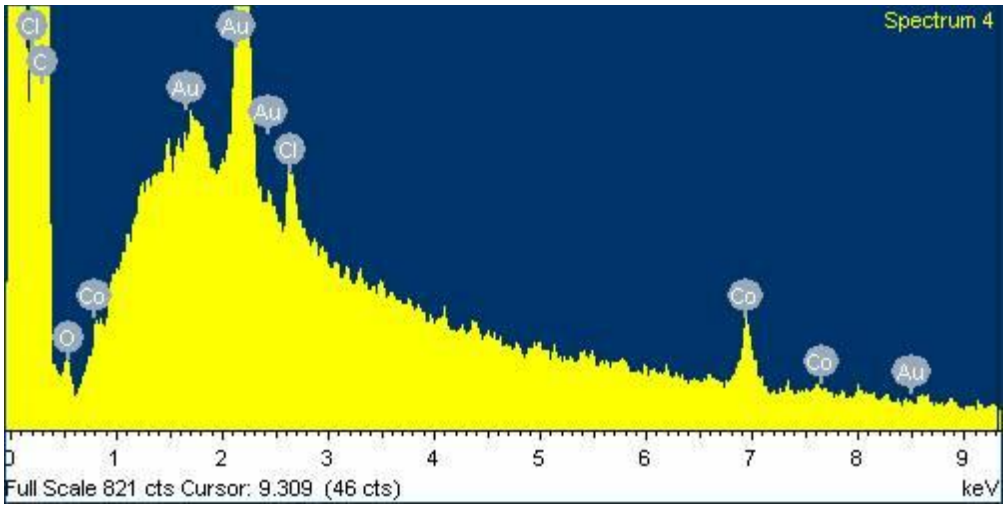

Figure 3.3: EDX analysis of GCE modified with (a) sonicated and (b) non-sonicated MWCNTs showing Co impurities.

3.2.1.2 *Electrochemical Characterisation of Electrodes Modified with MWCNTs using a $K_3Fe(CN)_6$ probe*

The electrode surfaces were characterised using cyclic voltammetry which is described in detail in Chapter 2. Briefly, this involves sweeping the applied electrical potential between two points and recording the resulting current. Although experimental parameters varied slightly throughout this work, generally the WE was cycled between -0.15 and 0.60 V vs. SCE for MWCNTs and vs. Ag^+/AgCl for graphene (due to the different laboratories where the experiments were carried out). For comparison purposes the potentials were corrected to SCE. The main substrate utilised in this study was glassy carbon, as it is used widely in graphene-based sensors,[87] showing superior performance in its modification with MWCNTs compared to metallic electrodes, most likely due to the similarity between their structures. A standard three electrode cell was used for the experiments based on GCE however a modified set up was commissioned to accommodate the use of basal plane HOPG as a working electrode (illustrated in Chapter 2).

To gain information about the electron transfer abilities of electrodes, redox reactions at the electrolyte interface are often analysed. The electrochemical probe used in this set of experiments was the redox couple $[Fe(CN)_6]^{3-}/[Fe(CN)_6]^{4-}$. Although the redox behaviour of this probe is used widely to describe the electrochemical properties of various electrodes, it is duly noted that it does not behave ideally, showing degradation with both time and light in particular.[197] To minimise the unreliability of this probe, fresh solutions were prepared regularly and kept under dark conditions. It was prepared as an aqueous solution containing 0.05 M KH_2PO_4 and 0.05 M KCl as a supporting electrolyte, to ensure that diffusion of the analyte was the only limitation to mass transport. This solution was also used to provide background currents for each voltammogram, ensuring that any peaks or waves observed were a result of the $[Fe(CN)_6]^{3-}/[Fe(CN)_6]^{4-}$ couple. The values

obtained in measurement of the faradaic current were estimated by removal of these background currents.

The effects of sonication on the electrochemical properties of MWCNTs samples cast on GCE is investigated in this section. This involved comparing the electrochemical response of the modified and bare electrodes to the redox behaviour of $K_3Fe(CN)_6$ using cyclic voltammetry. The peak potentials (E_p) and peak currents (I_p) of the redox probe were measured directly from the voltammograms and capacitance of the modified electrodes was calculated from a measurement of the background currents at various scan rates. The effect of increasing the cast volume for both non-sonicated and sonicated solutions is also investigated. Cyclic voltammetry in 1.00×10^{-3} M $K_3Fe(CN)_6$ was performed on the electrodes prior to modification, i.e. the bare electrode, to provide a comparison for the modified surfaces. The substrates were then replenished and cast with 5, 10, 15 or 20 µL of the 10 mg mL^{-1} MWCNTs/DMF samples. In both cases the volume cast was used to give a rough estimation of the mass of MWCNTs on the GC surface. The reproducibility of the results using various casting volumes indicate that in both cases, the MWCNTs were reasonably well dispersed throughout the solvent and it was estimated that 5 µL of the MWCNTs sample would result in approximately 0.05 mg MWCNTs on the GC surface.

3.2.1.2.1 The Effect of Sonication on the $[Fe(CN)_6]^{3-}/[Fe(CN)_6]^{4-}$ Peak Current

Cyclic voltammograms illustrating the redox behaviour of $[Fe(CN)_6]^{3-}$ /$[Fe(CN)_6]^{4-}$ at the modified electrodes can be seen in Figure 3.4, which compares GCEs modified with both non-sonicated and sonicated MWCNTs to the bare GCE. An increase in faradaic currents with both modifications of glassy carbon is apparent from these voltammograms, suggesting an increased surface area with enhanced electrochemical activity. As discussed in Chapter 2, the faradaic current refers only to the current arising from the transport of

electrons, whereas the capacitive currents can be referred to as those resulting from a build of a charge at the electrode/electrolyte interface.[174] The magnitude of this faradaic current is generally an indication of the amount of the species being oxidised or reduced, and therefore in this case can be indicative of an increased electroactive surface area in comparison to the bare electrode.

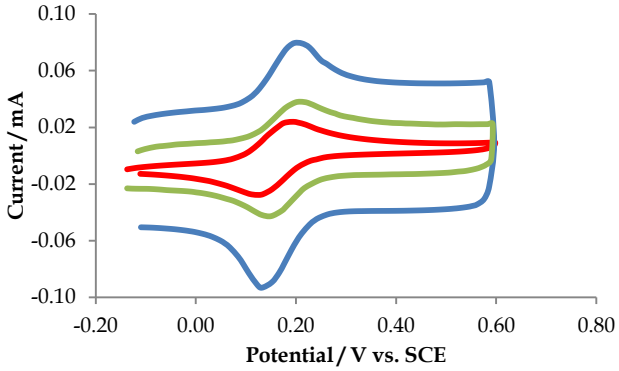

Electrode	I_{pa} (µA)	ΔE_p (V)	I_{pc} / I_{pa}
GCE (n=4)	22.8	0.102	1.04
GCE/MWCNTs sonicated (n=7)	65.0	0.075	1.27
GCE/MWCNTs non-sonicated (n=7)	28.6	0.060	1.15

Figure 3.4: Cyclic voltammograms comparing a 4 mm diameter GCE — bare, — modified with 5 µL non-sonicated MWCNTs (10 mg mL^{-1}) and — modified with 5 µL sonicated MWCNTs (10 mg mL^{-1}). All electrodes were cycled in 1.00×10^{-3} M $[Fe(CN)_6]^{3-}/[Fe(CN)_6]^{4-}$, with 0.05 M KCl and 0.05 M KH_2PO_4 as a supporting electrolyte system, at a scan rate of 100 mV s^{-1}. The average values of the anodic peak current, I_{pa}, and ΔE_p from the voltammograms are tabulated with the calculated reversibility ratio of I_{pc}/I_{pa}.

The average recorded anodic faradaic current (n=7) for the oxidation of $Fe(CN)_6^{4-}$ at a GCE modified with non-sonicated MWCNTs was 2.86×10^{-5} A, which was significantly larger than 2.28×10^{-5} A (n=4) at the bare electrode ($t = 32.59$, d.f. = 9, $P < 0.0001$). Modification of the GC electrode with dispersed MWCNTs showed a further enhancement of the faradaic currents. In this case the average peak current (n=7) measured was 6.50×10^{-5} A, which was also significantly larger than the bare GC electrode ($t = 29.76$, d.f. = 8, $P < 0.0001$). In the case of the non-sonicated MWCNTs, this increase is likely due to their superior surface area, as the nanotubes are known to have an extremely high

aspect ratio[34] that would provide a significant increase in the surface area of the electrode, regardless of their level of dispersion. The further increase observed in the average faradaic current at the electrode modified with sonicated MWCNTs is indicative of the dispersive effects of sonication on the MWCNTs. As the surface areas of the electrodes were expected to change relative to modifications, the currents were not normalised to the geometric surface area of the GCE in this work. It can therefore be presumed that the increase in currents seen at the modified GCE electrodes can be associated with an increase in surface area, achieved by sonicating the nanotube solution which would further expose the large aspect ratio of MWCNTs. The reversibility of the redox process was analysed by calculating the ratio of the peak currents and was found to be approximately 1 and behaved independently of scan rate (10 to 200 mV s^{-1}) indicating an electrochemically reversible process.[174]

In analysing the voltammograms of GCEs modified with various casting volumes (5, 10, 15 and 20 µL) of both samples, it is clear that there were slight increases observed in the faradaic currents of $[Fe(CN)_6]^{3-}/[Fe(CN)_6]^{4-}$ with additions of 5 to 15 µL of non-sonicated MWCNTs. This is shown in Figure 3.5 (a) and (b) for unsonicated and sonicated samples, respectively. In particular, the anodic peak currents increased steadily from 2.38×10^{-5} A at the bare electrode to 3.13×10^{-5} A at the GCE modified with 15 µL non-sonicated MWCNTs but did not further increase at the 20 µL casting. A one way ANOVA analysis of the data indicated, however, that the differences between the various casting volumes were statistically insignificant ($P>0.05$). The slight enhancement of the peak current can possibly be attributed to a small increase in the electroactive surface area of the modified electrode.

(a)

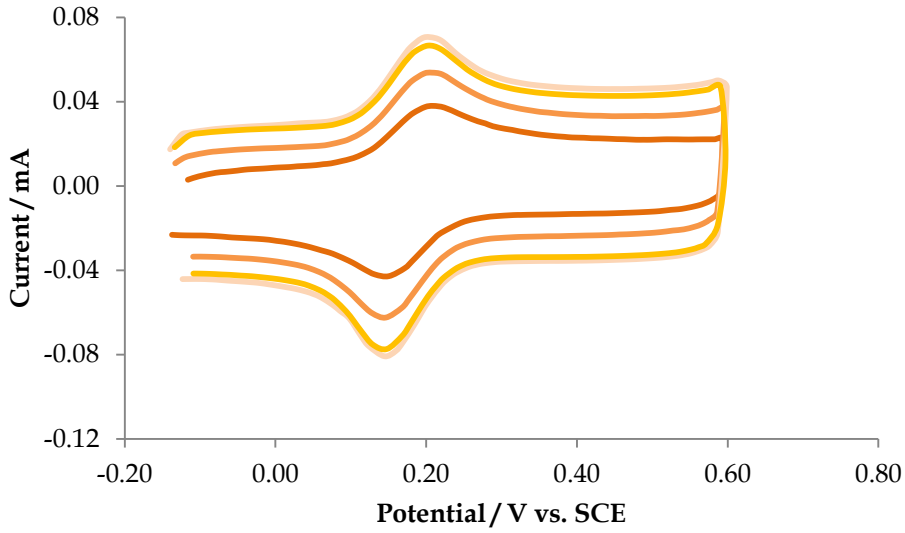

(b)

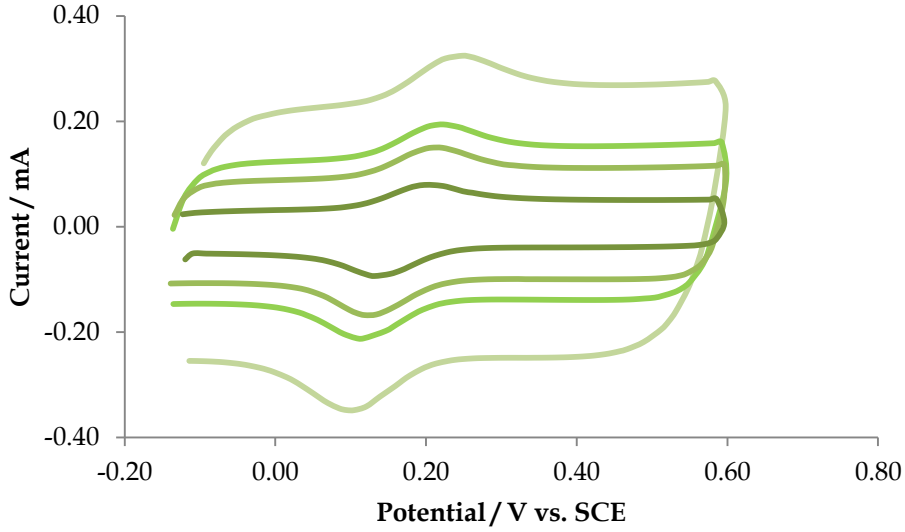

Figure 3.5: Cyclic voltammograms comparing successively increasing casting volumes of (a) — 5, — 10, — 15 and — 20 µL aliquots of non-sonicated and (b) — 5, — 10, — 15 and — 20 µL aliquots of sonicated MWCNTs. In all cases, modified electrodes were cycled in 1.00×10^{-3} M $[Fe(CN)_6]^{3-}/[Fe(CN)_6]^{4-}$ with 0.05 M KCl and 0.05 M KH_2PO_4 as a supporting electrolyte system, at a scan rate of 100 mV s^{-1}.

The voltammograms comparing increases in volumes cast of sonicated MWCNTs, seen in Figure 3.5 (b) shows that the peak currents increased from 2.38×10^{-5} A at the bare electrode to 5.22×10^{-5} and 7.46×10^{-5} A at the GCE modified with 5 and 10 µL sonicated MWCNTs, respectively. The surface area was likely to be increased with increasing cast volumes, which accounted for the increased peak currents, also observed by Borowiec *et al.*[44] Similar results were observed by Li *et al.*[206] in studying this redox couple at MWCNT tower electrodes. They found that the redox currents of $[Fe(CN)_6]^{3-}/[Fe(CN)_6]^{4-}$ were proportional to the film thickness, which was explained by the porous nature of nanotubes allowing the electrolyte access to the interior surface. Further increasing the casting volume of sonicated MWCNTs, to 15 and 20 µL, decreased the peak currents slightly to 6.02×10^{-5} and 6.29×10^{-5} A, respectively, which could possibly be caused by the large background capacitive currents masking the faradaic current. Statistical analysis of the modified electrodes however showed no significance in the observed differences. This indicated that the maximum increase in surface area was achieved with 5 to 10 µL casting of the sonicated MWCNTs solution.

3.2.1.2.2 Evaluation of the Capacitance of the Modified Electrodes

Capacitive currents are generated due to the charge stored at the electrode/electrolyte interface, and are therefore affected by the entire physical surface area of the material. The mesoporous structure of MWCNTs enables easy access of the solvated ions to this interface during charging of the electrical double layer[40] (further discussed in Chapter 2). It can be seen in Figure 3.5 (a) and (b) that sonication had a large affect on the capacitance of the modified electrodes.[40, 207] The capacitance was therefore calculated and compared for the sonicated and non-sonicated materials by measuring the current in the non-faradaic region (0.50 V) as a function of the scan rate. As mentioned previously, the currents are not normalised to the geometric surface area in this work. In this case, the gravimetric capacitance is reported,

similarly to the work reported by Barisci *et al.*,[208] where the currents were related to the approximate mass of MWCNTs on the modified electrode.

As the capacitance of bulk metals is dominated by the solution,[209] it is reasonable to measure the capacitance at the bare electrode, as a comparison for measurements at the modified substrates. Capacitance values of approximately 3.0×10^{-5} F were calculated for the bare GC electrode, confirming the minor contribution of the substrate to the capacitance measured at the modified electrode. The plot seen in Figure 3.6 shows the increase in the background current with increasing scan rate for the modified electrodes, where the slope is a measure of the capacitance.

The small increase in capacitance observed upon modification with non-sonicated MWCNTs, compared to the bare GC, to 2.3×10^{-4} F or 5.0 F g^{-1} is likely due to a slight increase in the surface area of the GCE. The average capacitance of the GC electrode modified with 5 µL sonicated MWCNTs (n=7) was calculated to be 5.8×10^{-4} F which results in a gravimetric capacitance of 11.6 F g^{-1}. This larger increase in capacitance observed upon modification with the sonicated MWCNTs sample can be owed to the dispersion of the MWCNTs which would have further increased the surface area of the modified electrode. It should also be noted that the DMF was not entirely removed from the MWCNT films and could have contributed to the observed capacitance. The different amounts of DMF in the sonicated and non-sonicated samples could therefore have contributed to the increase in capacitance observed upon sonication.[210]

The capacitance values calculated here are quite similar to those calculated in a similar fashion by Barisci *et al.*[208] of 14 to 16 F g^{-1} for sheets of SWCNTs, that they referred to as nanotube paper. In both cases it is apparent that the mass distribution of MWCNTs through the solution was reasonably homogenous, evident by the small error in the repeated experiments (n = 7), indicated by the small error bars, which highlighted that the amount cast was very

reproducible. However, as indicated by SEM analysis, the non-sonicated sample was more compact and therefore would likely have a smaller physical surface area than the more dispersed sonicated sample.

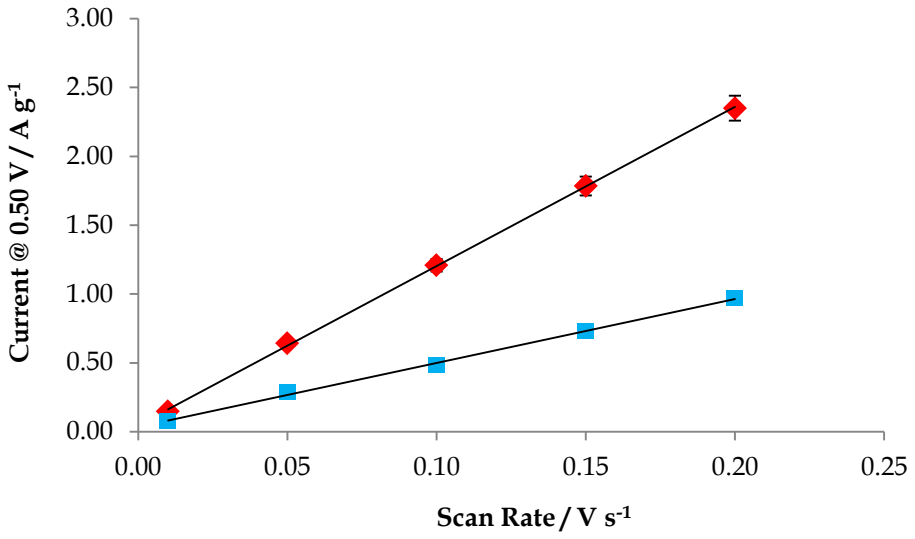

Figure 3.6: Plot of increasing background current (normalised to the approximate mass of MWCNTs in a 5 µL aliquot) with scan rate for GC electrode modified with MWCNTs ■ sonicated (R^2=0.999) and ■ non-sonicated (R^2=0.998), used to calculate the specific capacitance.

The capacitive currents were also compared for both samples by recording the current as a function of cast volume, which can be seen in Figure 3.7. Here it can be seen that increasing the volume cast of the non-sonicated sample did not drastically alter the background currents (measured at 0.50 V vs. SCE). A linear increase (R^2=0.997) was observed in the currents on increasing the cast volume of the sonicated sample. This suggests that the physical surface area did not increase with increasing cast volume due to the compactness of the non-sonicated sample, and highlights the dispersive effect of sonication on the MWCNTs film. This dispersion is expected to have increased the amount of DMF in the sonicated MWCNTs sample, which may also have contributed to the increased capacitance observed for the sonicated MWCNTs.

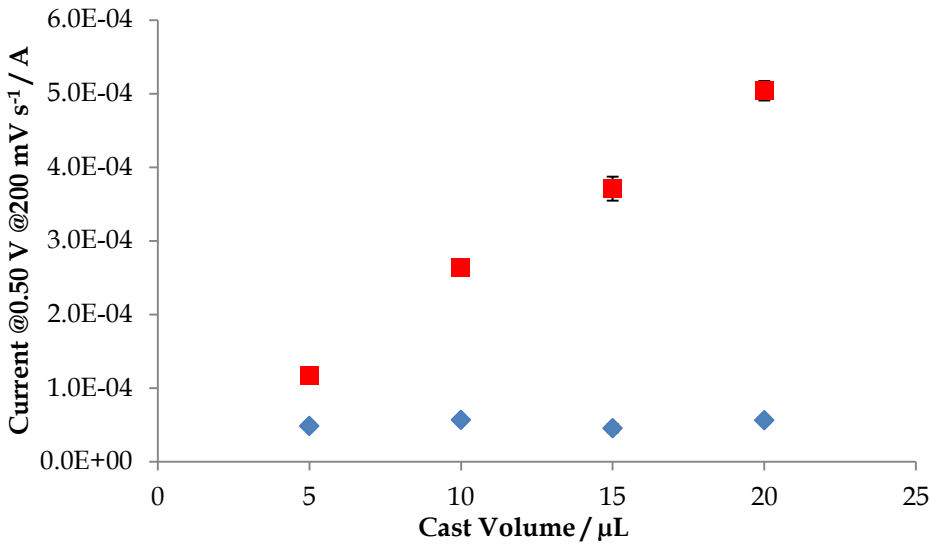

Figure 3.7: Plot comparing the capacitive currents recorded for ■ non-sonicated and ■ sonicated samples of MWCNTs at various casting volumes.

To further investigate the observed effect of the increase in capacitance with increased amount of sonicated MWCNTs, the currents normalised to their respective estimated mass of MWCNTs. The currents were then plot as a function of scan rate and it can be seen in Figure 3.8 that when normalised to the amount of MWCNTs on the surface, the capacitance was approximately the same at each electrode, and the relationship was linear. This is a good indication that the mesoporous structure of MWCNTs was exposed with sonication providing a more capacitive film with increasing cast volume.

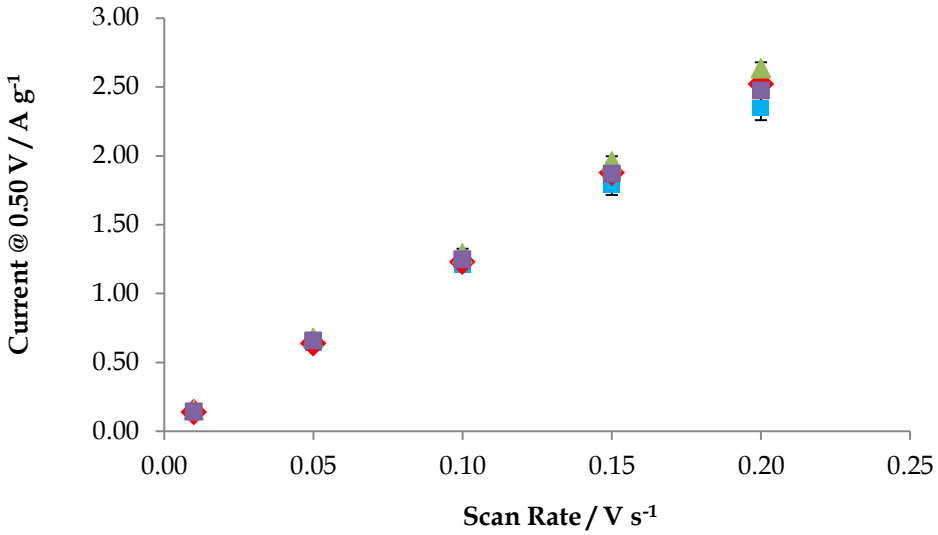

Figure 3.8: Plot representing the relationship between the background current and scan rate for various amounts of MWCNTs, ■ 5 ■ 10 ■ 15 and ■ 20 µL, from 10 mg mL^{-1} suspensions in DMF, used to calculate the capacitance of the MWCNTs used in this work (R^2=0.999).

3.2.1.2.3 The Effect of Sonication of MWCNTs on The Peak Separation for The Redox Reaction of $K_3Fe(CN)_6$

The peak potentials were measured for each reaction at the modified electrodes, E_p, and used to calculate the half wave potential, $E_{1/2}$, which is a thermodynamic measure of the reaction. The half wave potential was calculated to be 0.17 V and was independent of sonication and cast volume. Similar values were reported by Keeley and Lyons[177] for similarly prepared electrodes. The efficiency of electron transfer at each modified electrode was also measured and compared to that at the bare electrode by measuring the separation between the oxidation and reduction peak potentials, ΔE_p, of the $[Fe(CN)_6]^{3-}/[Fe(CN)_6]^{4-}$ couple at various scan rates. It was calculated that modification of the GCE with non-sonicated MWCNTs resulted in a significant decrease in the average ΔE_p to 0.064 V (n = 7) in comparison to the bare GC which gave an average peak separation of 0.102 V (n=3) for voltammograms recorded at 100 mV s^{-1} (t = 6.124, d.f. = 9, P < 0.001).

The modification of the GCE with MWCNTs sonicated for 30 min was evaluated and found to significantly decrease the ΔE_p to 0.075 V (n = 7), in comparison to that seen at the bare electrode (t = 29.76, d.f. = 8, P < 0.0001). The observations of enhanced electron transfer at GCE modified with MWCNTs agrees with studies by Bai *et al.*,[38] who proposed that the length of MWCNTs, had a significant influence on the conductivity of the resulting modified material. This conductivity was owed greatly to the linkage of small aggregates via intertube connections. As the MWCNTs in this study were sonicated for a short time or shaken gently without the use of surfactants, the enhanced electron transfer can be owed to the sufficient dispersion of larger aggregates into networks of MWCNTs and maintenance of the nanotube length in both samples.

In studying the separation between the oxidation and reduction peak positions for the GCE modified with various amounts of MWCNTs, (Figure 3.9) it was found that the electron transfer at the modified GCE was impeded as the casting volume of sonicated MWCNTs increased. The average ΔE_p recorded at 100 mV s^{-1} for the GCE modified with 5 µL sonicated MWCNTs was 0.075 V which was increased to 0.112 V at the 20 µL casting. One-way ANOVA statistical analysis of these data showed a significant difference in the peak separation (F = 7.252, d.f. = 30, P < 0.005) in comparing the bare GCE to the GCE cast with various volumes of sonicated MWCNTs (5, 10 15 and 20 µL). Bonferroni post-hoc analysis comparing the individual cast volumes however, showed mixed results. A plot measuring the change in ΔE_p with increasing cast volume was therefore generated and is shown in Figure 3.9, where poor linearity is noted and a plateau of the curve can be seen at higher casting volumes. This suggested that the thickness of the MWCNTs layer introduced a diffusional limitation or may have decreased the conductivity at the electrolyte interface.[211] This was not seen however at the GCE modified with non-sonicated MWCNTs (Figure 3.9). As the casting volume was increased for this modified electrode, the peak separation remained relatively constant at an average of 0.058 V. Under these specific conditions it appears that the non-

sonicated sample that was shaken gently to aid dispersion showed superior electron transfer to the sonicated sample. It is proposed that the increased cast volume may have slowed the diffusion of the analyte through the mesoporous structure of the sonicated MWCNTs. Additionally, it is likely that the increased thickness of the film led to an increase in the amount of DMF on the electrode surface which would decrease the conductivity at the electrode/electrolyte interface.

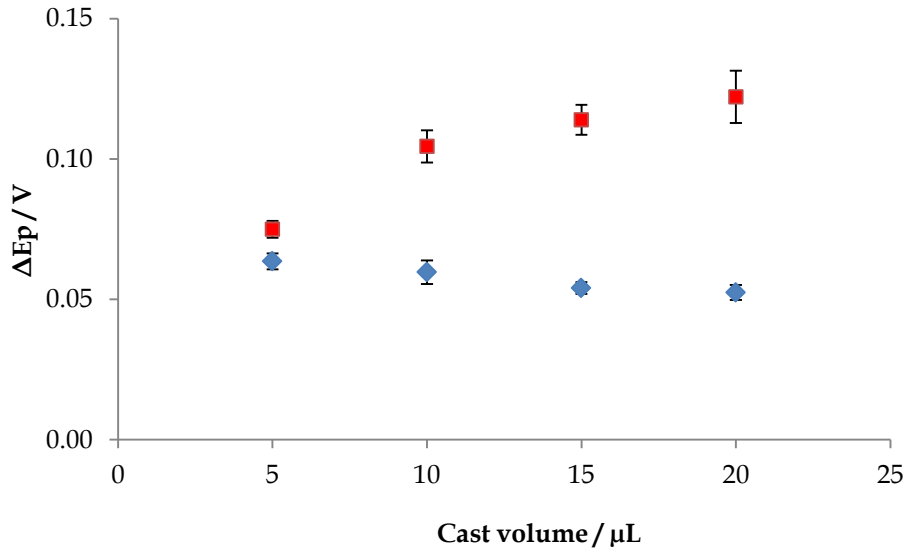

Figure 3.9: Plot of increasing ΔE_p with increasing cast volume. Potentials were recorded at GCEs modified with 5, 10, 15 and 20 µL MWCNTs ■ non-sonicated and ■ sonicated for 1 hr of the redox reactions of 1.00 × 10^{-3} M $[Fe(CN)_6]^{3-}$ /$[Fe(CN)_6]^{4-}$ with 0.05 M KCl and 0.05 M KH_2PO_4 as a supporting electrolyte system, at a scan rate of 100 mV s^{-1}.

3.2.1.2.4 Evaluation of Diffusional Effects at Electrodes Modified with MWCNTs

To investigate the diffusion process at the modified electrodes, the relationships between the log of the scan rate (log v) and the log of the recorded peak currents (log I_p) for all experiments in this section were measured by plotting the data, as shown in Figure 3.10. It is widely accepted

that a slope of 0.5 for this plot would indicate a diffusion controlled process whereas a slope of 1.0 would suggest an adsorption phenomenon. Values in between 0.5 and 1.0 indicate that both processes are important factors.[174, 212] The relative slope values for all of the modified electrodes can be seen in Table 3.1, where it is clear that a diffusional process is predominantly occurring for the redox couple of $[Fe(CN)_6]^{3-}/[Fe(CN)_6]^{4-}$ as all values are closer to 0.5 than to 1.0. The diffusional nature of this process was further supported by the linearity observed in plotting the peak current (I_p) against the square root of the scan rate ($\sqrt{v}$).[171] The average correlation coefficients recorded for modification with non-sonicated and sonicated MWCNTs were 0.99 and 0.98, respectively. Moreover, in monitoring the peak currents with cycle number it was found that they were stable and did not steadily increase with time, which also discounted any significant adsorption at the electrodes modified with sonicated MWCNTs samples. These observations coincide with the observed diffusive tail seen in cyclic voltammograms (Figure 3.11) confirming that adsorption to the nanotube surface is unlikely.

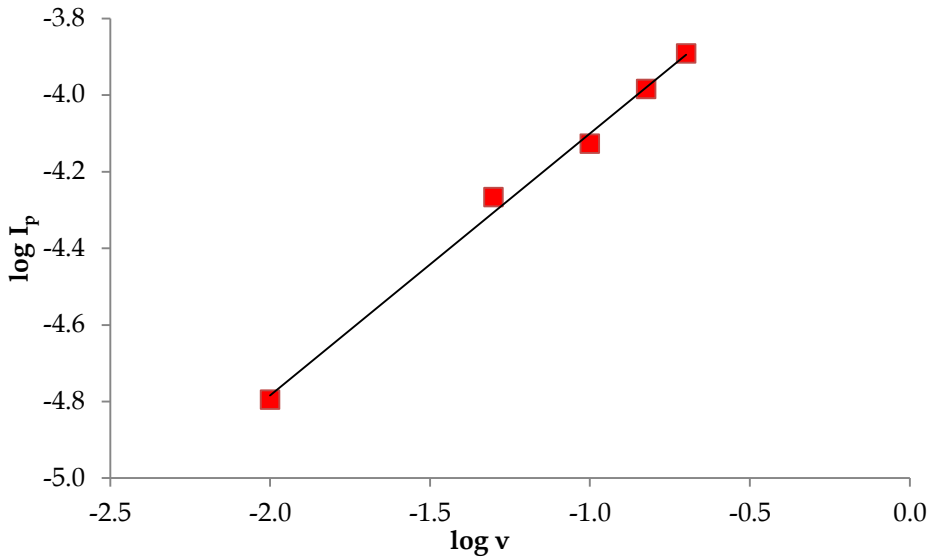

Figure 3.10: Typical plot showing the linear relationship (R^2=0.995) between the log of the scan rate and the log of the peak current. The slope of ~0.5 was used to determine the diffusional nature of the electron transfer.

Table 3.1: Values for the slope (m) obtained in plotting the log of the scan rate (log ν) against the log of the peak current (log I_p) for various cast volumes of sonicated and non-sonicated MWCNTs.

Cast Volume / µL	Sonicated MWCNTs	Non-sonicated MWCNTs
5	0.69	0.53
10	0.68	0.54
15	0.60	0.56
20	0.56	0.57

As mentioned previously, Keeley and Lyons[177] have highlighted that three possible processes may contribute to electron transfer in electrodes modified with carbon nanotubes; diffusion of an analyte through bulk solutions, diffusion through thin layers of solution within the networked nanotubes and adsorption to the surface of the nanotubes. As the diffusional nature of this system appears to be prevalent, from Table 3.1, it is likely that the diffusion through bulk solution and thin films are dominant factors in electron transfer at these modified electrodes. The effects of thin layer diffusion are explained in Chapter 2. In terms of electrodes modified with MWCNTs, it has been proposed that probe molecules or analytes can diffuse into "pockets" which form between networked nanotubes on the electrode surface. As the species is trapped at the electrode surface, it does not diffuse back into the bulk solution, as it would for semi-infinite diffusion, making electron transfer more efficient. Thin layer diffusion results in a small peak separation and is dependent on many factors, such as the thickness of the thin layer.

The small peak separation observed under certain conditions in Section 3.2.1.2.3 can be owed to the contribution of thin layer diffusion. Thin layer diffusion might be expected to have a bigger effect for the non sonicated MWCNTS, as an increase in the size of the thin layer "pockets" should occur in the sonicated MWCNTs agglomerations. Streeter *et al.*[178], have shown that an increase in the thin layer size will shift the anodic potential to more oxidative

potentials as the electron transfer becomes more difficult. Another important factor contributing to the slower electron transfer observed is the volume of solvent in the nanotube film. Keeley and Lyons[177] have suggested that the coating of nanotubes with solvent can inhibit electron transfer between the redox probe and the nanotube strands which is likely to be seen in the case of the sonicated MWCNTs. Sonication of the MWCNTs in DMF is likely to have coated the nanotubes more thoroughly than would be expected from gentle shaking. Although the solvent was evaporated under an IR lamp, it is unlikely that full removal of DMF was achieved. This increased level of solvent in the MWCNTs film may therefore also be responsible for the slower electron transfer at the sonicated MWCNTs film in comparison to the non-sonicated sample.

In comparing the voltammograms at various scan rates, evidence of thin layer diffusion at sonicated MWCNTs can be seen by the smaller peak separation (Figure 3.11 (a)) at slower scan rates. Significantly, while studying the peak separation of dopamine at a bare GCE and a single-walled nanotube modified electrode, Keeley and Lyons[177] observed that the peak separation for the modified electrode was smaller at low scan rates but larger at high scan rates than for the bare GCE. They explain that this is possibly due to time limitations of the diffusion process, in that at faster scan rates the diffusion of the analyte into the "thin layer pockets" of the MWCNTs does not have time to occur.

It can be seen in Figure 3.11 (b), by comparing the peak separations at each scan rate for the bare GCE to that modified with a sonicated sample of MWCNTs, the largest difference between the electrodes is seen at the slower scan rates. At higher scan rates the modified and bare electrodes behaved similarly, showing the contribution from semi-infinite planar diffusion for the GCE modified with sonicated MWCNTs. These results are consistent with the trend observed in Section 3.2.1.2.3 in the $[Fe(CN)_6]^{3-}/[Fe(CN)_6]^{4-}$ peak separation with increasing cast volume of sonicated MWCNTs. This suggests that the thin layer diffusion process is an important contribution to fast electron transfer at MWCNTs used in this work and that slow scan rates and low casting volumes are required to allow for the diffusion to occur in the sonicated sample.

(a)

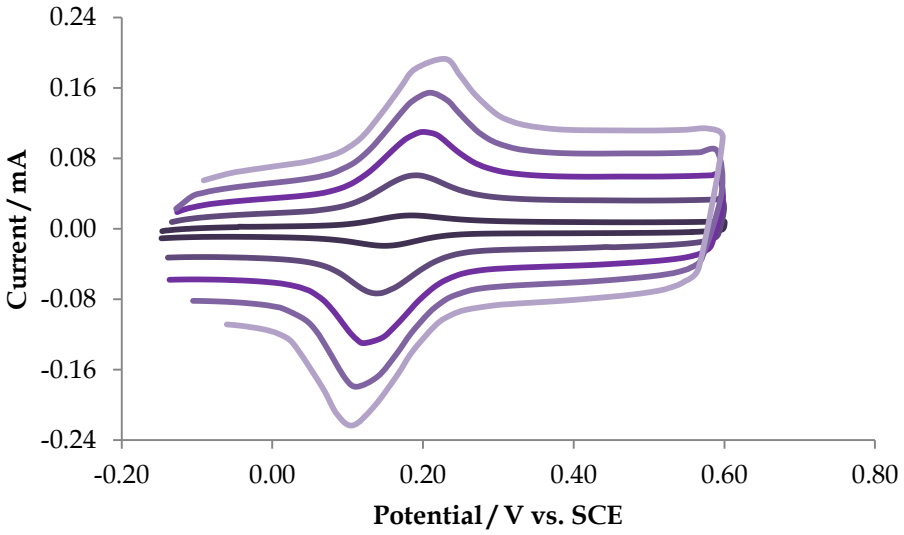

(b)

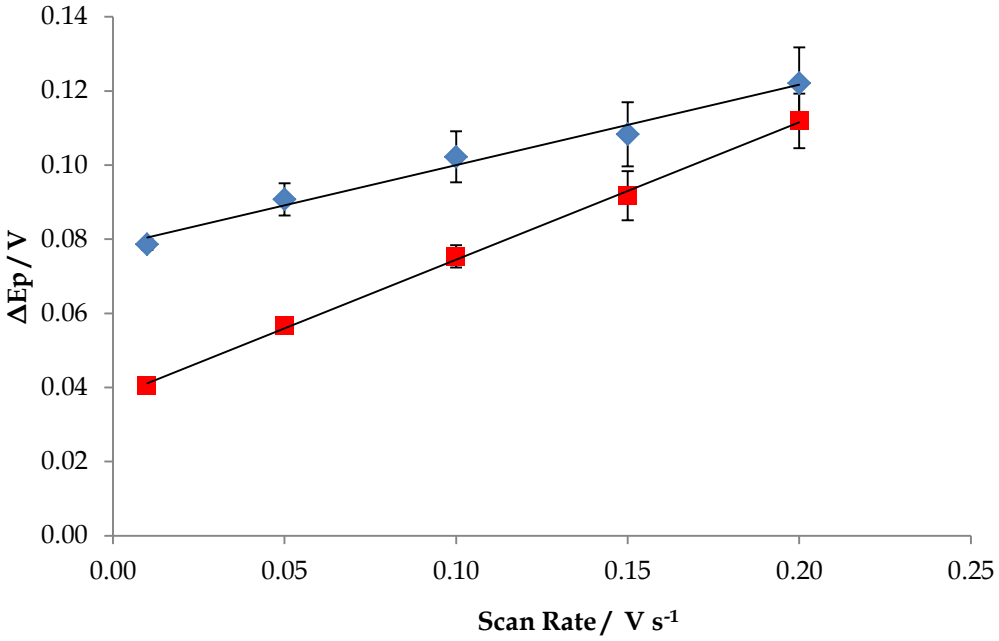

Figure 3.11: The redox behaviour of $K_3Fe(CN)_6^{3-/4-}$ with 0.05 M KCl and 0.05 M KH_2PO_4 as a supporting electrolyte system, at GCE modified with 5 µL sonicated MWCNTs shown by (a) voltammograms illustrating the effect of scan rates — 10 to — 200 mV s^{-1} and (b) plot highlighting the linear relationships of peak separation to scan rate for GCE ■ bare and ■ modified with 5 µL sonicated MWCNTs.

3.2.2 Electrodes Modified with Graphene

3.2.2.1 Electrochemical Characterisation of Electrodes Modified with Graphene

The effect of sonication on graphene samples is investigated in this section, similarly to that seen in Section 3.2.1.2.1 for MWCNTs. The experiments involving graphene were carried out at UNSW in Australia under the supervision of Prof. J.J. Gooding as part of an international exchange programme. Experiments involving the use of graphene required the use of two types of working electrodes (WEs). Glassy carbon (GC) and Platinum (Pt) pencil-style working electrodes of 3 mm diameter were prepared for use by polishing with alumina slurry (1.00, 0.30 and 0.05 μm grades) as described in Chapter 2. Highly ordered pyrolytic graphite (HOPG) was used to construct a basal plane HOPG working electrode as a comparative substrate (set up illustrated in Chapter 2). The quality of the basal plane HOPG was insured by stripping defected layers from the surface with adhesive tape, rinsing with EtOH and drying with N_2.[213, 214] The low level of remaining defects on the surface was confirmed by cyclic voltammetry whereby the electrode was cycled in 1.00×10^{-3} M $K_3Fe(CN)_6$ with 0.05 M KH_2PO_4 and 0.05 M KCl as supporting electrolytes. Voltammograms were recorded at various scan rates (10 to 200 mV s^{-1}) and a separation between the oxidation and reduction peak potentials, ΔE_p > 600 mV signified a suitable working surface containing a low level of defects.[213]

Graphene samples were prepared from 10 mg mL^{-1} suspensions in DMF, whereby non-sonicated samples were inverted to achieve their maximum dispersion without the aid of sonication and sonicated samples were dispersed using sonication for 30 min. The modified electrodes were prepared by drop casting 5 or 10 μL aliquots of the sample on the surface of the prepared working electrode and drying in an oven at 45 ^{o}C for 10 min. Cyclic voltammetry was carried out using the ferricyanide probe as described in

Section 3.2.1.2 with the peak currents, background currents and peak potentials recorded.

3.2.2.1.1 Effects of Dispersion on $K_3Fe(CN)_6$ Peak Currents at Glassy Carbon Modified with Graphene

The cyclic voltammograms in Figure 3.12 compare results obtained at bare GC to the GC electrode modified with non-sonicated graphene in $[Fe(CN)_6]^{3-}$ /$[Fe(CN)_6]^{4-}$ at 100 mV s^{-1}. There was a distinct decrease in the peak currents by modification of GCE with non-sonicated graphene, which can be seen in Figure 3.12 (a). The average anodic peak current measured at the bare GCE was 0.013 mA which decreased to 0.004 mA (n=3) upon modification with 5 µL of the non-sonicated graphene sample. The significance of this decrease was confirmed using a t-test (t = 10.04, d.f. = 5, P <0.001) and suggested that poorly dispersed graphene resulted in a lower active surface area of the modified electrode. Contrastingly, Figure 3.12 (b) shows an increase in faradaic currents at the GCE modified with sonicated graphene with the average anodic peak current (n=4) increased to 0.016 mA. However, this was not statistically different from the bare electrode (t = 2.014, d.f. = 6, P > 0.05). This slight increase was likely due to the increased surface area of the dispersed graphene sheets as was similarly shown for sonicated MWCNTs samples in Figure 3.4 but as the difference was insignificant, it suggested that the activity of the surface was very similar to that of glassy carbon.

It should be noted, however, that the difference observed between the GCE modified with non-sonicated and sonicated graphene was significant (t = 7.130, d.f. = 5, P < 0.001), highlighting the effect of sonication on the graphene sample. Similar results were recently obtained by Kang and co-workers[87] who studied the electrochemical detection of paracetamol at a graphene modified electrode prepared similarly to the sonicated sample in this work. They simply proposed that the graphene accelerated the electrochemical reaction at the

modified surface and the currents were further increased with increasing cast volume.

The volume of graphene cast on GCE was also varied and analysed similarly to that in Section 3.2.1.2.1. Results displayed in Figure 3.13 compare redox behaviour of the $[Fe(CN)_6]^{3-}/[Fe(CN)_6]^{4-}$ couple at 100 mV s^{-1} of the GCE modified with 5 and 10 µL (a) non-sonicated and (b) sonicated graphene, obtained using cyclic voltammetry as described before. It can be seen that by increasing the volume of non-sonicated material, the peak current varied insignificantly, ($t = 1.077$, d.f. = 4, $P > 0.05$). For modification of the GCE with sonicated graphene, the peak currents were increased from 1.56×10^{-5} A for 5 µL casting to 1.68×10^{-4} A upon modification with 10 µL. Statistical analysis of these data however, again showed no significance in this increase ($t = 0.6078$, d.f. = 6, $P > 0.05$), indicating that the increased volume did not significantly increase the active surface area of the modified electrode.

(a)

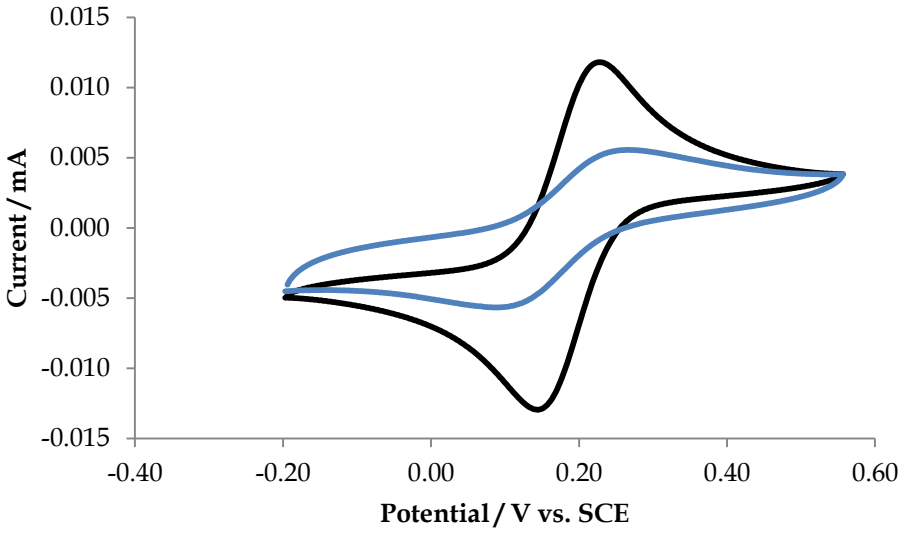

(b)

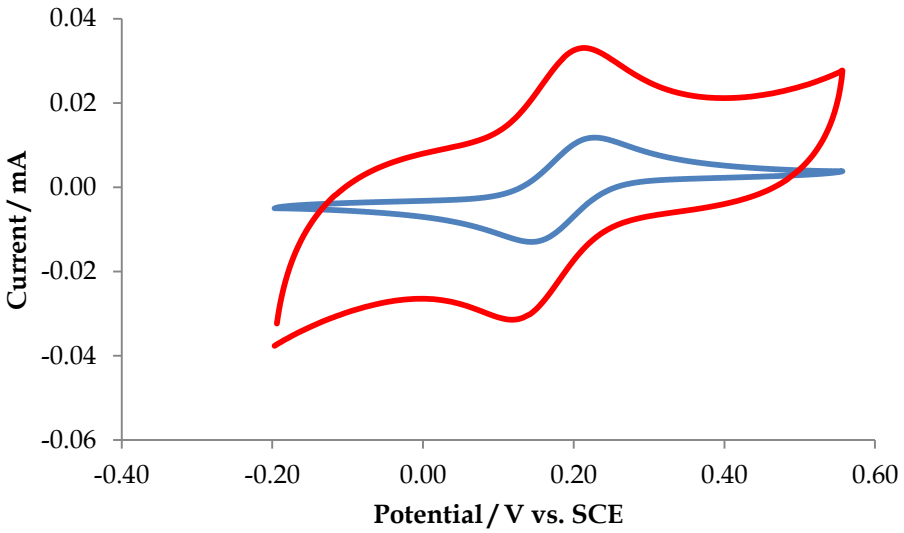

Figure 3.12: Cyclic voltammograms comparing 3 mm GCE (a) — bare to — modified with 5 µL non-sonicated graphene and (b) — bare to — modified with 5 µL sonicated graphene. All electrodes were cycled in 1.00×10^{-3} M $[Fe(CN)_6]^{3-}/[Fe(CN)_6]^{4-}$ with 0.05 M KCl and 0.05 M KH_2PO_4 as a supporting electrolyte system, at a scan rate of 100 mV s^{-1}.

(a)

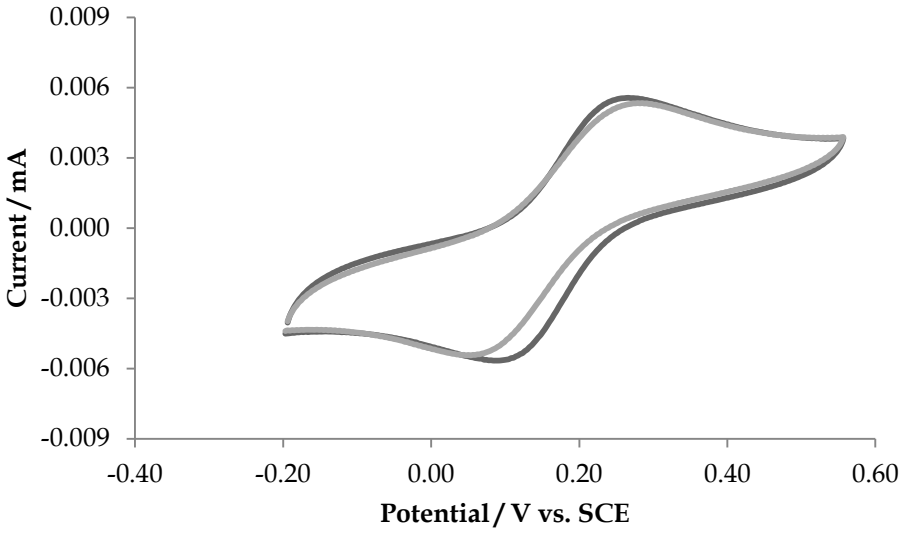

(b)

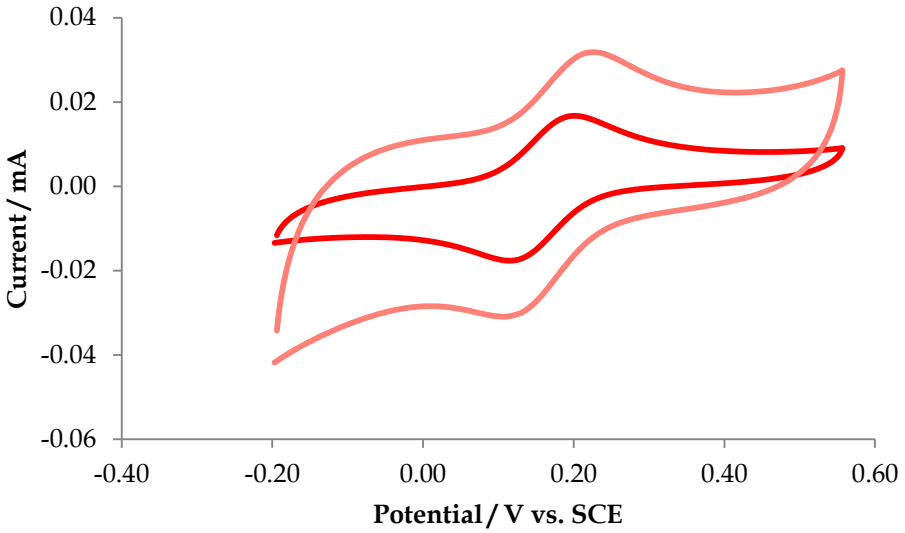

Figure 3.13: Cyclic voltammograms comparing (a) — 5 and — 10 µL casting volumes of non-sonicated graphene and (b) — 5 and — 10 µL casting volumes of sonicated graphene. The modified electrodes were cycled in 1.00×10^{-3} M $[Fe(CN)_6]^{3-}/[Fe(CN)_6]^{4-}$ with 0.05 M KCl and 0.05 M KH_2PO_4 as a supporting electrolyte system, at a scan rate of 100 mV s^{-1}.

Investigation of further increasing the volume of sonicated graphene cast on GC showed results contrasting to those obtained for MWCNTs. As can be seen in Figure 5.14, the increase from 10 to 15 and 20 µL in casting volume resulted in an apparent decrease in the faradaic currents. The peak currents in this case decreased slightly from 1.68 × 10^{-4} A at the GC modified with 10 µL to 5.85 × 10^{-5} and 1.13 × 10^{-5} A, respectively, for 15 and 20 µL castings. No statistical differences were found between the various casting volumes which further suggested that regardless of the volumes cast, the electrochemical activity was similar to that observed at the bare electrode, indicating that the graphene re-stacked on the GCE surface. This re-stacking is known to occur with pristine graphene as the individual sheets are relatively unstable[86] therefore the use of nanoparticles and chemical functionalisation of graphene is commonly implemented to aid in their separation.[89, 215] For the purpose of this study however, the materials in their pristine forms were solely examined.

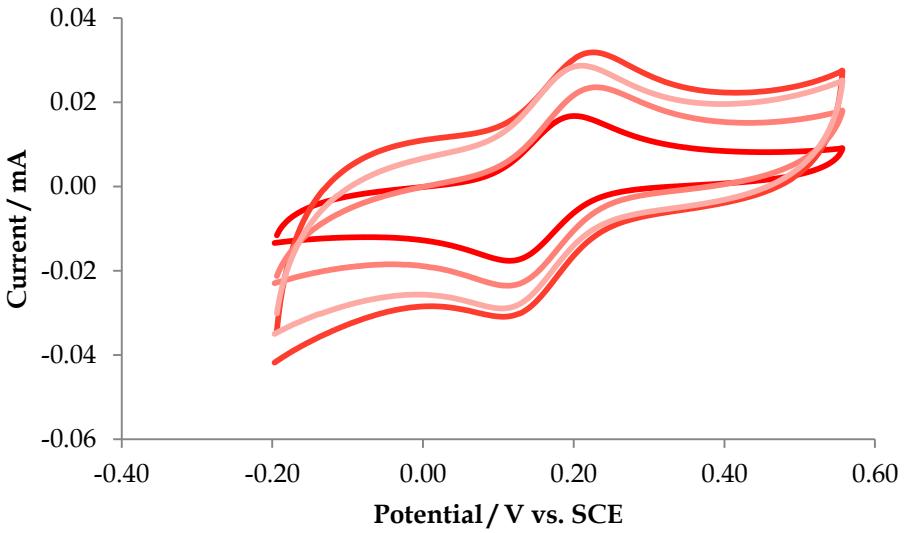

Figure 3.14: Cyclic voltammograms of GCE modified with increasing cast volumes of sonicated graphene: — 5, — 10, — 15 and — 20 µL. The modified electrodes were cycled in 1.00 × 10^{-3} M $[Fe(CN)_6]^{3-}/[Fe(CN)_6]^{4-}$ with 0.05 M KCl and 0.05 M KH_2PO_4 as a supporting electrolyte system, at a scan rate of 100 mV s^{-1}.

3.2.2.1.2 Evaluation of the Capacitive Properties of Electrodes Modified with Sonicated Graphene

The capacitance of the GCE modified with sonicated graphene was calculated by measuring the current at 0.50 V as a function of scan rate, as seen previously in Section 3.2.1.2.2 for the MWCNTs modified electrodes. It was found that upon modification with 5 µL sonicated graphene, the capacitance increased to 1.3×10^{-4} F from 3.0×10^{-5} F at the bare GCE. The measured capacitance was further increased to 1.8×10^{-4} F with the modification of GCE with 10 µL sonicated graphene. This suggested that sonication of the graphene sample separated individual graphene sheets allowing for the build up of charge at the edge planes of the sheets. The ordered layering between graphene sheets is known to introduce interfacial capacitive properties to the material which would have contributed to this increase.[198, 211] Kang *et al.*,[87] for example observed increased background currents with increasing amounts of graphene, which they ascribed to an increased surface area obtained in modification of their GCE surface with a graphene nanocomposite film. Wang *et al.*[211] have utilised a similar increase in observed capacitance to calculate the number of layers in their graphene samples, relating their observations to interfacial capacitance.

As outlined in Section 3.2.1.2.2, the measured capacitance was related to the mass of graphene cast on the surface to provide gravimetric capacitance values. It was calculated that the gravimetric capacitance of the electrode modified with 5 µL sonicated graphene (i.e. 0.05 mg) was 2.6 F g^{-1}. However, this decreased to 1.8 F g^{-1} at the GCE modified with 10 µL (i.e. 0.10 mg) sonicated graphene. This is indicative that the entire amount of graphene on the surface was not accessible to the electrolyte in this case. This can perhaps be explained by a decrease in the exposed edge planes of the graphene which can be caused by the agglomeration of undispersed sheets.[86] The agglomeration may have resulted in folding and disordered stacking of the graphene sheets which has been shown to have adverse effects on its

electronic properties.[216] From the results presented here, it is apparent that the modification of GCE with approximately 0.05 mg graphene provides the most significant enhancement of the capacitance.

3.2.2.1.3 Evaluation of Diffusional Properties of $K_3Fe(CN)_6$ at Electrodes Modified with Graphene

To investigate the differences in the I_p for the oxidation of $K_3Fe(CN)_6$ and the capacitance values noted thus far between MWCNTs and graphene modified electrodes, the mechanism of the observed reaction was assessed. The relationship between the log of the scan rate (log ν) and the log of the peak current (log I_p) was investigated, as used before for the MWCNTs modified electrodes in Section 3.3.1.4. Data are shown in Table 3.3 comparing the slope of these plots for sonicated and non-sonicated graphene confirming that a diffusional process remained dominant as the slopes for these plots remained at approximately 0.5 in both cases. Although in literature reports, semi-infinite planar diffusion is generally the only process considered, Hallam and Banks[217] have highlighted that, similarly for MWCNTs, electrochemical measurements on graphene-modified electrodes should consider the possibility of thin layer diffusion or discount it where necessary.

The decrease in electrochemical activity with increased casting volume of sonicated graphene suggested that some adsorption occurred at the electrode surface. In monitoring the peak currents with cycle number however, it was found that they were stable and did not steadily increase with time, discounting any significant adsorption at the electrodes modified with sonicated graphene samples. Based on the slope values presented in Table 3.2, it is unlikely that thin layer diffusion occurred for the graphene modified electrodes unlike that seen for MWCNTs.[217]

Table 3.2: Values for the slope (m) obtained in plotting the log of the scan rate (log ν) against the log of the peak current (log I_p) for various cast volumes of sonicated and non-sonicated MWCNTs.

Cast Volume / µL	Sonicated graphene	Non-sonicated graphene	Bare GC Electrode
5	0.53	0.38	0.48
10	0.48	0.32	

3.2.2.1.4 The Effect of Dispersion on Electron Transfer for the $[Fe(CN)_6]^{3-}/[Fe(CN)_6]^{4-}$ couple at Glassy Carbon Modified with Graphene

The peak potentials for the $[Fe(CN)_6]^{3-}/[Fe(CN)_6]^{4-}$ couple were measured at the modified electrodes, E_p, and used to calculate the half wave potential, $E_{1/2}$, as was carried out for MWCNTs. The half wave potential was calculated to be 0.16 V, similar to that calculated at MWCNTs modified electrodes and again was independent of sonication or cast volume. The efficiency of electron transfer at the modified electrodes was also investigated by calculating the separation of the anodic and cathodic peak positions, ΔE_p. The average (n=4) calculated ΔE_p at the GCE modified with non-sonicated graphene was slightly larger at 0.144 V than the bare GCE which was 0.102 V. Statistical analysis of these data however, showed no significance in the shift (t = 1.446, d.f. = 5, P > 0.05).

The peak separation for $[Fe(CN)_6]^{3-}/[Fe(CN)_6]^{4-}$ redox notably decreased from 0.102 V at the bare electrode to 0.088 V at the GCE modified with sonicated graphene. It was possible that this was due to partial oxidation of graphene during sonication, as Ji *et al.*[218] demonstrated an increase in electron transfer at graphitic materials with increasing oxygen-containing groups. Similarly to that seen for MWCNTs, as the graphene samples were not treated with strong acids, it was unlikely that they were significantly oxidised during sonication but a small increase in oxygen containing groups would be expected. The

statistical analysis however, showed that this was not a significant decrease ($t = 1.326$, d.f. = 6, $P > 0.05$) which highlights the importance of using such analytical techniques to clarify the significance of changes in voltammetric responses.

It was found that increasing the volume of sonicated graphene cast on the surface from 5 to 10 µL increased the peak separation slightly from 0.088 to 0.111 V. Further increasing the cast volume to 15 µL caused another slight increase in ΔE_p to 0.117 V, however increasing the volume to 20 µL decreased the peak separation to 0.098 V. Statistical analysis of the various cast volumes showed no significant difference overall, however Bonferroni post-hoc analysis showed variable significances between individual data sets. As these results contrast with that seen for MWCNTs, it is proposed that the increase in casting volume had no impact on the active area of this modified electrode due to stacking of graphene.

Data presented in Table 3.3 comparing the electrodes modified with sonicated and non-sonicated graphene solutions which shows that there is a clear decrease in the peak separation, ΔE_p, and a significant increase in peak current, I_p, at the electrode modified with sonicated graphene compared to that of non-sonicated graphene. These results indicate that the dispersion of graphene in DMF exposed the electrocatalytic properties of the material for small cast volumes of 5 to 10 µL. These properties, as discussed previously, arise due to extrinsic defects such as oxygenated groups or intrinsic defects such as the formation of 5 membered rings in the graphene sheet.

Table 3.3: Data obtained from cyclic voltammograms of non-sonicated and sonicated graphene cast on GCE. Table compares peak separation (ΔE_p) and anodic peak current (I_{pa}) for 5 and 10 µL casting volumes of both materials at 100 mV s^{-1}.

Electrode	**ΔE_p / V**		**I_{pa} / mA**	
GCE	0.102		0.0130	
	Volume Cast / µL			
	5	**10**	**5**	**10**
GC/non-sonicated graphene	0.144	0.188	0.0044	0.0037
GC/sonicated graphene	0.088	0.111	0.0156	0.1683

3.2.2.2 Electrochemical Comparison of Various Substrates Modified with Graphene using $K_3Fe(CN)_6$.

As the modification of GC with graphene has thus far shown similar electrochemical properties to that seen at the bare electrode, and in some cases impeded the electrochemical response, the influence of the substrate on the peak current and peak separation was investigated. In this study, 5 µL casts of the sonicated graphene sample were compared at GC, basal plane highly orientated pyrolytic graphite (HOPG) and platinum (Pt) electrodes.

3.2.2.2.1 The Electrochemical Properties of HOPG modified with Sonicated Graphene

The use of basal plane HOPG as a comparative substrate was investigated as it is known to have poor electron transfer properties.[213] This facilitated testing of the electrochemical properties of graphene without interference from the underlying substrate. In Figure 3.15 (a) and (b) results obtained by cycling bare glassy carbon and basal plane HOPG in the ferricyanide solution are compared to those modified with sonicated graphene. It is evident in Figure 3.15 (b) that redox cycling of the $[Fe(CN)_6]^{3-}/[Fe(CN)_6]^{4-}$ couple is inefficient at the bare

basal plane HOPG electrode. The slow electron transfer was identified by a broad ΔE_p of > 600 mV which is characteristic of this substrate when it is virtually free from defects.[213, 214] In Figure 3.15 (b), the slow electron transfer observed at the bare basal plane HOPG substrate was increased upon modification with sonicated graphene and exhibited a ΔE_p of 0.185 V (n=3). The large difference between this peak separation and that observed for the analogous experiment carried out at GCE (0.088 V) suggested that there was some interaction between the GC substrate and the graphene or that the electron transfer properties of GC contributed to the results observed in Section 3.3.2.1.

The increase in I_p for the oxidation of $K_3Fe(CN)_6$ to 0.0048 mA observed with modification of the basal plane HOPG with sonicated graphene was significant in comparison to the bare substrate, due to the low levels of defects achieved during preparation of the substrate. The peak currents monitored at the GCE modified with sonicated graphene were notably larger; at 0.0156 mA. These values were obtained by removal of the background capacitive currents and therefore indicated that there was some interaction between the graphene and the glassy carbon electrode that enhanced the electronic properties of the modified electrode. This could be explained by the structure of GC as it is reported to have fullerene–like structures and many edge-plane sites,[219] which would likely interact with graphene via π-π interactions. It could also indicate that some electroactivity occurred at the GC substrate. As no composite or filler materials were used, it was likely that some of the GC substrate was left uncovered and contributed to the reaction.

(a)

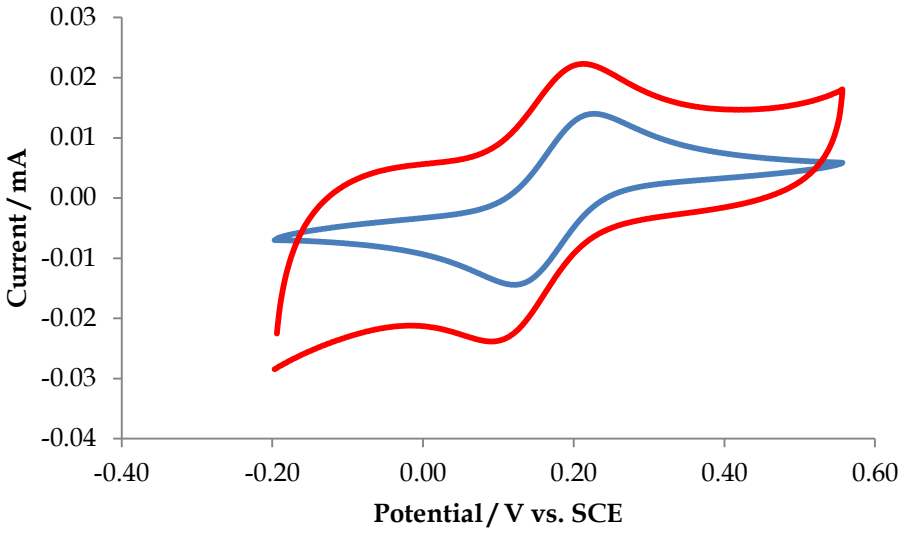

(b)

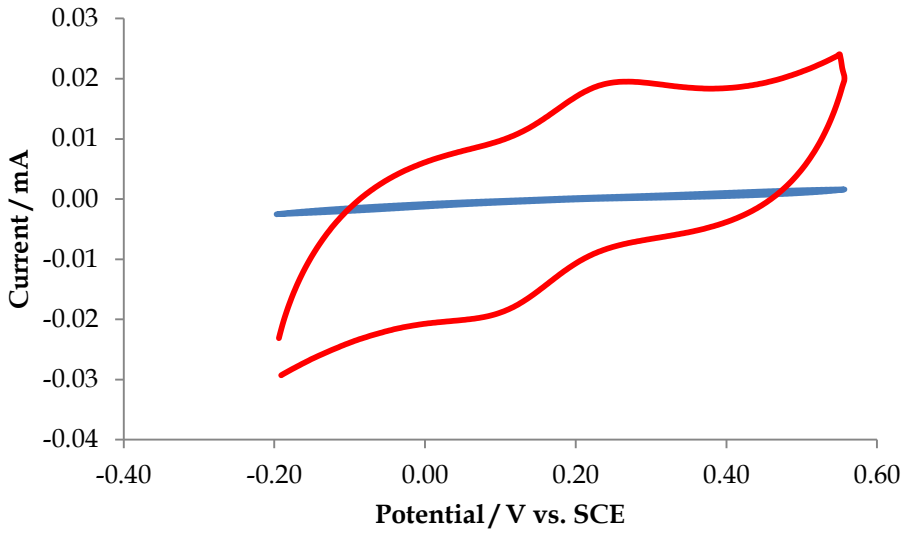

Figure 3.15: Cyclic voltammograms of (a) glassy carbon and (b) basal plane graphite electrodes comparing — bare surfaces and — surfaces modified with 5 µL sonicated graphene recorded in 1.00×10^{-3} M $K_3Fe(CN)_6$ with 0.05 M KCl and 0.05 M KH_2PO_4 as a supporting electrolyte system, at a scan rate of 100 mV s^{-1}.

3.2.2.2.2 *The Electrochemical Properties of Pt modified with Sonicated Graphene*

To further investigate the possibility of carbon-based interactions between the defects of glassy carbon and graphene, a platinum substrate was investigated as an electrode material. Figure 3.16 displays results similar to those in Figure 3.15 (a), whereby both the bare substrate and the substrate modified with 5 µL sonicated graphene were compared for their electrochemical properties. It appears from these voltammograms that the addition of graphene to the platinum surface increased the faradaic current response in comparison to the bare electrode. However, the anodic peak currents observed at the modified platinum electrode were substantially lower than the currents observed at GC modified with sonicated graphene (0.016 mA), which supported observations that some interaction between the GC substrate and the sonicated graphene enhanced the amount of analyte oxidised at the modified electrode. Also, as the redox behaviour of $K_3Fe(CN)_6$ is known to be largely affected by defects at the electrode surface such as edge-plane sites, it is a possibility that any uncoated parts of the GCE reacted directly with the $K_3Fe(CN)_6$.

The findings outlined above support observations of the contribution of GC to the observed electronic properties of graphene and suggested that there were electrostatic interactions between the graphene and the glassy carbon substrate.[57] Similar results have been reported by Borowiec *et al.*[44] in comparing MWCNTs cast on Pt, Au and GC electrodes for the oxidation of ketoconazole. They found that GCEs modified with MWCNTs provided the highest current response for ketoconazole detection in comparison to Au and Pt modified electrodes. A decrease in the peak separation from 0.076 V at the bare platinum to 0.066 V was observed as a result of modification with sonicated graphene. This indicated that electron transfer at the platinum modified electrode was faster than that observed at the modified GC substrate (0.088 V); however the bare platinum was also superior to GC in this respect. This observation further highlights the contribution of the substrate to the

electrochemical response of the modified electrodes to the redox behaviour of the ferricyanide couple.

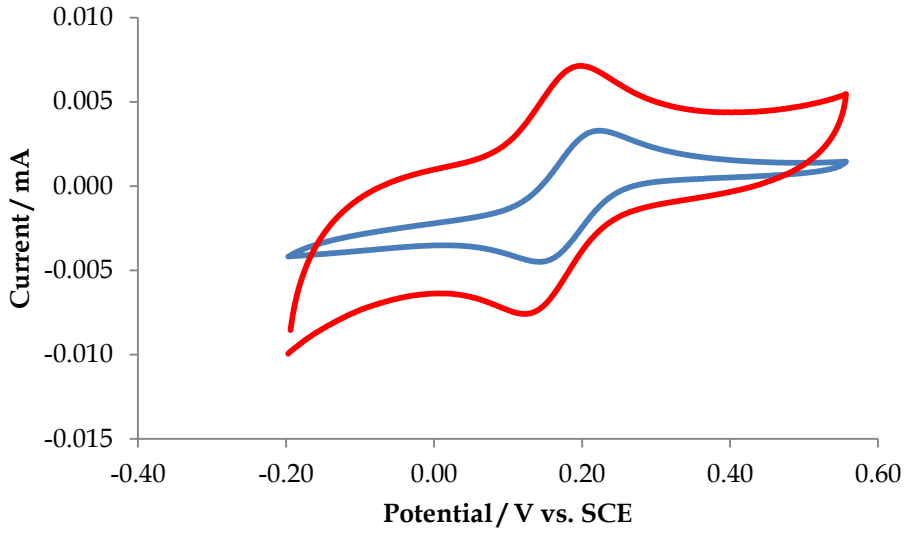

Figure 3.16: Cyclic voltammograms comparing the redox couple of 1.00×10^{-3} M $[Fe(CN)_6]^{3-}/[Fe(CN)_6]^{4-}$ with 0.05 M KCl and 0.05 M KH_2PO_4 as a supporting electrolytes, at — bare Pt electrode and — Pt electrode modified with 5 µL sonicated graphene.

3.2.2.3 SEM Analysis of Graphene

High resolution micrographs obtained of the cast graphene samples can be seen in Figures 3.17 (a) and (b). The images show agglomeration of the carbon material without sonication (a) and the image in Figure 3.17 (b) highlights that some order was achieved in the sample by sonication. The non-sonicated image in Figure 3.17 (a) is similar to that initially reported by Choucair *et al.* [167] in the production of this graphene sample. They describe the structure as a fusion of individual graphene sheets creating a porous structure. The order achieved by sonication seen in Figure 3.17 (b) resembles the individual folded graphene sheets observed by Kang *et al.*[87] also on a GC substrate, however at this magnification, it is likely that an ordered stack of graphene sheets is

observed as π-stacking interactions would create a certain degree of order between individual sheets.[92]

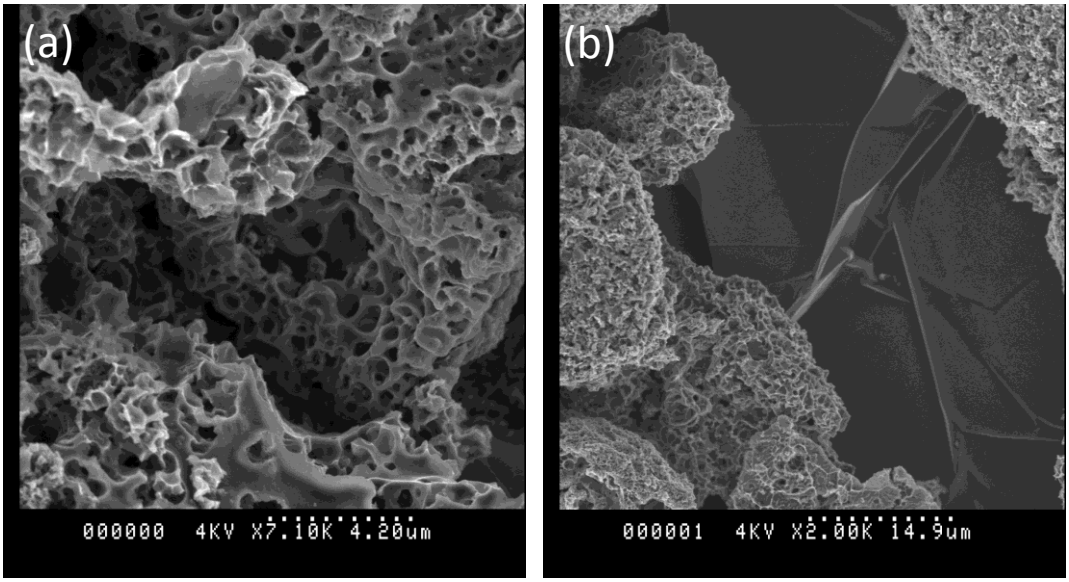

Figure 3.17: SEM images for (a) non-sonicated and (b) sonicated graphene samples.

3.2.3 Electrochemical Analysis of GC Electrodes Modified with Sonicated MWCNTs and Graphene

Observations of increased peak currents in Section 3.2.1.2.1 and 3.2.2.1.1 at GCE modified with MWCNTs and graphene indicated that an increase in the electroactive surface area was achieved upon sonication of both materials. The peak separations observed in Section 3.2.1.2.3 and 3.2.2.1.4 indicated that sonication also increased the rate of electron transfer at the modified electrodes in comparison to the bare GCE. The data obtained from cyclic voltammetry experiments were therefore used to calculate the electroactive surface areas and specific rate constants at GC electrodes modified with sonicated MWCNTs and sonicated graphene samples in this section. The calculation of the rate constants, k_s, involved using the peak separations (ΔE_p) of the $[Fe(CN)_6]^{3-}/[Fe(CN)_6]^{4-}$ redox couple as described in Section 3.2.3, for

each electrode at various scan rates; 10, 50, 100, 150 and 200 mV s^{-1}. As the diffusional nature of the $[Fe(CN)_6]^{3-}/[Fe(CN)_6]^{4-}$ redox couple at each electrode was confirmed in Section 3.2.3, the peak separations were applied to two kinetic equations that assume a diffusion-controlled current, namely the Kochi and Klingler Equation and the Nicholson theory, which are both discussed in detail in Chapter 2.

3.2.3.1 Calculation of the Diffusion Coefficient of $K_3Fe(CN)_6$ at GCE

Firstly the diffusion coefficient, *D*, was calculated as it is a widely used value in analytical equations used to describe diffusion controlled process that describes the transport of the electrochemical probe to the electrode surface. In order to further characterise both MWCNTs and graphene modified electrodes, the diffusion coefficient of the probe, $K_3Fe(CN)_6$ was calculated at the bare GC electrode, using the Randles Sevcik[220] Equation, 3.1.

$$I_p = 0.4463\, n\, F\, A \left(\frac{nF}{RT}\right)^{1/2} D^{1/2}\, v^{1/2}\, c \qquad 3.1$$

In this equation I_p is the peak current (A), *F* is Faraday's constant 96,485 C mol^{-1}, *R* is the gas constant (8.314 J mol^{-1}), *T* is the temperature (K), *n* is the number of electrons involved in the redox reaction, *A* represents the electroactive surface area (cm^2), *D* is the diffusion coefficient of the analyte ($cm^2\ s^{-1}$), *c* is the concentration (mol cm^{-3}) and *v* is the scan rate (V s^{-1}). Cyclic voltammetry of the bare GCE was carried out in 1.00×10^{-3} M $K_3Fe(CN)_6$ at various scan rates as detailed in Section 3.2.3. The recorded peak currents were plot against the square root of the scan rate, and as illustrated in Figure 3.18, linear plots were observed. This linearity was used to calculate a diffusion coefficient of 3.58×10^{-6} $cm^2\ s^{-1}$, which agrees quite well with previous literature reports (6.3×10^{-6} $cm^2\ s^{-1}$).[221]

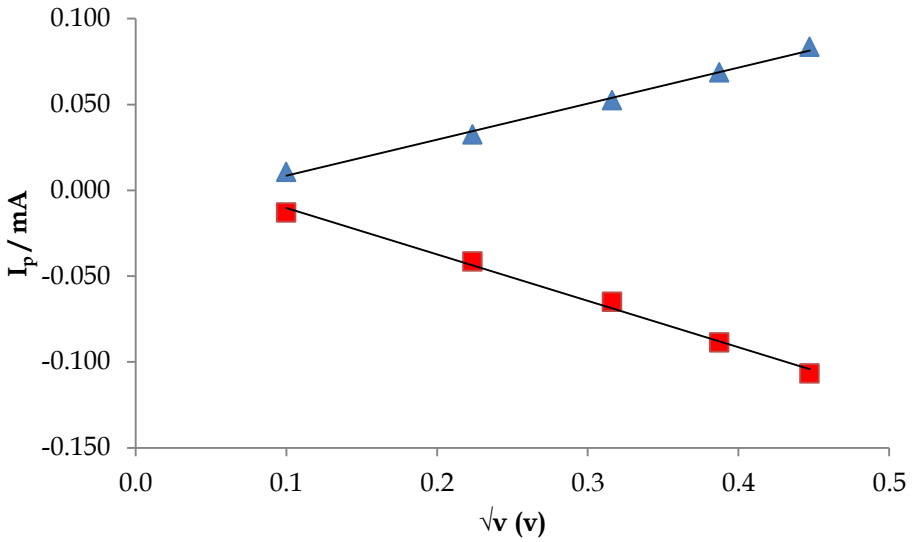

Figure 3.18: Typical plot monitoring change in ■ oxidative and ■ reductive peak currents (I_p) of 1.00 × 10^{-3} M $K_3Fe(CN)_6$ with 0.05 M KCl and 0.05 M KH_2PO_4 as a supporting electrolyte system, with the square root of the scan rate (√v) used to calculate the diffusion coefficient, D.

3.2.3.2 Calculation of the Heterogeneous Electron Transfer Rate Constant using The Nicholson Theory

The use of the Nicholson theory to calculate rate constant, k_s, involved the derivation of the kinetic parameter Ψ from a working curve. Theoretical values of decreasing Ψ with increasing peak separation, ΔE_p, were proposed in the classic paper by Nicholson.[179] In plotting $1/\Psi$ against $1/\Delta E_p$, a polynomial relationship was observed which was used to calculate values of Ψ based on experimental ΔE_p values. According to Equation 3.2, Ψ was then used to calculate k_s. This theory is further discussed in Chapter 2.

$$\Psi = \frac{\gamma^{\alpha} k_s}{\left(\frac{\pi D n \nu F}{RT}\right)^{\frac{1}{2}}} \qquad 3.2$$

Here, the value of γ is 1 which indicates the assumption that the oxidised and reduced species have small differences in concentration and diffusion

coefficients, α is the transfer coefficient which is assumed to 0.5, and k_s is the heterogeneous electron transfer rate constant. D is the diffusion coefficient calculated in Section 3.2.3.1 (3.58×10^{-6} cm^2 s^{-1}) the number of electrons transferred is represented by n, ν is the scan rate (V s^{-1}), F is Faraday's constant (96,485 C mol^{-1}), R is the gas constant (8.314 J K^{-1} mol^{-1}) and T is the temperature (K). It is noteworthy that this method is limited by ΔE_p values between 61 and 212 mV and intermediate scan rates, to maintain Ψ values in the quasi-reversible range.

The Nicholson Theory was used to calculate rate constants at each peak separation and the average rate constant was then determined. This was carried out for both MWCNTs and graphene at a range of cast volumes and the results are illustrated in Table 3.4. It is clear from this table that the rate constants for both MWCNTs and graphene in this case are very similar. The largest difference between the rate constants in this case occurs at the 5 µL casting, where thin layer diffusion is most effective, as indicated in Section 3.2.1.2.3 by the relatively small peak separation. As the predominant characteristic of thin layer diffusion is small peak separation,[222] it could not be accurately accounted for with the Nicholson Theory, which is limited by peak separations greater than 61 mV. Therefore, in calculating the average electron transfer rate constant at GCE modified with MWCNTs, peak separations smaller than 61 mV were not included. The Nicholson theory generally assumes that semi-infinite planar diffusion is the only contributing mode of transport in the electrochemical cell, and that no iR compensation is required.

The heterogeneous electron transfer rate constant calculated using 5 µL casting of MWCNTs reported here is similar to the 1.7×10^{-3} cm s^{-1} calculated by Ambrosi *et al.*[223] for MWCNTs containing nano graphite impurities, also using the Nicholson Theory. The peak separations in the case of graphene modified electrodes were between 61 and 212 mV, further indicating that semi-infinite planar diffusion was the most dominant form of mass transport for electron transfer. The rate constant calculated using 5 µL casting of graphene

is similar to that calculated for stacked graphene nanofibers by Ambrosi *et al.*[224] In comparing the effects of inter-sheet folds on the electron transfer rate, they calculated k_s of 6.9×10^{-3} cm s^{-1} for electrodes modified with "open" stacks of graphene, prepared similarly to this work.

It generally can be seen that increasing the cast volume of MWCNTs on GCE resulted in slower rate constants. This was expected as the ΔE_p measured in Section 3.2.1.2.3 increased with increasing cast volume. This was attributed to the influence of thin layer diffusion on the electron transfer at smaller casting volumes that was not seen with larger cast volumes due to the thickness of the mesoporous film which is further supported here. The cast volume had little effect on the rate constant at the graphene-modified electrode which indicated that the graphene sheets re-stacked upon drying on the electrode surface and suggested that electroactivity was resided to the top layer of graphene which is at the electrode-electrolyte interface.

Table 3.4: Average rate constants calculated using the Nicholson Theory for GCE modified with various casting volumes of sonicated MWCNTs and graphene.

Casting Volume / µL	**Rate Constant (k_s) / cm s^{-1}**	
	MWCNTs	**graphene**
5	4.29×10^{-2}	7.29×10^{-3}
10	3.75×10^{-3}	5.44×10^{-3}
15	2.05×10^{-3}	2.91×10^{-3}
20	1.63×10^{-3}	4.64×10^{-3}

3.2.3.3 Calculation of the Heterogeneous Electron Transfer Rate Constant Using The Kochi and Klingler Method

The Kochi and Klingler[180] Equation 3.3 was applied to data obtained from cyclic voltammetry to calculate rate constants at both modified and bare electrodes for the $[Fe(CN)_6]^{3-}/[Fe(CN)_6]^{4-}$ redox couple which could include values outside the threshold of the Nicholson Theory.

$$k_s = 2.18 \left(\frac{\beta DnFv}{RT}\right)^{\frac{1}{2}} exp\left(-\frac{\beta^2 nF}{RT}\left(E_p^a - E_p^c\right)\right) \qquad 3.3$$

Here, k is the rate constant (cm s^{-1}), β is a derivation of the transfer coefficient α, where β = 1-α, D is the diffusion coefficient (cm^2 s^{-1}), n is the number of electrons transferred, F is Faraday's constant (96,485 C mol^{-1}), v is the scan rate (V s^{-1}), R is the gas constant (8.314 J K^{-1} mol^{-1}) and T is the temperature (K). Equation 3.3 was rearranged to form Equation 3.4 to correlate the natural logarithm of the scan rate, lnv, to ΔE_p.

$$lnv = \frac{2\beta^2 nF}{RT}\Delta E_p + 2lnk - 2ln\ 2.18 - ln\frac{\beta DnF}{RT} \qquad 3.4$$

In obtaining a linear correlation, as can be seen in Figure 3.19, the slope (m) was used to calculate values for β and the intercept was therefore used to calculate values for the rate constant, k.

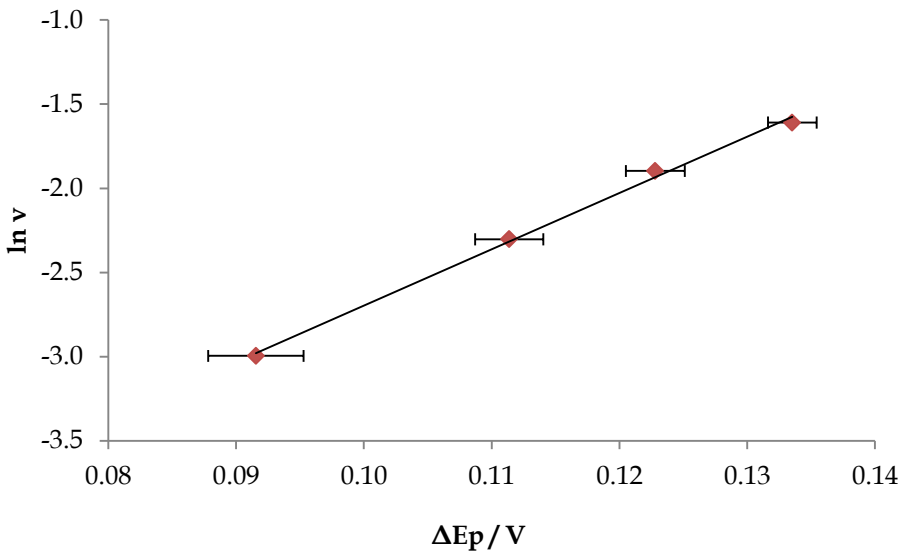

Figure 3.19: Typical plot of the logarithm of the scan rate as a function of peak separation, the slope of which was used in the calculation of β.

The values calculated for β indicated values for the transfer coefficients which are in good agreement with literature obtained by Kochi and Klingler[180] in their original paper in 1981 using the $[Fe(CN)_6]^{3-}/[Fe(CN)_6]^{4-}$ couple. The heterogeneous electron transfer rate constants that were calculated using Equation 3.3 for both sonicated MWCNTs and graphene of various casting volumes are displayed in Table 3.5. The values of β calculated at MWCNTs modified electrodes ranged between 0.41 and 0.56 and the rate constants ranged from 1.35 to 2.36 × 10^{-3} cm s^{-1} which agree well with literature reports from Sanchez *et al.*[49] The values calculated for β at graphene modified electrodes ranged between 0.65 and 0.80 and the heterogeneous electron transfer rate constants ranged from 8.16 × 10^{-4} to 1.07 × 10^{-3} cm s^{-1} which coincide with results obtained by Keeley *et al.*[61]

The rate constants are similar at both graphene and MWCNTs modified electrodes for casting volumes from 5 to 20 µL, with a slight variance observed at the GCE modified with 5 µL graphene. This can be explained by the β value of 0.80 calculated at this electrode which deviates from the other modified electrodes. The rate constant decreased steadily for MWCNTs with increasing

cast volume, as expected from observed peak separations in Section 3.2.1.2.3. This indicated that the mesoporous structure decreased the rate constant of the MWCNTs modified electrodes as it introduced diffusional limitations. There was little effect on rate constant at the graphene modified electrode again, which highlights that the stacked structure of the graphene limited any effects of cast volume.

Table 3.5: Heterogeneous electron transfer rate constants calculated for the $[Fe(CN)_6]^{3-}/[Fe(CN)_6]^{4-}$ couple using Kochi and Klingler Equation for GCE modified with various casting volumes of sonicated MWCNTs and graphene.

Casting Volume / µL	**Rate Constant (k_s) / cm s^{-1}**	
	MWCNTs	**Graphene**
5	2.36×10^{-3}	8.16×10^{-4}
10	2.35×10^{-3}	1.02×10^{-3}
15	1.53×10^{-3}	1.03×10^{-3}
20	1.35×10^{-3}	1.07×10^{-3}

3.2.3.4 Comparison of Kinetic Analyses

The rate constants calculated using both the Nicholson theory and the Kochi and Klingler method were compared to evaluate the discrepancies between the two methods. In Section 3.2.3.3 the relationship between a range of peak separations and scan rates was used to determine the rate constants, k_s, for the Kochi and Klingler method. Conversely, rate constants were determined at each peak separation for the Nicholson method with the average rate constant reported. To compare both methodologies k_s was calculated for each peak separation using the calculated β values in the case of the Kochi and Klingler method. As shown in Figure 3.20 (a) and (b), the relationship of k_s with peak separation can be therefore displayed for both methods. Similar to results presented by Kochi and Klingler in 1981,[180] the plots rapidly converge at larger peak separations, showing the equivalence of both methods in calculating rate constants under certain conditions.

Although it is very difficult to compare the amount of material at a graphene and MWCNT modified electrode due to their different morphologies and therefore dispersion in solution, it is estimated under these conditions that a similar mass of both materials was deposited on the surface. This was assumed as experiments which were repeated with the same cast volume of each material showed good reproducibility. In both cases, the heterogeneous electron transfer constant was larger at the GCE modified with MWCNTs than with graphene. This can be explained by the thin layer effects seen at the MWCNTs modified electrode in Section 3.2.1.2.4 that were not seen for the graphene modified electrode. The electroactive surface area of both materials was also expected to have affected the calculated rate constants at these electrodes.

(a)

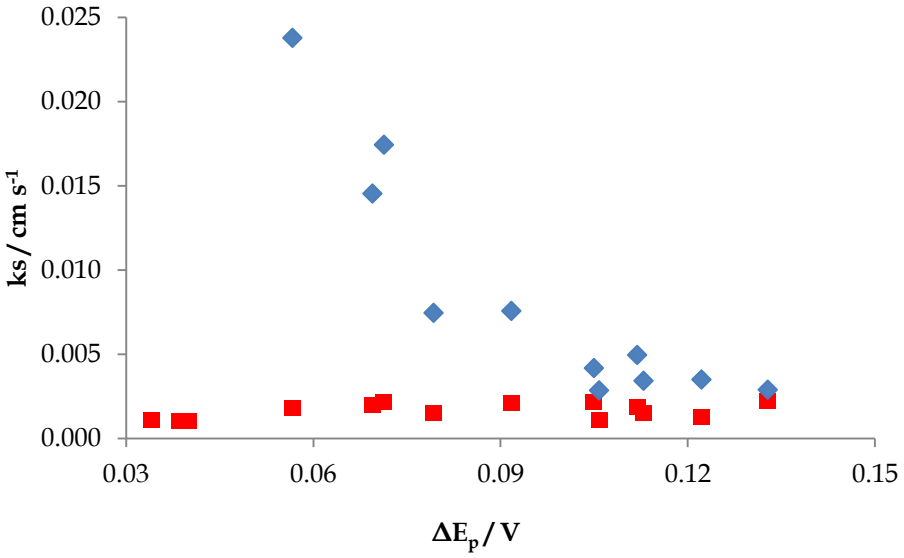

(b)

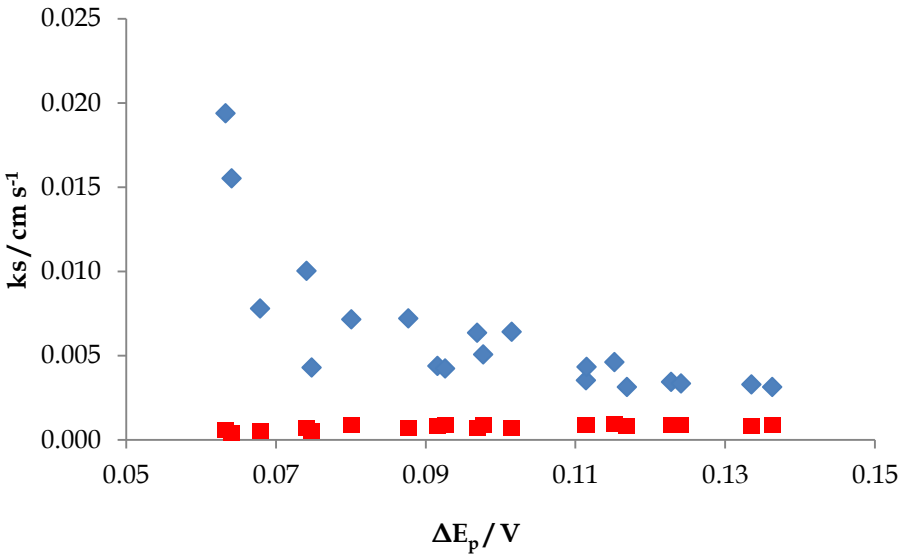

Figure 3.20: Comparison of the standard rate constant, k_s evaluated by ■ the Nicholson theory and ■ the Kochi and Klingler method for (a) MWCNTs and (b) graphene modified GC electrodes.

3.2.3.5 Calculation of Electroactive Surface Areas of GCEs Modified with Sonicated Graphene and MWCNTs.

As discussed in Chapter 1, among the most important benefits to using MWCNTs and graphene in the modification of electrodes, is their large surface area, however as the morphology of both materials are vastly different, it was expected that the electroactive surface areas of the modified electrodes would also be different. This may have also contributed to differences observed in the heterogeneous electron transfer rate constant observed in Sections 3.2.3.2 and 3.2.3.3. Literature reports often focus on the physical surface area of MWCNTs samples, for example, Pumera *et al.*[71] have shown graphene to have a larger physical surface area than carbon nanotubes in evaluating the influence of nitric acid treatment on carbon materials, with reported BET surface areas of 2630 m^2 g^{-1} and 1315 m^2 g^{-1} for acid treated graphene and carbon nanotubes, respectively. The reported physical surface area of the graphene used in this work by Choucair *et al.*[167] is 1692 m^2 g^{-1} calculated by methylene blue adsorption for samples dispersed in ethanol. In this section however, the area of the modified electrodes used in electrochemical measurements of the $K_3Fe(CN)_6$ probe, i.e. the electroactive surface areas, were calculated by re-arrangement of the Randles Sevcik equation, 3.1. By plotting the peak current, I_p, as a function of the square root of the scan rate, $v^{1/2}$, the slope, m, was used to calculate the surface area according to Equation 3.5:

$$m = 0.4463\, n\, F\, A \left(\frac{nF}{RT}\right)^{1/2} D^{1/2} c \qquad 3.5$$

The use of $K_3Fe(CN)_6$ as an electrochemical probe is known to be sensitive to defects which are an indication of the Density of States of an electrode.[218, 225] It can therefore be deduced that the electroactive surface area in this case, refers to the area of the electrode that is active towards $K_3Fe(CN)_6$. It was therefore expected that the electroactive surface areas calculated using this method would differ to those calculated by adsorption techniques such as BET.

The average (n=7) of the calculated surface areas of GCEs modified with sonicated samples of both MWCNTs and graphene are displayed in Figure 3.21 and compared to their respective bare electrodes. Firstly, the calculated surface area of a 3 mm diameter (0.071 cm^2) GCE modified with 5 µL sonicated graphene is compared to the bare electrode. It can be seen here that this modification increased the electroactive surface area from 0.071 cm^2 to 0.092 cm^2, which can be due to the dispersion of graphene in the DMF solution exposing the defect areas by revealing the smaller stacks of sheets, as seen in SEM images in Figure 3.9. Luo *et al.*[226] have calculated the surface area of a 0.071 cm^2 GCE modified with a CuO-nanocube/graphene composite using the Randles Sevcik Equation and found it to be 0.062 cm^2. This decrease in electroactive surface area from the bare GCE could be a result of the use of Nafion® in the composite which possibly impeded the access of the electrolyte to the electroactive sites of the modified electrode. Most recently, Rajesh *et al.*[93] have calculated the surface areas of 0.071 cm^2 GCEs modified with platinum modified graphene using the Randles-Sevcik method to be 0.074 cm^2. They have elegantly combined the electronic and structural properties of MWCNTs and graphene to dramatically increase this surface area to 0.121 cm^2 by vertically growing the nanotubes on a single sheet of graphene.

Figure 3.21 also compares the surface areas of a 4 mm diameter GCE (0.1257 cm^2) modified with 5 µL sonicated MWCNTs to the bare electrode. This modification impressively increased the electroactive surface area of the electrode from 0.1257 cm^2 to 0.413 cm^2. This large increase can be attributed to the dispersion of MWCNTs exposing their high aspect ratio. This dispersion would have increased the mesoporosity of the resulting film by reducing the size of MWCNT aggregates and improving internetworking of the smaller bundles.[38] Recently, Kun *et al.*[78] have used the Randles-Sevcik equation to calculate the surface area of MWCNTs modified with platinum nanoparticles, and found an increase by a factor of 1.79 with 5 µL castings in comparison to the bare GCE which is significantly less than the 3 fold increase in surface area calculated in this work for 5 µL castings of pristine MWCNTs. This could be

explained by the use of Nafion® in fabrication of the former electrode as seen also for graphene modified electrodes. The increase of about 3 fold in the surface area achieved with this modification also supersedes that achieved by Xiao *et al.*[227] who observed a 1.5 fold increase in the calculated surface area of a similarly prepared GCE. This can possibly be attributed to the larger aspect ratio of the MWCNTs employed here, as the length of MWCNTs used in this work ranged from 2.5 to 20 μm in comparison to lengths of 1 to 2 μm used by Xiao *et al.*[227]

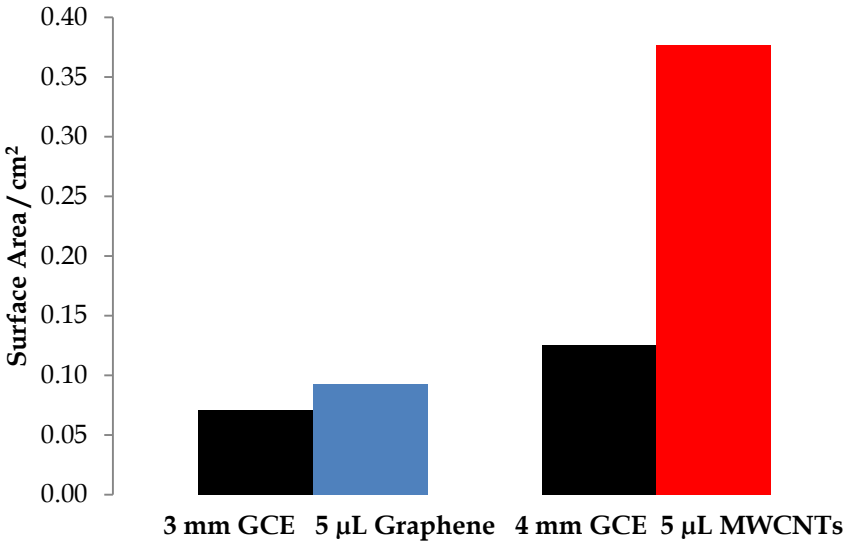

Figure 3.21: Bar charts comparing electroactive surface areas of ■ bare GCE to GCE modified with 5 μL ■ graphene and ■ MWCNTs samples from 10 mg mL^{-1} DMF suspensions, sonicated for 1hr.

The electroactive surface areas of electrodes modified with various cast volumes of both graphene and MWCNTs were also calculated, and are displayed in Figure 3.22 as a percentage change in surface area from the bare GCE for each cast volume and the individual surface areas are tabulated. It can be seen from this chart that further increasing the cast volume of sonicated graphene to 10, 15 and 20 μL decreased the electroactive surface area of the modified GCE. This is possibly due to the π-stacking interactions between the graphene sheets that may have decreased the level of exposed electroactive

sites of the graphene.[86] Conversely, it can be seen that increasing the volume of sonicated MWCNTs cast on the GCE further enhanced the electroactive surface area to up to 0.580 cm^2. In 2009, Hegde *et al.*[228] calculated the surface area for a GCE modified with acid treated MWCNTs using this method and found a 4.0-4.5 fold increase with the addition of a 15 µL casting in the surface area compared to the bare GCE. The results obtained in this study are comparable with up to 4.6 fold increase for cast volumes of 15-20 µL castings of untreated MWCNTs.

In comparing the increase in surface area of the GCE upon modification with sonicated graphene to that of sonicated MWCNTs, it is clear that MWCNTs provided a significantly larger surface area than graphene when cast on the GCE surface. This can be explained by the large aspect ratio of MWCNTs which is between 416.67 and 1538.46. Choucair *et al.*[167] have characterised the graphene used here as consisting of sheets that extend laterally in the range of 1×10^{-7} to 1×10^{-5} m, however to accurately compare both materials, it is best to consider their morphologies as they aggregate. In studying the effects of cutting SWCNTs, Haas *et al.*[229] observed that decreasing the aspect ratio caused them to exhibit a more layered sheet–like assembly. This is very likely to have occurred in sonicating graphene samples as their sheet-like morphology favours π-stacking assembly that does not occur with untreated MWCNTs. This group also measured the porosity of the SWCNTs of different aspect ratios. They found that materials of larger aspect ratios displayed mesoporosity and larger pores were created in spaces between the bundles of SWCNTs. It was observed that SWCNTs of lower aspect ratios assembled into dense layered structures and this porosity was lost. It is likely that similar differences occurred between MWCNTs and graphene samples in this study, as other literature reports have also shown that MWCNTs tend to form bundles of networked nanotubes[38] and that graphene can form more densely packed, layered coatings when cast on the electrode surface[89].

It has been reported by Wang *et al.*[90] that the inclusion of carbon nanoparticles in a graphene composite effectively increased the surface area by reducing stacking between graphene sheets. The incorporation of these nanoparticle resulted in an increase of the BET surface area from 77 to 1256 $m^2 g^{-1}$. They attribute this increase in surface area to the formation of a mesoporous composite, and show the absence of mesopores in the composite prepared without nanoparticles, indicating a high level of re-stacking in graphene. The differences in calculated surface areas of the MWCNTs and graphene modified GCEs in this work agree well with the differences observed by Haas *et al.*[229] in calculating the BET surface areas of the SWCNTs with different aspect ratios. However, although BET and methylene blue methods allow for sufficient calculation of the physical surface area of both materials, for the purpose of electrochemical characterisation, it can be seen that the use of the Randles Sevcik Equation to determine the electroactive surface areas of the modified electrodes is more accurate for defining the active or defect sites of modified electrodes.

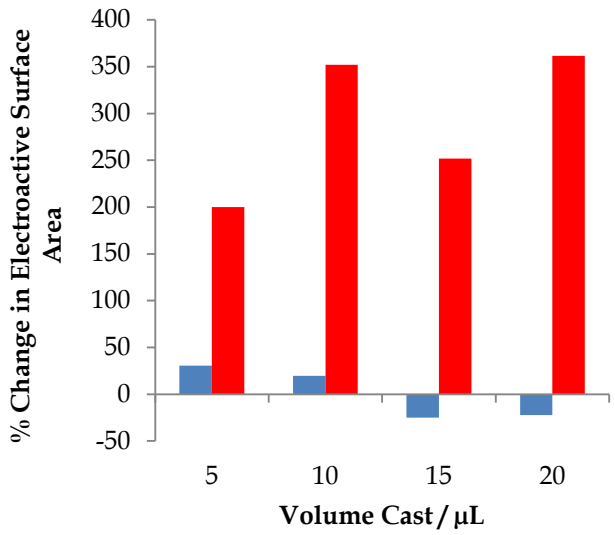

Volume Cast / µL	Surface Area / cm²	
	Graphene	MWCNTs
5	0.092	0.377
10	0.085	0.568
15	0.053	0.442
20	0.055	0.580

Figure 3.22: Bar charts comparing the relative change in electroactive surface areas of modified GCEs with respect to the geometric surface area of the bare electrodes. Data are compared for GCEs modified with 5, 10, 15 and 20 µL ■ Graphene and ■ MWCNTs samples from 10 mg mL^{-1} DMF suspensions, sonicated for 1hr. Table inset illustrates calculated surface areas of each modified electrode.

3.3 Conclusion

The electrochemistry at GCEs modified with MWCNTs and graphene has been evaluated in this chapter. Dispersed suspensions of 10 mg mL^{-1} MWCNTs and graphene were prepared in DMF using sonication and were compared to non-sonicated samples. The redox couple of $[Fe(CN)_6]^{3-}/[Fe(CN)_6]^{4-}$ was monitored using cyclic voltammetry and the peak potentials and peak currents were recorded. The rate constants for the redox couple were also calculated at the modified electrodes using both the Kochi and Klingler Equation and the Nicholson Theory as the diffusional nature of the reaction was confirmed. Overall it was found that GCEs modified with MWCNTs exhibited faster electron transfer kinetics than GCEs modified with graphene which has been explained by the mesoporous structure of MWCNTs providing superior electrochemical properties to the modified electrodes in this study, most likely due to thin layer diffusion processes.

The electroactive surface areas of the modified electrodes were calculated from the peak currents using the Randles Sevcik Equation and it was found that modification of the GCE with sonicated MWCNTs provided a larger increase in surface area in comparison to that of graphene modified electrodes. In comparing the electrochemistry at MWCNTs modified electrodes to graphene modified electrodes (Table 3.6), the rate constants and electroactive surface areas are greater for the GCEs modified with MWCNTs. In recent reports, Borowiec *et al.*[44] have attributed an improved electrochemical response to ketoconazole at similarly prepared MWCNTs modified electrodes to their increased surface area and also recognised their ability to promote electron transfer.

Table 3.6: Surface areas and rate constants for GCE modified with 5 and 10 µL sonicated MWCNTs and graphene.

	5 µL		**10 µL**	
	graphene	MWCNTs	graphene	MWCNTs
Surface Area / cm^2	0.092	0.377	0.085	0.568
Rate of Reaction / cm s^{-1}	8.16×10^{-4}	2.36×10^{-3}	1.02×10^{-3}	2.35×10^{-3}

Chapter 4:

The Electrochemical Detection of Cr(VI) using Electrodes Modified with Multiwalled Carbon Nanotubes

4.1 Introduction

Chromium (VI) is a toxic metal ion which is found in many parts of the environment due to its ability to leach great distances in groundwater. Chromium metal is found naturally in many rocks and the hexavalent ion, Cr(VI), is therefore often leached into groundwater and can be found in soil and plants as a result. Cr(VI) is also a common waste product of industries such as mining and electroplating. As Cr(VI) is classified as a human respiratory carcinogen[230] and is known to cause a multitude of skin disorders,[6] it is important to be able to detect it at low levels. The Environmental Protection Agency has set a mandatory limit of 9.61×10^{-7} M (50 μg L^{-1}) Cr(VI) in drinking water.[12] It is therefore crucial to enable its specific detection at low levels by a simple and fast method. As discussed in Chapter 1, there are many benefits to the use of electrochemical sensors in environmental monitoring of toxic species such as Cr(VI), including real-time analysis and on-site monitoring.

A review of the current literature based on electrochemical sensors and the current methods used to detect Cr(VI) are presented in Chapter 1. Briefly, it can be noted that current methodologies used in the detection of chromium such as ICP-MS, do not provide real-time, on site detection and thus are costly, time consuming and can be exposed to contamination or other problems associated with the transport of samples before testing. Electrochemical sensors provide the opportunity to test on-site with remote operation which would be time saving and cost effective. The electrochemical detection of Cr(VI) in particular allows for its specific identification, as current methodologies do not distinguish between Cr(VI) and Cr(III), a less toxic chromium ion which is essential for glucose metabolism at low levels.

The drop cast method of modifying electrodes with MWCNTs was investigated in Chapter 3 and compared to the use of graphene as a modification material. It was found that the mesoporous structure of MWCNTs further enhanced the electron transfer abilities and provided a larger surface area than was seen at graphene modified electrodes. MWCNTs are therefore investigated in this chapter for their use in the electrochemical sensing of Cr(VI). The use of MWCNTs in electrochemical sensors has increased over the past decade,[48, 196, 231] as they have many desirable properties such as fast electron transfer[43] and an immense length to diameter ratio.[41] Many electrochemical sensors have been investigated using the drop cast method discussed here with successful results, for example in the detection of cytochromes and ketoconazole.[44, 232] However, concerns for the stability of the cast MWCNTs film have led to an increase in the development of carbon nanotube / polymer composites, using conducting polymers such as polyaniline[233] and polypyrrole[146]. The conductivity of such polymers, however, can contribute to the large capacitance of the carbon nanotubes which can be overcome by the use of overoxidised polymers.[234] The use of polypyrrole (Ppy), with its partial overoxidation, in the modification of electrodes with MWCNTs is therefore also explored in this chapter.

The use of nanoparticles to modify MWCNTs has been reported with impressive enhancements in sensitivity of the resulting materials. Kun *et al.*, [78] for example have shown the impressive increase in peak currents of potassium ferricyanide redox reactions at Pt nanoparticle modified MWCNTs in comparison to a Pt nanoparticle modified GCE and a MWCNTs modified GCE, indicating an increase in surface area. The authors saw a correlated enhancement of current for the oxidation of propranolol hydrochloride at the Pt nanoparticle modified MWCNTs with this increase in surface area. As the peak currents for the reduction of Cr(VI) have been shown to be optimum at an Au substrate by Welch *et al.,*[235] the modification of MWCNTs with gold nanoparticles (AuNPs) was explored in this chapter to enhance the detection of Cr(VI).

The work outlined in this chapter was aimed to investigate three main materials for their ability to sense Cr(VI) electrochemically; MWCNTs, MWCNT/Ppy composite films and MWCNT/AuNPs films. For the main part, the MWCNTs were not pre-treated, however for the modification of MWCNTs with AuNPs, both pristine and oxidised MWCNTs were used (MWCNTsOx/AuNPs). Investigations were carried out using solely the MWCNTs to determine the influence the pH of the solution, the conductivity of the solution, and the substrate had on the detection of Cr(VI). A study was also carried out to investigate the detection of Cr(VI) at MWCNTs in the presence of three possible interferants; Cl^-, NO_3^- and Cu^{2+} ions; and in real water samples. Finally, a study was carried out to investigate the use of differential pulse voltammetry and constant potential amperometry with a rotating disc electrode to improve the detection of Cr(VI).

4.2 Results and Discussion

4.2.1 Investigating the use of a MWCNT Modified Electrode in the Detection of Cr(VI)

In Chapter 3, it was shown that MWCNTs could be reproducibly cast (20 µL) onto a glassy carbon surface (0.126 cm^2) from a 10 mg mL^{-1} sonicated dispersion in DMF to produce an electrode with an increased electroactive surface area of 0.580 cm^2 (GCE/MWCNTs). In this section, the same dispersion and cast volume were used to modify a GCE for the detection of Cr(VI). Good surface coverage of the electrode was achieved and was confirmed using SEM imaging of the modified surface. Figure 4.1 (a) and (b) displays the micrographs obtained, confirming that the nanotubes were reasonably well dispersed with small agglomerations of networked MWCNTs formed, highlighted in Figure 4.1 (b).

(a) (b)

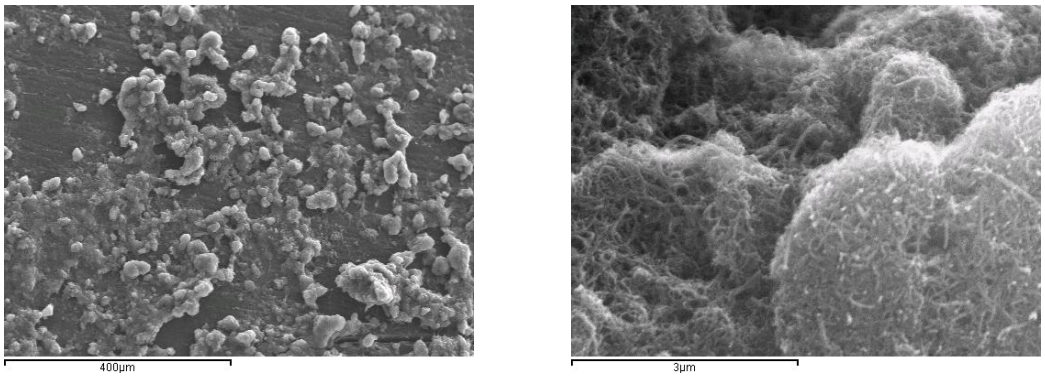

Figure 4.1: High resolution SEM micrographs at different magnifications (a) and (b) showing 20 µL cast on 4 mm diameter glassy carbon surface from 10 mg mL^{-1} MWCNTs/DMF solution.

The electrochemical detection of Cr(VI) in this work was based on its reduction to the less toxic Cr(III) using cyclic voltammetry. As the reduction reaction is favoured in acidic solutions, according to Equation 4.1, it was initially carried out in an aqueous media of H_2SO_4 at pH 2.0.

$$Cr_2O_7^{2-}{}_{(aq)} + 14\ H^+{}_{(aq)} + 6e^- \rightarrow 2\ Cr^{3+}{}_{(aq)} + 7\ H_2O_{(l)} \qquad 4.1$$

The detection of this reduction was compared at a bare glassy carbon electrode (GCE) and the MWCNTs modified GCE (GCE/MWCNTs). The electrodes were firstly cycled in the supporting electrolyte solution without Cr(VI) to obtain stable background readings and the voltammograms were recorded between -0.25 and +0.90 V vs. SCE, at 10 mV s^{-1}. The detection of 6.00×10^{-4} M Cr(VI) at both bare GCE and at GCE/MWCNTs is compared in Figure 4.2, and the average (n=4) peak position (E_p) and peak current (I_p) values are tabulated inset. The bare GCE showed a broad reduction peak at approx. 0.25 V vs. SCE which is analogous to that seen by Welch *et al.*[235] amongst others, who found the reduction peak to be electrochemically irreversible and controlled by diffusion. Upon modification of the GCE with MWCNTs, a shift in peak position was observed (Figure 4.2) to a more favourable position of 0.65 V vs. SCE, which could be attributed to the fast electron transfer properties of MWCNTs. In the reduction of Cr(VI) to Cr(III) many factors such as the increased wettability of the surface and the presence of defects,[43] as well as the presence of oxygenated groups at defect sites on MWCNTs,[46] may have contributed to this catalytic effect. In addition, thin layer diffusion may have led to higher local concentrations of Cr(VI) within the networked bundle, as seen in Chapter 3 for the ferricyanide couple.[177]

It is of note that the reduction of Cr(VI) at GCE/MWCNTs in comparison to the bare GCE showed a significant increase in peak current from 3.02×10^{-6} to 1.73×10^{-5} A (Figure 4.2). This can most likely be explained by the increased surface area of the electrode, and possibly an increased density of states at the

electrode/electrolyte interface. In 2001, Nugent *et al.*[43] reported Nernstian behaviour at MWCNTs modified electrodes for a one-electron transfer process, where the nanotubes were well aligned in the form of micro-bundles. The researchers proposed that the density of states and wettability of electrodes modified with MWCNTs were responsible for increases in electron transfer rates.

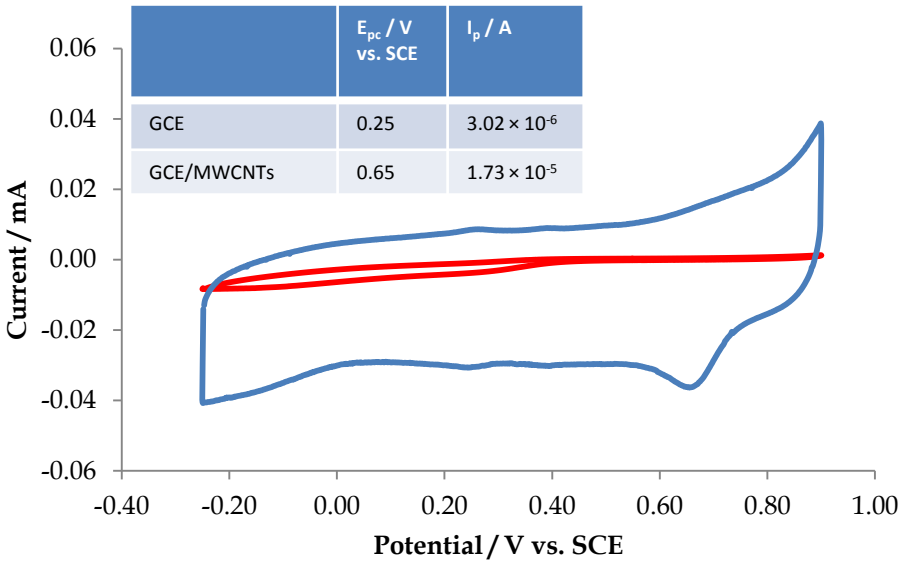

Figure 4.2: Cyclic voltammograms in 6.00×10^{-4} M Cr(VI) in H_2SO_4 pH 2.0, at 10 mV s^{-1}, of — bare GCE and — GCE modified with 20 µL 10 mg mL^{-1} MWCNTs in DMF. Average electrochemical properties for n=4 repeated experiments are tabulated inset.

A possible concern of using MWCNTs to develop an electrochemical sensor for Cr(VI) comes from recent reports by Gu *et al.*[236] on the interactions of MWCNTs with Cr(VI) under highly acidic conditions (pH 1.0). These researchers showed, using Fourier transform infra-red (FTIR) spectroscopy to identify the modification imposed on the MWCNTs after Cr(VI) treatment, that Cr(VI) can spontaneously oxidise MWCNTs and thus itself be reduced. They confirmed however, that at pH 2.0 no measurable oxidation of the MWCNTs had occurred and as the Cr(VI) reduction process was

electrochemically monitored at pH 2.0 in this work, contribution from such competing processes was very unlikely. To confirm this, a cyclic voltammetry study was carried out to detect Cr(VI) as outlined above, but at pH 1.0, and the reduction reaction was not observed electrochemically.

In examining the currents at approximately 0.40 V vs. SCE in Figure 4.2 a pair of distinctively reversible redox peaks was observed. They can be attributed to the presence of oxygen-containing species on the nanotube surface, recently identified by Zheng and co-workers.[237] The researchers identified the presence of oxygen containing functional groups on the MWCNTs by FTIR spectroscopy. The electrochemical activity of the groups was observed by the authors using cyclic voltammetry and it was found that the peak positions were dependent on pH according to Equation 4.2,[237] determined using an Ag^{+}/AgCl reference. The observed processes were therefore assigned to the reduction of carbonyl groups on the carbon nanotubes by the authors. In this current work, as the peaks did not appear to interfere with the peak associated with the reduction of Cr(VI), the acidic solution was used in further studies.

$$E^{0}\ V\ = 0.4001 - 0.0508\ pH \qquad 4.2$$

It is clear that overall, the detection of Cr(VI) was dramatically enhanced at the MWCNTs surface in comparison to the bare GCE by the shift in peak potential of 0.40 V vs. SCE and the increase in peak current of 5.7 fold. In summary, the results showed that that the reduction of Cr(VI) to Cr(III) at the MWCNTs surface exhibited a better defined peak at a more favourable position in comparison to the bare GCE, therefore this modified electrode was deemed promising for the detection of Cr(VI).

4.2.1.1 Investigation of the Parameters Affecting Cr(VI) Reduction at a GCE modified with MWCNTs

The effect of the conductivity of the supporting electrolyte and the pH of the sample solution on the detection of Cr(VI) was explored in the development of the sensor in this section. Where considered appropriate, statistical analysis was carried out on the recorded data in order to verify the significance of the parameters on the detection of Cr(VI). A one way ANOVA followed by a Bonferroni test was performed using Prism (GraphPad Software Inc., CA, USA). Significance levels were calculated based on the probability that the result was caused by varying the specific parameter, with $P < 0.05$ considered to be significant.

4.2.1.1.1 Influence of Solution Conductivity on Cr(VI) Reduction

The supporting electrolyte plays a key role in electrochemical experiments as it is required to provide adequate conductivity for the transport of ions to the electrode surface and for the transfer of electrons from the solution to the working electrode (WE) in the electrochemical cell. A study was therefore conducted comparing the response at the GCE/MWCNTs electrode in electrolyte solutions of varying conductivities. To accurately compare the effects of such parameters on this reduction process, the data are compared from the 10^{th} cycle in 1.00×10^{-3} M Cr(VI) with varying concentrations of Na_2SO_4 supporting electrolyte and the pH was adjusted to 2.0 using concentrated sulfuric acid. Table 4.1 highlights the influence of varying the conductivity on both the potential at which reduction occurred (E_p) and the amount of Cr(VI) that was reduced (I_p).

Table 4.1: Data comparing E_p and I_p values for the reduction of 1.00 × 10^{-3} M Cr(VI) in Na_2SO_4 at 0.10, 0.15 and 0.20 M concentrations.

Supporting Electrolyte	**Conductivity / mS cm^{-1}**	**E_p / V vs. SCE**	**I_p / A**
0.10 M Na_2SO_4	22.0	0.589 (+/- 0.004)	5.38 ×10^{-5} (+/-1.3 × 10^{-6})
0.15 M Na_2SO_4	26.5	0.537 (+/- 0.001)	4.10 ×10^{-5} (+/- 1.17 × 10^{-6})
0.20 M Na_2SO_4	32.8	0.549 (+/- 0.002)	3.26 × 10^{-5} (+/- 1.40 × 10^{-6})

It can be seen from Table 4.1 that changing the concentration of the supporting electrolyte correlatively increased the conductivity of the solutions, which, did not appear to affect the reduction peak potential of Cr(VI) at the modified electrode to the same extent. Statistical analysis showed in this case that the overall difference between the peak potentials was significant (F = 11.33; *d.f.* = 2,10; P < 0.01). However, it was calculated that the difference between the potentials recorded in 0.10 and 0.20 M solutions specifically was insignificant, using Bonferroni post-hoc analysis. As the changes in peak potential did not correlate with the changes in conductivity, it appears that they were not necessarily related and the changes observed could be an effect of slight changes in the pH of the solution, which is further explored in Section 4.2.1.1.2.

The peak currents for the reduction of Cr(VI) surprisingly appeared to correlatively decrease with increasing conductivity of the supporting electrolyte solution, which was also calculated to be significant (F = 32.48; *d.f.* = 2,10; P < 0.0001). Bonferroni post-hoc analysis in this case showed significant differences, (P < 0.0001) between 0.1 and 0.2 M solutions and (P < 0.05) between 0.1 and 0.15 M solutions of Na_2SO_4. This decrease in peak current was unexpected, as it is generally observed that an increase in conductivity would enhance the electron transfer kinetics in a solution, thus

increasing the peak current. It can therefore be assumed that increasing the concentration of Na_2SO_4 may have led to some SO_4^{2-} adsorption on the MWCNTs.[238]

4.2.1.1.2 Influence of pH on Cr(VI) Reduction

It was discussed previously, that the reduction of Cr(VI) to Cr(III) from $Cr_2O_7^{2-}$ requires 6 electrons and 14 protons (Equation 4.1) and therefore is highly influenced by the pH of the sample solution.[239] The potential at which this reduction reaction is observed electrochemically (E_p), is therefore also dependent on the pH of the solution. The E_p-pH relationship of the reduction of Cr(VI) to Cr(III), in the pH range of 0.00 to 6.75 can be described by Equation 4.3:[239]

$$E_p = 1.333 - 0.138\,pH \qquad 4.3$$

The effect of pH on the reduction of Cr(VI) was investigated specifically from pH 1.9 to 4.8 at a GCE/MWCNTs electrode using Na_2SO_4 as a supporting electrolyte modified with appropriate amounts of concentrated H_2SO_4. Figure 4.3 (a) compares voltammograms obtained for 6.00×10^{-3} M Cr(VI) in solutions of pH 1.9, 2.4 and 2.8. The shift in peak potential from 0.65 to 0.44 V vs. SCE with increasing the pH from 1.9 to 2.4 is characteristic of the decrease in H^+ concentration. By further increasing the pH of the solution to 2.8 the reduction peak decreased to 0.39 V vs. SCE, however a second peak also appeared at this pH at 0.13 V vs. SCE, which is further discussed in Section 4.2.1.1.2. The voltammograms seen in Figure 4.3 (b), also compare the reduction of Cr(VI) to Cr(III) at pH 4.8, 3.6 and at 2.8. It can be seen here that only the second reduction peak is observed at the higher pH values and that the peak potential decreased slightly from 0.13 V vs. SCE at pH 2.8, to 0.10 V vs. SCE at pH 3.6. It is noted that no further decrease in peak potential was seen in further increasing the pH to 4.8, indicating that Nernstian behaviour was not being followed.

(a)

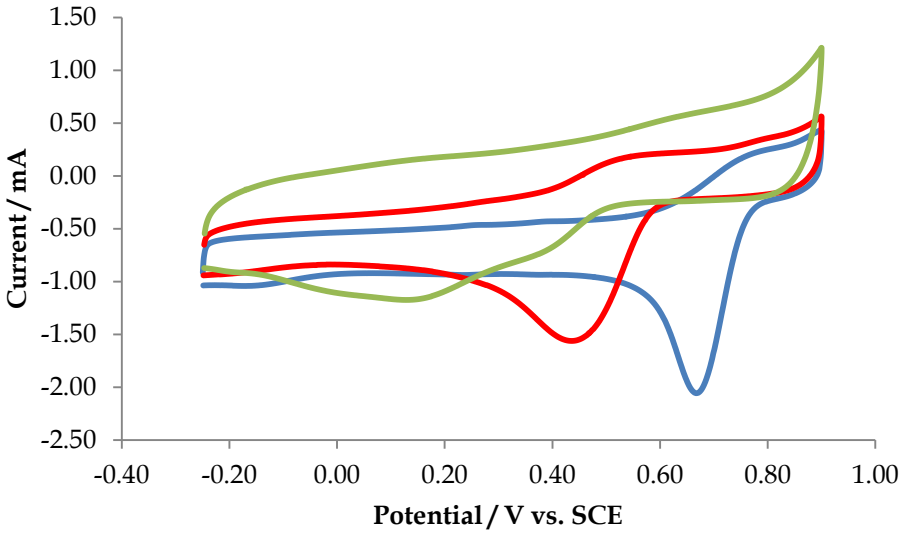

(b)

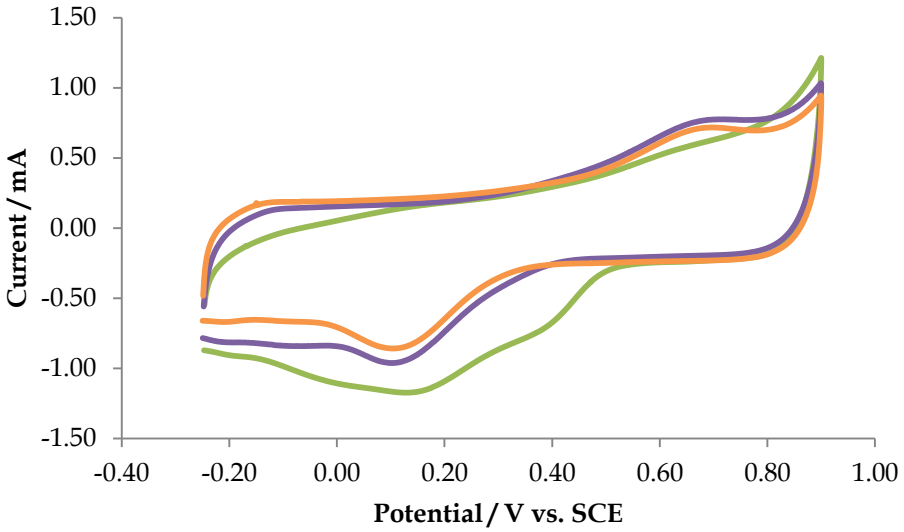

Figure 4.3: Cyclic voltammograms showing reduction of 6.00 × 10^{-3} M Cr(VI) in 0.10 M Na_2SO_4 at 10 mV s^{-1} for (a) pH — 1.9, — 2.4 and — 2.8 and (b) pH — 2.8, — 3.6 and — 4.8.

The peak potentials for the reduction of Cr(VI) to Cr(III), predicted by Equation 4.3 (derived from the Nernst Equation) are shown in Figure 4.4 where they show the linear response of E_p to pH. This relationship is compared to the experimentally recorded potentials (from Figure 4.3) and it can be seen that the linear response was not observed, further indicating that Nernstian behaviour was not followed. The large variation between the predicted potentials and the observed values may be explained to some extent by the reduction pathway followed by Cr(VI) reduction, which is further discussed in the next section.

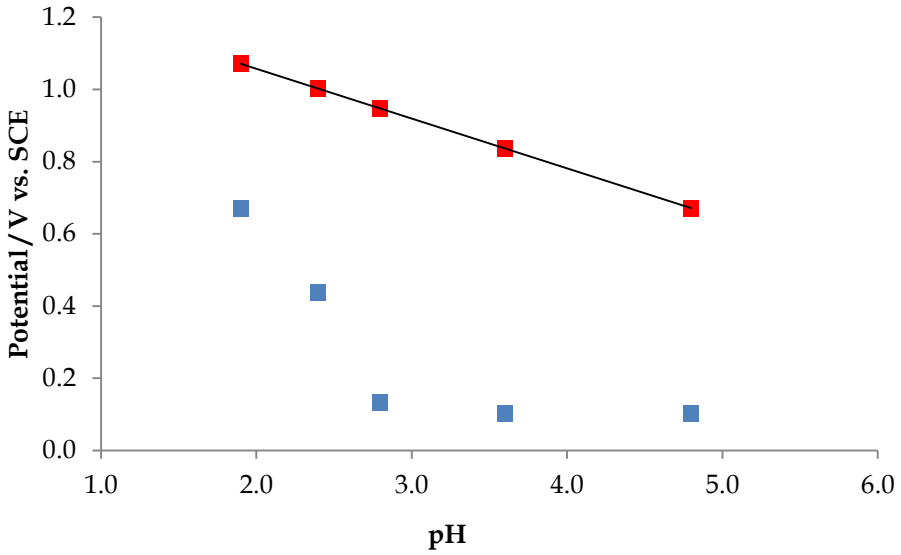

Figure 4.4: Plot comparing the peak potentials ■ predicted and ■ observed as a function of pH for the reduction of 6.00 × 10^{-3} M Cr(VI) in 0.1 M Na_2SO_4 modified with H_2SO_4.

The effects of changing the pH of the solution on the peak currents were also compared as can be seen in Figure 4.5. The lowest currents were recorded for the solution of pH 4.8 and the highest currents were found at pH 1.9, indicating that the reduction of Cr(VI) to Cr(III) at the modified electrode was most kinetically favourable in acidic conditions. It can be seen here that the error in the peak current dramatically increased at pH below 2.0, which as discussed earlier, could indicate the chemical oxidation of MWCNTs by Cr(VI)

which would have altered the concentration of Cr(VI) in solution. The optimum pH for the electrochemical detection of Cr(VI) was therefore chosen to be 2.0.

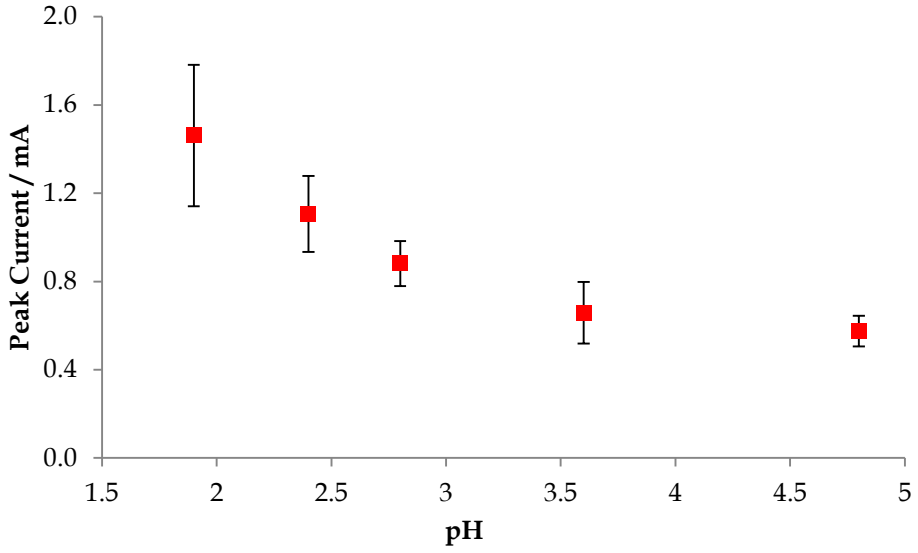

Figure 4.5: Plot of peak current for the reduction of 6.00×10^{-3} M Cr(VI) in 0.1 M Na_2SO_4 modified with H_2SO_4 as a function of pH (n=3).

(i)*Evidence for the Reduction Pathway of Cr(VI) to Cr(III)*

It is clear from the relationship between the reduction peak potential of Cr(VI) and pH in Section 4.2.1.1.2, that the electrochemical reaction does not follow simple Nernstian behaviour at the GCE/MWCNTs electrode. A reduction mechanism of Cr(VI) to Cr(III) was proposed by Welch *et al.*,[235] whereby the initial reduction of Cr(VI) occurred via a rate determining, one electron transfer step to form Cr(V), seen in Equation 4.4. They suggested that at low pH levels, this Cr(V) can rapidly form Cr(III), via a disproportionation reaction illustrated in Equations 4.5 and 4.6. Welch *et al.*[235] observed a pre-shoulder wave for the reduction of Cr(VI) at a GCE similar to that observed in Figure 4.3, in a 0.010 M HCl solution that they did not observe in 0.100 or 0.001 M HCl solutions. They attributed this shoulder peak to the reduction of Cr(VI) to

Cr(V) and found it to be more electrochemically reversible than the more dominant reduction peak.

$$Cr\ VI\ +\ e^{-}\ \rightleftharpoons\ Cr(V) \qquad 4.4$$

$$2Cr\ V\ \rightleftharpoons\ Cr\ IV\ +Cr\ VI \qquad 4.5$$

$$Cr\ IV\ +Cr\ V\ \rightleftharpoons\ Cr\ III\ +Cr(VI) \qquad 4.6$$

or

$$2Cr\ IV\ \rightleftharpoons Cr\ III\ +Cr(V)$$

In the work shown here; at pH 1.9, it can be assumed that the high concentration of protons enabled the fast electron transfer at the MWCNTs modified electrode, which produced a voltammogram with one intense sharp reduction peak, as seen in Figure 4.3 (a). It is therefore possible that by increasing the pH of the solution to 2.8, the rate of reduction of Cr(VI) to Cr(V) decreased and was observed as a pre-shoulder peak at 0.40 V vs. SCE (Figure 4.3 (a)). The rate of disproportionation of Cr(V) to Cr(III) was therefore also decreased so that the direct reduction of Cr(VI) to Cr(III) was observed at 0.13 V vs. SCE.

In comparing the voltammogram at pH 2.8 to those at pH 3.6 and 4.8, seen in Figure 4.3 (b) the rapid reduction of Cr(VI) to Cr(III) was observed with a successive decrease in peak potential, however the pre-shoulder peak representing Cr(VI) reduction to Cr(V) was not observed at higher pH values. This was most likely because the initial reduction of Cr(VI) to Cr(V) is a slow, proton dependent step. In a less acidic medium this reaction would be less

favourable and also be of small magnitude and therefore the peak representing the reduction of Cr(VI) to Cr(V) would have shifted to lower potentials and would possibly occur at the same potential as the reduction of Cr(VI) to Cr(III). This appeared as one reduction peak representing the entire process at 0.10 V vs. SCE for pH 3.6 and 4.8. Figure 4.6 (c) confirms that the reduction of Cr(VI) to Cr(V) had become even more difficult with the increase in pH, as this feature appeared at a less favourable potential. It showed the feature identified previously as the reduction of Cr(V) to Cr(III) to occur as the dominant feature in the plot, and the reduction of Cr(VI) to Cr(V) to occur as a pre-wave that was not observed by cyclic voltammetry.

To investigate the observation of the possible slow reduction step from Cr(VI) to Cr(V) at higher pH values, the voltammograms from Figure 4.3 were further analysed. The change in currents were analysed with respect to the change in potential to identify any secondary processes contributing to the observed reduction peaks. By calculating *dI*, the differential of the current and *dE*, the differential of the potential and plotting *dI*/*dE* as a function of potential, the contributing processes were observed for the reduction of Cr(VI) at pH 1.9, 2.8 and 3.6 (Figure 4.6 (a), (b) and (c)). The results obtained in analysing these data coincided well with the original observations, that in acidic conditions, the reduction of Cr(VI) to Cr(III) is very fast and by decreasing the concentration of protons, the slower reduction of Cr(VI) to Cr(V) can be observed electrochemically. Figure 4.6 (a) illustrates the efficient reduction of Cr(VI) to Cr(III) under acidic conditions (pH 1.9), indicated by the symmetry of the feature, crossing the x-axis at the reduction peak potential and clarifies that only one process can be observed. The increase in pH to 2.8 in Figure 4.6 (b) allowed for a second feature to be observed clearly and highlighted the decrease in peak potential as well as the decrease in currents, which were also observed in the voltammograms (Figure 4.6). This is indicative of the slow reduction of Cr(VI) to Cr(V) and the observation of Cr(V) reduction to Cr(III).

(a)

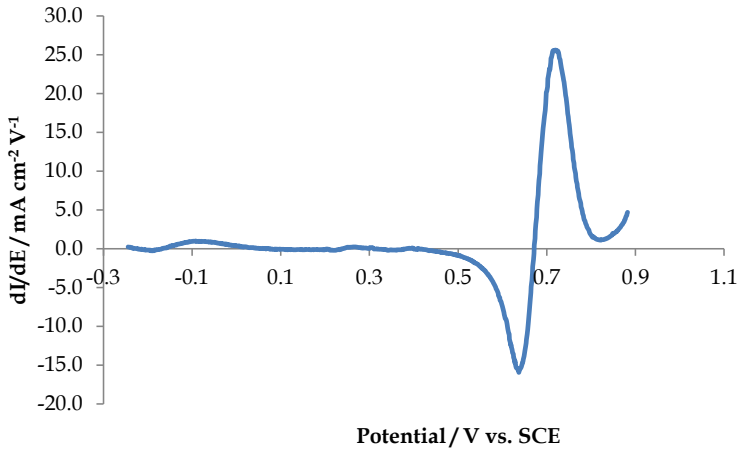

(b)

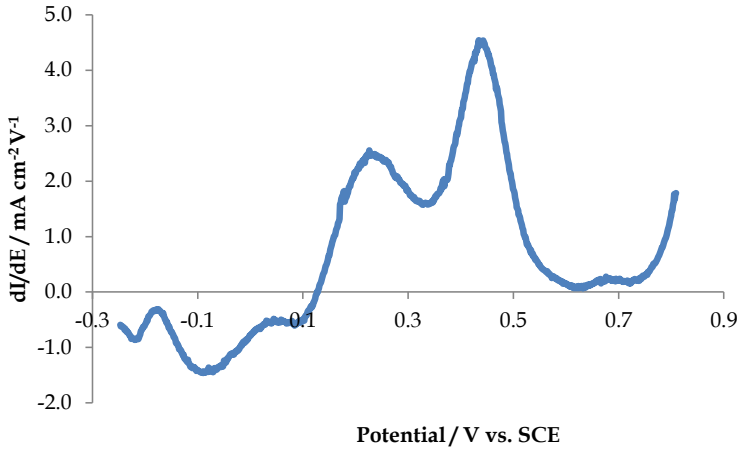

(c)

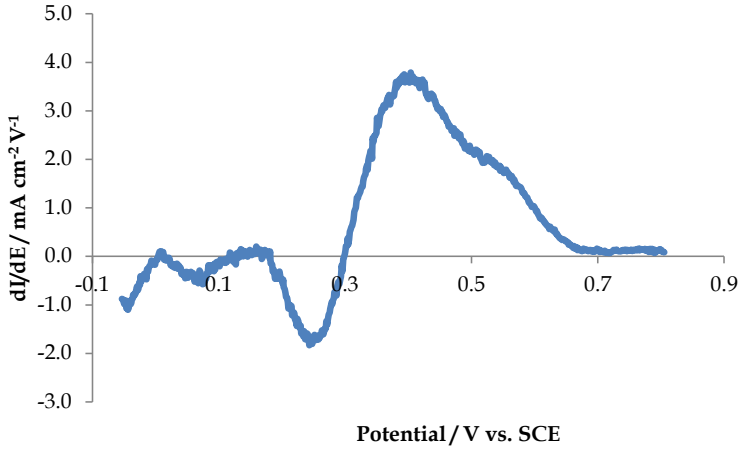

Figure 4.6: Analysis of voltammograms recorded at (a) pH 1.9, (b) pH 2.8 and (c) pH 3.6. Data are presented for the changes in current (dI) with respect to the changes in potential (dE) and are displayed as a function of potential.

4.2.2 Evaluation of a MWCNTs Modified Electrode as an Electrochemical Sensor for Cr(VI) Detection

To evaluate the use of MWCNTs modified electrodes for their use in the detection of Cr(VI), their stability, selectivity and sensitivity were evaluated. This was carried out using a GCE modified as described in Section 4.2.1 whereby 20 μL of a 10 mg mL^{-1} sonicated dispersion of MWCNTs in DMF was cast on a 4 mm diameter GCE (GCE/MWCNTs). The electrode was then dried at an IR lamp. The detection of Cr(VI) was evaluated at this electrode from a solution of $Na_2CrO_7.2H_2O$ in H_2SO_4 at pH 2.0.

4.2.2.1 Stability of a MWCNTs modified Electrode in Cr(VI)

The stability of the peak current for Cr(VI) reduction was monitored as a function of cycle number at the GCE/MWCNTs electrode using cyclic voltammetry. The modified electrode was cycled in 6.00×10^{-4} M Cr(VI) at 10 mV s^{-1} for 100 cycles. It was found that the current dropped by approx. 50% over the first 10 cycles until it reached a steady state, as displayed in Figure 4.7. The currents remained relatively constant at this point over the remaining 90 cycles, showing reasonable stability in the acidic solution. This suggested that the electrode was not spoiled by adsorbing molecules under these conditions. All current responses were therefore recorded after 10 cycles to ensure a stable, reliable value. Reasonable electrochemical stability has also been reported for similarly prepared electrodes both in investigating their capacitive properties,[240] and in the detection of other molecules such as morphine.[241]

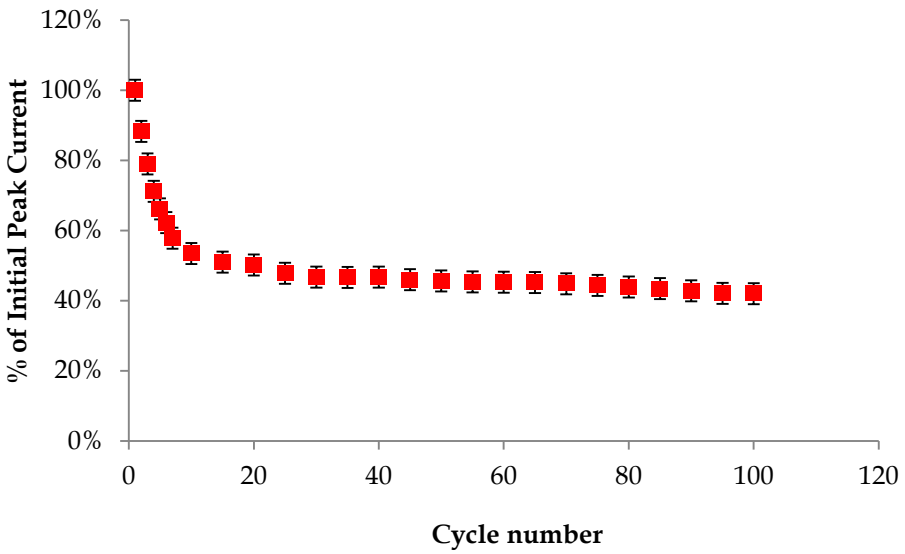

Figure 4.7: Plot representing the stability of the peak current for the reduction of 6.00 × 10^{-4} M Cr(VI) at 10 mV s^{-1} over 100 cycles (n=3) using GCE/MWCNTs. The currents are measured as a percentage of the initial magnitude of the peak and are plot as a function of cycle number.

4.2.2.2 Selectivity of Cr(VI) Detection at a MWCNTs Modified Electrode

The efficiency of the sensor in the presence of potentially interfering substances is very important as the sensor response may be impaired or the electrode surface may be spoiled in real water samples. Nitrate (NO_3^-) pollution is widespread and therefore is very likely to be found in real water samples, according to recent reports from the EPA[12] which show that in Ireland some exceedances of the NO_3^- mandatory limit were recorded in 2010. The presence of Cl^- in water is generally utilised as an indication of pollution from sewage or industrial effluent,[12] therefore it is also likely to be present in contaminated water samples. The efficiency of the sensor in Cr(VI) reduction was also tested in the presence of Cu^{2+} ions as both metal ions are known pollutants from similar industrial waste, for example electroplating and timber treatment facilities.[15] In this section, the interference of Cu^{2+}, Cl^- and NO_3^- were investigated over a range of concentrations based on their individual parametric values. Standard parametric values are the mandatory limits

allowed in drinking water, as outlined by the EPA. The limits for each species are given in Table 4.2, with the respective concentrations in molarity.

Table 4.2: Standard parametric values (g L^{-1}) and the equivalent concentrations (M) for Cr(VI) and the interferants tested.[12]

Substance	**Concentration**	
Chromium	50 µg L^{-1}	9.6×10^{-7} M
Copper	2 mg L^{-1}	3.2×10^{-5} M
Nitrate	50 mg L^{-1}	7.0×10^{-4} M
Chloride	250 mg L^{-1}	7.0×10^{-3} M

The GCE/MWCNTs was prepared as previously described in Section 4.3.1. The modified electrodes were then cycled in a solution containing 4.00×10^{-4} M Cr(VI) to provide an original reduction peak for comparison. The interferants were added to the sample solution in separate experiments and the concentration was increased gradually. The interferant solutions prepared were of relatively high concentration and contained both the supporting electrolyte and 4.00×10^{-4} M Cr(VI) to ensure the composition of the sample solution was not greatly altered. The stability of the sensor at the parametric concentration of each interfering substance was tested by continuous cycling without further addition of the interfering solution.

In all cases, the peak potential of Cr(VI) reduction to Cr(III) did not shift with varying concentrations of interferants, which indicated that the substances did not interfere with the reduction process. The peak currents were also investigated with varying concentrations of each interferant. The recorded data were analysed by comparing the peak current (I_p) measured after each addition of interferant and measuring it as a percentage of the original peak current (recorded prior to the addition of the interferant), according to Equation 4.7. In other words, the original peak current was taken as 100% and the % change in peak current was monitored as a function of increasing

concentration of each interferant. All peak currents were measured after stability had been reached as mentioned previously in Section 4.2.2.1.

$$\% \text{ of Original Ip} = \frac{\text{Ip}_{(\text{Cr VI +Interferant})}}{\text{Ip}_{(\text{Cr VI })}} \times 100 \qquad 4.7$$

The effect of Cl^- on the reduction of Cr(VI) can be seen in Figure 4.8 (a). As the sites of Cr(VI) contamination are generally inland, the concentration of Cl^- is not expected to exceed the parametric value specified by the EPA which takes into account areas of high Cl^- such as coastal areas. The concentrations utilised in this study however ranged from 0.0 to 9.0×10^{-3} M Cl^- to take any exceeding values into account. There was a slight decrease observed in I_p to approximately 75% with the addition of 2.0×10^{-3} M Cl^-, however, the currents remained stable with further additions of Cl^-, which suggested that the modified electrode was not greatly affected by this ion.

The interference of Cu^{2+} ions was tested from 0.0 to 4.2×10^{-5} M as the parametric limit for copper in drinking water is approximately 3.20×10^{-5} M, as set by the EPA. The data obtained in this range are presented in Figure 4.8 (b), where it can be seen that the stability of the peak current was slightly increased by the presence of this substance until the parametric value was exceeded. To further analyse this interferant, statistical analysis was carried out using a paired t-test. It was found that the addition of 6.00×10^{-6} to 4.20×10^{-5} M concentrations of Cu^{2+} had no significant effect on the Cr(VI) reduction peak current with $P > 0.05$ in all cases.

The addition of NO_3^- ion to the Cr(VI) solution was monitored over the concentration range 0.0 to 7.0 × 10^{-4} M. There was some increase in peak current in the case of this substance, suggesting it interfered with the detection of Cr(VI). As can be seen in Figure 4.8 (a), the currents increased to approximately 120% of the original peak current after addition of relatively low concentrations of nitrate. The currents decreased with further increase in NO_3^- concentration and at higher concentrations the currents increased greatly with large errors recorded between repeated experiments. This variable response can be explained by possible adsorption of NO_3^- to the electrode surface and its subsequent reduction which would contribute to the reduction current measured.[242] This indicated that for this modified electrode to work efficiently in the detection of Cr(VI), any nitrate contamination of the sample should be firstly removed.

(a)

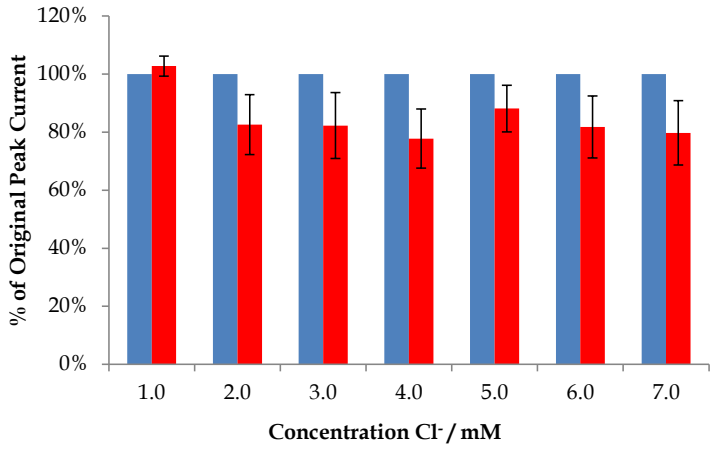

(b)

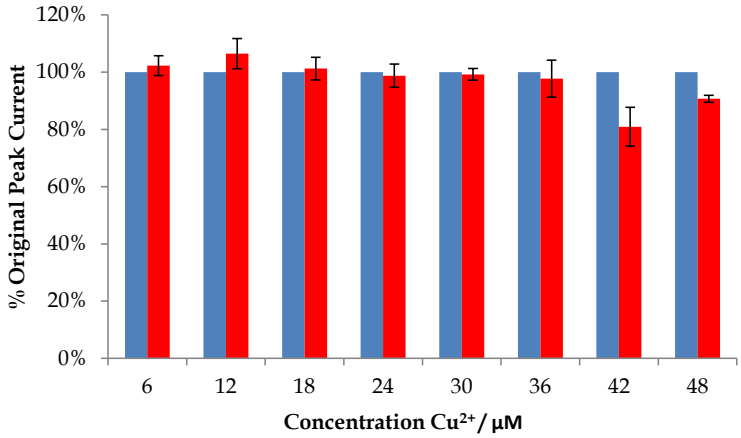

(c)

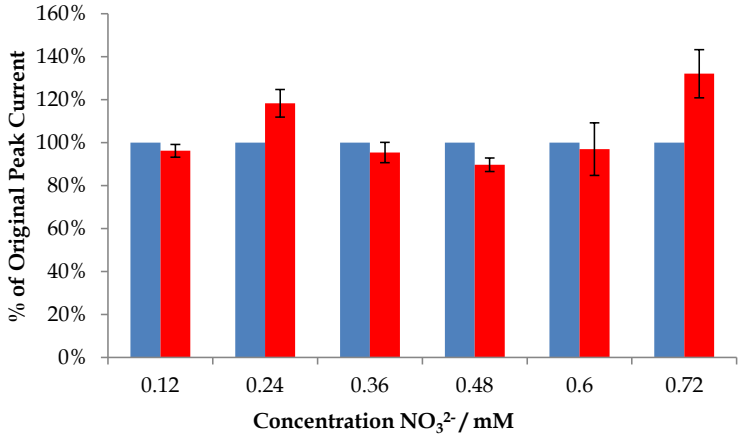

Figure 4.8: Stability of peak current for the reduction of 4.00×10^{-4} M Cr(VI) at 10 mV s^{-1} ■ with increasing concentration of interferant and ■ without interferant for (a) Cl^-, (b) Cu^{2+} and (c) NO_3^-.

The stability of Cr(VI) reduction at the parametric value of each interferant was also tested over 10 cycles. It was found that the Cr(VI) reduction peak current decreased to 90% in the presence of 7.0×10^{-3} M Cl^-, 81% in the presence of 3.2×10^{-5} M Cu^{2+} and 87% in the presence of 7.0×10^{-4} M NO_3^-. This suggests that the GCE/MWCNTs electrode showed reasonable selectivity for Cr(VI) reduction in the presence of these common interferants, but from Figure 4.8 it should be noted that the nitrate response is not likely to be reliable.

4.2.2.3 Limit of Detection of Cr(VI) at GCE modified with MWCNTs

To assess the limits of detection for Cr(VI) at GCE/MWCNTs, a calibration curve was constructed by plotting the peak current response from cyclic voltammetry against Cr(VI) concentration. The calibration curve was constructed for Cr(VI) at pH 2.0 and a linear relationship was observed which can be seen in Figure 4.9. The limit of detection (LOD) at this electrode was determined using Equation 4.8;

$$C_m = \frac{3S_b}{m} \qquad 4.8$$

Where C_m denotes the error in the background signal, S_b is the standard deviation of the blank response and m is the slope of the linear region of the calibration curve. The error in the intercept of the calibration curve was accounted for by assuming the concentration (x value) at which no current was observed (where y = 0), illustrated in Equation 4.9, to be the lowest possible concentration detectable. This value was therefore added to C_m to give a more accurately calculated LOD.

$$y = mx + c \quad \therefore \ @\, y = 0, \ x = \frac{-c}{m} \qquad 4.9$$

Here, y represents the peak current (mA), x indicates the concentration (mM) and m and c are the slope and gradient from the resulting plot of peak current vs. concentration. It was determined using these calculations that the lowest detectable concentration of Cr(VI) at GCE/MWCNTs by cyclic voltammetry was 1.95×10^{-4} M, which is significantly higher than the mandatory limit of 5.2×10^{-6} M set by the EPA. This high LOD can be explained by the poor linearity observed at lower concentrations of Cr(VI) as shown in the plot inset of Figure 4.9.

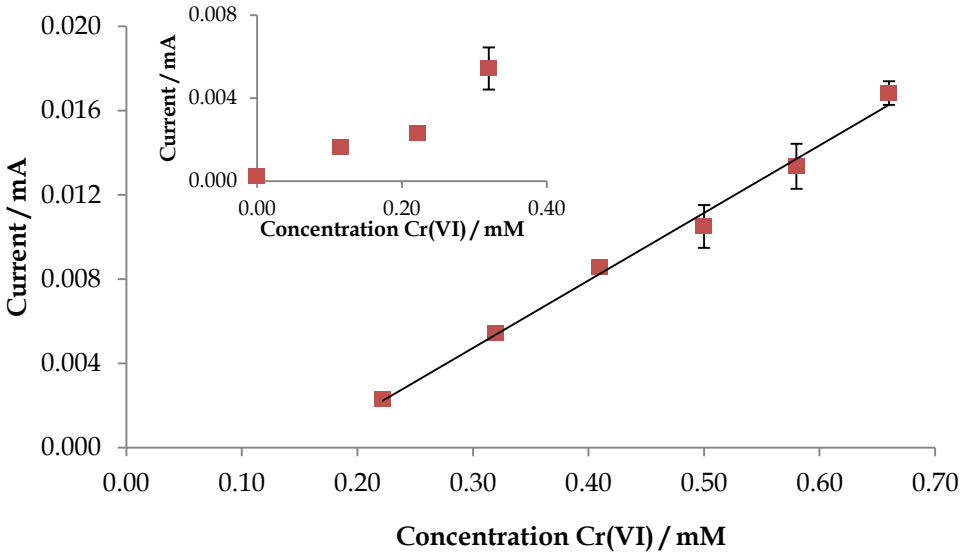

Figure 4.9: Calibration curve measuring the current response from cyclic voltammograms of a GCE modified with 20 µL 10 mg mL^{-1} MWCNTs/DMF at various concentrations of Cr(VI) in H_2SO_4 (pH 2.0) (n=3). $R^2 = 0.99$, $y = 0.0321x - 0.0049$, LOD = 1.95×10^{-4} M.

4.2.2.4 Cr(VI) Detection in Real Water Samples

To investigate the application of this Cr(VI) sensor, real water samples were obtained from Emerald Environmental who obtained the samples from local rivers in north Kildare. The analytical data provided with the samples is illustrated in Table 4.3, showing that samples A and B only differed in their ammonia and chloride content and both had a pH value of ~5.0.

Table 4.3: Analytical data provided with real water samples.

Concentration / mg L^{-1}	**A (pH 4.96)**	**B (pH 4.97)**
Solids	<1	<1
Total Phosphorous	0.05	0.05
Ammonia	0.03	0.02
Nitrate	<0.3	<0.3
Nitrite	<0.002	<0.002
Orthophosphate	0.03	0.03
Chloride	8.4	8.1

The real water samples were tested after modification with concentrated H_2SO_4 to obtain a pH level of 2.0, as this level provided the largest current response for the reduction of Cr(VI) in Section 4.2.1.1.2. Both samples were tested with the addition of various concentrations of Cr(VI) and exhibited reduction peaks at 0.57 V vs. SCE, as was also seen in laboratory prepared samples. The results are displayed in Table 4.4 and calibration curves for both samples with gradients of 0.033 mA mM^{-1} and 0.027 mA mM^{-1} calculated for samples A and B respectively, can be seen in Figure 4.10. These values are similar to the 0.032 mA mM^{-1} gradient calculated for the samples prepared in de-ionised water, showing the similarity between the results (illustrated inset of Figure 4.10). The poor reproducibility in the real water samples however was indicated by the large error bars seen in the calibration curves in Figure 4.10. This signifies that the water samples were unsuitable for the electrochemical

detection of Cr(VI) which may be due to the solid content in both cases, which may have adsorbed some of the Cr(VI).[7]

Table 4.4: Data illustrating the average peak current (n=3) for the reduction of Cr(VI) in real water samples A and B at pH 2.0.

[Cr(VI)] added / M	Average I_p / mA	
	Sample A	**Sample B**
1.7×10^{-4}	1.12×10^{-3}	7.73×10^{-4}
3.2×10^{-4}	4.58×10^{-3}	3.68×10^{-3}
4.7×10^{-4}	9.54×10^{-3}	7.23×10^{-3}
6.0×10^{-4}	1.58×10^{-2}	1.30×10^{-2}

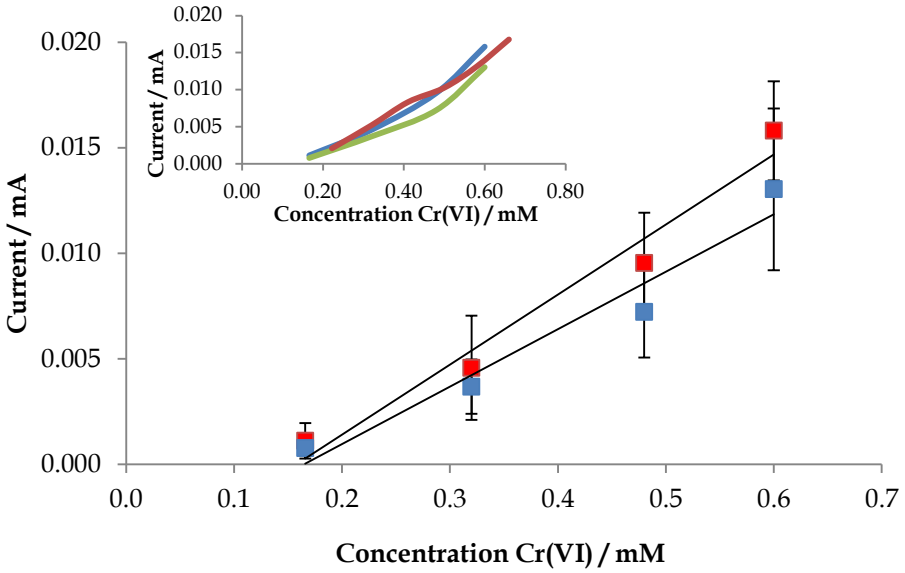

Figure 4.10: Calibration curves obtained from cyclic voltammograms of GCE/MWCNTs in real water samples ■ A (m = 0.033 mA mM^{-1}) and ■ B (m = 0.027 mA mM^{-1}). Plot inset compares calibration curves of real water samples — A and — B to — de-ionised water sample from Figure 4.9 (m = 0.032 mA mM^{-1}).

4.2.3 The Screening of Various Electrode Materials for the Electrochemical Detection of Cr(VI)

The electrochemical reduction of Cr(VI) to Cr(III) is well known to occur at a range of electrode substrates such as glassy carbon and gold.[235] In this section a study was carried out to investigate if the electrochemical response analysed in Section 4.2.2 could be enhanced to improve the detection of Cr(VI). A number of different approaches were attempted and in this Section, the preparation and characterisation of the electrode materials and a voltammetric study, to screen their ability to sense Cr(VI), is described.

4.2.3.1 Detection of Cr(VI) at a Gold Electrode Modified with MWCNTs

As the method employed for the modification of a GCE was shown to be successful in Section 4.3.1.1, the same procedure was carried out using a gold substrate (Au/MWCNTs). The Au electrode was polished and cast with 20 µL MWCNTs/DMF from a 10 mg mL^{-1} solution. The electrode was dried under an IR lamp and SEM micrographs were again obtained as can be seen in Figure 4.11. The images show that a similar coverage of the Au electrode surface was obtained as was seen previously for the GC substrate in Figure 4.1.

(a) (b)

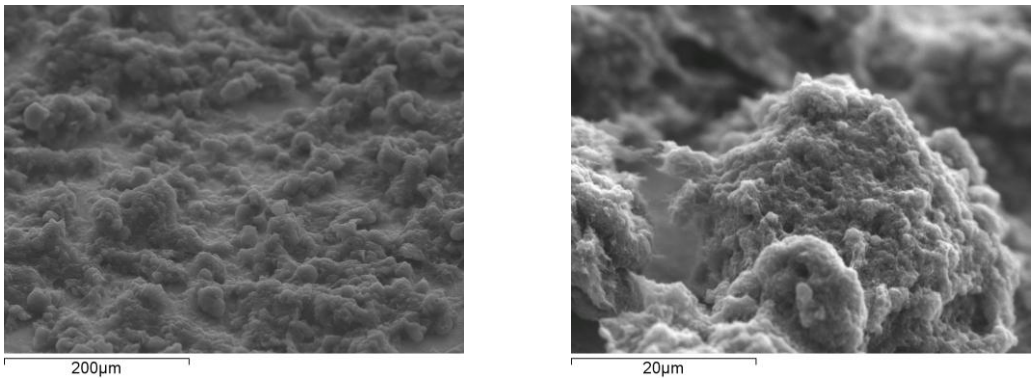

Figure 4.11: High resolution SEM micrographs at different magnifications (a) and (b) showing a 20 µL cast on a 4 mm diameter Au surface from 10 mg mL^{-1} MWCNTs/DMF suspension.

The reduction of Cr(VI) at the Au/MWCNTs electrode is compared to that at a bare Au electrode in Figure 4.12 with the relevant properties tabulated inset. The reduction peak appears at 0.41 V vs. SCE at the bare Au electrode, which shows a more efficient reduction of Cr(VI) in comparison to that seen at the bare GCE in Section 4.3.1.1, as it appears at a more favourable potential with a more symmetrical and intense peak. This is also comparable to the study by Welch *et al.*[235] The reduction peak at the Au/MWCNTs electrode appears at a more favourable potential of 0.57 V vs. SCE, in comparison to that seen at the bare electrode, however the peak currents in this case appear to be enhanced only by 1.6 fold at the electrode modified with MWCNTs. The reversible peaks at approx. 0.40 V vs. SCE are visible again at the Au/MWCNTs electrode, similar to that seen in Figure 4.2 due to the presence of oxygen containing molecules.[237]

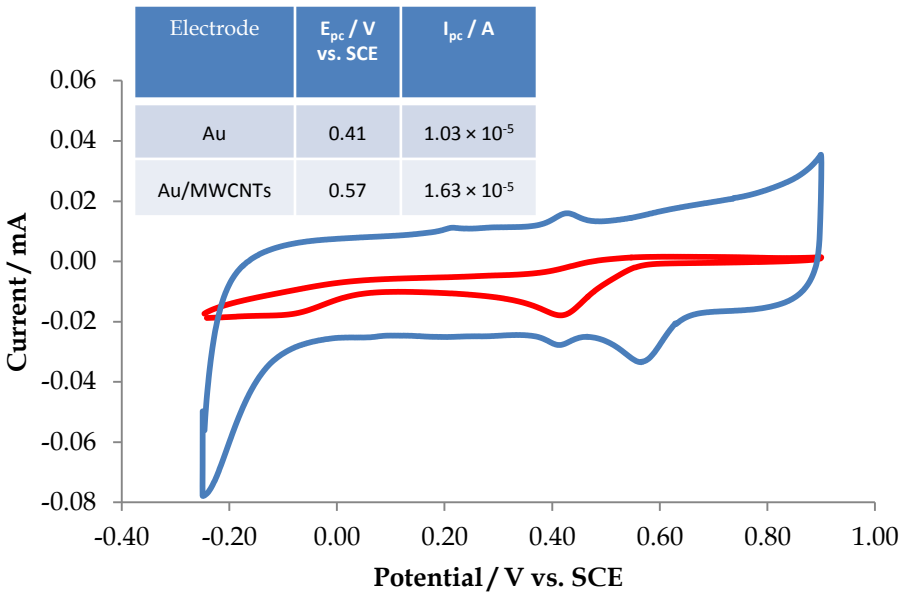

Figure 4.12: Cyclic voltammograms of — bare Au and — Au modified with 20 µL 10 mg mL^{-1} MWCNTs in DMF recorded in 5.0×10^{-4} M Cr(VI) in H_2SO_4 pH 2.0, at 10 mV s^{-1} The relevant electrochemical properties are tabulated inset.

It can be seen that the reduction peak at the Au/MWCNTs electrode (0.57 V vs. SCE), is very similar in shape and position to that seen in Section 4.3.1.1 at GCE/MWCNTs. The peak currents are also comparable at both substrates when modified with MWCNTs. This highlights that the MWCNTs dominated the detection at both modified electrodes, irrespective of the substrate. The peak currents at the bare Au substrate appear to be comparable to that seen at the Au/MWCNTs, however it is noteworthy that the reproducibility of the bare Au electrode was poor in comparison to the MWCNTs modified electrodes.

4.2.3.2 *Detection of Cr(VI) at a Gold Electrode Modified with MWCNT-Polypyrrole Composites*

Many literature studies report the modification of electrodes with MWCNTs by drop casting the MWCNTs directly on the electrode surface from solution but there are some concerns about the electrode stability. One means reported of overcoming this issue is to immobilise the MWCNTs in a polymer matrix which is strongly adherent to the electrode surface. A number of studies have investigated the use of polypyrrole in this regard, for example Prakash *et al.*[243] used MWCNT drop cast on a polypyrrole film as a nitrous oxide (NO) sensor which showed evidence of catalysis and increased surface area. The catalytic properties of such CNT/polypyrrole composites are reportedly due to the conductivity of the polymer providing an enhanced connection for the MWCNTs to the underlying substrate.[244] Another method employed by many researchers is similar to that reported by Arami *et al.*[245] who deposited polypyrrole on a copper substrate in the presence of MWCNTs, forming a co-deposited composite. The researchers observed the deposition of polypyrrole on the nanotubes and used thermo-gravimetric analysis to show that the incorporation of nanotubes enhanced the thermal stability of the polymer film.

In this section, MWCNT-polypyrrole composite electrodes were formed in two ways; the first composite was prepared by modifying a gold substrate with a polypyrrole film and then drop casting a layer of MWCNTs on the surface (Ppy/MWCNTs), using an adaptation of the method outlined by Prakash *et al.*[243] The second composite formed was prepared by polymerisation of pyrrole in the presence of MWCNTs to form a co-deposited composite (PpyMWCNTs) similar to that carried out by Arami *et al.*[245]

4.2.3.2.1 Formation and Characterisation of Ppy and PpyMWCNTs

The Ppy and PpyMWCNTs films were electrochemically deposited on the electrode surface from 0.10 M pyrrole in H_2SO_4 (pH 2.0) using a potentiostatic method which involved the application of a constant potential of 0.75 V vs. SCE to the gold WE surface to initiate oxidation of the monomer and sustain the growth of the polymeric film.[171] The potential was applied until a specific charge of 0.03 C was consumed which allowed for the production of uniform polymers in each experiment.[246] The current values given for the deposition of both polymers has been normalised to the geometric surface area of the WEs.

In the first instance, a Ppy film was deposited and in the second case, a PpyMWCNTs film was deposited. The growth profiles outlined in Figure 4.13 (a) and (b) compare the electropolymerisation of pyrrole, to that containing 0.07 mg mL^{-1} MWCNTs. Figure 4.13 (a) shows the currents monitored as a function of polymerisation time where it can be seen that that the initial current for electrodeposition was slightly lower for the solution containing MWCNTs. Similar results were obtained by Hu *et al.*[247] in the co-deposition of acid-treated MWCNTs and non-conducting polymers which they ascribed to the "inferior mobility of the anionic CNTs". Although the MWCNTs in this work were unfunctionalised, it is likely that sonication in H_2SO_4 introduced some anionic moieties to the ends of the nanotubes and/or to defect areas,[72, 248] allowing them to partially dope the Ppy.

Higher currents were observed from 0.1 s onwards for the electrodeposition of the polymer from the solution containing MWCNTs and H_2SO_4 (1.67×10^{-2} A cm^{-2}) compared to that deposited from H_2SO_4 alone (1.24×10^{-2} A cm^{-2}) which is illustrated in Figure 4.13 (a). This is consistent with the work reported by Hu *et al.*[247] who also observed higher currents for the electrodeposition of the polymer in comparison to that prepared from KCl. This can likely be attributed to the physical entrapment of MWCNTs during polymerisation increasing the conductivity of the resultant polymer with possible partial doping of the

polymer by the MWCNTs. Snook *et al*.[151] have observed the doping of Ppy with oxidised carbon nanotubes. This group accredit the increase in the conductivity of the material to the incorporation of MWCNTs into the polymer structure created, as they provided ion and electron conducting paths in the polymer matrix. The nanotubes used in the present research were not pre-treated and this should have led them to exhibit a higher aspect ratio which is known to contribute to the conductivity of resulting composites as discussed by Bai *et al*.[38]

The charge-time plot in Figure 4.13 (b) shows a linear relationship for both polymers between the charge consumed and polymerisation time. This indicates that polymerisation occurred efficiently and formed a uniform film across the substrate in both cases. The slope of the charge-time plot for the Ppy film was 1.15×10^{-2} C cm^{-2} s^{-1}, lower in comparison to that for the Ppy film containing MWCNTs which was 1.56×10^{-2} C cm^{-2} s^{-1}, indicating a faster rate of polymerisation. This can be attributed to the aggregation of MWCNTs at the electrode/electrolyte interface. Due to the immense length to diameter ratio of MWCNTs, it is likely that their large active surface area would allow for faster formation of the polymer film.[245] Moreover, the mesoporosity of MWCNTs would make the resultant surface more accessible to the electrolyte, which would in turn increase the rate of polymerisation.[39] Khajeamiri[249] similarly used H_2SO_4 as a supporting electrolyte in depositing the conducting polymer polyaniline, modified with MWCNTs, and found the incorporation of MWCNTs to increase the surface area of the polymer during deposition.

(a) (b)

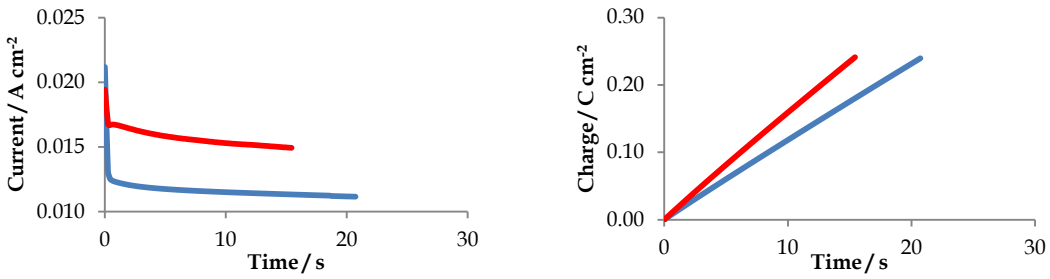

Figure 4.13: The electropolymerisation of 0.1 M pyrrole in 0.1 M H_2SO_4 — without and — with 0.07 mg mL^{-1} MWCNTs, grown at 0.75 V vs. SCE on a 4 mm diameter gold substrate displayed as (a) current vs. time and (b) charge vs. time.

The reproducibility of both films was tested to ensure that the electrochemical polymerisation of the pyrrole solution produced consistent films, particularly with the incorporation of MWCNTs. The polymerisation data of three repeated experiments for both Ppy and PpyMWCNTs are presented as current-time plots in Figure 4.14 (a) and (b) respectively. For each repeat of the experiment, the gold substrate was polished (as outlined in Chapter 2) and a fresh polymerisation solution was prepared. The data for the three repeated experiments almost directly overlapped in all cases, showing that the electrochemical polymerisation of the solutions provided reproducible films.

(a) (b)

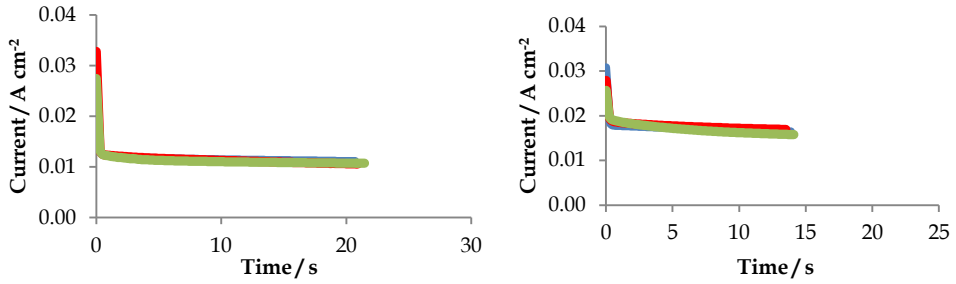

Figure 4.14 Current-time plots showing the reproducibility of (a) Ppy growth and (b) PpyMWCNTs growth on a gold substrate. All polymers were grown at 0.75 V vs. SCE to 0.03 C from 0.10 M pyrrole in 0.10 M H_2SO_4 solutions with (b) containing 0.07 mg mL^{-1} MWCNTs.

The Ppy films prepared from H_2SO_4 with and without MWCNTs were compared for their electrochemical activity using cyclic voltammetry in H_2SO_4 (pH 2.0), seen in Figure 4.15. Redox waves arose in both polymers as they were cycled from their oxidised to neutral forms, due to anion intercalation and loss, to balance the charge. The cyclic voltammograms of both polymers were relatively similar and showed the general shape of an anion exchange polymer, whereby the oxidation peak is distinctly sharper than that of the reduction peak. This has been attributed to the high mobility of the anions and to the ionic concentration gradient between the bulk electrolyte and the polymer.[250] Therefore, the oxidation of the polypyrrole film involving the incorporation of SO_4^{2-} ions from the solution phase into the film is a relatively fast and efficient process, whereas the reduction of the polymer is slower due to the slow release of the SO_4^{2-} ions. Similar voltammograms were observed by Mangold *et al.*[250] for Ppy, using Na_2SO_4 as an electrolyte. This would indicate that the major dopant to balance the charge for the PpyMWCNTs film is the SO_4^{2-}. This would suggest that the MWCNTs are mainly neutral in charge and are just held within the PPy film due to physical entrapment.

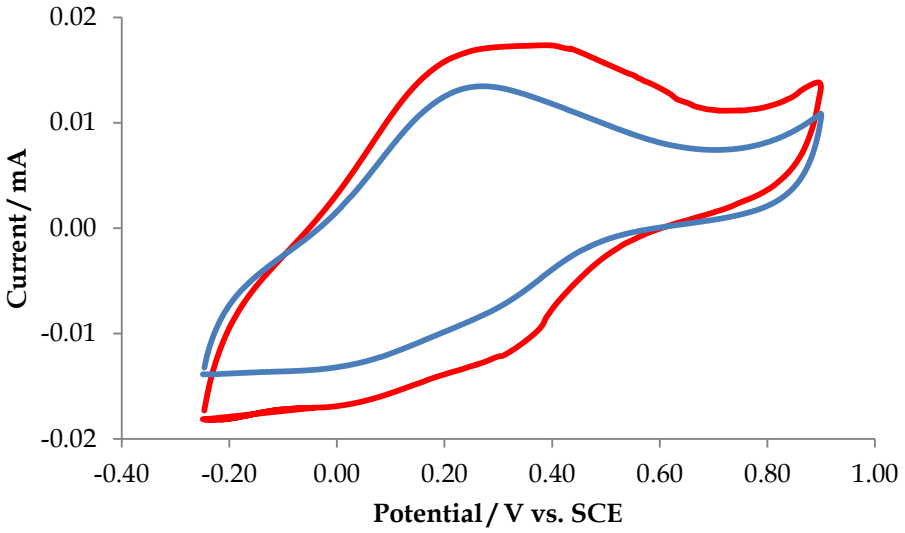

Figure 4.15: Cyclic voltammograms of — Ppy and — PpyMWCNTs cycled in H_2SO_4 (pH 2) at 10 mV s^{-1}.

Direct evidence for the incorporation of MWCNTs into the Ppy for the PpyMWCNTs film was obtained using SEM. The images of both the PpyMWCNTs and the Ppy surfaces obtained using SEM are displayed in Figure 4.16. The polymers in this case were grown to a higher charge (0.30 C) to produce thicker films, as thinner films were difficult to image. It can be assumed that for the thinner polymer the morphology was somewhat different.[138, 139] However, one aim of this characterisation was to confirm that Ppy maintained its regular cauliflower morphology when grown in the presence of MWCNTs, which would not likely depend on the film thickness. The image in Figure 4.16 (a) shows the overall surface morphology with agglomerations of MWCNTs which appeared to be coated by the PPy visible throughout the film. Snook *et al.*[151] recorded SEM micrographs of a composite consisting of polypyrrole and acid-treated MWCNTs prepared by cyclic voltammetry, shown in Figure 4.17 (a) and (b). They also observed agglomerations of the MWCNTs across the polymer surface, although these appeared to be smaller in size compared to those observed in the current work. This is likely due to the fact that the MWCNTs used here were not acid-

treated and so even though sonication was employed to disperse the MWCNTs in solution, they would have a greater probability of forming agglomerations even in well dispersed solutions.[53]

On closer inspection of the agglomerations in the work presented here, it was found that many of the agglomerated nanotubes formed distinct spherical clusters which were coated in Ppy (Figure 4.16 (b)). The mesoporous nature of the MWCNTs could be identified in Figure 4.16 (c) where pores between the networked agglomerations of MWCNTs were coated in Ppy. Very similar images were obtained by Arami *et al.*,[245] who deposited PpyMWCNTs films on a copper substrate using a potentiometric technique. The cauliflower morphology observed in Figure 4.16 (d), a magnification of the coated aggregate, was identical to that observed in the Ppy film produced without MWCNTs, seen in Figure 4.16 (e) and (f). This morphology is characteristic of Ppy electrosynthesis in aqueous solutions,[132,251] indicating that the MWCNTs did not alter the growth morphology.

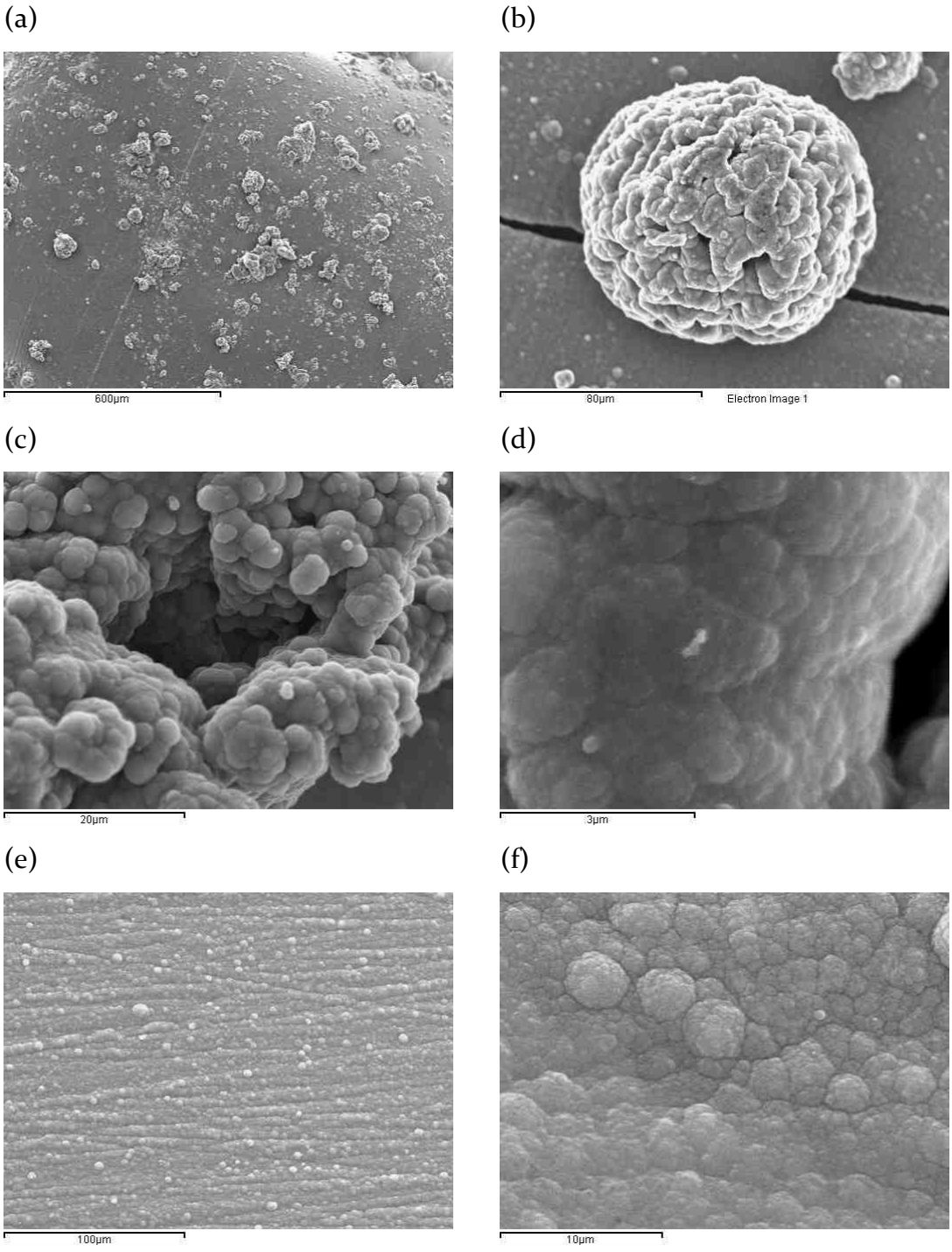

Figure 4.16: High resolution SEM micrographs of (a) – (d) PpyMWCNTs and (e) & (f) regular Ppy film. Both films grown on a gold substrate at 0.75 V vs. SCE to a charge of 0.30 C from 0.10 M pyrrole solutions in H_2SO_4 at pH 2.0, with (a) – (d) containing 0.07 mg mL^{-1} MWCNTs.

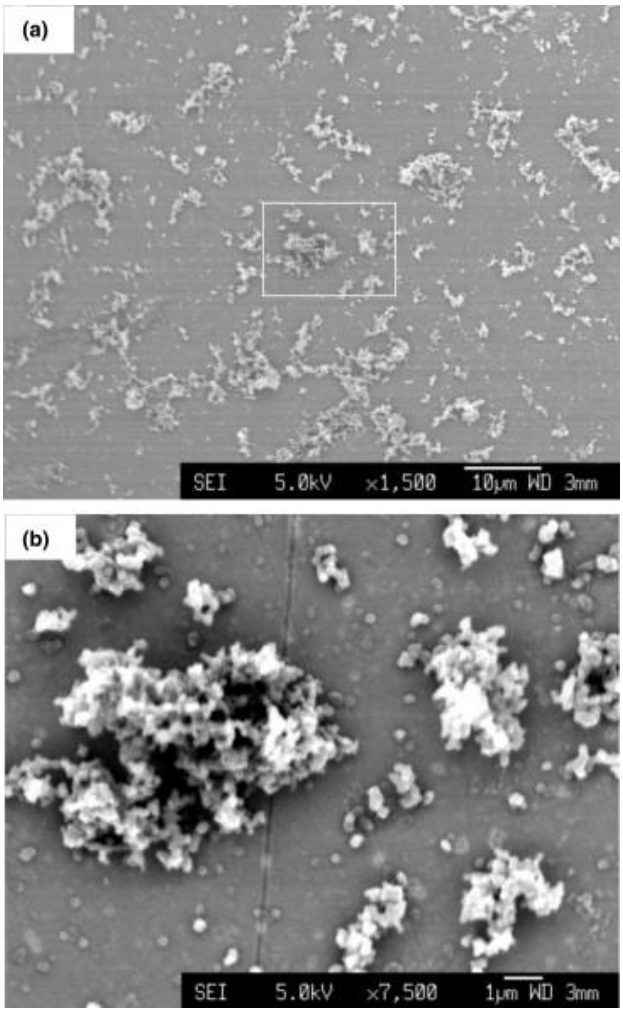

Figure 4.17: SEM images reprinted from Snook *et al.*[151] showing (a) a pyrrole/carbon nanotube layer deposited onto the quartz crystal using cyclic voltammetry. In (b) is shown the details of the region enclosed in the box indicated in (a).

EDX analysis was carried out on two differing regions of the PpyMWCNTs film prepared in this work, and is displayed in Figure 4.18 (a) and (b). Analysis of an aggregation of MWCNTs coated in Ppy is shown in the spectrum in Figure 4.18 (a) and in an aggregate free region in the spectrum in Figure 4.18 (b). A signal for sulfur was present in both spectra confirming that the SO_4^{2-} ion was extensively doping the PPy as previously indicated by the voltammogram of the PpyMWCNTs film.

(a) (b)

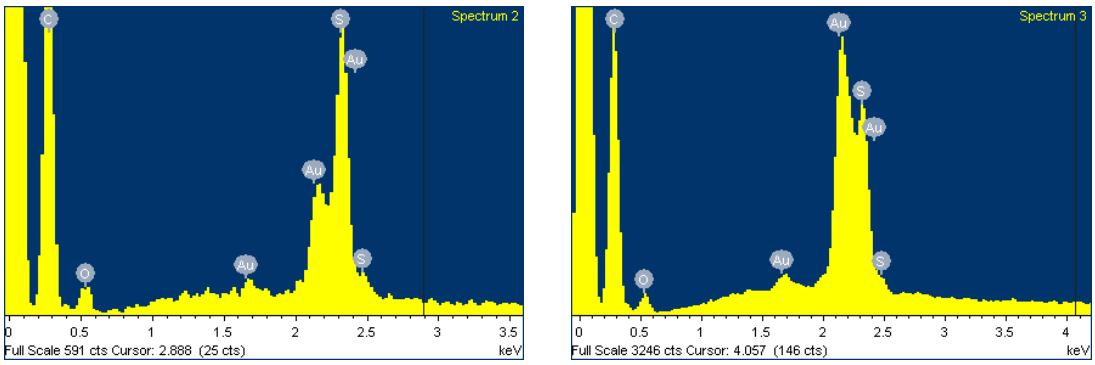

Figure 4.18: EDX spectra of PpyMWCNTs (a) obtained at the rough, clustered region of the surface and (b) obtained from the smooth region of the surface. Au peaks arise as the film was sputtered coated with gold before EDX analysis.

4.2.3.2.2 Formation and SEM characterisation of Ppy/MWCNT

In the modification of GC with the Ppy/MWCNTs film; the Ppy polymer was grown as outlined above, with only H_2SO_4 used as a supporting electrolyte and the coating was rinsed with distilled water. A 10 µL aliquot was drop cast onto the surface from a 7.0 mg mL^{-1} MWCNTs dispersion in DMF and the surface was dried under an IR lamp. High resolution SEM images were obtained of the formed films (Figure 4.19), and show that the MWCNTs formed aggregates on the surface (illustrated in Figure 4.19 (a)). Upon magnification of these aggregates (Figure 4.19 (b) and (c)) the structure of the aggregates appeared to be quite irregular, having both smooth and porous regions. Further magnification of these areas however revealed networked entanglements of nanotubes in the agglomerations of MWCNTs (Figure 4.19 (d),(e) and (f)). These micrographs provided an indication of the magnitude by which the surface area increased with the addition of MWCNTs to the polymer surface and highlighted the morphology of the resulting surface which suggests an improved wettability of the electrode.

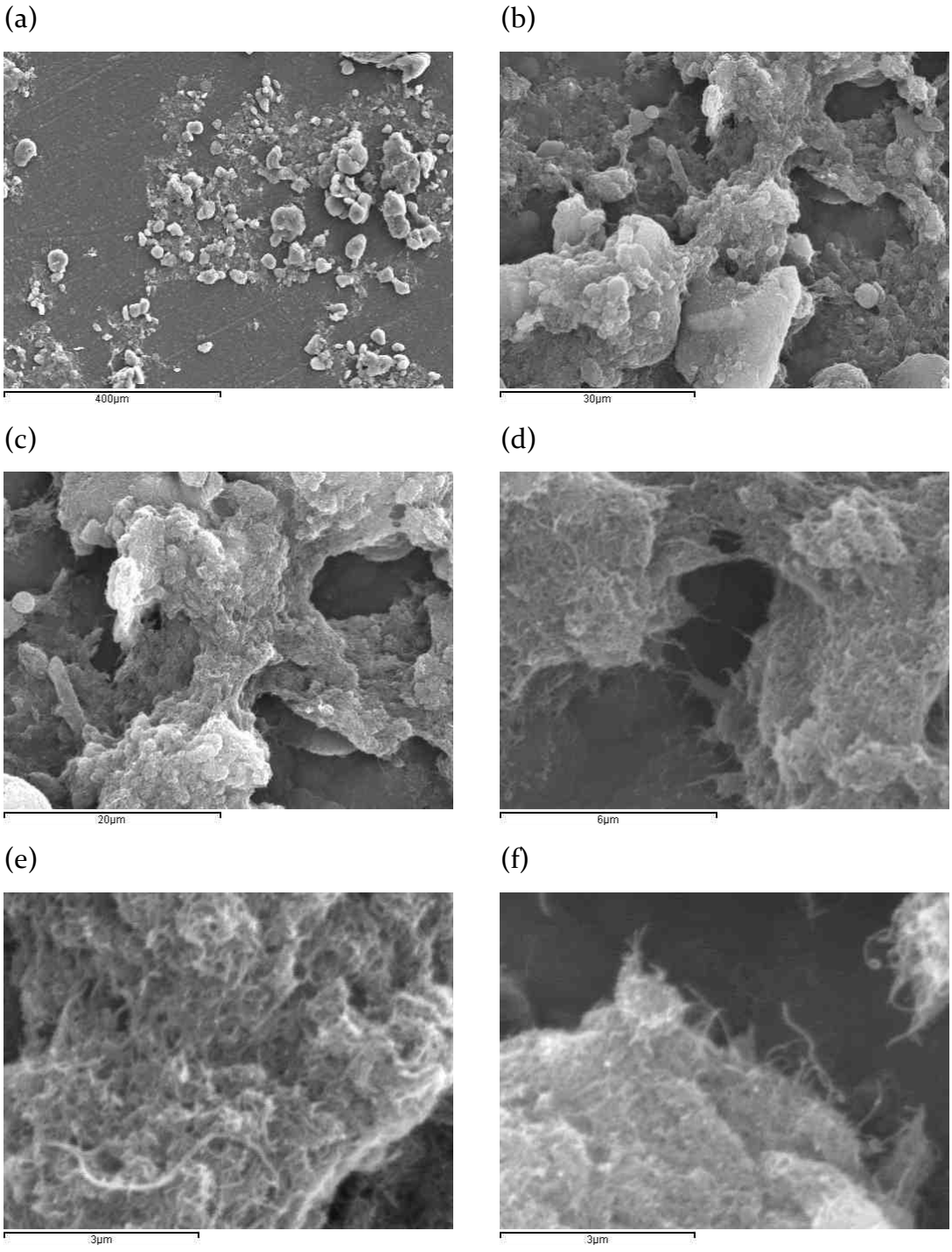

Figure 4.19: High resolution SEM micrographs of the Ppy film modified with cast MWCNTs at various magnifications (a) – (f). The polypyrrole film was deposited at 0.75 V vs. SCE to a charge of 0.30 C from a solution containing 0.1 M pyrrole in H_2SO_4 at pH 2.0. A volume of 10 µL was cast on the surface from a 7.0 mg mL^{-1} MWCNTs suspension.

4.2.3.2.3 *Chromium(VI) Detection at Electrodes modified with MWCNTs Composites*

A number of researchers have used Ppy modified electrodes for the sensing of Cr(VI). For example; Ansari *et al.*[252] developed an ion selective electrode by growing a Ppy film in the presence of CrO_4^{2-} under basic conditions and Ge *et al.* [253] used an overoxidised Ppy and the Cr(VI) was pre-concentrated at the polymer surface by holding the electrode at a potential of 0.80 V vs. SCE. It is of note that the sensors described above are all based on the ability of Ppy to adsorb the Cr(VI) anion. The ability of PPy to adsorb Cr(VI) is well known from remediation studies in which the anion exchange properties can assist in the removal of Cr(VI) from waste water.[254] This adsorption was therefore taken into consideration as a possible method of detection at the polymer-modified electrodes. A further concern with using a Ppy modified electrode for Cr(VI) detection is that it is also known that, as Cr(VI) is a strong oxidising agent, it can spontaneously (or upon electrochemical reduction of the Ppy) oxidise Ppy, as shown by Wei *et al.* and Senthurchelvan *et al.* repectively.[53,50] This chemical reaction could compete with the electrochemically monitored electron transfer process and alter the concentration of Cr(VI) in the sample solution. In order to avoid the chemical reduction of Cr(VI) by the PPy-MWCNT composites, prior to cycling in the Cr(VI) solution, both polymers were cycled in the supporting electrolyte, H_2SO_4, to partially overoxidise the Ppy.[255, 256] The Ppy-MWCNT were cycled in H_2SO_4 at pH 2.0 between -0.25 and +0.90 V vs. SCE for 10 cycles at 10 mV s^{-1}. A striking reduction in the capacitance current was observed, indicating that the polymer conductivity had decreased, which in turn would limit the chemical reduction of Cr(VI).

The detection of Cr(VI) at both MWCNTs composites; PpyMWCNTs and Ppy/MWCNTs is compared in Figure 4.20 and the relevant electrochemical properties can be seen in the table inset. The peak potential for the reduction of Cr(VI) occurred at 0.47 V vs. SCE for the PpyMWCNTs modified electrode

and was shifted to a more positive potential of 0.65 V vs. SCE at the Ppy/MWCNTs modified electrode. This suggested that the electron transfer was further facilitated by the direct access of Cr(VI) to the MWCNTs on the electrode surface, in comparison to the PpyMWCNTs film. A partially overoxidised Ppy modified electrode was also tested for its ability to electrochemically reduce Cr(VI) to Cr(III). The polymer displayed a reduction peak for Cr(VI) at 0.40 V vs. SCE which is the same potential as that observed at the bare Au electrode in Section 4.2.3.1. This suggested that the polymer was sufficiently degraded so that any reduction of Cr(VI) was actually occurring at the gold substrate.[256] This did not appear to be the case for the electrode modified with Ppy/MWCNTs, as the reduction peak potential was more favourable than seen previously for the MWCNTs modified Au electrode. This suggested that the polypyrrole film assisted in the reduction of Cr(VI) despite its pre-treatment.

In comparing the peak currents (Table inset of Figure 4.20), observed at the PpyMWCNTs film to those at the Ppy/MWCNTs modified electrode, there is an impressive enhancement with the latter modification. The dramatic improvement in detection may be partially accredited to the increased wettability of the MWCNTs as they were at the electrode/electrolyte interface, allowing for their properties to be fully exploited. By casting MWCNTs at the polymer/electrolyte interface in the case of Ppy/MWCNTs, the mesoporous morphology and increased surface area of the nanotubes likely enhanced the electrolyte access, thus improving the ionic conductivity of the surface.[146] This would account for the 4.7 fold increase in capacitive currents and the increase in faradaic currents from 6.97×10^{-6} to 1.67×10^{-5} A (2.4 fold) observed at the Ppy/MWCNTs film. However, the Ppy film without the incorporation of MWCNTs was not completely overoxidised, as evident by the Ppy redox currents seen in Figure 4.20. This suggested that chemical reduction of Cr(VI) by the polymer may have occurred and this would alter the concentration of Cr(VI) in the sample solution, making electrochemical detection unreliable.

Further studies using Ppy were not pursued due to this contribution which is further discussed later in Section 4.2.3.4.

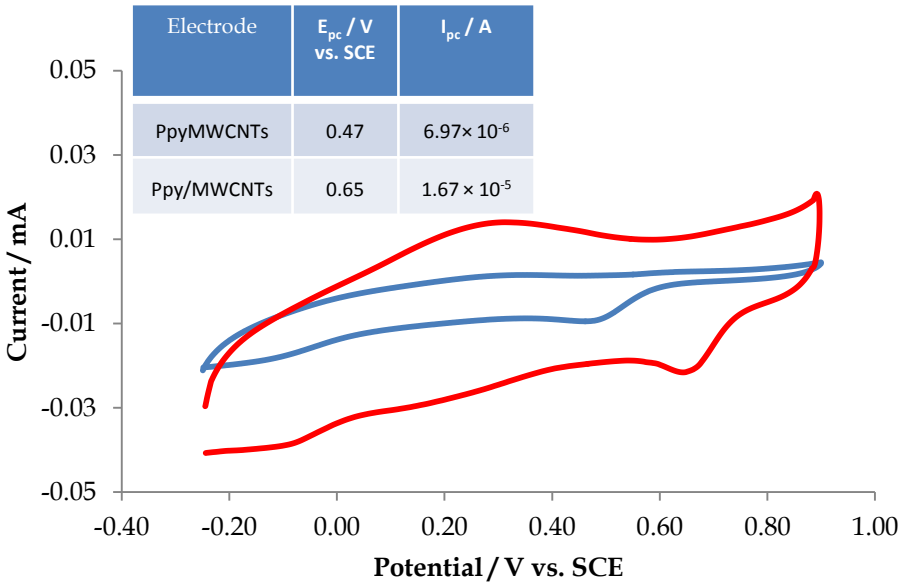

Figure 4.20: Cyclic voltammograms of modified gold electrodes in a 6.0 × 10^{-4} M Cr(VI) in H_2SO_4 (pH 2.0) at 10 mV s^{-1}. Plot shows gold electrode modified with — PpyMWCNTs compared to — MWCNTs/Ppy.

4.2.3.3 *Detection of Cr(VI) at a Gold Electrode Modified with Gold Nanoparticles and MWCNTs*

The modification of MWCNTs with gold nanoparticles (AuNPs) has been implemented in this section with the aim of improving the LOD of Cr(VI). AuNPs were chosen as a means of modification due to the impressive peak currents observed in Section 4.2.3.1 at an Au compared to a GC substrate. It has been reported that Au can exhibit catalytic behaviour when prepared as particles in the nanometre range,[257] which spurred the use of AuNPs in sensing. The modification of MWCNTs with AuNPs has been reported for many uses such as protein detection,[258] humidity detection,[259] and mercury ion detection.[79] It has been reported that AuNPs can increase the conductivity and catalytic redox activity of MWCNTs,[243] and they have been described as electron antennae on MWCNTs when shown to further improve in the efficiency of electron transfer.[80] In 2007, Liu *et al.*[260] reported the detection of Cr(VI) at a screen-printed electrode modified with AuNPs in a medium with a pH value of 4.6. The detection was based on the adsorption of Cr(VI) which they did not observe at lower pH values, and was enhanced 10 fold in comparison to that observed at the solid Au substrate. As Zakharova *et al.*[261] have more recently shown the detection of Cr(VI) at Au microelectrodes with good sensitivity for linear potential sweep voltammetry using acidic conditions, the use of MWCNTs/AuNPs in acidic solutions was used here for the diffusion-controlled detection of Cr(VI) at pH 2.0.

The modification of MWCNTs with nanoparticles generally involves the initial oxidation of MWCNTs to assist in their dispersion and the carboxylate groups have been reported to provide binding sites for nanoparticles to be deposited,[77] therefore both pristine MWCNTs and oxidised MWCNTs (MWCNTsOx) were modified with Au nanoparticles,[262] and compared as materials for the detection of Cr(VI).

4.2.3.3.1 Formation and Characterisation of MWCNTs/AuNPs and MWCNTsOx/AuNPs

The modification of MWCNTs with AuNPs was carried out by another member of the research group, Mr David Branagan,[263] via a method similar to that reported by Alexeyeva *et al.*[262] in 2006. Briefly, in the preparation of MWCNTs/AuNPs, the pristine MWCNTs were used as received and in the case of MWCNTsOx/AuNPs the MWCNTs were acid treated to modify any defect areas with oxygen containing functional groups. The MWCNTsOx and pristine MWCNTs were both firstly dispersed in SDS by sonication in highly concentrated solutions (1% w/v). This step provided well dispersed suspensions and is likely to have provided nucleation sites for the AuNPs to form.[77] The AuNPs were formed by the addition of an aqueous solution of $HAuCl_4$ to the MWCNTs suspension under vigorous stirring, and the subsequent slow addition of $NaBH_4$ aqueous solution. The modified suspension was then filtered and rinsed with copious amounts of H_2O.

The MWCNTsOx/AuNPs were characterised physically using transmission electron microscopy (TEM) and both the MWCNTs/AuNPs and MWCNTsOx/AuNPs were characterised using atomic adsorption (A.A.) spectroscopy. The TEM analysis was carried out at the C.R.A.N.N. centre based in TCD, Dublin by Mr Clive Downing and the A.A. spectroscopy was carried out by a member of the research group, Mr David Branagan, using a 1 mg mL^{-1} Au standard solution in 0.50 M HCl. It was found using A.A. spectroscopy that the MWCNTsOx/AuNPs samples used in this work consisted of 2% wt. Au and the MWCNTs/AuNPs samples consisted of 1% wt. The TEM images taken at various magnifications can be seen in Figure 4.21 (a)-(d). It was found using this sensitive imaging, coupled with EDX analysis, that the MWCNTs were indeed decorated with AuNPs. The image in Figure 4.21 (a) shows the overall view of a MWCNT agglomeration with AuNPs scattered throughout and in Figure 4.21 (b) it would appear that the AuNPs are adsorbed on the outer walls of the MWCNTs. Figure 4.21 (c) shows the distribution of various sizes of the

AuNPs in a magnified image of the MWCNTs agglomeration and Figure 4.21 (d) highlights the spherical morphology of the AuNPs.

The distribution of the particle sizes (diameter) was analysed and is displayed as a histogram in Figure 4.21 (e). It was found that the majority of the particles measured were of 7.5 nm in diameter; and the range of sizes was 5.5 to 12.5 nm. This analysis is direct evidence that the Au particles used to modify the MWCNTs were nanoparticulate.

(a)

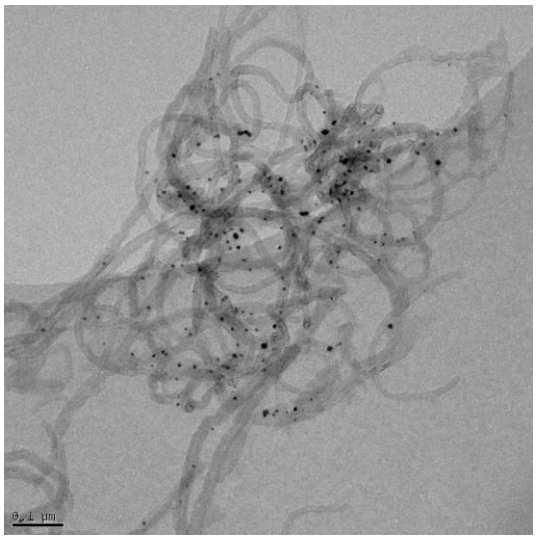

(b)

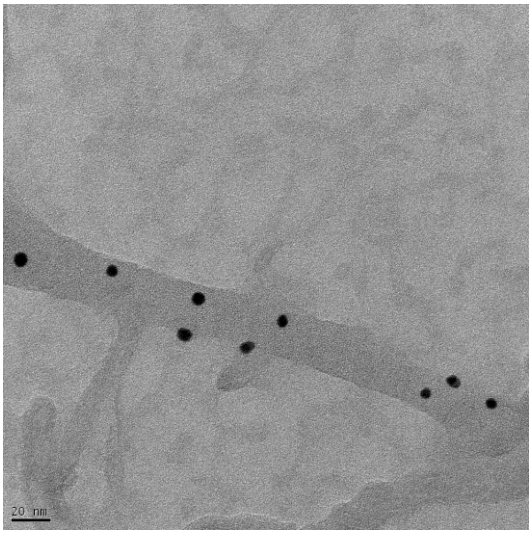

(c)

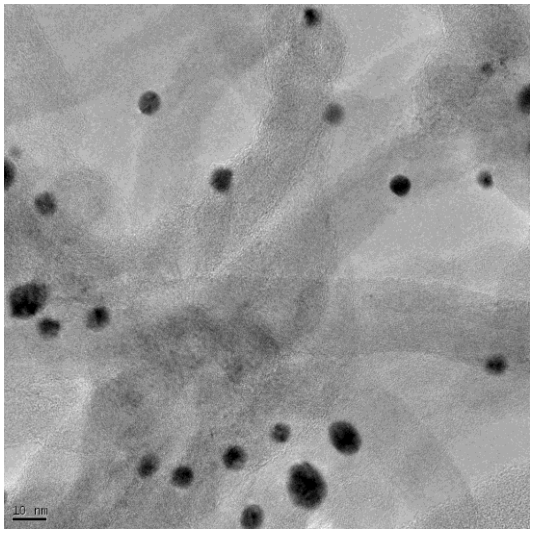

(d)

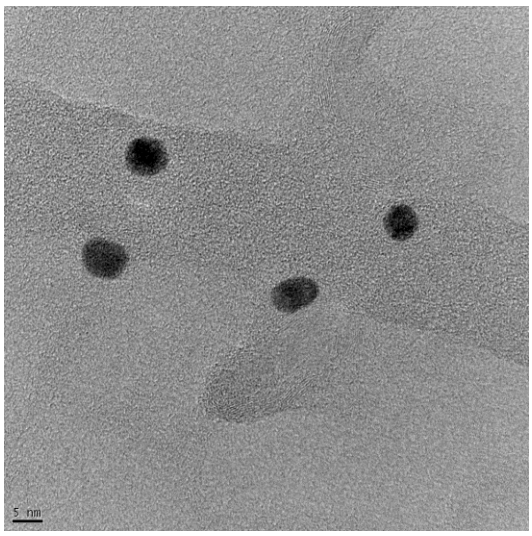

(e)

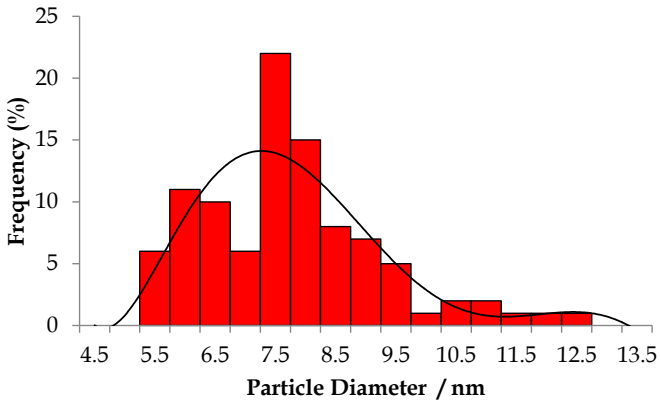

Figure 4.21: (a)–(d). TEM images of MWCNTsOx/AuNPs at various magnifications and (e) Particle size distribution histogram of 100 AuNPs.

4.2.3.3.2 Chromium(VI) Detection at Electrodes modified with MWCNTs and Au Nanoparticles

The MWCNTsOx/AuNPs and MWCNTs/AuNPs suspensions were prepared by dispersing 10 mg mL^{-1} modified MWCNTs in DMF via sonication for 30 min. The Au electrodes were then drop cast with 20 µL MWCNTsOx/AuNPs or MWCNTs/AuNPs and dried under an IR lamp. The voltammetric response of MWCNTsOx/AuNPs and MWCNTs/AuNPs is compared in Figure 4.22 in the reduction of 5.00×10^{-4} M Cr(VI) in H_2SO_4 at pH 2.0 with the peak potentials and currents tabulated inset. The broad redox pair at 0.20/0.30 V vs. SCE seen at the MWCNTsOx/AuNPs modified electrode most probably arose from the oxygen functionalities on the oxidised MWCNTs, as has previously been reported in the literature.[262, 264] There was no clear reduction peak observed at this modified electrode, likely as a result of this redox pair masking the peak, however rough estimates of both peak potential and peak current were made from the voltammogram. The approximate peak position of 0.52 V vs. SCE and peak current of 8.11×10^{-6} A, appear to be lower than those seen at the MWCNTs/AuNPs. It would appear, however, that cyclic voltammetry was unsuitable for the detection of Cr(VI) at the MWCNTsOx/AuNPs modified electrode.

A clear reduction peak was observed at the electrode modified with MWCNTs/AuNPs, where it is of note that there was a shift in peak position from 0.56 V at bare MWCNTs to 0.60 V vs. SCE at MWCNTs/AuNPs. This indicates that some sensing occurred at both the AuNPs surface and the MWCNTs, which resulted in a lower over-potential than for the MWCNTs alone. The peak currents in this case were 8.92×10^{-6} A for the reduction of 5.0×10^{-4} M Cr(VI).

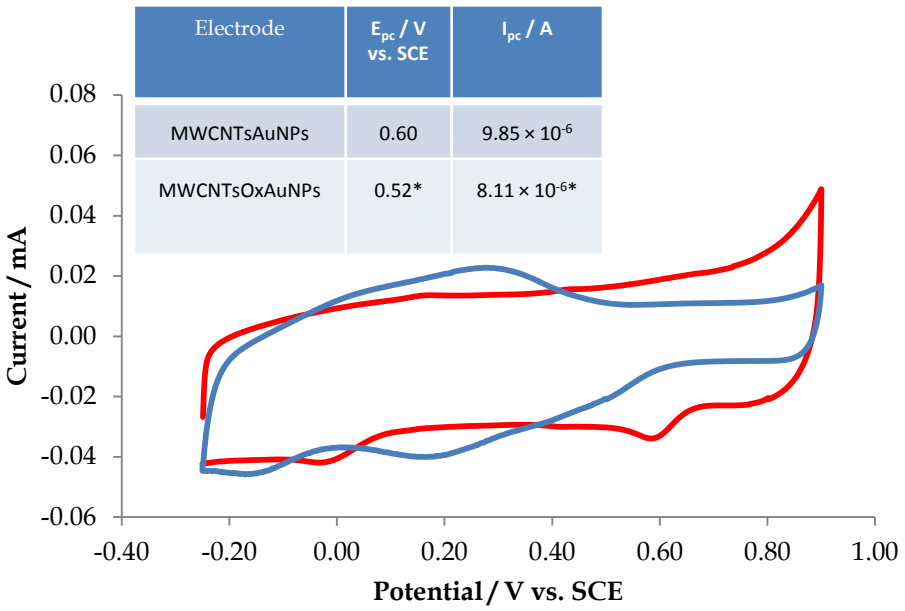

Figure 4.22: Cyclic voltammograms of modified gold electrodes in a 5.0×10^{-4} M Cr(VI) in H_2SO_4 (pH 2.0) at 10 mV s^{-1}. Plot shows gold electrode modified with — MWCNTsOx/AuNPs compared to — MWCNTs/AuNPs. The relevant electrochemical properties are tabulated inset.

*Approximate peak position and current values were determined from cyclic voltammetry.

4.2.3.4 Comparison of the Electrode Materials Studied with respect to Cr(VI) Reduction using Cyclic Voltammetry

To accurately compare the various electrodes, their sensitivity was calculated from the observed current response with respect to the concentration of Cr(VI) tested (Current / Concentration). The resulting sensitivities are shown in Figure 4.23. In comparing the bare substrates studied, the peak current for the reduction of Cr(VI) was clearly larger at the Au electrode in comparison to the GCE. Signals were observed for the reduction of Cr(VI) at the MWCNT modified electrodes, the polypyrrole MWCNT composite electrodes and the MWCNTs/AuNPs modified electrode. As cyclic voltammetry was deemed

unsuitable for use in monitoring the detection of Cr(VI) reduction at the MWCNTsOx/AuNPs modified electrode, it was not compared in this table.

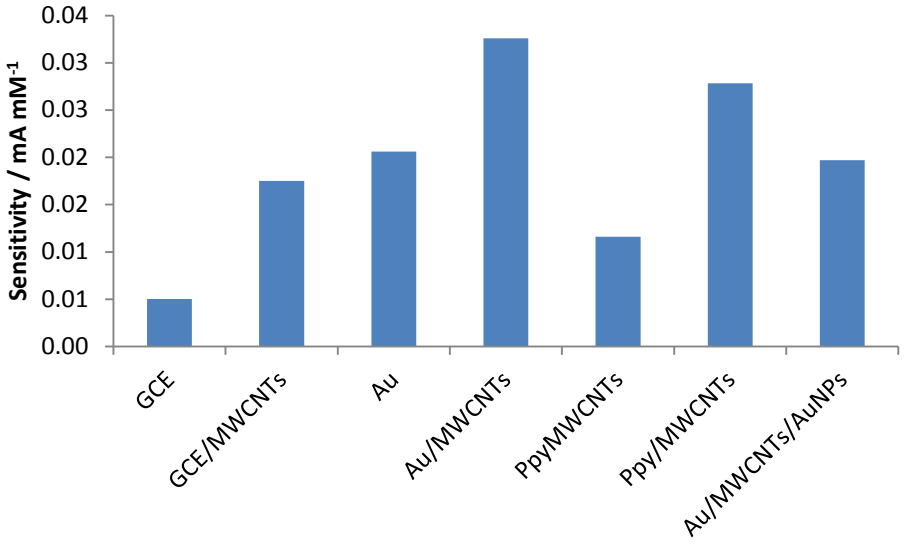

Figure 4.23: Bar chart comparing the current response of the various modified and bare electrodes for the detection of Cr(VI), with respect to the concentration of Cr(VI) tested.

It is clear from the screening study that the largest current response in relation to the concentration of Cr(VI) observed via cyclic voltammetry was at the Au electrode modified with MWCNTs (Au/MWCNTs). Furthermore, it appeared that the next most promising material for sensing Cr(VI) using cyclic voltammetry was the polypyrrole modified electrode (Ppy/MWCNTs), however the amount of MWCNTs cast in both cases differed. Therefore further analysis of the data was carried out in order to compare the performance of these two electrodes. The casting was carried out from a 7.0 mg mL^{-1} MWCNTs suspension in both cases to investigate the role of the underlying Ppy film. As can be seen in Table 4.5, the peak potential recorded at the Au electrode cast with MWCNTs was the same as that recorded at the Ppy film cast with MWCNTs. In comparing the peak currents however, there was a slight increase observed at MWCNTs/Ppy in comparison to the Au/MWCNTs electrode, suggesting that the polymer layer contributed to the process in some way most likely by Cr(VI) adsorption as discussed earlier.

Table 4.5: Comparison of peak potential and peak current values for the detection of 6.0×10^{-4} M Cr(VI) at electrodes cast with 7.0 mg mL^{-1} MWCNTs, both with and without the underlying Ppy film.

Electrode	E_p / V vs. SCE	I_p / A
MWCNTs	0.65	1.41×10^{-5}
Ppy/MWCNTs	0.65	1.67×10^{-5}

In comparing the stability of the Ppy/MWCNTs electrode to the MWCNTs, seen in Figure 4.24, it was clear that over the course of 10 cycles in Cr(VI), the polymer layer of the Ppy/MWCNTs degraded gradually as the currents dropped off to a similar level observed for the MWCNTs casting, which exhibited a relatively constant current over the 10 cycles. This suggested that in the early cycles, the Ppy component of the electrode contributed to Cr(VI) detection but that the Ppy was not stable in the Cr(VI) solution. Therefore as Ppy provided no benefit to the construction of the sensor, it was concluded that the most efficient detection of Cr(VI) in this work was achieved at the electrode modified with solely MWCNTs and Ppy was no longer utilised in the modification of the electrode.

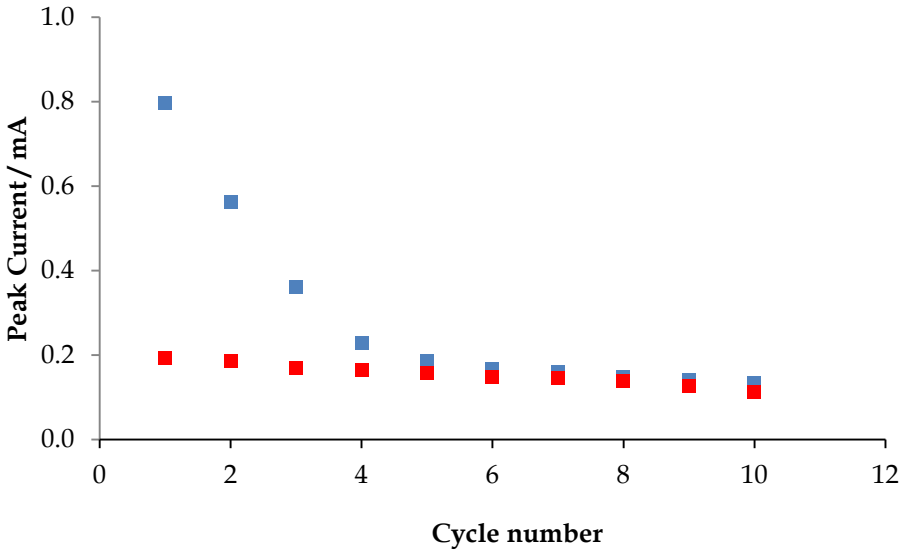

Figure 4.24: Comparison of peak current stability over 10 cycles for ■ Ppy/MWCNTs and ■ MWCNTs.

4.2.4 Investigating the Limit of Cr(VI) Detection at Various Electrode Materials using Different Electrochemical Techniques

The screening study highlighted that the best current response was observed at an electrode cast with MWCNTs from a DMF suspension, a bare gold electrode and a gold electrode cast with AuNPs modified MWCNTs therefore the LODS of these electrodes are further investigated herein. The electrode cast with MWCNTsOx/AuNPs is also further investigated in this section as cyclic voltammetry was deemed as an unsuitable technique for its evaluation in Cr(VI) detection (Section 4.2.3.3.2).

The use of differential pulse voltammetry (DPV) and constant potential amperometry at a rotating disc electrode (CPA/RDE) are investigated in this section to improve the limit of Cr(VI) detection. Both techniques are described in Chapter 2 which briefly illustrates that the improved sensitivity of DPV occurs as it allows for decaying of the capacitive currents and the improved sensitivity of CPA/RDE arises from enhanced mass transport to the electrode surface.

In all cases the LOD of the electrode towards the reduction of Cr(VI) was calculated by constructing calibration curves from plots of peak current vs. Cr(VI) concentration. The relationship between the slope of the calibration curve and the standard deviation of the background signal was used to calculate the LOD, as was illustrated in Section 4.2.2.3.

4.2.4.1 Detection of Cr(VI) using Cyclic Voltammetry

In Section 4.2.2.3 the limit of Cr(VI) detected at GCE/MWCNTs using cyclic voltammetry was calculated to be 1.95×10^{-4} M. The screening study in Section 4.2.3.4 showed that the reduction of 6.00×10^{-4} M Cr(VI) was also promising at the bare Au electrode, the Au/MWCNTs electrode and the Au/MWCNTs/AuNPs electrode using cyclic voltammetry. The calibration

curves of these electrodes can be seen in Figure 4.25 (a) to (c). It can be seen at the bare Au electrode in Figure 4.25 (a) that although the reproducibility was poor, good linearity was achieved between 1.22×10^{-4} M and 5.00×10^{-4} M Cr(VI). The LOD was calculated as 7.47×10^{-5} M, which is lower than that detected at GCE/MWCNTs. A calibration curve for the Au substrate cast with 20 µL 10 mg mL^{-1} MWCNTs can be seen in Figure 4.25 (b). The LOD achieved at this modified electrode, using cyclic voltammetry, was shown to be 1.45×10^{-4} M. The higher LOD at this electrode in comparison to the bare Au electrode can possibly be explained by the use of cyclic voltammetry. At the lower concentrations, poor linearity was observed in the calibration curve, therefore the LOD was calculated from the slope between 2.22×10^{-4} and 5.80×10^{-4} M Cr(VI). This is indicative of the slow diffusion of Cr(VI) through the MWCNTs film, as discussed in Chapter 3.

The GCE modified with 10 mg mL^{-1} MWCNTs/AuNPs also showed efficient detection of Cr(VI) in the screening study in Section 4.2.3.4, therefore its LOD was also calculated from the calibration curve in Figure 4.25 (c). For the MWCNTs/AuNPs modified electrode, a detection limit of 1.55×10^{-4} M was determined using cyclic voltammetry, which is also higher than that achieved at the bare Au electrode. This high LOD occurred again as a result of the deviation from linearity at lower concentrations of Cr(VI) in the cyclic voltammetry experiments. In this case the LOD was calculated from the slope between 2.22×10^{-4} and 5.00×10^{-4} M Cr(VI). This LOD was very similar to that recorded at the bare MWCNTs, which agrees well with the physical characterisation of the sample that shows a low loading of Au on the pristine MWCNTs.

(a)

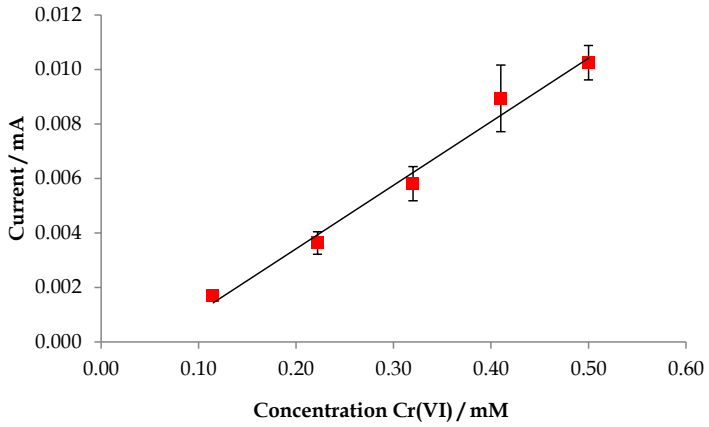

(b)

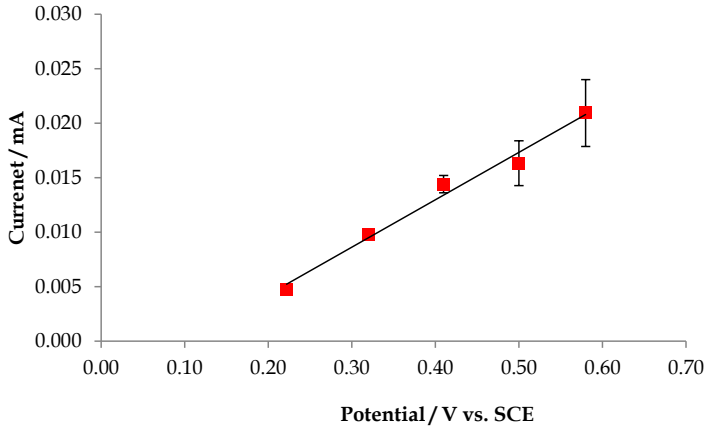

(c)

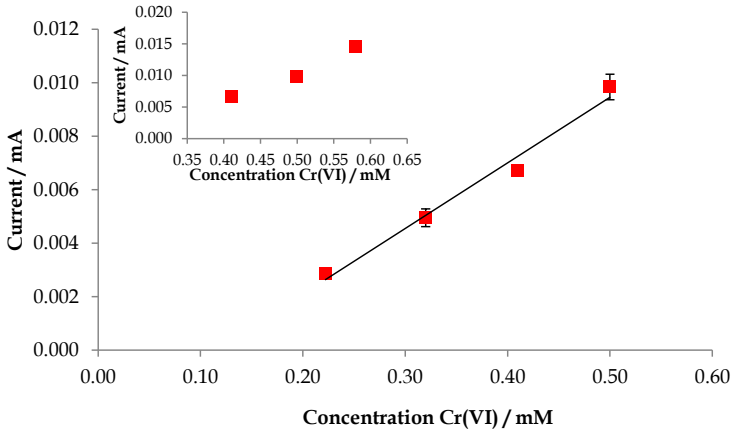

Figure 4.25: Calibration curves measuring the current response from cyclic voltammograms of (a) a bare Au electrode (b) Au/MWCNTs and (c) GCE/MWCNTs/AuNPs at various concentrations of Cr(VI) in H_2SO_4 (pH 2.0, n=3).

4.2.4.2 *Detection of Cr(VI) at a MWCNTs modified Glassy Carbon Electrode using Differential Pulse Voltammetry*

An attempt was made to further improve the LOD of the MWCNTs modified electrode by implementing differential pulse voltammetry to reduce Cr(VI) to Cr(III). DPV is detailed in Chapter 2, briefly it involves applying the potential in pulses which allows the capacitive current to decay, preventing its build up. This generally enhances the redox signals, making it a more sensitive technique. It was shown in Chapter 3 that MWCNTs are highly capacitive, therefore DPV was used in this section to lower the limit of Cr(VI) detection at the MWCNTs modified electrode. The conditions utilised for differential pulse voltammetry measurements are outlined in Table 4.6.

Table 4.6: Relevant parameters used in differential pulse voltammetry experiments.

Parameter	Value
Initial Potential	0.80 V vs. SCE
Final Potential	-0.25 V vs. SCE
Potential Increment	5 mV
Pulse Amplitude	50 mV
Pulse Period	0.30 s
Sample Width	0.01 s
Pulse Width	0.15 s

In principle, DPV should be very useful in this system as MWCNTs are highly capacitive[40] thus, as the background currents were relatively large, it appeared that they masked the faradaic currents. However, a calibration curve was constructed to determine the LOD achieved and it can be seen from Figure 4.26 that the linearity of the current response was extremely poor, in particular at lower concentrations. This was likely due to the limitations of diffusion

through the mesoporous MWCNTs layer. This technique was therefore discounted for further use.

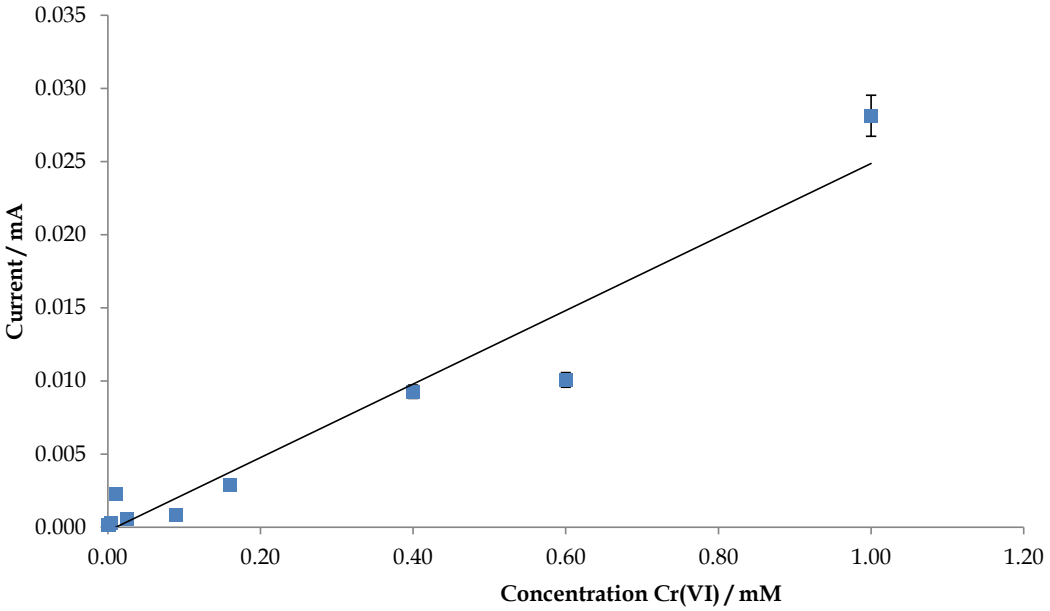

Figure 4.26: Peak currents for the reduction of Cr(VI) in 0.1 M H_2SO_4 recorded at GCE/MWCNTs using differential pulse voltammetry, plot as a function of Cr(VI) concentration. R^2 = 0.98 for n=3.

4.2.4.3 *Detection of Cr(VI) using Constant Potential Amperometry at a Rotating Disc Electrode*

The use of rotating disc voltammetry and constant potential amperometry are shown in this section to lower the limit of Cr(VI) detection at the various electrodes. The use of rotating disc electrodes in electrochemical detection is often implemented to aid in the transport of the analyte to the electrode surface by removing diffusion limitations by means of convection. This technique could therefore possibly be utilised to enhance diffusion of an analyte through the mesoporous MWCNTs layer. This technique is generally coupled with constant potential amperometry as the sufficient transport of the analyte to the surface ensures a consistent supply from the bulk solution, which therefore can provide sensitive detection. Calibration curves for this technique are constructed using the standard addition method and produce staircase amperograms. Based on the response obtained in Section 4.2.3 using cyclic voltammetry, the bare rotating disc Au electrode was tested for its response to Cr(VI) reduction at a constant applied potential of 0.20 V vs. SCE. The use of an RDE in these experiments was to ensure fresh reactant was brought to the working surface which is achieved when the electrode is rotated at a particular rotation speed in solution. The calibration curves (n=1) for the bare electrode at two different rotation speeds; 900 and 1900 rpm, are shown in Figure 4.27 where it can be seen that the rotation speed of 1900 rpm showed a more sensitive current response by the higher currents.

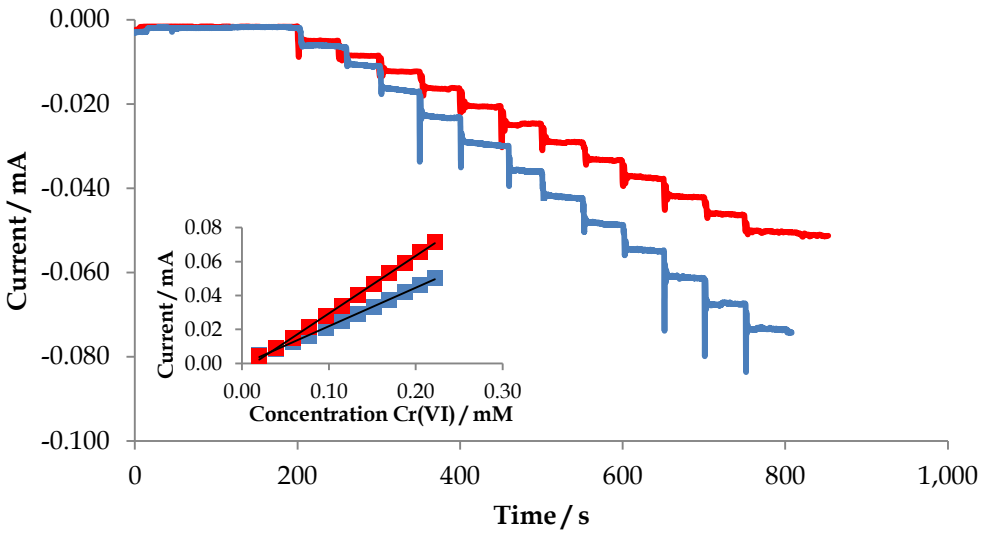

Figure 4.27 : Staircase amperograms (n=1) comparing the current response of bare Au electrodes at various concentrations of Cr(VI) in H_2SO_4 at pH 2.0, measured at a constant potential of 0.2 V vs. SCE for a rotation speed of ■ 900 and ■ 1900 rpm. Plot inset shows (n=1) calibration curves recorded at both speeds.

A calibration curve was constructed of the bare Au rotating disc electrode at the rotation speed of 1900 rpm, which can be seen in Figure 4.28 (a). It can be seen here that the bare electrode exhibited poor reproducibility, causing the plot to deviate from linearity at lower concentrations (inset Figure 4.28 (a)). A LOD of 5.07×10^{-5} M was calculated from the linear region of the plot at the bare Au substrate using this technique. A gold rotating disc electrode modified with MWCNTs (20 µL 10 mg mL^{-1} MWCNTs/DMF) was also tested using constant potential amperometry to introduce convection in the electrochemical cell. A constant potential of 0.40 V vs. SCE was applied to the Au/MWCNTs electrode to ensure a sufficient over-potential was applied to achieve complete conversion of Cr(VI) to Cr(III) based on the cyclic voltammetry experiments in Section 4.2.3. A calibration curve was then constructed for the Au/MWCNTs electrode using constant potential amperometry at 0.40 V vs. SCE on a rotating disc at 1900 rpm. It can be seen that a linear response with good reproducibility was produced using this technique and lower LOD of 2.22×10^{-6} M Cr(VI) was achieved.

(a)

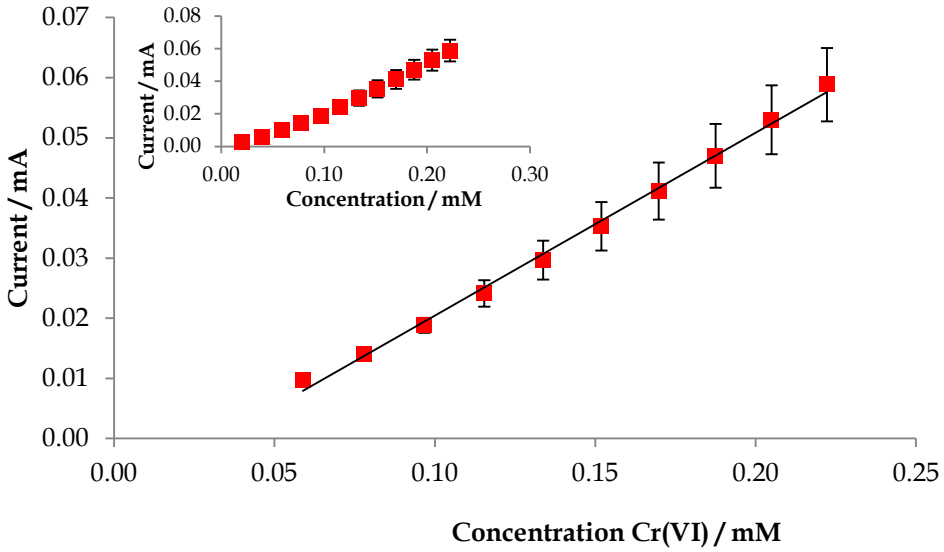

(b)

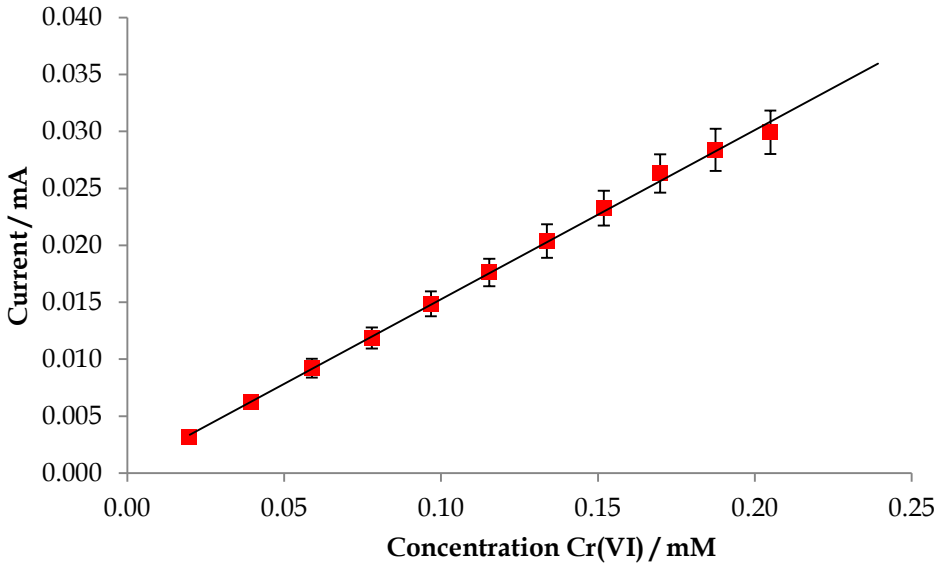

Figure 4.28: Calibration curves representing the current response of (a) a bare Au electrode and (b) an Au electrode modified with 20 µL 10 mg mL^{-1} MWCNTs to various concentrations of Cr(VI) in H_2SO_4 at pH 2.0, at a constant potential (0.2 and 0.4 V vs. SCE, respectively) using a rotating disc electrode at 1900 rpm.

The physical characterisation of the modified MWCNTs showed that MWCNTsOx/AuNPs had a higher loading of Au than the pristine MWCNT/AuNPs, therefore the MWCNTsOx/AuNPs were solely investigated in this case. The constant potential amperogram was measured for the reduction of Cr(VI), similarly to that in Figure 4.27, at 900 and 1900 rpm. It can be seen in Figure 4.29 (a) that the faster rotation speed of 1900 rpm, showed an increase in the current response of this electrode also. A calibration curve was therefore constructed of the Au/MWCNTsOx/AuNPs electrode and is displayed in Figure 4.29 (b). A LOD of 1.20×10^{-6} M was calculated, at a constant potential of 0.40 V vs. SCE and a rotation speed of 1900 rpm, which is in the region of the mandatory limits set by the EPA. The excellent reproducibility of this modified electrode is highlighted by the small error bars and linear current response. The lower limit of detection can be accredited to the increased amount of AuNPs (2% wt.) which are known to act as electron antennae in electrochemical sensing.[80]

(a)

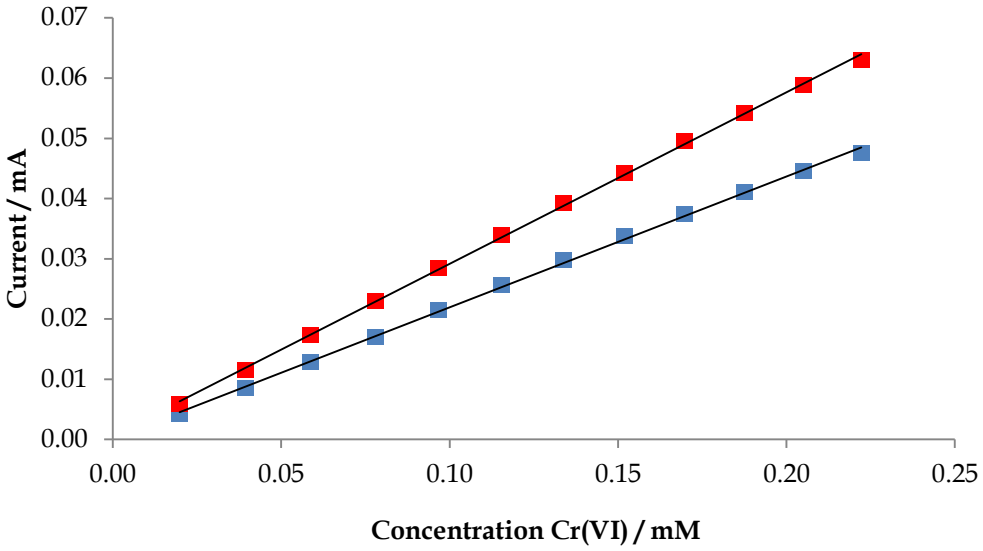

(b)

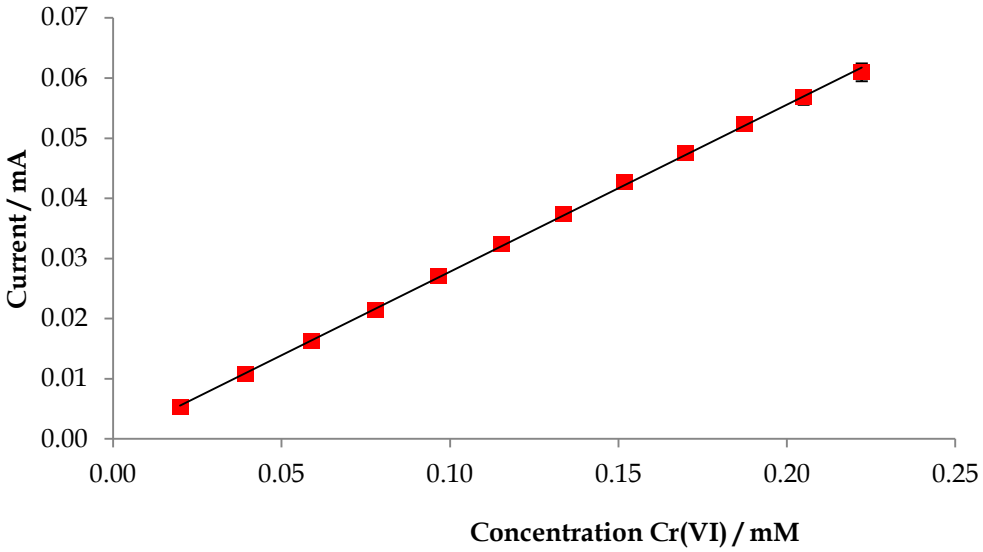

Figure 4.29: Calibration curves recorded for the reduction of various concentrations of Cr(VI) in H_2SO_4 at pH 2.0 measured at a constant potential of 0.40 V vs. SCE using an Au electrode modified with 20 µL 10 mg mL^{-1} MWCNTsOx/AuNPs (a) (n=1) for a rotation speed of ■ 900 and ■ 1900 rpm and (b) (n=3) at 1900 rpm.

The limits of detection (LOD) that have been calculated for various electrodes using cyclic voltammetry and constant potential amperometry with rotating disc electrodes (CPA/RDE) are shown in Table 4.7. It is clear from this table that the most sensitive electrode using cyclic voltammetry for the detection of Cr(VI) was the bare Au electrode which was slightly enhanced by the use of CPA/RDE. A lower LOD was achieved by the use of CPA/RDE for the MWCNTs modified electrodes, with almost 100 fold increase achieved at the Au electrode modified with MWCNTs. This can most likely be explained by the increase in mass transport obtained with the use of an RDE. The lowest LOD of Cr(VI) was achieved at the MWCNTsOx/AuNPs, where the detection was enhanced 2 fold further by the modification of MWCNTs with AuNPs. The use of CPA/RDE with the MWCNTsOx/AuNPs modified Au electrode provided a LOD of 1.20×10^{-6} M (62 μg L^{-1}) which is approaching the mandatory limit set by the EPA of 9.61×10^{-7} (50 μg L^{-1}).

Table 4.7: Limits of detection (LOD) for Cr(VI) at the various modified electrodes using cyclic voltammetry and constant potential amperometry at a rotating disc electrode (CPA/RDE).

Electrode	**Limit of Detection / M Cr(VI)**	
	Cyclic Voltammetry	CPA/RDE
Au	7.47×10^{-5}	5.07×10^{-5}
Au/MWCNTs	1.45×10^{-4}	2.22×10^{-6}
GCE/MWCNTs	1.95×10^{-4}	†
Au/MWCNTs/AuNPs	1.55×10^{-4}	†
Au/MWCNTsOx/AuNPs	‡	1.20×10^{-6}

† Electrodes were not tested for Cr(VI) detection using this technique.

‡ Technique was not suitable for Cr(VI) detection at this electrode.

4.3 Conclusion

In this chapter it was found that a MWCNTs modified glassy carbon electrode could be used to detect the electrochemical reduction of Cr(VI). The reduction peak was monitored at 0.65 V vs. SCE using cyclic voltammetry and a LOD of 1.95×10^{-4} M was determined. A reasonably stable peak current was monitored over 30 cycles which was not influenced by the potential interferants Cl^- and Cu^{2+}. Some interference was noted in the presence of NO_3^- however, and poor reproducibility was seen in real water samples. As expected, the peak potential for the reduction of Cr(VI) to Cr(III) was influenced greatly by the pH of the sample solution, however, it did not follow simple Nernstian behaviour. Surprisingly, the peak current did not increase with an increase in the conductivity of the sample solution, perhaps due to adsorption of SO_4^{2-} on the MWCNTs surface.

Different modifications were explored in the construction of the Cr(VI) sensor in attempt to enhance the limits of detection. Ppy was initially utilised as a scaffold for the MWCNTs due to its ease of preparation, good conductivity and relative stability.[265, 266] The growth of PpyMWCNTs was compared to that of Ppy under the same conditions and PpyMWCNTs was characterised electrochemically using cyclic voltammetry and imaged using SEM. The inherent properties of Ppy are known to both spontaneously adsorb[267] and reduce[268] Cr(VI) therefore, partial overoxidation of the Ppy film was carried out to supress any chemical interference. The electrochemical properties of the resultant films showed Ppy redox activity that was supressed by overoxidation in the acidic Cr(VI) solution by cycling in a large potential window at a relatively slow scan rate of 10 mV s^{-1}. The current response for the reduction of Cr(VI) to Cr(III) was markedly improved by the presence of MWCNTs in the Ppy matrix. This modification of the electrode was then further enhanced by the addition of MWCNTs as a drop-cast coating on Ppy (MWCNTs/Ppy). This modification was compared to the original MWCNTs modified electrode, without the use of the Ppy matrix. Initial cycles showed an enhanced current

response at the MWCNTs/Ppy modified electrode, however, the signal was unstable possibly due to a chemical reaction between the Ppy film and Cr(VI). As similar detection was achieved at both electrodes by the 10^{th} cycle, it was concluded that the use of MWCNTs alone was preferential for the electrochemical reduction of Cr(VI) to Cr(III). The second modification of the electrode with MWCNTs investigated to optimise the detection of Cr(VI) was by the incorporation of AuNPs. Samples of MWCNTs both pristine and oxidised were modified with AuNPs and it was found, using atomic adsorption spectroscopy, that the MWCNTsOx contained substantially more AuNPs than the pristine MWCNTs after modification. A LOD of 1.55×10^{-4} M was achieved at the Au/MWCNTs/AuNPs, which was quite similar to that obtained for GCE/MWCNTs. A LOD was not calculated, however for Au/MWCNTsOx/AuNPs using cyclic voltammetry due to the electroactivity of the MWCNTsOx.

Constant potential amperometry at a rotating disc electrode was therefore investigated as a means of decreasing the limit of Cr(VI) detection. This technique was used to compare the various electrodes; bare Au, Au/MWCNTs, and Au/MWCNTsOx/AuNPs using a rotating speed of 1900 rpm. The lowest LOD achieved using this technique was 1.20×10^{-6} M at the Au/MWCNTsOx/AuNPs electrode.

In summary, although it would appear that simple modification of an electrode with MWCNTs can be used to detect Cr(VI), there are problems with its LOD. The AuNPs modified MWCNTs however show enhanced detection of Cr(VI). Future recommendations for this work would include optimising the modification of the MWCNTs with AuNPs to maximise the amount of AuNPs on the modified surface. Studies to investigate the selectivity of the optimised electrode and its use in real water samples would also be recommended.

Chapter 5:

The Electrochemical Detection of Cu(II) in Aqueous Solutions using N,N-Diethyldithiocarbamate

5.1 Introduction

Copper is a transition metal that is found naturally in some rock sediments and forms monovalent and divalent cations in solution. Its pollution generally stems from anthropogenic uses such as copper piping and wiring where it can be leached into drinking water. Although it is an essential dietary requirement, it can cause organoleptic (taste) problems when ingested at levels above 1 mg L^{-1}. At lower doses it can cause symptoms typical of food poisoning, and the acute lethal dose for adults lies between 1 and 400 mg of copper (II) per kg of body weight.[15] As copper is found naturally in the environment at low concentrations, its sensitive detection is very important. The EPA have thus imposed a parametric value, i.e. a mandatory limit, of 3.15×10^{-5} M Cu(II) in drinking water in Ireland. For the most part, copper is detected using techniques such as ICP-MS, which are expensive, time-consuming and do not provide real-time analysis. The development of electrochemical sensors for metal ion detection would allow for simple, on-site detection remote access to data, making it a very attractive technique for environmental monitoring. The electrochemical detection of metals has mainly been reported using stripping voltammetry,[158, 269, 270] and ion selective membranes.[271, 272, 273] Recently, there have been developments in the production of voltammetric sensors for the fast and simple detection of copper which include the use of self assembled monolayers and ion-selective ligands.[274, 275] The main advantages of these electrodes are that they are quickly and simply prepared at a relatively low cost and they have the potential for being used on a miniature scale for use in disposable sensors such as screen printed electrodes.[274, 276]

Herein, both a glassy carbon electrode (GCE) and platinum (Pt) mesh electrode are modified with a diethyldithiocarbamate (DDC) ligand. Dithiocarbamates are simple analogues of carbamates whereby both oxygen atoms are replaced by sulfur atoms, as illustrated in Figure 5.1 (a). They have been investigated for several decades in the detection of copper as the sulfur atoms are known to co-ordinate with transition metal cations.[271] They are

known to form highly stable complexes with copper, in particular copper diethyl-dithiocarbamate ($Cu(DDC)_2$), which is illustrated in Figure 5.1 (b), has a reported stability constant in EtOH of log K = 28.8. The complex is poorly soluble in water (log k_{sp} = -31)[277] which was beneficial in this work as the complex formed on the electrode surface and was not easily leached into the aqueous sample solution.

(a) (b)

N,N-diethyl-dithiocarbamic acid diethylammonium (DDC)

$Cu(DDC)_2$

Figure 5.1: Structure of (a) the diethylammonium salt of diethyldithiocarbamate (DDC) and (b) $Cu(DDC)_2$, the complex formed between diethyldithiocarbamate and Cu(II).

The detection of Cu(II) in this chapter is based on the formation of the $Cu(DDC)_2$ complex[278] at the electrode surface, using cyclic voltammetry to detect the presence of copper. As highlighted in Chapter 1, the $Cu(DDC)_2$ complex is generally studied in organic solvents as it is poorly soluble in aqueous media. Many reports have been made of the interactions between copper and dithiocarbamates in solution[122, 279] and in polymeric matrices,[280] however in this work we discuss the use of a Nafion perfluorinated ionomer film as a structured support for the formation of the copper complex. Nafion is chemically and thermally inert, non-electroactive and insoluble in water and is therefore, particularly suitable for the modification of electrodes.[158, 281] It has been shown particularly by Chen *et al.,*[124] that electrodes modified with DDC and Nafion can be used for the detection of metal ions in stripping voltammetry, a technique that involves the deposition of the metal on the electrode surface. The technique investigated herein involves cycling the metal

ion between its oxidation states within the formed complex which would allow for the fast detection of the metal ion without the need for multiple steps.[282]

5.2 Results and Discussion

5.2.1 The Electrochemical Characterisation of Modified Electrodes

The use of DDC/Nafion modified electrodes in aqueous systems is investigated in this section. Firstly, the simple drop-cast method is used to modify a GCE to investigate the electrochemical properties of the film as a basis for an electrochemical sensor. The use of a Pt mesh WE is then explored to provide a flexible electrode with potential application in spectrophotometric studies.

5.2.1.1 The Electrochemical Characterisation of DDC immobilised in a Nafion film on a GCE

The modified electrode was prepared using the drop-casting method whereby 0.030 g of DDC was dispersed in 1.50 mL 5% wt. Nafion (in lower aliphatic alcohols and 15-20% water) to form the DDC/Nafion solution. A 10 µL aliquot of DDC/Nafion was cast on a polished GCE surface which was then dried for 10 min under an IR lamp. Cyclic voltammetry was performed on the modified electrode in 0.10 M NaCl at 50 mV s^{-1} for 10 cycles each in two different potential windows, -0.10 to +1.10 V and -0.10 to +0.90 V vs. SCE which can be seen in Figure 5.2 (a). The electrochemical oxidation of the DDC can be seen here at 0.20 V vs. SCE in the first cycle in both potential windows. The voltammograms in Figure 5.2 (b) compare the first and final cycles of the voltammograms cycled between -0.10 and +1.10 V vs. SCE. Here it can be seen that with continued cycling, the oxidation peak diminished which indicated the complete and electrochemically irreversible oxidation of DDC under these conditions.

(a)

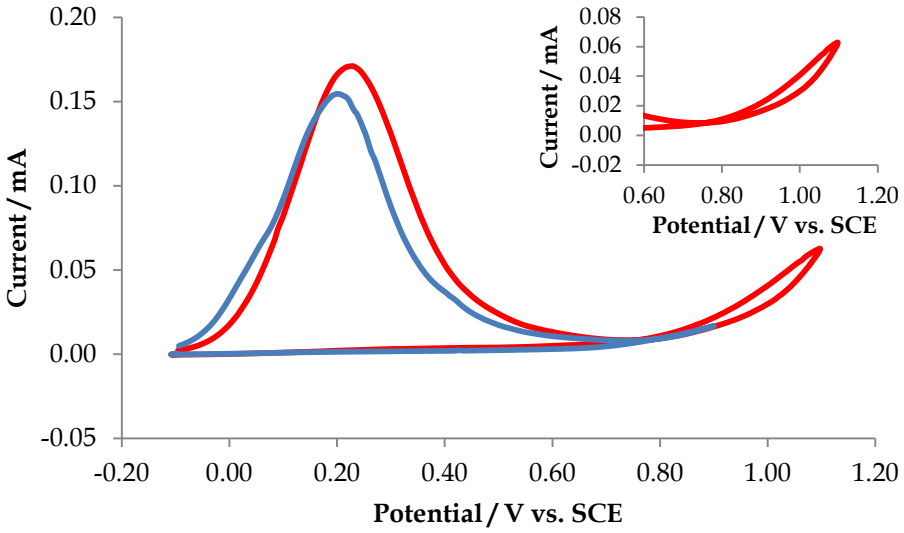

(b)

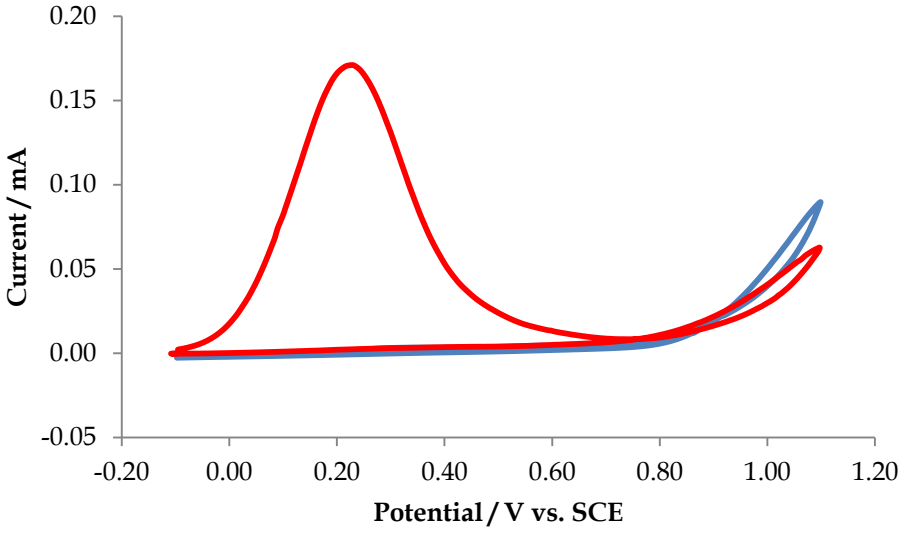

Figure 5.2: Cyclic voltammograms of GCE cast with 10 µL of DDC/Nafion (0.030 g / 1.50 mL) in 0.10 M NaCl (a) comparing the initial cycles when scanned from -0.10 to — +1.10 and — +0.90 V vs. SCE and (b) comparing the — initial and — final cycle (cycle 10) when scanned between -0.10 and +1.10 V vs. SCE.

The electrochemical activity of the immobilised DDC, can most likely be identified as the oxidation of DDC to its radical DDC$^{\bullet}$, according to the mechanism illustrated in Scheme 5.1. This has been shown both chemically[283] and electrochemically[284] in the literature to be subsequently followed by its rapid coupling to form Bis(N,N-diethylthiocarbamoyl) disulfide, better known as disulfiram (DSF). The further chemical oxidation of DSF to bis(dialkyliminium)tetrathiolane dication (Bitt-4^{2+}) has also been reported by Cen *et al.*,[283] which can also be seen in Scheme 5.1 and was also considered as a possible electrochemical step herein.

The oxidation of a dissolved DDC polymer in solution was shown by Lieder[285] to occur as a prewave from 0.1 to 0.30 V and a dominant oxidation peak at 0.70 V vs. SCE. The author describes how the polymer was prepared by reacting a linear poly(ethylenimine) polymer with CS_2, to give a DDC polymer which was dissolved in organic solvent for electrochemical analysis. The dominant peak at 0.70 V vs. SCE was assigned by Lieder[284, 285] to the oxidation of DDC to its radical, DDC$^{\bullet}$, and the pre-wave observed between 0.1 and 0.30 V vs. SCE was assigned to the oxidation of DDC bound to the electrode surface, occurring at a relatively low potential due to a decrease in activation energy. In the initial oxidation cycle of the modified electrode in this current work a similar decrease in activation energy can be attributed to the ligand being attached to the electrode surface, as no radicals would be present in this case. This would allow for the oxidation of DDC to occur at the lower potential of 0.20 V vs. SCE.

It is notable that the oxidation of the ligand in the larger potential window was further verified by a hysteresis loop, highlighted inset in Figure 5.2 (a). Here the currents of the reverse scan were higher than the forward scan between 1.10 and 1.00 V vs. SCE, and crossed to form a loop in the voltammogram. Hysteresis loops are generally regarded as an indication of polymerisation or deposition in cyclic voltammetry,[286, 287] and have been explained by Smie *et al.*[288] as a slow second order coupling step between dimeric species in the case of the oligimerisation of 3-methylthiothiophene. In this present case, it is therefore possible that the dimerisation of DDC$^{\bullet}$ to form DSF was observed as a hysteresis loop.

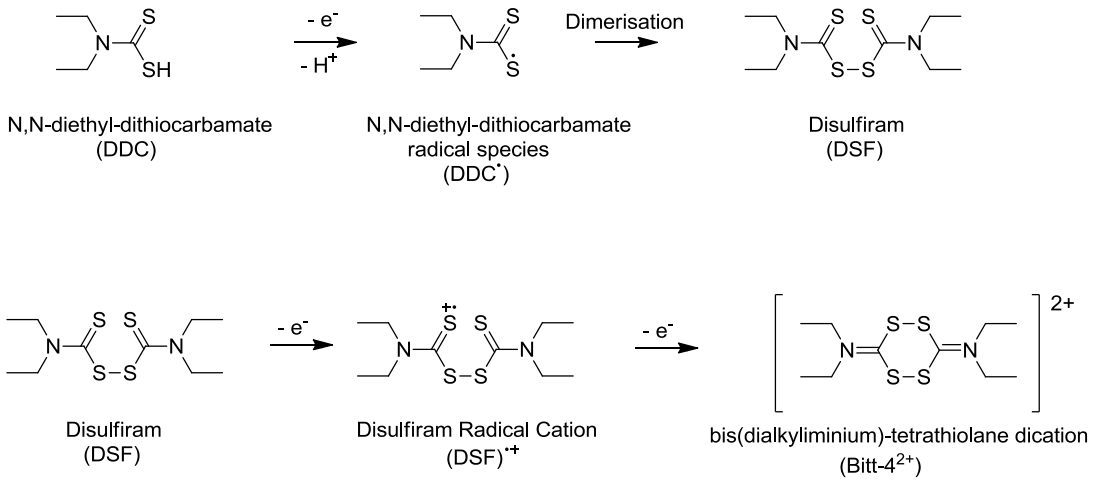

Scheme 5.1: Schematic illustration[283] of the possible mechanism for the oxidation of DDC to DSF and of DSF to Bitt-4^{2+}.

The lower limit of the potential window was then extended to scan from -1.00 to 0.90 V vs. SCE, and cycles 1 and 10 are again shown in Figure 5.3 (a). Similarly to that seen in Figure 5.2, an oxidation peak was observed at approximately 0.20 V vs. SCE in the initial cycle which was not visible in the final cycle. In this larger potential window however, a small reduction peak was observed at -0.70 V vs. SCE which increased with cycle number, indicating that some DSF was reduced back to DDC under these conditions. The control experiment of the GCE cast with 5% wt. Nafion (in lower aliphatic alcohols and

15-20% water) alone can be seen in Figure 5.3 (b) where the large oxidation peak is absent. In the initial cycle of Figure 5.3 (b), smaller redox peaks can be observed which may be attributed to reactions of the solvated protons fixed on the SO_3^- sites, as described by Sanmatias *et al.*[289] according to reaction 5.1.

$$H_{solv}^{+} + e^{-} \rightarrow \frac{1}{2} H_2 \qquad 5.1$$

The uptake of water in Nafion films has been discussed in the literature with reference to its effect on the morphology of the film and its conductivity,[290] however, regardless of the origin of these small redox peaks, it is clear that the large oxidation peak at 0.20 V vs. SCE observed in Figure 5.3 (a) must occur due to the presence of DDC.

(a)

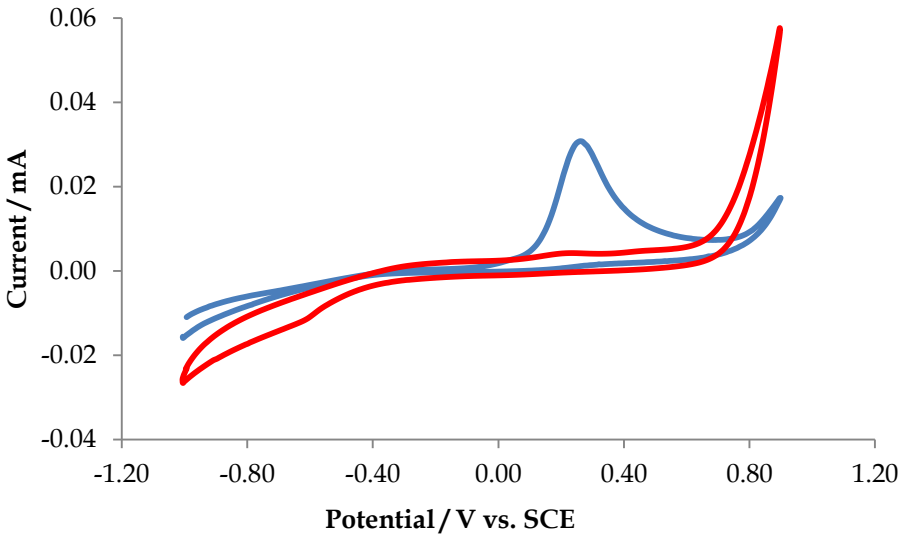

(b)

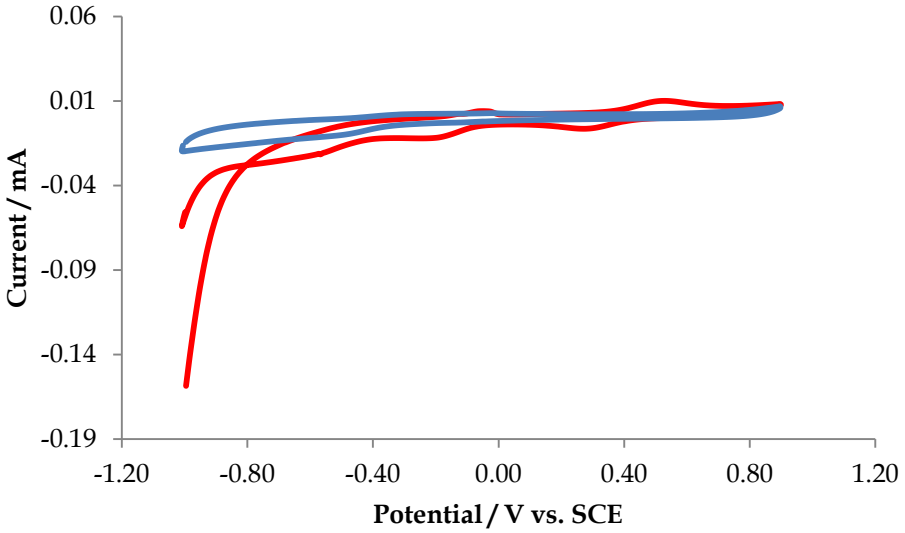

Figure 5.3: Cyclic voltammograms of GCE cast with 10 µL of (a) DDC/Nafion 0.030 g / 1.50 mL and (b) 5% wt. Nafion (in lower aliphatic alcohols and 15-20% water); in 0.10 M NaCl comparing the — initial and — final cycles when scanned between -1.00 and +0.90 V vs. SCE.

5.2.1.2 The Electrochemical Analysis of DDC/Nafion on a Pt mesh Electrode

5.2.1.2.1 The Electrodeposition of DDC/Nafion on a Pt mesh electrode

A Pt mesh working electrode (WE) was investigated as a substrate for modification with DDC/Nafion due to its small apertures allowing for its possible use in UV-vis spectroscopy as well as electrochemical experiments. As drop-casting the DDC/Nafion solution onto the mesh gave poorly controlled coverage and immeasurable loading of the film to the substrate, the DDC/Nafion solution was electrodeposited onto the mesh. This involved the application of a positive potential to the WE so as to attract the negatively charged Nafion and DDC ions from solution to the electrode surface, resulting in a relatively even coverage. The deposition required a larger volume of DDC/Nafion solution to allow for complete coverage of the mesh in the electrochemical cell and a high concentration of DDC to ensure its sufficient loading. A solution consisting of 0.240 g DDC dispersed in 6.00 mL 5% wt. Nafion (in lower aliphatic alcohols and 15-20% water) was prepared, giving a 0.2 M solution of DDC. The charge-time plot in Figure 5.4 shows the linear increase in charge passed with time by applying 1.00 V vs. SCE to the mesh for 120 s, indicating a gradual and controllable increase in the thickness of the film in this work. The plot highlights the reproducibility achieved in the electrodeposition, with 4 repeated experiments showing an error of 0.016 C (3.4%). The solvent was evaporated as before by drying the modified mesh under an IR lamp for 10 min (Pt/DDC/Nafion). This method has been used by many, for example, Hashemi *et al.*[291] have shown it to provide thin, uniform coatings of Nafion to carbon micro-fibre electrodes.

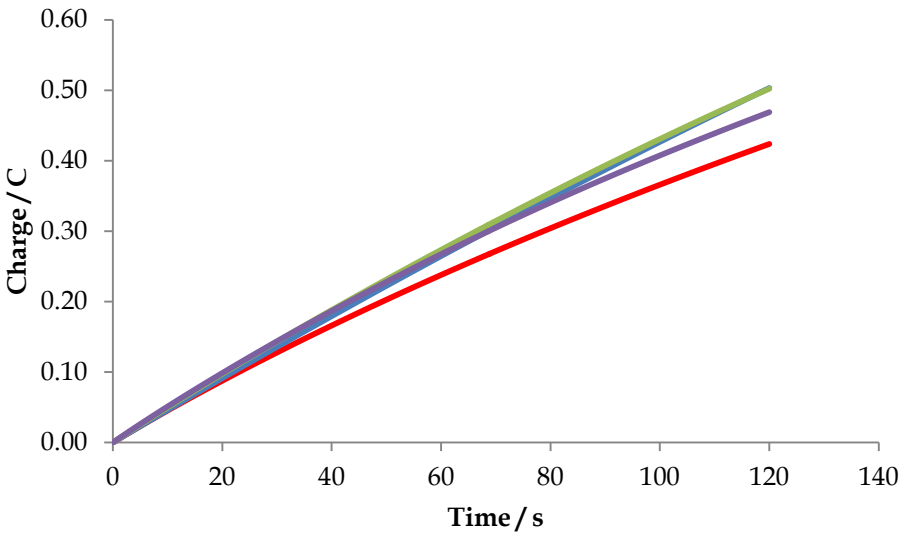

Figure 5.4: Plot showing the increase in charge as a function of time for the electrodeposition of DDC/Nafion on Pt mesh from a 0.02 M DDC 5% wt. Nafion solution at 1.00 V vs. SCE for 120 s (n=4).

5.2.1.2.2 Oxidation of DDC/Nafion on a Pt Mesh Electrode

The electrochemical characterisation of the modified electrode (Pt/DDC/Nafion) was carried out as discussed before in Section 5.2.1.1, by cycling the modified mesh in 0.10 M NaCl at 50 mV s^{-1} for 10 cycles. The potential window in this case was limited to cycle between -0.50 and 0.90 V vs. SCE. As can be seen in Figure 5.5, the oxidation peak potential, for the oxidation of DDC to its radical, was the same as that previously observed for the modified GCE in the same potential window (0.20 V vs. SCE). The film thickness, and therefore the amount of DDC deposited on the sensor could possibly be increased by varying the duration of electrodeposition. In this work, however, the electrodeposition time was kept at 120 s and a reproducible amount of DDC was incorporated into the Nafion film, confirmed by the intensity of the oxidation peak for each experiment. Figure 5.5 also shows the complete oxidation of DDC to DDC$^{\bullet}$ after 10 cycles and the hysteresis loop indicating the dimerisation of the radicals to form DSF, similar to that seen in Section 5.2.1.1.

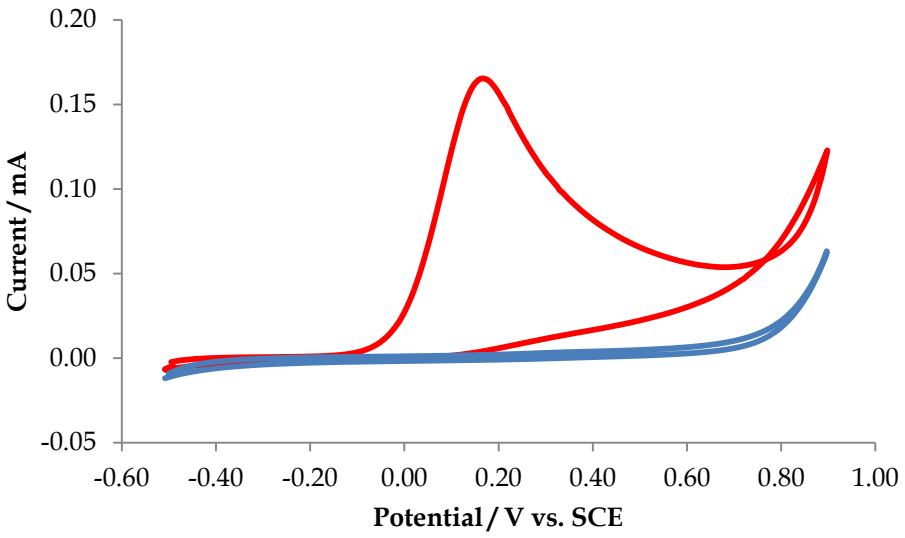

Figure 5.5: Cyclic voltammograms showing cycles — 1 and — 10 of the oxidation of DDC/Nafion coating on a Pt mesh in 0.10 M NaCl at 50 mV s^{-1}.

5.2.1.2.3 Stability of DDC/Nafion on a Pt mesh Electrode

After DDC was electrochemically converted to DSF within the Nafion film, the stability of Pt/DDC/Nafion was investigated. The modified electrode was placed in a fresh solution of 0.10 M NaCl and scanned for 100 cycles at 50 mV s^{-1} between -0.50 and +0.90 V vs. SCE. Figure 5.6 (a) shows every 10^{th} cycle scanned and it can be seen that small oxidation and reduction peaks appeared at +0.80 and -0.50 V vs. SCE respectively in the initial cycles. The peak currents diminished over the first 40 cycles, and then reached a steady state. These are possibly due to the oxidation and reduction of platinum and its oxide. The stability of the modified Pt mesh was therefore investigated in a smaller potential window by repeating the experiment but scanning the potential from -0.10 to +0.60 V vs. SCE. It can be seen from Figure 5.6 (b), where every 10^{th} cycle again is displayed, that there was no redox process occurring in 0.10 M NaCl within this potential window. The electrode remained stable throughout the 100 cycles tested, indicating a more controlled and reliable background for further experiments.

(a)

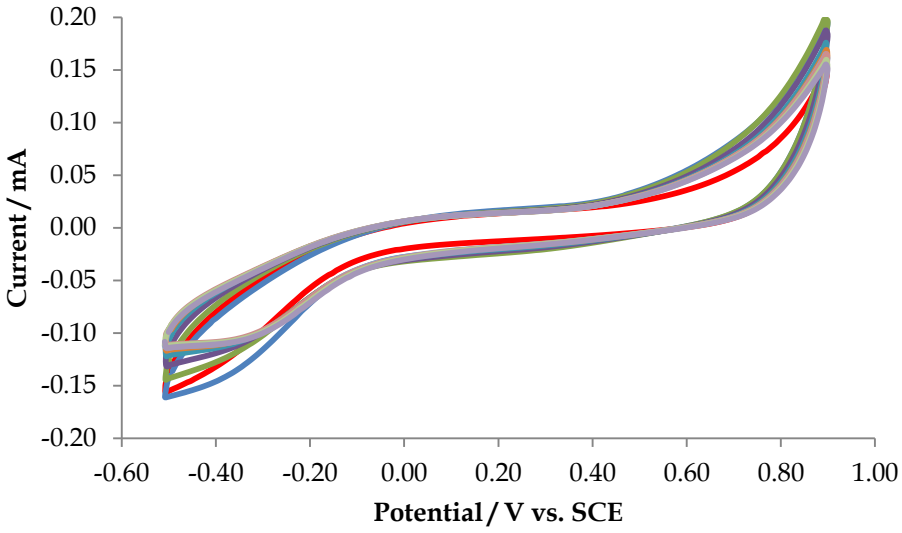

(b)

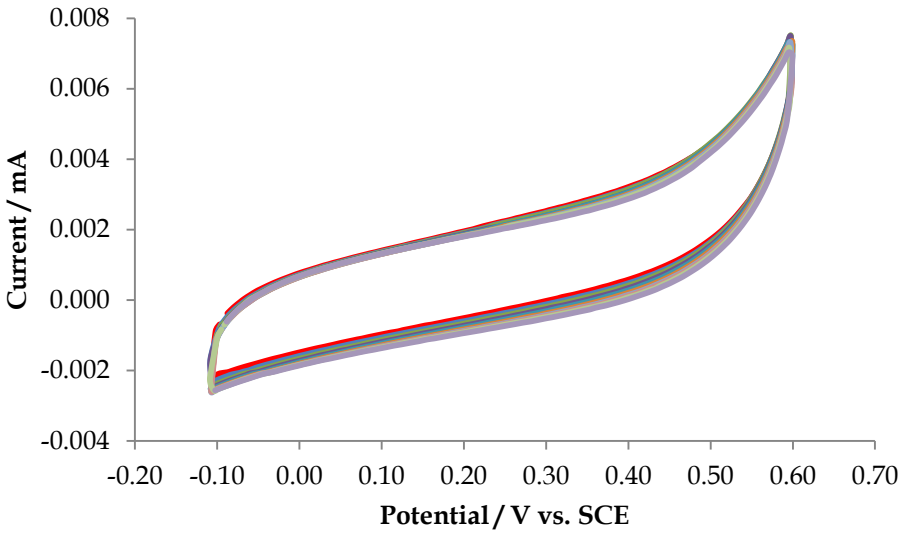

Figure 5.6: Cyclic voltammograms of the DDC/Nafion film on a Pt mesh electrode showing stability over 100 cycles in 0.10 M NaCl at 50 mV s^{-1} comparing the potential windows of (a) -0.50 to +0.90 V vs. SCE and (b) -0.10 to +0.60 V vs. SCE.

5.2.1.2.4 *The Electrochemical Characterisation of Nafion/DSF on a Pt mesh Electrode*

The electrochemical characterisation of both GCE and Pt mesh modified with DDC in Nafion showed the oxidation of DDC which indicated that the resulting modified electrodes consisted of DSF in the Nafion film. To confirm this, the Pt mesh electrode was modified with DSF/Nafion directly from a solution containing 0.030 g DSF in 6.00 mL 5% wt. Nafion (in lower aliphatic alcohols and 15-20% water). The electrode was modified via electrodeposition at 1.00 V vs. SCE for 120 s and dried under an IR lamp for 10 min as in Section 5.2.1.2.1. The electrochemical characterisation of this modified electrode was carried out similarly to the DDC/Nafion modified electrode, whereby the modified mesh was cycled in 0.10 M NaCl for 10 cycles at 50 mV s^{-1}. Figure 5.7 (a) and (b) compares the first and final cycles of this electrochemical characterisation carried out in two different potential windows. Figure 5.7 (a) displays voltammograms in the smaller potential window of -0.10 to +0.60 V vs. SCE, which shows very little change between the initial and final cycles, and shows no significant redox reactions. This shows that both oxidised DDC/Nafion and DSF/Nafion modified electrodes show no electrochemical activity under these conditions, producing a suitable background voltammogram.

Figure 5.7 (b) conversely shows the reduction of DSF at -0.70 V vs. SCE, which was visible as the window was extended to scan from -1.00 to +1.00 V vs. SCE. This is analogous to the reduction peak seen in the final cycle of Figure 5.3 (a) where the DDC/Nafion modified GCE was cycled in a similar potential window. In the previous case, the reduction was seen after the DDC had been converted to DSF; however in this case, the reduction can be seen in the initial cycle as the DSF is readily available. This further supports evidence of DSF formation from the oxidation of DDC. There is no coupled oxidation peak to the reduction of DSF, showing an electrochemically irreversible reaction, suggesting that when the small amount of DSF was reduced to DDC, it was

leached from the Nafion film. This is likely to occur as DDC is a water soluble anion whereas DSF is poorly soluble in aqueous solutions, and is therefore likely to have remained in the Nafion film until it was reduced to DDC. It was therefore deduced that the smaller potential window was most suitable to prevent the loss of DSF from the Nafion film.

(a)

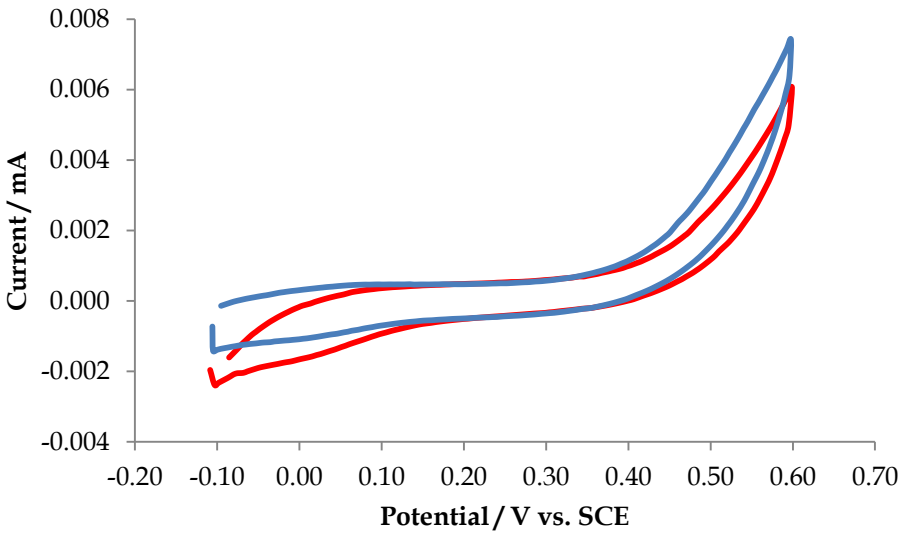

(b)

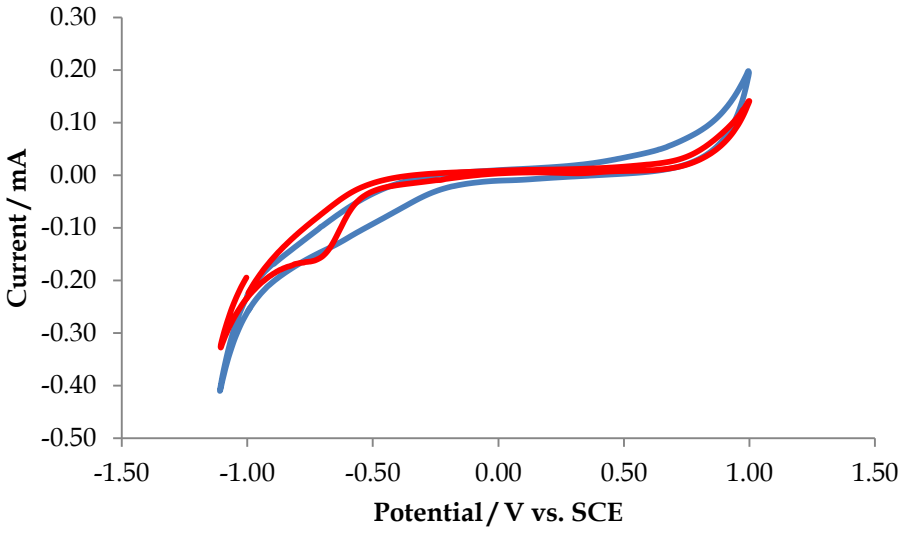

Figure 5.7: Cyclic voltammograms showing cycle — 1 and — 20 of the DSF/Nafion modified Pt mesh in 0.10 M NaCl at 50 mV s^{-1} in various potential windows (a) -0.10 to +0.60 V vs. SCE and (b) -1.00 to +1.00 V vs. SCE.

5.2.2 Copper Detection at a Modified Pt mesh Electrode

The Pt mesh electrode that was characterised in Section 5.2.1 is used in this section for the detection of Cu(II). Firstly, the complexation of DDC and DSF to Cu(II) is explained with reference to the literature. A calibration curve is then used to examine the sensitivity of Pt/DDC/Nafion in the detection of Cu(II). The formation of $Cu(DDC)_2$ at Pt/DDC/Nafion is then verified using cyclic voltammetry and UV-vis spectroscopy.

5.2.2.1 The complexation of DDC and DSF to Cu(II)

It has been shown that the oxidation of a Pt mesh electrode modified with DDC/Nafion film results in the formation of a DSF/Nafion modified electrode. The formation of $Cu(DDC)_2$ from DSF is therefore discussed herein.[283, 292] Tonkin *et al.*,[293] for example, propose that its formation occurs via the 2 electron reduction of DSF to DDC and Victoriano[294] describes the oxidising properties of DSF with the reduction of the ligand breaking the S-S bond. In particular, Burkitt *et al.*[121] have demonstrated the formation of $Cu(DDC)_2$ from DSF in the presence of Cu(II) using electron paramagnetic resonance (EPR). They propose a mechanism whereby with the oxidation of either Cu(I) to Cu(II) or Cu(II) to Cu(III), DSF can undergo a one electron reduction to form the DDC anion and one thiyl radical, as illustrated in Scheme 5.2. Two DDC anions are reported to coordinate with Cu(II) to form the square planar $Cu(DDC)_2$ complex. Similar reactions have also been reported by Jeliakova and Doicheva[295] in studying mixed ligand complexes.

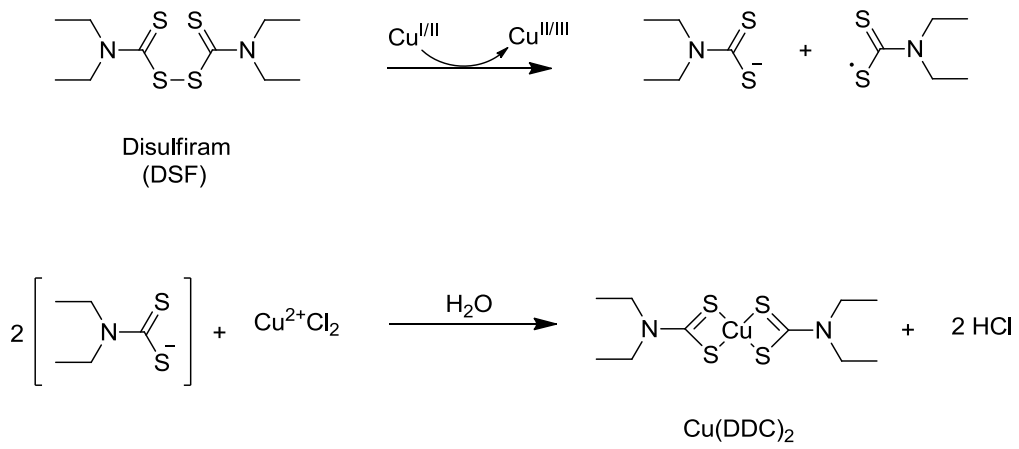

Scheme 5.2 Schematic representation of the complexation of DSF to Cu(II) via the chemical reduction of DSF to DDC and DDC•.

Although in the work discussed herein, Cu(II) was added to the sample solution, the redox cycling would enable the production of Cu(I) which in turn would facilitate the formation of the $Cu(DDC)_2$ complex. The further oxidation of DSF to Bitt-4^{2+} has also been discussed as a possible reaction, depending on the upper limit of the potential window and Cen *et al.*[283] have shown that it is possible for Bitt-4^{2+} to react with Cu(I) to make the $Cu(DDC)_2$ complex. They synthesised the complex shown in Scheme 5.3, and showed that under hydrolysis it can form $Cu(DDC)_2$. Accordingly, it is possible that DDC, DSF and Bitt-4^{2+} all form the $Cu(DDC)_2$ complex in the presence of Cu(II) or Cu(I).[283]

(a)

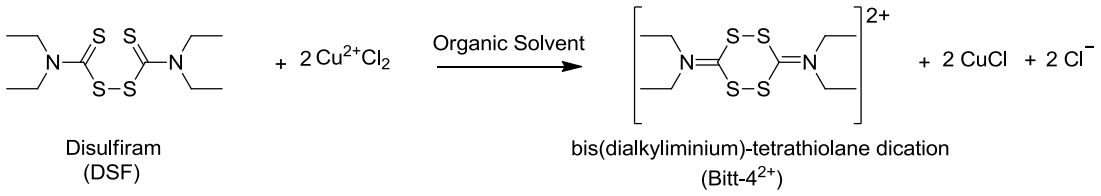

(b)

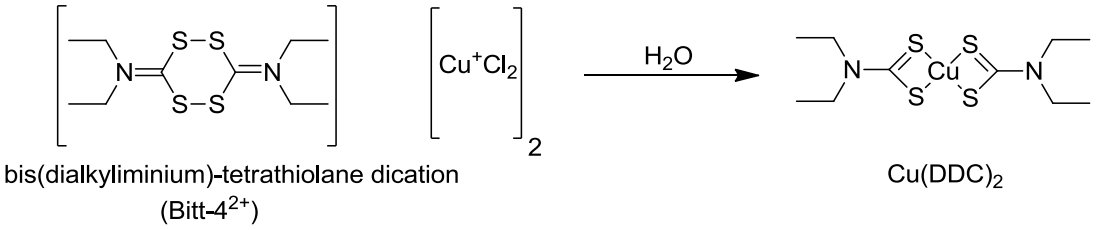

Scheme 5.3: Schematic representation of (a) oxidation of DSF to Bitt-4^{2+} in the presence of Cu(II), and (b) the hydrolysis of [Bitt-4][$CuCl_2$] forming $Cu(DDC)_2$.[283]

5.2.2.2 The Electrochemical Detection of Cu(II) at Nafion/DDC on a Pt Mesh Electrode

The detection of Cu(II) was investigated in this section at a Pt mesh electrode modified with DDC/Nafion using cyclic voltammetry. The Pt mesh was modified as before and cycled in 0.10 M NaCl for 10 cycles to complete the oxidation of DDC to DSF and retrieve a steady baseline. The modified electrode was transferred to a fresh solution of 0.10 M NaCl and a solution containing Cu(II) was added gradually by standard addition. Figure 5.8 shows the electrochemical response of the modified electrode to 2.44×10^{-5} M $CuCl_2$ in comparison to the background of 0.10 M NaCl. The reduction peak at 0.08 V vs. SCE is indicative of the reduction of Cu(II) to Cu(I), also seen at a bare GCE (data not shown) and the coupled oxidation peak at 0.32 V vs. SCE is most likely the oxidation of Cu(I) to Cu(II). Significantly, the redox couple exhibited

in Figure 5.8 is similar to that seen by Bond and Wallace who observed the oxidation of $Cu(DDC)_2$ in 0.10 M acetonitrile which occurred at 0.40 V and 0.47 V vs. Ag/AgCl at a platinum electrode.[122] The peak separation for the redox couple seen in Figure 5.8 is 0.24 V, which is larger than the values of 0.06 V and 0.15 V reported in tetra-n-butyl ammonium bromide (TBAB)/acetone and EtOH respectively, by Dunbar *et al.*[296] for the $Cu(DDC)_2$ complex. This is possibly due to the immobilisation of the complex in the Nafion film which is poorly conducting, making electron transfer less efficient. The $E_{1/2}$ value in this case is 0.22 V which is lower than the values reported of 0.57 V and 0.51 V in TBAB and EtOH respectively,[296] indicating a more thermodynamically favoured reaction, which can be attributed to the immobilisation of the complex on the electrode surface. In restricting the lower potential to -0.10 V vs. SCE, and thus probably inhibiting the reduction of Cu(I) to Cu(0), the majority of Cu(I) was oxidised to Cu(II), resulting in good electrochemical reversibility, indicated by the ratio of the peak currents of 1.28.

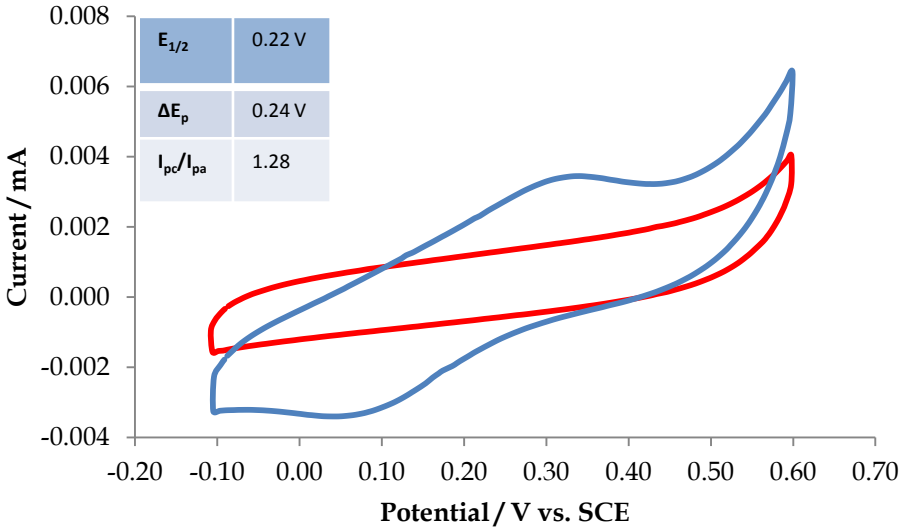

Figure 5.8: Cyclic voltammogram of Pt mesh modified with DDC/Nafion cycled at 50 mV s^{-1} in — 0.10 M NaCl and — 0.10 M NaCl with 2.44×10^{-5} M $CuCl_2$. Electrochemical properties of the redox couple are tabulated inset.

Figure 5.9 (a) shows the detection of various concentrations of Cu(II) at Pt/DDC/Nafion where it can be seen that the peak currents increased linearly (R^2 = 0.96) with increasing concentration of Cu(II). The stability of the modified electrode after the final addition of $CuCl_2$, in the solution of 2.44×10^{-5} M $CuCl_2$, can be seen inset of Figure 5.9 (a) which displays every 10^{th} cycle for 50 cycles. The modified electrode showed good stability in this case, as both the peak potentials and currents remained stable throughout the 50 cycles. A calibration curve was constructed relating the peak current to increasing Cu(II) concentration, and is displayed in Figure 5.9 (b). The standard deviation of the background signal and the slope of the calibration curve were used to calculate the limit of detection of 5.40×10^{-5} M at Pt/DDC/Nafion. This is close to the recommended limit of 3.15×10^{-5} M set by the EPA for drinking water.[12]

(a)

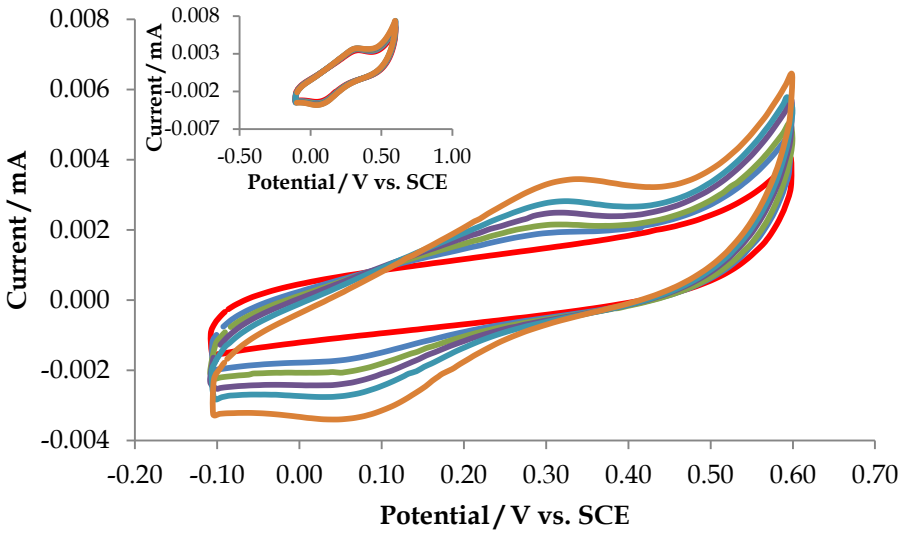

(b)

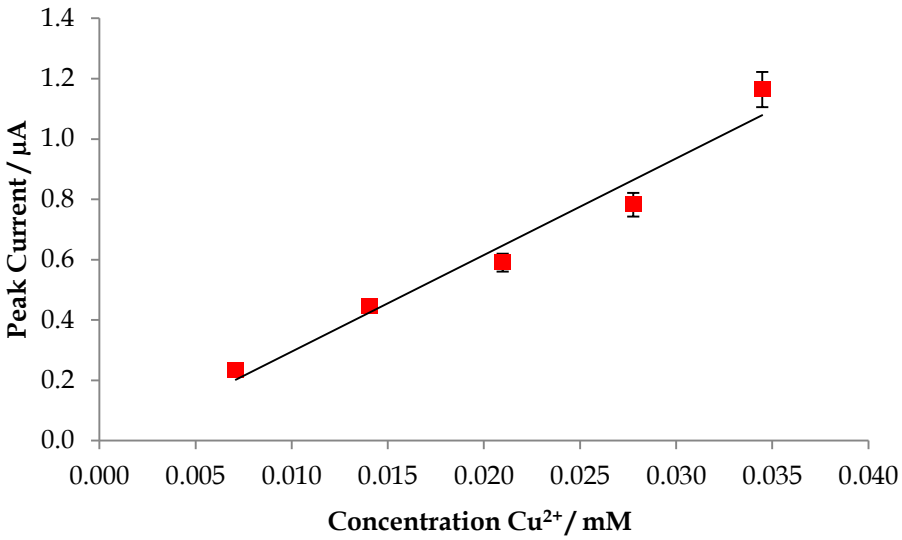

Figure 5.9: Detection of Cu(II)at Pt/DDC/Nafion (a) Cyclic voltammograms scanned between -0.10 and 0.60 V vs. SCE at 50 mV s^{-1} in 0.10 M NaCl and — 0.00, — 4.98×10^{-6}, — 9.90×10^{-6}, — 1.48×10^{-5}, — 1.96×10^{-5} and — 2.44×10^{-5} M $CuCl_2$. Inset plot shows stability of electrode in 2.44×10^{-5} M $CuCl_2$ over 50 cycles. (b) Plot showing the correlation between the peak current and the concentration of Cu(II) used to calculate a limit of detection of 5.40×10^{-5} M. (R^2=0.96).

5.2.2.2 The Verification of Complex Formation at Modified Pt mesh Electrodes

5.2.2.2.1 Electrochemical Investigation to Complex Formation

To confirm that the detection of Cu(II) observed in Section 5.2.2.1 occurred via the formation of $Cu(DDC)_2$, and that the electrochemical response monitored was characteristic of the complex immobilised on the Pt mesh electrode, a number of control experiments were carried out. Firstly, to ensure that the redox response was due to complex formation, the various components of the modified electrode were compared for their response to Cu(II) detection under the same conditions. The detection of Cu(II) is then compared at Pt/DDC/Nafion and at Pt/DSF/Nafion to investigate the complexation mechanism outlined in Section 5.2.2.1.

(i) Bare Pt mesh and Pt/Nafion

Figure 5.10 (a) shows voltammograms of the bare Pt mesh under the specified conditions used previously in Figure 5.8 at two concentrations of Cu(II): 3.50×10^{-5} M and 1.00×10^{-3} M and Figure 5.10 (b) shows the same voltammograms for the Pt mesh coated in 5% wt. Nafion (in lower aliphatic alcohols and 15-20% water). It can be seen from these voltammograms that at the relatively low concentration of 3.50×10^{-5} M Cu(II) (red traces), in the specific potential window of -0.1 to 0.60 V vs. SCE, no copper signal could be identified at either electrode. The voltammogram of the bare Pt electrode cycled in a significantly higher concentration, 1.00×10^{-3} M of Cu(II), (Figure 5.10 (a) blue trace) shows oxidation peaks at 0.17 and 0.40 V vs. SCE and a reduction peak at 0.05 V vs. SCE. The Pt mesh electrode modified with Nafion (Figure 5.10 (b) blue trace) shows oxidation peaks at -0.05 and 0.12 V vs. SCE, and shows a reduction peak at -0.05 V vs. SCE. The absence in both cases of the second reduction peak is likely due to the limit of the potential window; however the voltammograms

indicate the poor sensitivity of the Pt mesh and of the Pt mesh modified with Nafion under these conditions in comparison to Pt/DDC/Nafion.

(a)

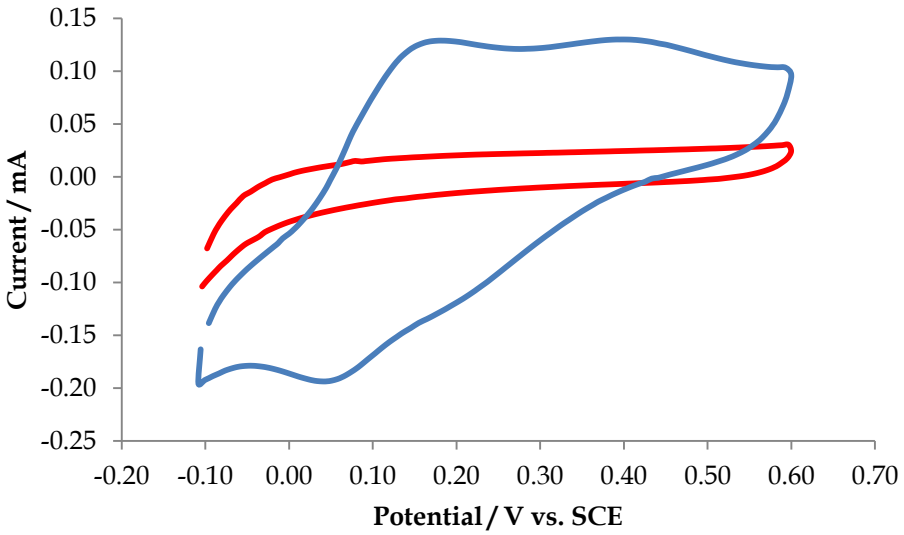

(b)

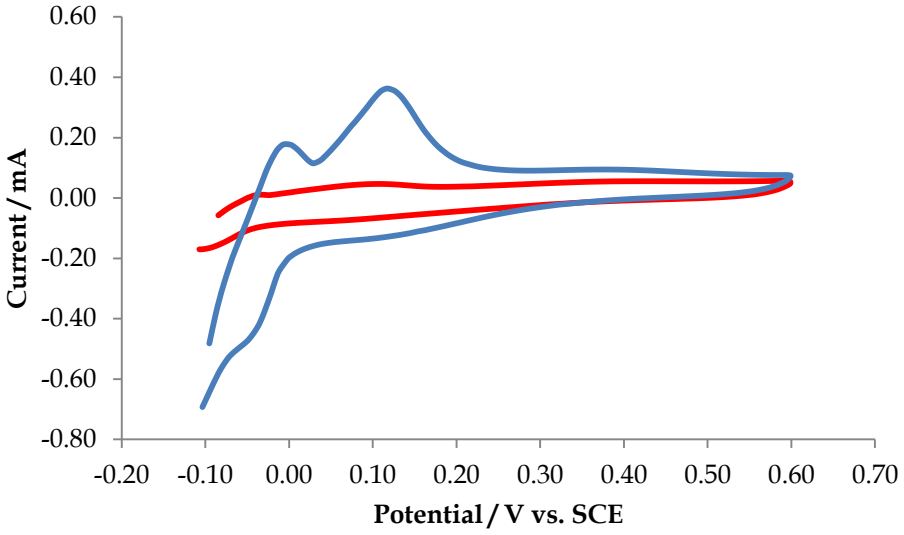

Figure 5.10: Cyclic voltammograms of (a) bare Pt mesh electrode and (b) Pt mesh electrode modified with 5% wt. Nafion (in lower aliphatic alcohols and 15-20% water) via electrodeposition at 1.00 V vs. SCE for 120 s; cycled in — 3.50×10^{-5} M and — 1.00×10^{-3} M Cu(II) in 0.10 M NaCl at 50 mV s^{-1}.

(ii) Pt/DSF/Nafion

The electrochemical conversion of DDC to DSF was carried out in Section 5.2.1.2, which indicated that both electrodes inevitably contained DSF, therefore, the Pt mesh electrode modified with DSF/Nafion was investigated for its ability to detect Cu(II). In Figure 5.11 (a) the detection of Cu(II) can be identified by a redox couple similar to that seen in Figure 5.8 for the oxidised DDC/Nafion modified electrode. Here the predominant oxidation peak can be seen at 0.34 V vs. SCE and the reduction peak can be seen at 0.09 V vs. SCE which are analogous to those seen at the oxidised DDC/Nafion modified electrode.

In Figure 5.11 (b), the detection of Cu(II) at the DSF/Nafion modified mesh is compared to that at the DDC/Nafion modified mesh. It is noteworthy that the concentration of DDC in DDC/Nafion was ten fold that of DSF in DSF/Nafion due to their different solubility. It was also noted that the amount of DSF deposited on the mesh was not measured but was expected to be less than DDC, as DSF is neutral and electrodeposition is dominated by the attraction of opposite charges. In the case of DDC and Nafion, which both are negatively charged, the amount of ligand deposited was therefore expected to be larger and better controlled. The peak currents observed for the detection of Cu(II) at the modified electrodes are therefore only compared relative to their preparation in this preliminary study and as expected, the currents were significantly larger at the oxidised DDC/Nafion modified electrode. Under the specific conditions used here, the use of DDC as opposed to DSF in the preparation of this electrode resulted in a significant increase in the peak currents for the detection of Cu(II) which is illustrated in the table inset of Figure 5.11 (b). The peak positions, however, indicated that the oxidised DDC and DSF modified electrodes detected Cu(II) by the same means, most likely via the formation of $Cu(DDC)_2$.

(a)

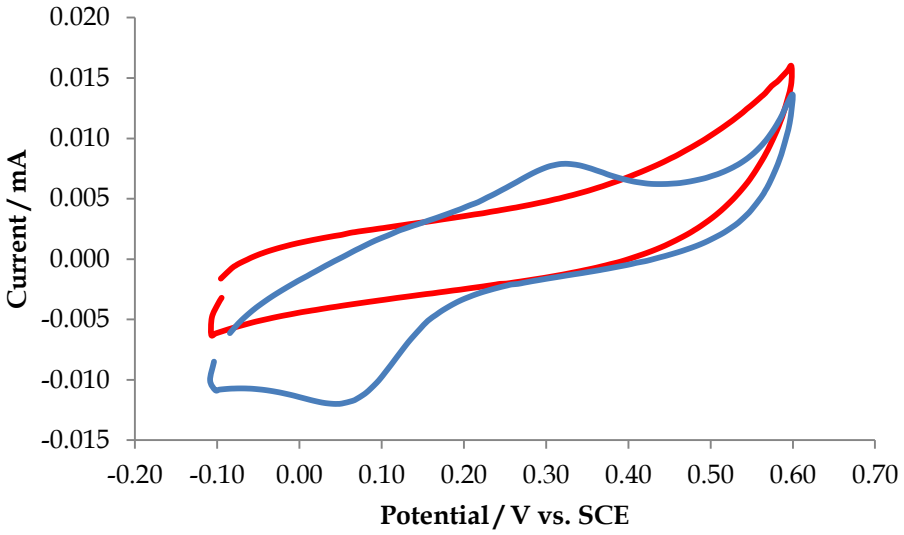

(b)

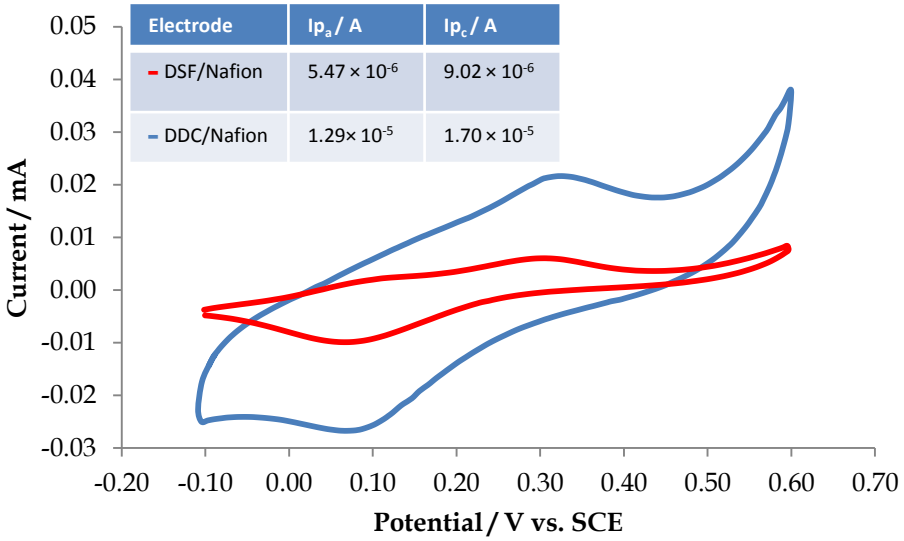

Figure 5.11: Cyclic voltammograms of (a) DSF/Nafion modified Pt mesh in — 0.00 M and — 4.10 × 10^{-5} M Cu(II) in 0.10 M NaCl at 50 mV s^{-1} and (b) Pt mesh modified with — DDC/Nafion (firstly oxidised by cycling in 0.10 M NaCl at 50 mV s^{-1} for 10 cycles) and — DSF/Nafion cycled in 1.40 × 10^{-5} M Cu(II) in 0.10 M NaCl at 50 mV s^{-1} with peak current values tabulated inset.

(iii) Pt/Cu(DDC)$_2$/Nafion

To confirm that the detection of Cu(II) at the modified electrodes occurred via the formation of Cu(DDC)$_2$, a Pt mesh electrode was modified with commercially available Cu(DDC)$_2$. This was carried out by mixing 0.060 g Cu(DDC)$_2$ with 3.00 mL 5% wt. Nafion (in lower aliphatic alcohols and 15-20% water). This provided a 0.06 M solution of Cu(DDC)$_2$, which, according to the Beer-Lambert law, when confined to the Pt mesh electrode, would give a sufficient absorbance to be detected by UV-vis spectroscopy. The Pt mesh electrode was modified with Cu(DDC)$_2$/Nafion similarly to that in Section 5.2.1.2.1 by electrodeposition at 1.00 V vs. SCE for 120 s; and drying under an IR lamp for 10 min.

The electrochemical activity of Cu(DDC)$_2$ has been shown previously in organic solution,[296] however it has not been investigated whilst confined to an electrode in aqueous solution. The electrochemical activity of the complex immobilised in Nafion on the Pt mesh electrode was therefore measured by cyclic voltammetry in 0.10 M NaCl and can be seen in Figure 5.12. Here, a redox couple can be seen at Pt/Cu(DDC)$_2$/Nafion similar to that seen at Pt/DDC/Nafion which had previously been cycled in 0.10 M NaCl and 3.45×10^{-5} M Cu(II). The increased magnitude and slight shift in peak position can be attributed to the both the difference in the Nafion content of both modified electrodes and the different amounts of Cu(DDC)$_2$ in both films which would result in a difference in the conductivity and thickness of the film. However, the similarity in the symmetry of the peaks and their reversibility supports previous evidence that the complex formed at the DDC/Nafion modified electrode is the Cu(DDC)$_2$ complex.

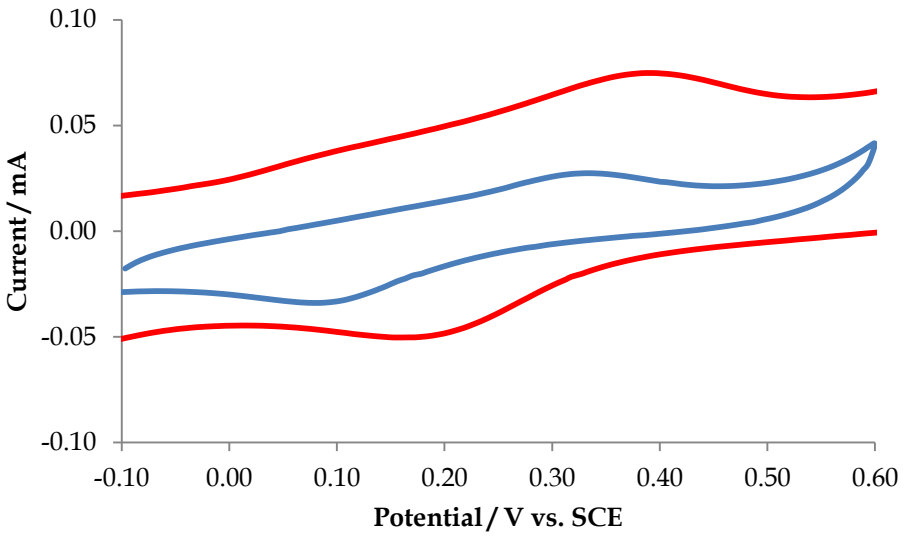

Figure 5.12: Cyclic voltammograms comparing the redox activity of a Pt mesh electrode modified with — $Cu(DDC)_2$/Nafion and — DDC/Nafion cycled in 3.45×10^{-5} M Cu(II); both electrodes cycled in 0.10 M NaCl at 50 mV s^{-1}.

5.2.2.2.2 *UV-vis Analysis of Complex Formation at Modified Pt mesh Electrode*

In Section 5.2.2.2 a Pt mesh electrode was modified with Nafion and DDC, and used to detect Cu(II) via cyclic voltammetry. Electrochemical data in Section 5.2.2.2.1 indicated that the detection occurred as a result of $Cu(DDC)_2$ formation. UV-vis spectroscopy was therefore used in this section to help confirm that the complex formed on the electrode surface was in fact $Cu(DDC)_2$. To investigate the formation of $Cu(DDC)_2$ at the modified Pt mesh electrode, the absorbance spectra of the ligand, DDC and commercially available $Cu(DDC)_2$, were compared to the absorption spectra of the modified electrodes used in the detection of Cu(II).

(i) UV-vis analysis of DDC and $Cu(DDC)_2$

As can be seen in Figure 5.13 (a) and (b), respectively, the absorbance spectrum of 1.70×10^{-5} M DDC was recorded in 0.1 M NaCl and shows absorbance bands at 257 and 282 nm, representing electronic transitions associated with the S-C=S and the N-C=S moieties, respectively.[112] The linear correlation between the absorbance of the peaks with increasing concentration was used to calculate the extinction coefficients (ε) for DDC as 9941 and 10078 $M\ cm^{-1}$, giving absorptions bands of log ε = 4.0 in both cases which agrees with literature reports by Shankaranarayana and Patel.[112]

The colorimetric reaction between DDC and copper, was discovered by Callan and Henderson in 1929,[114] whereby the addition of Cu(II) to the solution of DDC resulted in the formation of the $Cu(DDC)_2$ complex, indicated by its golden-brown colour. According to Dunbar *et al.*,[296] the complex exhibits absorbance bands at 269, 289 and 433 nm in EtOH, with respective extinction coefficients of 11,900, 6,400 and 5,100 $M^{-1}\ cm^{-1}$. The spectrum of 4.20×10^{-6} M $Cu(DDC)_2$ was recorded in EtOH which can be seen in Figure 5.13 (b). The spectrum shows absorbance bands at 434, 270 and 290 nm with absorbance ratios of 2.6 : 1.8 : 1 which agree reasonably well with the literature values reported by Dunbar *et al.*[296]

(a)

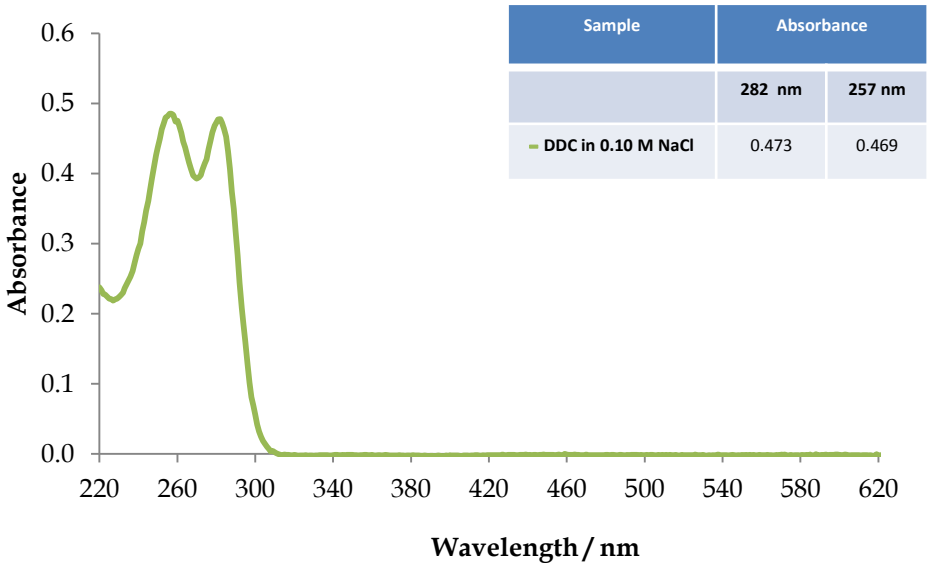

(b)

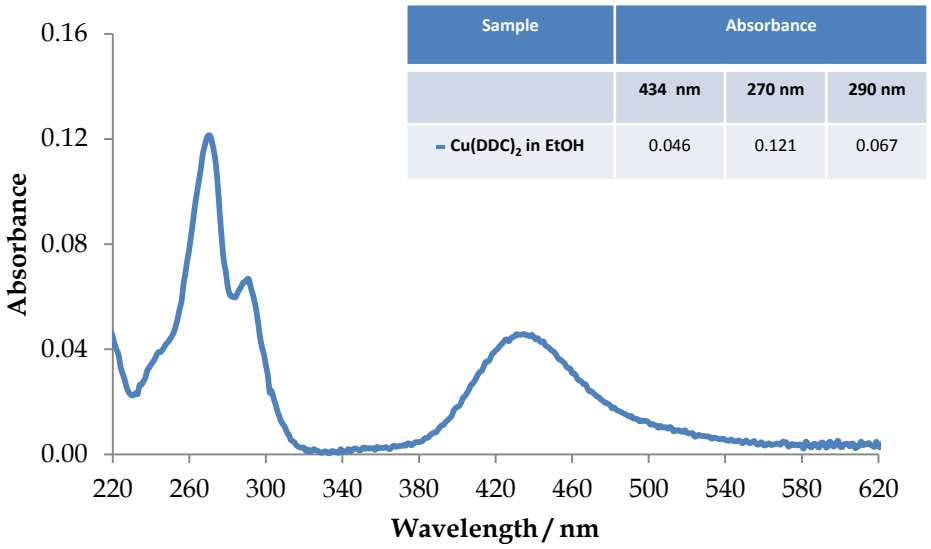

Figure 5.13: Uv-vis absorbance spectra of (a) 1.70×10^{-5} M DDC in 0.10 M NaCl and (b) 4.20×10^{-6} M $Cu(DDC)_2$ in EtOH with absorbance data for relevant peaks tabulated inset.

(ii) *UV-vis analysis of Nafion Films dissolved in EtOH from Modified Electrodes*

To confirm that the complex formed at the DDC/Nafion modified electrode was $Cu(DDC)_2$, the UV-vis spectra of the modified electrodes used in Section 5.2.2.2 were obtained by dissolving the Nafion films in EtOH. This was carried out for the mesh modified with DDC/Nafion oxidised and used to detect Cu(II) and for the Pt mesh modified with $Cu(DDC)_2$/Nafion. The resulting spectra can be seen in Figure 5.14 where absorbance peaks at 434, 290 and 270 nm can be seen in both cases. The ratio of the absorbance of the peaks, (434 nm: 290 nm: 270 nm) were calculated for each sample and it was found that the ratios were 2.4 : 1.9 : 1 and 2.3 : 2.0 : 1 which agree reasonably well with the extinction coefficients reported in the literature.[296] This further indicates that the complex formed at the electrode surface was most likely to be $Cu(DDC)_2$.

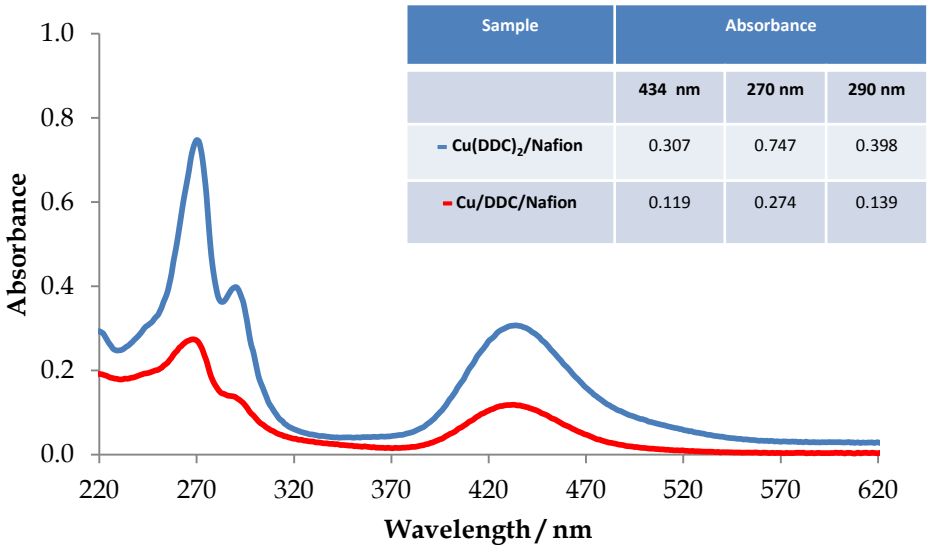

Figure 5.14: UV-vis spectra of Nafion films containing — $Cu(DDC)_2$ and —DDC and Cu(II) dissolved in EtOH.

(iii) UV-vis Analysis of Modified Pt mesh Electrodes

The Pt mesh was used as a WE to allow for the characterisation of the modified electrode using UV-vis spectroscopy. Spectra were therefore obtained of the electrode modified with DDC/Nafion that had been cycled in Cu(II) and the Pt mesh modified with Nafion/$Cu(DDC)_2$ by suspending the electrodes in cuvettes containing H_2O. The resulting spectra can be seen in Figure 5.15 (a) with a magnification of the DDC/Nafion modified electrode inset. Absorbance peaks at 261 nm can be observed in both spectra, however, the absorbance bands in the visible region of the spectra are slightly different at each electrode, which is highlighted in the magnification of the spectra inset of Figure 5.15 (a). At the Pt mesh modified with $Cu(DDC)_2$, the absorbance shows a λ_{max} at 416 nm, however, for the complexed DDC/Nafion modified electrode, the absorbance appears to have a λ_{max} of 406 nm. This is likely due to the poor signal to noise ratio causing asymmetry of the latter peak and poor accuracy in the determination of λ_{max}, as a much lower concentration of the complex was formed at this electrode. However, it is noteworthy that the absorbance peaks occur in the same region (480 – 360 nm) in both cases. This further supports evidence that the complex formed at the electrode surface was $Cu(DDC)_2$, however, further use of the modified mesh electrode in spectrophotometric analysis was not recommended due to its poor sensitivity under these conditions. It is noteworthy, however, that the peaks observed at the modified electrode however, did not coincide with those observed from solution based samples in Figure 5.14, therefore, the film used in Figure 5.14 (a) was dissolved in EtOH to ensure that the peaks were in fact characteristic of the $Cu(DDC)_2$ complex. Figure 5.15 (b) shows UV-vis spectra of the complex immobilised on the Pt mesh electrode in comparison to that dissolved in EtOH. It can be seen here that the peak in the visible region has shifted from 434 to 416 nm, confirming that the absorbance band observed in Figure 5.15 (a) was that of $Cu(DDC)_2$ and indicates that the immobilisation of the complex on the electrode caused the shift in wavelength.

(a)

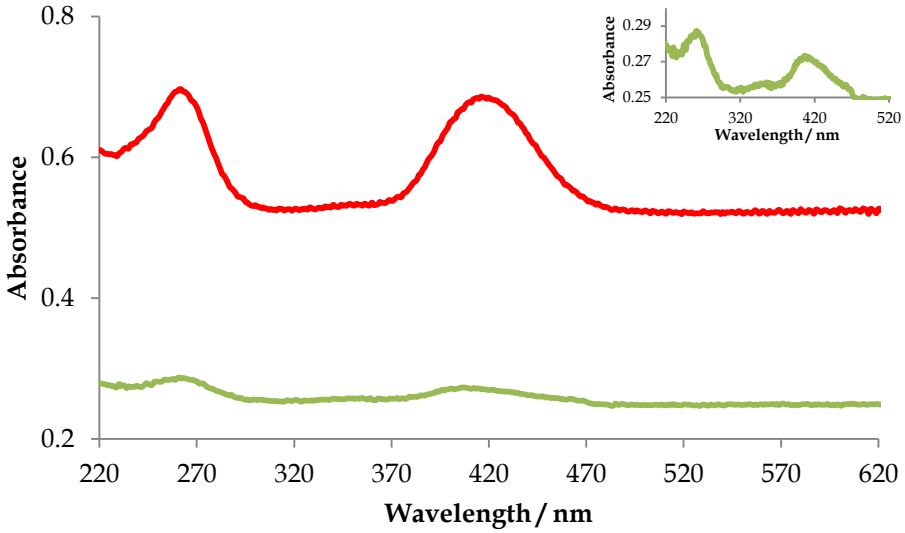

(b)

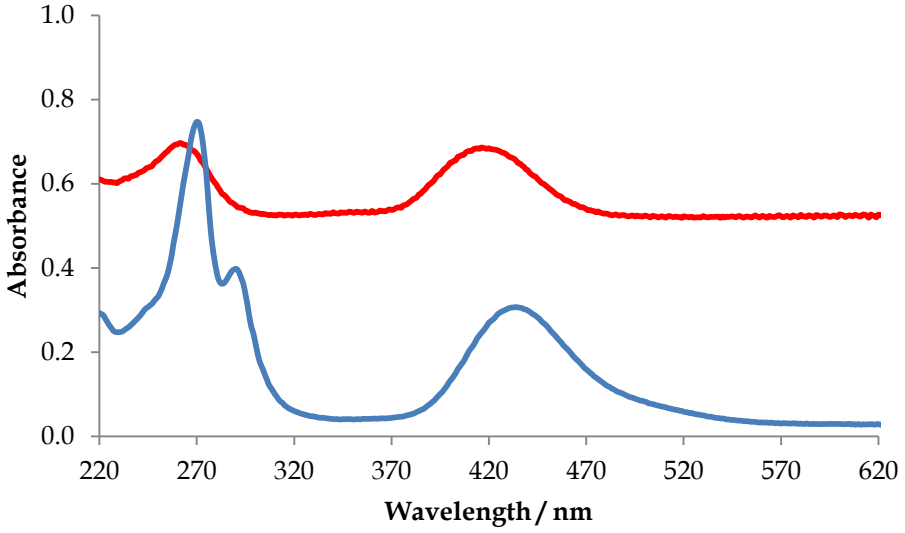

Figure 5.15: UV-vis absorbance spectra of Nafion films (a) immobilised on Pt mesh containing — $Cu(DDC)_2$ (λ = 262 and 416 nm) and — DDC cycled in Cu(II) (λ = 261 and 406 nm), both suspended in H_2O and (b) containing $Cu(DDC)_2$ — immobilised on Pt mesh electrode in H_2O (λ = 262 and 416 nm) and — dissolved in EtOH (λ = 270, 290 and 434 nm).

5.2.3 *Investigating the use of MWCNTs to Enhance the Detection of Cu(II) at a DDC/Nafion Modified Pt mesh Electrode*

It has been shown that a Pt mesh electrode modified with Nafion and DDC has the potential to be used as a Cu(II) sensor thus far, therefore, an attempt was made in this section to enhance the sensitivity of the sensor. MWCNTs have been widely used in the formation of composites[51, 297] and have shown to be very beneficial in electrochemical sensors as the MWCNTs can increase the conductivity and electrochemical performance of the resulting film.[298] This is particularly true of Nafion films as they are poorly conducting, which can hinder their electrochemical performance.[165] In this section, MWCNTs were incorporated into the Nafion film to investigate their effect on the detection of Cu(II).

5.2.3.1 *The Electrochemical Oxidation of DDC at DDC/Nafion/MWCNTs Modified Pt mesh Electrode*

There are many variations reported in the literature for the preparation of nanotube composites,[70] including the modification of MWCNTs , and generally it is found that acid-treated MWCNTs provide a well dispersed matrix.[281] It was found in Chapter 4 however, that acid-treated MWCNTs exhibit a large, broad redox couple at 0.20/0.30 V vs. SCE which is very close to the redox couple of Cu(II) monitored in this work (0.08/0.32 V vs. SCE), therefore large amounts of interference was expected from their use. Pristine MWCNTs were therefore used in the formation of Nafion/MWCNTs composites in this work with note taken that some agglomerations would be present.[46, 299] In this preliminary testing, a 1.0 mg mL^{-1} solution of pristine MWCNTs in 5% wt. Nafion (in lower aliphatic alcohols and 15-20% water) was prepared using sonication for 30 min. The ligand (0.20 M DDC) was added to the Nafion/MWCNTs solution and stirred for 10 min. The Pt mesh electrode was modified with DDC/Nafion/MWCNTs by electrodeposition, as before, by applying 1.00 V vs. SCE to the WE for 120 s. The composite was then dried

under an IR lamp for 10 min. As discussed in Section 5.2.1.1.1, the oxidation of DDC to its radical was observed by cycling the modified electrode in 0.10 M NaCl at 50 mV s^{-1} for 10 cycles. Figure 5.16 (a) shows the initial and final cycles of this oxidation step, where it can be seen that the oxidation peak at 0.03 V vs. SCE had diminished by the 10^{th} cycle. In this case however, unlike the DDC/Nafion modified electrode, a reduction peak was observed at 0.06 V vs. SCE. With continued cycling, the reduction peak increased and an oxidation peak appeared at 0.38 V vs. SCE. This could indicate the oxidation of DSF to Bitt-4^{2+} and its reduction back to DSF, possibly facilitated by the fast electron transfer properties of the MWCNTs. The redox couple reached stable currents and in Figure 5.16 (b) it can be seen that a stable background voltammogram was obtained in a fresh solution of NaCl.

(a)

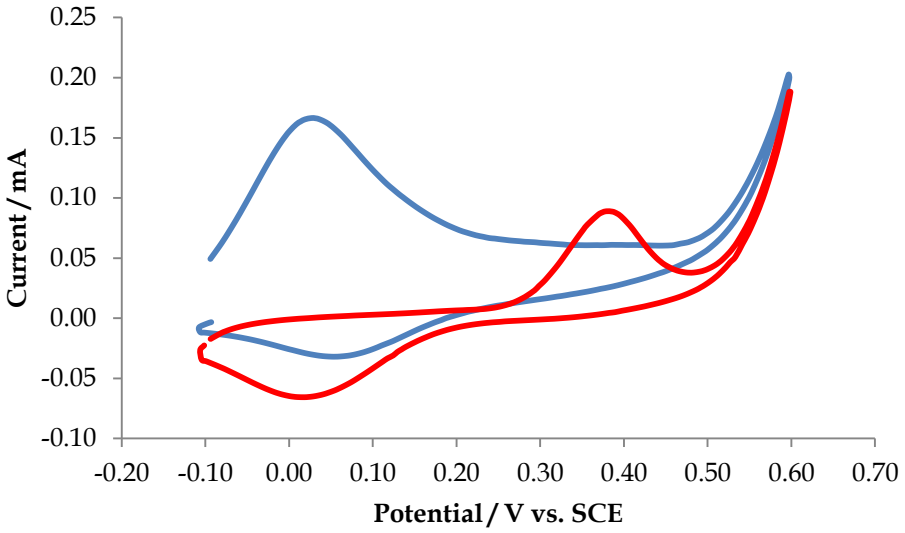

(b)

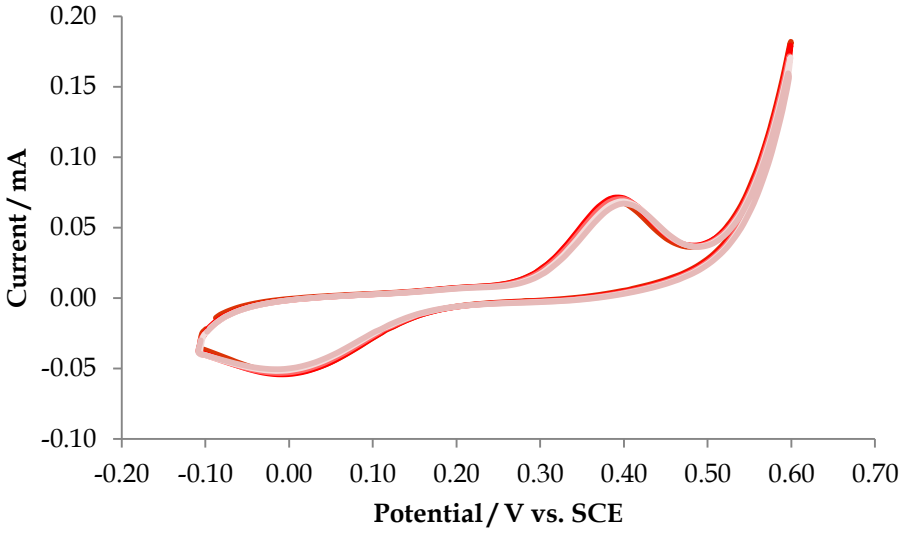

Figure 5.16: Cyclic voltammograms in 0.10 M NaCl at 50 mV s^{-1} of a Pt mesh electrode modified with DDC/Nafion/MWCNTs from 0.20 M DDC and 1.0 mg mL^{-1} MWCNTs in 5% wt. Nafion via electrodeposition at 1.00 V vs. SCE for 120 s (a) cycles — 1 and — 10 showing oxidation of DDC and (b) 10 subsequent overlaying cycles showing the stability of the background.

5.2.3.2 *Electrochemical Detection of Cu(II) at DDC/Nafion/MWCNTs Modified Pt mesh Electrode*

The detection of Cu(II) was investigated at the oxidised DDC/Nafion/MWCNTs modified Pt mesh electrode, similarly to that in Section 5.2.2.1 whereby the electrode was cycled in 0.10 M NaCl and the concentration of Cu(II) was increased gradually by standard addition. It can be seen from these voltammograms, shown in Figure 5.17 (a), that upon addition of Cu(II), the redox couple seen in the background (at 0.06/0.38 V vs. SCE) gradually diminished and a redox pair similar to that seen at the DDC/Nafion modified electrode gradually appeared. This is indicative that the detection mechanism was similar in both cases, however, further work would be required to identify the significance of the background peaks. The voltammograms in Figure 5.17 (b) compare the detection of Cu(II) at Pt/DDC/Nafion to that at Pt/DDC/Nafion/MWCNTs and the calculated electrochemical properties are tabulated inset. The peak positions of this redox couple recorded at Pt/DDC/Nafion/MWCNTs were 0.14/0.24 V vs. SCE giving an $E_{1/2}$ value of 0.19 V with a ΔEp of 0.10 V in this case. These values are lower than the $E_{1/2}$ = 0.22 and ΔEp = 0.24 V seen at Pt/DDC/Nafion which can be explained by the conductivity and the fast electron transfer properties of the MWCNTs. The peak currents were also dramatically enhanced (2.6 fold) by the incorporation of MWCNTs into the DDC/Nafion film and the electrochemical reversibility at the DDC/Nafion modified Pt mesh electrode was improved with the incorporation of MWCNTs; from I_{pc}/I_{pa} = 1.28, to I_{pc}/I_{pa} = 1.10. This is also a good indication that the incorporation of MWCNTs into the DDC/Nafion film would lead to more sensitive detection of Cu(II). To preliminarily screen the sensitivity of Pt/DDC/Nafion/MWCNTs in comparison to Pt/DDC/Nafion, the current response at each electrode was compared at the same concentration. The current response for the reduction of 3.45×10^{-5} M Cu(II) at Pt/DDC/Nafion was 1.16×10^{-6} A. The current response under the same conditions at Pt/DDC/Nafion/MWCNTs was recorded as 4.71×10^{-5} A, which is an increase of over 40 fold.

(a)

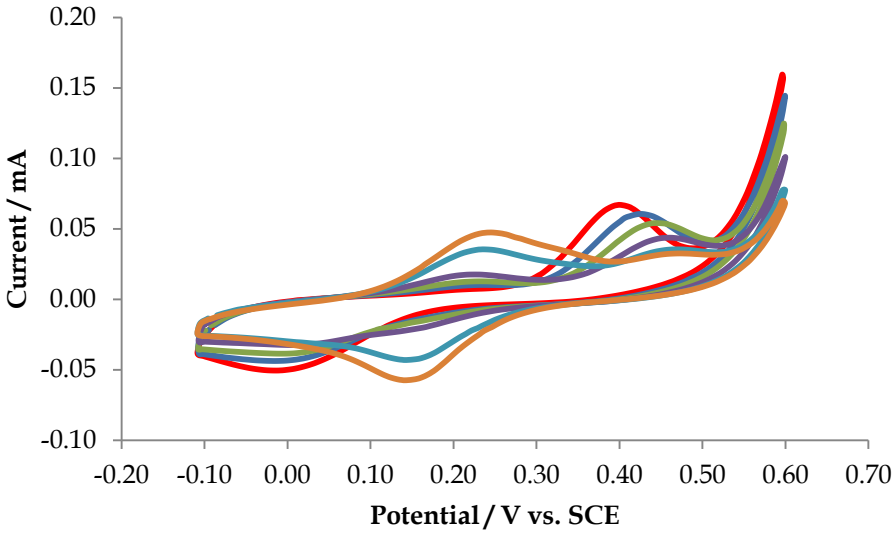

(b)

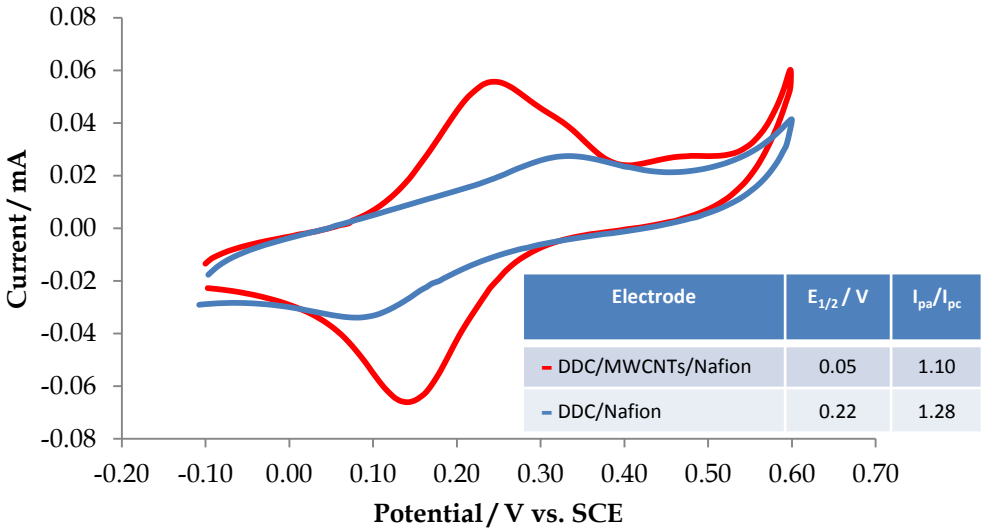

Figure 5.17: Cyclic voltammograms of Pt mesh electrode modified with (a) —DDC/Nafion/MWCNTs from 0.20 M DDC and 1.0 mg mL^{-1} MWCNTs in 5% wt. Nafion via electrodeposition at 1.00 V vs. SCE for 120 s; cycled in 0.10 M NaCl with additions of — 0.00, — 7.09 × 10^{-6}, — 1.40 × 10^{-5}, — 2.10 × 10^{-5}, — 2.78 × 10^{-5} and — 3.45 × 10^{-5} M $CuCl_2$ and (b) — DDC/Nafion/MWCNTs and —DDC/Nafion from 0.20 M DDC in 5% wt. Nafion, both in 0.10 M NaCl containing 3.45 × 10^{-5} M $CuCl_2$ with relevant data tabulated inset.

5.2.3.3 Verification of Complex formation at DDC/Nafion/MWCNTs Modified Pt mesh Electrode

To confirm that the detection of Cu(II) at the DDC/Nafion/MWCNTs modified electrode was via the formation of the $Cu(DDC)_2$ complex, the detection of Cu(II) was compared to that at a Pt mesh modified with Nafion/MWCNTs. The Pt mesh was modified via electrodeposition as before from a solution of 1.0 mg mL^{-1} MWCNTs in 5% wt. Nafion (in lower aliphatic alcohols and 15-20% water) at 1.00 V vs. SCE for 120 s. The modified electrode was dried at an IR lamp for 10 min and cycled in the background electrolyte of 0.10 M NaCl to obtain a steady background current. The voltammogram in Figure 5.18 shows the response of the modified electrode to 3.45×10^{-5} M $CuCl_2$ in comparison to that at the DDC/Nafion/MWCNTs modified Pt mesh. It is clear from this voltammogram that the detection at both electrodes is very different with the Nafion/MWCNTs modified mesh showing similar peak positions to the Nafion modified mesh seen in Figure 5.10 (b), but with enhanced peak currents. This indicates that the detection of Cu(II) at the DDC/Nafion/MWCNTs modified electrode occurred via the complexation of Cu(II) to DDC, which as shown previously, results in the formation of $Cu(DDC)_2$ complex.

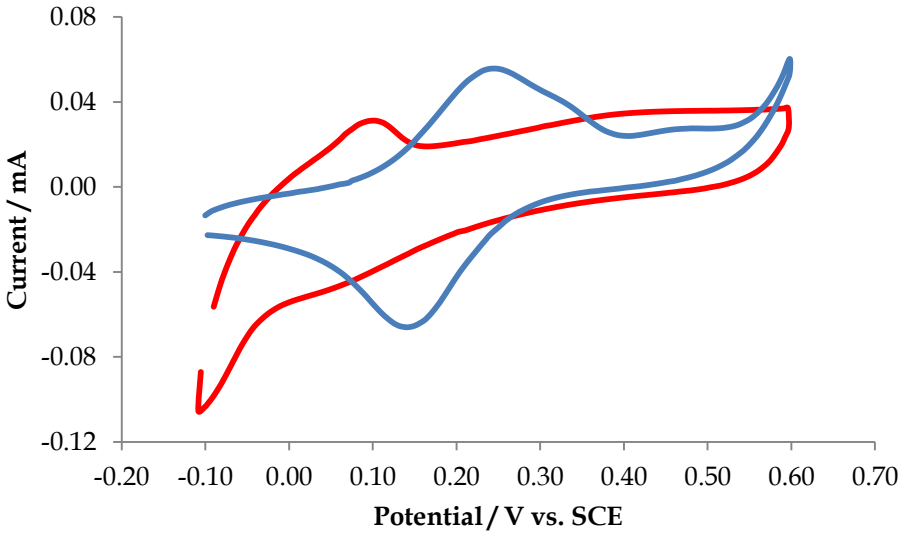

Figure 5.18: Cyclic voltammograms of Pt mesh electrode modified with — DDC/Nafion/MWCNTs from 0.20 M DDC and 1.0 mg mL^{-1} MWCNTs in 5% wt. Nafion, and — Nafion/MWCNTs from 1.0 mg mL^{-1} MWCNTs in 5% wt. Nafion, via electrodeposition at 1.00 V vs. SCE for 120 s, both in 0.10 M NaCl containing 3.45×10^{-5} M $CuCl_2$.

5.2.3.4 Reproducibility of DDC/Nafion/MWCNTs Modified Pt mesh Electrode

The reproducibility of the DDC/Nafion/MWCNTs modified Pt mesh was investigated in the detection of Cu(II) and 3 repeated experiments can be seen in Figure 5.19. The voltammograms highlight the poor reproducibility of the sensor which is most likely due to poor reproducibility in the incorporation of MWCNTs into the Nafion film. As discussed previously, the electrodeposition of Nafion and DDC is based on the attraction of their negatively charged moieties to the positive potential applied to the WE. As the MWCNTs used in this section were not modified and thus were expected to contain very few negatively charged sites, their incorporation into the Nafion film is likely to be predominantly due to physical entrapment. It is therefore suggested that the reported method of preparation is unsuitable for the modification of an electrode with MWCNTs. As the electrochemical response of the

DDC/Nafion/MWCNTs modified electrode was clearly enhanced as a result of the incorporation of MWCNTs, the experimental design should be revised to optimise its use for further work.

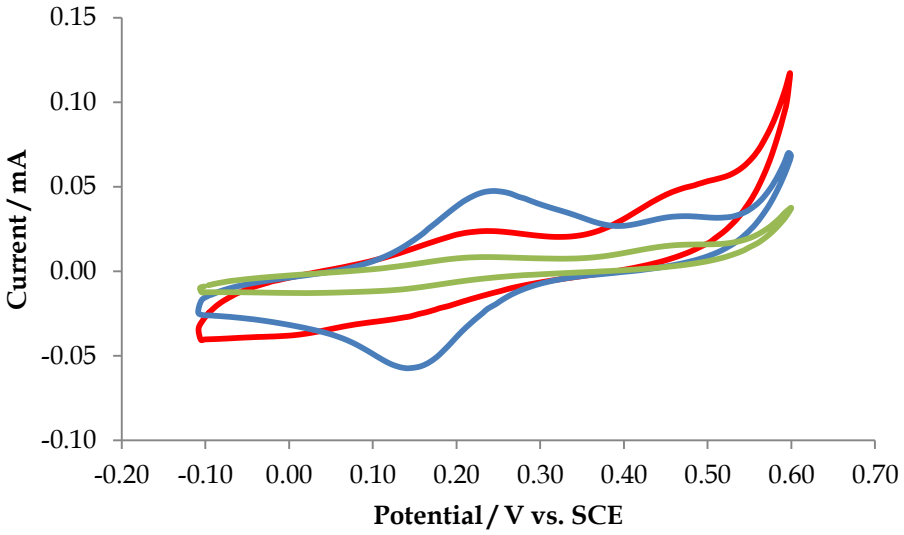

Figure 5.19: Cyclic voltammograms of Pt mesh modified with DDC/Nafion/MWCNTs from 0.20 M DDC and 1.0 mg mL^{-1} MWCNTs in 5% wt. Nafion in 2.44 × 10^{-5} M $CuCl_2$ in 0.10 M NaCl for repeated experiments — n=1 — n=2 and — n=3 showing poor reproducibility.

5.3 Conclusion

This chapter has demonstrated the modification of a Pt mesh electrode with the ligand DDC immobilised in a Nafion film and its subsequent oxidation to DSF. It has been shown that this resulting modified electrode can be used as a simple sensor for the detection of Cu(II) ions in solution and a detection limit of 5.40×10^{-5} M was determined using cyclic voltammetry.

The electrodeposition of the ligand, DDC, in Nafion on the Pt mesh and its electrochemical oxidation has been monitored using cyclic voltammetry. The oxidation of DDC was consistent with the formation of DSF, which was confirmed by independent studies, carried out on Pt/DSF/Nafion. Control studies involving Pt/DSF/Nafion, Pt/Nafion and bare Pt were also carried out to confirm that the sensing of Cu(II) occurred at the oxidised DDC/Nafion film. It was evident from these studies that the interactions of DSF/Nafion and oxidised DDC/Nafion with Cu(II) were very similar, however, it was found that due to its solubility and electroactivity, DDC was the favoured ligand for use in the preparation of the modified electrode.

Studies were also carried out in this chapter to identify the complexation of Cu(II) at the modified electrode with the formation of $Cu(DDC)_2$. In order to confirm the formation of the complex, cyclic voltammetry was carried out on a $Cu(DDC)_2$/Nafion modified electrode and compared to the oxidised DDC/Nafion modified electrode cycled in Cu(II). A similar redox couple was observed at both electrodes. UV-vis spectroscopy of the Pt mesh was also utilised as a means of confirming the complexation of Cu(II) at the modified electrode. It was found however, that the poor signal to noise ratio at the Pt mesh electrode, due to the short path length, decreased the sensitivity of the absorbance spectra, and a definitive characterisation could not be made at the oxidised DDC/Nafion modified electrode. The spectra were obtained for the films deposited on both electrodes by dissolving the Nafion films in EtOH, and it was found that both films exhibited very similar absorbance spectra giving

good evidence that $Cu(DDC)_2$ was formed at the oxidised DDC/Nafion modified electrode cycled in Cu(II).

An attempt was made to enhance the sensitivity of the oxidised DDC/Nafion modified electrode towards the detection of Cu(II) by introducing MWCNTs into the film. Preliminary investigations suggested that the MWCNTs enhanced the electrochemical response of the modified electrode and a larger current response was observed, which would signify greater sensitivity. Problems arose with the reproducibility of this modified electrode however, with variable amounts of MWCNTs incorporated into each DDC/Nafion film formed.

In summary these preliminary studies would indicate that an oxidised DDC/Nafion modified electrode could form the basis of a simple sensor for the detection of Cu(II) using cyclic voltammetry. Further studies would be recommended however to optimise the loading of DDC in the Nafion film and to optimise the film thickness. There is also the possibility of altering the morphology, and thus the physical properties of the film using heat treatments.[300] Studies would also be required to determine the effects of interferants such as Pb(II) and Fe(III) which form well known complexes with DDC,[122] on the electrochemical detection of Cu(II).

Chapter 6:

Conclusions and Future Work

6.1 Introduction

The work presented in this thesis has shown the characterisation and ultimate use of electrochemical sensors in the detection of metal ions. The design of the electrochemical sensors was based on the use of carbon nanomaterials on electrode substrates. The nanomaterials were characterised electrochemically using the redox probe: potassium ferricyanide $[Fe(CN)_6]^{3-}/[Fe(CN)_6]^{4-}$ in Chapter 3 and the electrochemical detection of Cr(VI) and Cu(II) were explored in Chapters 4 and 5 respectively.

6.2 Results

6.2.1 The Electrochemical Characterisation of Carbon–based Nanomaterials

The basic electrochemical sensors prepared were (i) GCE/MWCNTs and (ii) GCE/graphene, for characterisation with the ferricyanide probe. In the characterisation of the GCE/MWCNTs, the currents and potentials were measured as a function of both scan rate and of the amount of the nanomaterial on the electrode surface using cyclic voltammetry. Analysis of the voltammograms showed that sonication of both materials combined with low casting volumes (5-10 μL) resulted in an enhanced electrochemical response to that exhibited at the bare GCE which is illustrated in Table 6.1.

The capacitance values for the electrodes modified with MWCNTs and graphene were calculated from the background currents as a function of the amount of material on each electrode, i.e. the gravimetric capacitance. It was found that sonication of the MWCNTs provided a gravimetric capacitance of 11.6 F g^{-1}, which was significantly larger than that calculated at the electrodes modified with non-sonicated MWCNTs (5.0 F g^{-1}). The capacitance measured at the GCE modified with 5 μL sonicated graphene was somewhat lower than

that measured at the MWCNTs modified electrodes, however, giving a gravimetric capacitance of 2.6 F g^{-1}.

The peak potentials representing the oxidation and reduction of the $[Fe(CN)_6]^{3-}/[Fe(CN)_6]^{4-}$ redox probe were also examined for the MWCNTs modified electrodes. Analysis of the peak separations with respect to the amount of material cast on the electrode and scan rate indicated that transport of the analyte through to the electrode surface inhibited electron transfer. It also indicated that when the sample had diffused into the MWCNT film, thin layer diffusion was an important contributor to the electrochemical response observed. The rate constants for the $[Fe(CN)_6]^{3-}/[Fe(CN)_6]^{4-}$ redox couple were calculated from these peak separations using the Kochi and Klingler equation and the Nicholson Theory. Both equations provided different rate constants which is likely due to the fact that α=0.5 and that only semi-infinite planar diffusion of the analyte occurs in the Nicholson Theory. In comparing the two methods of calculating the rate constant at the various modified electrodes, it was found that the Kochi and Klingler method gave a more accurate calculation. The heterogeneous rate of electron transfer was calculated in all cases and the GCE modified with 5 µL sonicated MWCNTs (2.36×10^{-3} cm s^{-1}) was found to have faster rate of electron transfer than the GCE modified with 5 µL sonicated graphene (8.16×10^{-4} cm s^{-1}).

The peak currents measured at the modified electrodes were used to give an indication of the electroactive surface area at the modified electrodes. In general, the peak currents measured at the GCE modified with sonicated MWCNTs were larger then those seen at the GCE modified with sonicated graphene (illustrated in Table 6.1). The Randles Sevcik equation was used to calculate the electroactive surface areas of the modified electrodes, based on the diffusion coefficient at the bare GCE. As the diffusion of the analyte was expected to be different at both modified electrodes in comparison to the bare GCE, this surface area is used purely as a comparative tool. The so determined surface area of the MWCNTs modified electrode (0.377 cm^2) was significantly

larger than the graphene modified electrode (0.092 cm^2), which is likely due to the entangled morphology and large aspect ratio of the MWCNTs. It can be seen by the electrochemical characterisation illustrated in Table 6.1 that overall, the GCE modified with MWCNTs displayed more impressive properties than the GCE modified with graphene.

Table 6.1: Electrochemical characterisation of GCE modified with 5 µL sonicated MWCNTs and graphene.

Parameter	MWCNTs	Graphene
Peak Current (I_{pa} / mA)	0.065	0.016
Peak Separation (ΔE_p / V)	0.075	0.088
Capacitance (F g^{-1})	11.6	2.6
Rate Constant (k / cm s^{-1})	2.36×10^{-3}	8.16×10^{-4}
Surface area (cm^2)	0.377	0.092

6.2.2 The Application of a MWCNTs Modified Electrode in the Detection of Cr(VI)

The electrochemical detection of Cr(VI) was measured by the reduction of Cr(VI) to Cr(III) using a variety of electrochemical techniques. Initially, cyclic voltammetry was implemented to investigate the important factors affecting the electrochemical detection at a GCE modified with MWCNTs. It was seen that the reduction could be monitored by a reasonably stable peak at 0.65 V vs. SCE at this electrode. It was found that this process was not significantly affected by the conductivity of the sample solution or by the interference of Cl^- or Cu^{2+}. The presence of NO_3^- however, interfered with the reduction peak current and poor reproducibility was noted when using real water samples. The most important parameter in the electrochemical detection of Cr(VI) was found to be the pH of the sample solution, however, the process did not follow

simple Nernstian behaviour. The optimum pH for Cr(VI) reduction in this case was found to be 2.0.

A wide range of modified electrodes were studied for their ability to reduce Cr(VI), which was generally measured by the peak potential and peak current using cyclic voltammetry. The range of modifications carried out on the electrodes included the use of polypyrrole and the use of Au nanoparticles. Limits of detection for the reduction of Cr(VI) were calculated using the slope of the calibration curve and the standard deviation of the background current. The sensitivity of the detection was also enhanced by the use of constant potential amperometry at a rotating disc electrode. The lowest limit of detection for the reduction of Cr(VI) was 1.20×10^{-6} M which was achieved at an Au rotating disc electrode modified with oxidised MWCNTs decorated with Au nanoparticles using constant potential amperometry.

6.2.3 The Electrochemical detection of Cu(II)

The detection of Cu(II) was measured by the complexation of Cu(II) to a DDC ligand and its subsequent reduction to Cu(I) and re-oxidation to Cu(II). This was carried out at a Pt mesh electrode modified with Nafion containing the DDC ligand using constant potential to electrodeposit the film on the substrate. The DDC ligand was oxidised prior to complexation to form DSF, however, UV-vis studies were carried out to show that the reaction of Cu(II) with DDC and DSF both resulted in the formation of $Cu(DDC)_2$, therefore this was not an issue. As DDC was more suitable for the modification of the electrode, it's use was continued. The oxidation and reduction cycling of the modified electrode in Cu(II), forming $Cu(DDC)_2$, was used to electrochemically detect Cu(II). This provided a limit of detection of 5.40×10^{-5} M using cyclic voltammetry.

MWCNTs were incorporated into the Nafion/DDC film in an attempt to increase the sensitivity of the detection. The peak currents for the oxidation

and reduction of Cu(I)/Cu(II) increased dramatically with this modification, however, reproducibility was poor which suggested that differing amounts of MWCNTs were incorporated into the Nafion film for each experiment.

6.3 Future Work

The most promising route to progress with the detection of Cr(VI) from Chapter 4, would involve the use of the rotating disc electrode and the use of Au nanoparticles. The parameters that could be optimised are the Au nanoparticle loading and the method of deposition for the Au nanoparticles. I would also suggest the use of an Au alloy nanoparticle such as Au-Pd. Further work on the detection of Cu(II) should involve optimising the incorporation of MWCNTs into the Nafion/DDC film as well as exploring the use of different electrochemical techniques, such as differential pulse voltammetry.

Bibliography

1. Agency, E. P. *Water Quality in Ireland 2007 - 2009*; Environmental Protection Agency: Ireland, 2009, 2009.
2. Nriagu, J. O., *Chromium in the Human and Natural Environment*. Wiley: 1988.
3. Pourbaix, M., *Atlas of electrochemical equilibria in aqueous solutions*. National Association of Corrosion Engineers: 1974.
4. Franchini, J.; Magnani, E.; Mutti, A., *Scand. J. Work Env. Hea.* **1983,** *9*, 247.
5. Dixon, F. W., *J. Amer. Med. Asoc.* **1929,** *93*, 837.
6. Bigby, M., *Arch. Dermatol.* **1990,** *126*, 1247.
7. Mayer, L. M.; Schick, L. L., *Environ. Sci. Technol.* **1981,** *15*, 1482.
8. Shannon, M. W.; Borron, S. W.; Burns, M. J.; Haddad, L. M.; Winchester, J. F., *Haddad And Winchester's Clinical Management of Poisoning And Drug Overdose*. Elsevier Science Health Science Division: 2007.
9. Bucossi, S.; Ventriglia, M.; Panetta, V.; Salustri, C.; Pasqualetti, P.; Mariani, S.; Siotto, M.; Rossini, P. M.; Squitti, R., *J. Alzheimers Dis.* **2011,** *24*, 175.
10. Brewer, G. J., *J. Am Coll. Nutr.* **2009,** *28*, 238.
11. Myers, J. R.; Cohen, A., *American Waterworks Association* **1984**.
12. Agency, E. P. *The Provision and Quality of Drinking Water in Ireland : A Report for the Year 2010* Environmental Protection Agency: 2010, 2010.
13. Matlock, M. M.; Howerton, B. S.; Atwood, D. A., *Water Res.* **2002,** *36*, 4757.
14. Querol, X.; Viana, M.; Alastuey, A.; Amato, F.; Moreno, T.; Castillo, S.; Pey, J.; de la Rosa, J.; de la Campa, A. S.; Artinano, B.; Salvador, P.; Dos Santos, S. G.; Fernandez-Patier, R.; Moreno-Grau, S.; Negral, L.; Minguillon, M. C.; Monfort, E.; Gil, J. I.; Inza, A.; Ortega, L. A.; Santamaria, J. M.; Zabalza, J., *Atmos Environ* **2007,** *41*, 7219.

15. Clenaghan, C.; O'Neill, N.; Page, D. *Dangerous Substances Regulations National Implementation Report, 2005*; Environmental Protection Agency: Ireland, 2005.
16. Liu, J.; Wang, Q.; Li, D., *Res. J. Chem. Environ.* **2011,** *15*, 372.
17. Kozono, S.; Itoh, T.; Yoshinaga, A.; Ohkawa, S.; Yakushiji, K., *Anal. Sci.* **1994,** *10*, 477.
18. Janata, J., Electrochemistry Encyclopedia. Sensors, E., Ed. 2010.
19. Haber, F.; Klemensiewicz, Z. Z., *Phys. Chem.* **1909,** *67*.
20. Windmiller, J. R.; Wang, J., *Electroanal.* **2013,** *25*, 29.
21. Kim, D. H.; Lu, N.; Ma, R.; Kim, Y. S.; Kim, R. H.; Wang, S.; Wu, J.; Won, S. M.; Tao, H.; Islam, A.; Yu, K. J.; Kim, T. I.; Chowdhury, R.; Ying, M.; Xu, L.; Li, M.; Chung, H. J.; Keum, H.; McCormick, M.; Liu, P.; Zhang, Y. W.; Omenetto, F. G.; Huang, Y.; Coleman, T.; Rogers, J. A., *Science* **2011,** *333*, 838.
22. Chuang, M.-C.; Yang, Y.-L.; Tseng, T.-F.; Chou, T.; Lou, S.-L.; Wang, J., *Talanta* **2010,** *81*, 15.
23. Zou, J.; Liu, J.; Karakoti, A. S.; Kumar, A.; Joung, D.; Li, Q.; Khondaker, S. I.; Seal, S.; Zhai, L., *ACS Nano* **2010,** *4*, 7293.
24. Bolger, F. B.; McHugh, S. B.; Bennett, R.; Li, J.; Ishiwari, K.; Francois, J.; Conway, M. W.; Gilmour, G.; Bannerman, D. M.; Fillenz, M.; Tricklebank, M.; Lowry, J. P., *J. Neurosci. Meth.* **2011,** *195*, 135.
25. Finnerty, N. J.; O'Riordan, S. L.; Palsson, E.; Lowry, J. P., *J. Neurosci. Meth.* **2012,** *209*, 13.
26. Sequeira, M.; Bowden, M.; Minogue, E.; Diamond, D., *Talanta* **2002,** *56*, 355.
27. McGraw, C. M.; Stitzel, S. E.; Cleary, J.; Slater, C.; Diamond, D., *Talanta* **2007,** *71*, 1180.
28. Cleary, J.; Slater, C.; McGraw, C.; Diamond, D., *Sensors* **2008,** *8*, 508.
29. Feier, B.; Floner, D.; Cristea, C.; Bodoki, E.; Sandulescu, R.; Geneste, F., *Talanta* **2012,** *98*, 152.
30. Noyhouzer, T.; Mandler, D., *Electroanal.* **2013,** *25*, 109.

31. Kroto, H. W.; Heath, J. R.; O'Brien, S. C.; Curl, R. F.; Smalley, R. E., *Nature* **1985,** *318*, 162.
32. Csiszár, M.; Szucs, Á.; Tölgyesi, M.; Mechler, Á.; Nagy, J. B.; Novák, M., *J. Electroanal. Chem.* **2001,** *497*, 69.
33. Seetharamappa, J.; Yellappa, S.; D'Souza, F., *Interface* 2006, 23.
34. Iijima, S., *Nature* **1991,** *354*, 56.
35. Geim, A. K.; Novoselov, K. S., *Nat Mater* **2007,** *6*, 183.
36. Delzeit, L.; Nguyen, C. V.; Chen, B.; Stevens, R.; Cassell, A.; Han, J.; Meyyappan, M., *J. Phys. Chem. B* **2002,** *106*, 5629.
37. Journet, C.; Bernier, P., *Appl Phys A* **1998,** *67*, 1.
38. Bai, J. B.; Allaoui, A., *Compos. Part A- Appl. S.* **2003,** *34*, 689.
39. Frackowiak, E.; Béguin, F., *Carbon* **2001,** *39*, 937.
40. Frackowiak, E.; Metenier, K.; Bertagna, V.; Beguin, F., *Appl. Phys. Lett.* **2000,** *77*, 2421.
41. Ajayan, P. M., *Chem. Rev.* **1999,** *99*, 1787.
42. Frank, S.; Poncharal, P.; Wang, Z. L.; de Heer, W. A., *Science* **1998,** *280*, 1744.
43. Nugent, J. M.; Santhanam, K. S. V.; Rubio, A.; Ajayan, P. M., *Nano Lett.* **2001,** *1*, 87.
44. Borowiec, J.; Wei, L.; Zhu, L.; Zhang, J., *Anal. Methods* **2012,** *4*, 444.
45. Fang, W.-C.; Huang, J.-H.; Chen, L.-C.; Su, Y. O.; Chen, K.-H.; Sun, C.-L., *Electrochem. Solid St.* **2006,** *9*, A5.
46. Chou, A.; Bocking, T.; Singh, N. K.; Gooding, J. J., *Chem. Commun.* **2005**, 842.
47. Wu, K.; Fei, J.; Hu, S., *Anal. Biochem.* **2003,** *318*, 100.
48. Liu, G.; Riechers, S. L.; Mellen, M. C.; Lin, Y., *Electrochem. Commun.* **2005,** *7*, 1163.
49. Sanchez, S.; Pumera, M.; Fabregas, E.; Bartroli, J.; Esplandiu, M. J., *Phys. Chem. Chem. Phys.* **2009,** *11*, 7721.
50. Kwok-Siong, T.; Liwei, L., *J. Micromech. Microeng.* **2005,** *15*, 2019.
51. Choi, J.-H.; Jegal, J.; Kim, W.-N., *J. Membr. Sci.* **2006,** *284*, 406.

52. Tóth, A.; László, K., Chapter 5 - Water Adsorption by Carbons. Hydrophobicity and Hydrophilicity. In *Novel Carbon Adsorbents*, Tascón, J. M. D., Ed. Elsevier: Oxford, 2012; pp 147.
53. Jiang, L.; Gao, L.; Sun, J., *J. Colloid Interf. Sci.* **2003,** *260*, 89.
54. Girifalco, L. A.; Hodak, M.; Lee, R. S., *Phys. Rev. B* **2000,** *62*, 13104.
55. Rosen, M. J., *Surfactants and Interfacial Phenomena*. John Wiley & Sons: 2004.
56. Verwey, E. J. W., *J. Phys. Colloid. Chem.* **1947,** *51*, 631.
57. Grossiord, N.; Regev, O.; Loos, J.; Meuldijk, J.; Koning, C. E., *Anal. Chem.* **2005,** *77*, 5135.
58. Yu, J.; Grossiord, N.; Koning, C. E.; Loos, J., *Carbon* **2007,** *45*, 618.
59. Islam, M. F.; Rojas, E.; Bergey, D. M.; Johnson, A. T.; Yodh, A. G., *Nano Lett.* **2003,** *3*,269.
60. Matarredona, O.; Rhoads, H.; Li, Z.; Harwell, J. H.; Balzano, L.; Resasco, D. E., *J. Phys. Chem. B* **2003,** *107*, 13357.
61. Keeley, G. P.; O'Neill, A.; McEvoy, N.; Peltekis, N.; Coleman, J. N.; Duesberg, G. S., *J. Mater. Chem.* **2010,** *20*, 7864.
62. Liu, J.; Casavant, M. J.; Cox, M.; Walters, D. A.; Boul, P.; Lu, W.; Rimberg, A. J.; Smith, K. A.; Colbert, D. T.; Smalley, R. E., *Chem. Phys. Lett.* **1999,** *303*, 125.
63. Ausman, K. D.; Piner, R.; Lourie, O.; Ruoff, R. S.; Korobov, M., *J. Phys. Chem. B* **2000,** *104*, 8911.
64. Nanolab COOH Functionalised Suspensions. http://www.nano-lab.com/nanotubesuspensions.html.
65. Al-Jamal, K. T.; Nunes, A.; Methven, L.; Ali-Boucetta, H.; Li, S.; Toma, F. M.; Herrero, M. A.; Al-Jamal, W. T.; ten Eikelder, H. M.; Foster, J.; Mather, S.; Prato, M.; Bianco, A.; Kostarelos, K., *Angew Chem Int Ed Engl* **2012,** *51*, 6389.
66. Li, J.; Luan, X.; Huang, Y.; Dunham, S.; Chen, P.; Rogers, J. A.; Chan-Park, M. B., *RSC Advances* **2012,** *2*, 1275.
67. Menzel, R.; Bismarck, A.; Shaffer, M. S. P., *Carbon* **2012,** *50*, 3416.
68. Lawrence, N. S.; Deo, R. P.; Wang, J., *Electroanalysis* **2005,** *17*, 65.

69. Nguyen, T. T.; Nguyen, S. U.; Phuong, D. T.; Nguyen, D. C.; Mai, A. T., *Adv. Nat. Sci.: Nanosci. Nanotechnol.* **2011,** *2*, 035015.
70. Huang, Y. Y.; Terentjev, E. M., *Polymers* **2012,** *4*, 275.
71. Pumera, M.; Smid, B.; Veltruska, K., *J. Nanosci. Nanotechno.* **2009,** *9*, 2671.
72. Buang, N. A.; Fadil, F.; Majid, Z. A.; Shahir, S., *Dig. J. Nanomater. Bios.* **2012,** *7*, 33.
73. Han, C.; Doepke, A.; Cho, W.; Likodimos, V.; de, l. C. A. A.; Back, T.; Heineman, W. R.; Halsall, H. B.; Shanov, V. N.; Schulz, M. J.; Falaras, P.; Dionysiou, D. D., *Adv. Funct. Mater.* **2013,** *23*, 1807.
74. Chebil, S.; Macauley, N.; Hianik, T.; Korri-Youssoufi, H., *Electroanal.* **2013,** *25*, 636.
75. Wang, J.; Bian, C.; Tong, J.; Sun, J.; Xia, S., *Thin Solid Films* **2012,** *520*, 6658.
76. Ouyang, R.; Bragg, S. A.; Chambers, J. Q.; Xue, Z.-L., *Anal. Chim. Acta* **2012,** *722*, 1.
77. Kim, B.; Sigmund, W. M., *Langmuir* **2004,** *20*, 8239.
78. Kun, Z.; Yi, H.; Chengyun, Z.; Yue, Y.; Shuliang, Z.; Yuyang, Z., *Electrochim. Acta* **2012,** *80*, 405.
79. Lu, X.; Dong, X.; Zhang, K.; Zhang, Y., *Anal. Methods* **2012,** *4*, 3326.
80. Zhang, L.; Yi, M., *Bioprocess Biosyst. Eng.* **2009,** *32*, 485.
81. Novoselov, K. S.; Geim, A. K.; Morozov, S. V.; Jiang, D.; Zhang, Y.; Dubonos, S. V.; Grigorieva, I. V.; Firsov, A. A., *Science* **2004,** *306*, 666.
82. Peres, N. M. R., *J. Phys.- Condens. Mat.* **2009,** *21*, 323201.
83. Yang, W.; Ratinac, K. R.; Ringer, S. P.; Thordarson, P.; Gooding, J. J.; Braet, F., *Angew. Chem. Int. Ed. Engl.* **2010,** *49*, 2114.
84. Hedberg, J. http://www.jameshedberg.com/about.php.
85. Ohno, Y.; Maehashi, K.; Yamashiro, Y.; Matsumoto, K., *Nano Lett.* **2009,** *9*, 3318.
86. Pumera, M., *Chem. Rec.* **2009,** *9*, 211.
87. Kang, X.; Wang, J.; Wu, H.; Liu, J.; Aksay, I. A.; Lin, Y., *Talanta* **2010,** *81*, 754.

88. Wang, Y.; Li, Y.; Tang, L.; Lu, J.; Li, J., *Electrochem. Commun.* **2009,** *11*, 889.

89. Si, Y.; Samulski, E. T., *Chem. Mater.* **2008,** *20*, 6792.

90. Wang, M. X.; Liu, Q.; Sun, H. F.; Stach, E. A.; Zhang, H. Y.; Stanciu, L.; Xie, J., *Carbon* **2012,** *50*, 3845.

91. Choucair, M.; Tse, N. M. K.; Hill, M. R.; Stride, J. A., *Surface Science* **2012,** *606*, 34.

92. Compton, O. C.; An, Z.; Putz, K. W.; Hong, B. J.; Hauser, B. G.; Brinson, L. C.; Nguyen, S. T., *Carbon* **2012,** *50*, 3399.

93. Rajesh; Paul, R. K.; Mulchandani, A., *J. Power Sources* **2013,** *223*, 23.

94. Jiang, H.; Zhang, S.; Cui, Y.; Xie, Y.; Shi, Q., *Afr. J. Pure Appl. Chem.* **2011,** *5*, 136.

95. Merce, A. L. R.; Nicolini, J.; Khan, M. A.; Bouet, G., *Carbohydr. Polym.* **2009,** *77*, 402.

96. El-Shal, M. A.; Attia, A. K.; Abdulla, S. A., *J. Adv. Sci. Res.* **2013,** *4*, 25.

97. Cheraghi, S.; Taher, M. A.; Fazelirad, H., *Microchim Acta* **2013,** *180*, 1157.

98. Juarez-Gomez, J.; Perez-Garcia, F.; Ramirez-Silva, M. T.; Rojas-Hernandez, A.; Galan-Vidal, C. A.; Paez-Hernandez, M. E., *Talanta* **2013,** *114*, 235.

99. Upadhyay, A.; Singh, A. K.; Bandi, K. R.; Jain, A. K., *Talanta* **2013,** *115*, 569.

100. Afkhami, A.; Soltani-Felehgari, F.; Madrakian, T.; Ghaedi, H.; Rezaeivala, M., *Anal. Chim. Acta.* **2013,** *771*, 21.

101. Kucukkolbasi, S.; Erdogan, Z. O.; Barek, J.; Sahin, M.; Kocak, N., *Int. J. Electrochem. Sci.* **2013,** *8*, 2164.

102. Jahandari, S.; Taher, M. A.; Fazelirad, H.; Sheikhshoai, I., *Microchim Acta* **2013,** *180*, 347.

103. Fu, F.; Zeng, H.; Cai, Q.; Qiu, R.; Yu, J.; Xiong, Y., *Chemosphere* **2007,** *69*, 1783.

104. Ali, M.; Tan, A.; Mirza, A.; Santos, J.; Abdullah, A., *Transit. Metal Chem.* **2012,** *37*, 651.

105. Kanchi, S.; Saraswathi, K.; Venkatasubba, N. N., *Environ. Monit. Assess.* **2011,** *183*, 531.
106. Noll, C. A.; Betz, L. D., *Anal. Chem.* **1952,** *24*, 1894.
107. Chilton, J. M., *Anal. Chem.* **1953,** *25*, 1274.
108. Andrus, M. E., *Met. Finish.* **2000,** *98*, 20.
109. Bonamico, M.; Dessy, G.; Mugnoli, A.; Vaciago, A.; Zambonelli, L., *Acta Crystallogr* **1965,** *19*, 886.
110. Gersmann, H. R.; Swalen, J. D., *J. Chem. Phys.* **1962,** *36*, 3221.
111. Hendrickson, A. R.; Martin, R. L.; Rohde, N. M., *Inorg. Chem.* **1976,** *15*, 2115.
112. Shankaranarayana, M. L., *Acta Chem. Scand.* **1965,** *19*, 1113.
113. Warshawsky, A.; Rogachev, I.; Patil, Y.; Baszkin, A.; Weiner, L.; Gressel, J., *Langmuir* **2001,** *17*, 5621.
114. Callan, T.; Henderson, R. J. A., *Analyst* **1929,** *54*, 650.
115. Endo, M.; Suzuki, K.; Abe, S., *Anal. Chim. Acta.* **1998,** *364*, 13.
116. Ashraf-Khorassani, M.; Combs, M. T.; Taylor, L. T., *Talanta* **1997,** *44*, 755.
117. Li, Y.; Zeng, X.; Liu, Y.; Yan, S.; Hu, Z.; Ni, Y., *Sep. Purif. Techno.* **2003,** *31*, 91.
118. Fu, H.; Lv, X. S.; Yang, Y. P.; Xu, X. H., *Desalination and Water Treatment* **2012,** *39*, 103.
119. Weldegebriel, Y.; Chandravanshi, B. S.; Wondimu, T., *Ecotox. Environ. Safe.* **2012,** *77*, 57.
120. Suzuki, Y.; Fujii, S.; Tominaga, T.; Yoshimoto, T.; Yoshimura, T.; Kamada, H., *Biochimica et Biophysica Acta (BBA) - General Subjects* **1997,** *1335*, 242.
121. Burkitt, M. J.; Bishop, H. S.; Milne, L.; Tsang, S. Y.; Provan, G. J.; Nobel, C. S.; Orrenius, S.; Slater, A. F., *Arch Biochem Biophys* **1998,** *353*, 73.
122. Bond, A. M.; Wallace, G. G., *Anal. Chem.* **1981,** *53*, 1209.
123. Bond, A. M.; Wallace, G. G., *Anal. Chem.* **1982,** *54*, 1706.
124. Chen, Z.; Pourabedi, Z.; Hibbert, D. B., *Electroanalysis* **1999,** *11*, 964.

125. deCarvalho, L. M.; do Nascimento, P. C.; Bohrer, D.; Stefanello, R.; Pilau, E. J.; da Rosa, M. B., *Electroanalysis* **2008,** *20*, 776.

126. Dong, Y. P.; Huang, L.; Zhang, J.; Chu, X. F.; Zhang, Q. F., *Electrochim. Acta* **2012,** *74*, 189.

127. Dong, Y. P.; Pei, L. Z.; Chu, X. F.; Zhang, W. B.; Zhang, Q. F., *Analyst* **2013,** *138*, 2386.

128. Azapagic, A.; Emsley, A., *Polymers: The Environment and Sustainable Development*. John Wiley and Sons: 2003.

129. Menon, R., *Curr. Sci. India* **2000,** *79*, 1632.

130. Campos, M. In *Conducting polymer sensors*, American Scientific Publishers: 2006; pp 229.

131. Dallollio, A.; Dascola, G.; Varacca, V.; Bocchi, V., *Comptes Rendus Hebdomadaires Des Seances De L'Academie Des Sciences Serie C* **1968,** *267*.

132. Ko, J. M.; Rhee, H. W.; Park, S. M.; Kim, C. Y., *J. Electrochem. Soc.* **1990,** *137*, 905.

133. Senthurchelvan, R.; Wang, Y.; Basak, S.; Rajeshwar, K., *J. Electrochem. Soc.* **1996,** *143*, 44.

134. Ogino, H.; Oishi, T.; Murakami, M. Manufacture of conductive polypyrrole capacitors with low impedance and high capacitance by chemical polymerization using organic bases. JP2009164187A, 2009.

135. Fenelon, A. M.; Breslin, C. B., *Corros. Sci.* **2003,** *45*, 2837.

136. Ryan, E. M.; Breslin, C. B.; Moulton, S. E.; Wallace, G. G., *Electrochim. Acta* **2013,** *92*, 276.

137. Schlenoff, J. B.; Xu, H., *J. Electrochem. Soc.* **1992,** *139*, 2397.

138. Hahn, S. J.; Stanchina, W. E.; Gajda, W. J.; Vogelhut, P., *J. Electron. Mater.* **1986,** *15*, 145.

139. Garcia-Belmonte, G., *Electrochem. Commun.* **2003,** *5*, 236.

140. McCarthy, C. P.; McGuinness, N. B.; Alcock-Earley, B. E.; Breslin, C. B.; Rooney, A. D., *Electrochem. Commun.* **2012,** *20*, 79.

141. Sahoo, N. G.; Rana, S.; Cho, J. W.; Li, L.; Chan, S. H., *Prog. Polym.Sci.* **2010,** *35*, 837.

142. Sha, Y.; Qian, L.; Ma, Y.; Bai, H.; Yang, X., *Talanta* **2006,** *70*, 556.

143. Spitalsky, Z.; Tasis, D.; Papagelis, K.; Galiotis, C., *Prog. Polym.Sci.* **2010**, 357.

144. Zanganeh, A. R.; Amini, M. K., *Electrochim. Acta* **2007,** *52*, 3822.

145. Wang, M.; Meng, G.; Huang, Q.; Xu, Q.; Liu, G., *Anal. Methods* **2012,** *4*, 2653.

146. Hughes, M.; Chen, G. Z.; Shaffer, M. S. P.; Fray, D. J.; Windle, A. H., *Chem. Mater.* **2002,** *14*, 1610.

147. Salam, M. A.; Al-Juaid, S. S.; Qusti, A. H.; Hermas, A. A., *Synthetic Metals* **2011,** *161*, 153.

148. Hermas, A. A.; Al-Juaid, S. S.; Al-Thabaiti, S. A.; Qusti, A. H.; Abdel Salam, M., *Prog. Org. Coat.* **2012,** *75*, 404.

149. Mi, H.; Zhang, X.; Xu, Y.; Xiao, F., *Appl. Surf. Sci.* **2010,** *256*, 2284.

150. Ioniță, M.; Prună, A., *Prog. Org. Coat.* **2011,** *72*, 647.

151. Snook, G. A.; Chen, G. Z.; Fray, D. J.; Hughes, M.; Shaffer, M., *J. Electroanal. Chem.* **2004,** *568*, 135.

152. Tsai, Y.-C.; Li, S.-C.; Liao, S.-W., *Biosens. Bioelectron.* **2006,** *22*, 495.

153. Grot, W., *Chem.-Ing.-Tech.* **1978,** *50*, 299.

154. Xue, T.; Trent, J. S.; Osseo-Asare, K., *J. Membrane Sci.* **1989,** *45*, 261.

155. Abuin, G. C.; Fuertes, M. C.; Corti, H. R., *J. Membrane Sci.* **2013,** *428*, 507.

156. Seeliger, D.; Hartnig, C.; Spohr, E., *Electrochim. Acta* **2005,** *50*, 4234.

157. Seen, A. J., *J. Mol. Catal. A-Chem.* **2001,** *177*, 105.

158. Kokkinos, C.; Economou, A., *Talanta* **2011,** *84*, 696.

159. Xu, M.; Cui, L.; Han, R.; Ai, S., *J. Solid State Electrochem.* **2012,** *16*, 2547.

160. Thangavel, S.; Ramaraj, R., *J. Colloid Interf. Sci.* **2011,** *355*, 293.

161. Casciola, M.; Alberti, G.; Sganappa, M.; Narducci, R., *Desalination* **2006,** *200*, 639.

162. Chen, K. Y.; Tseung, A. C. C., *J. Electrochem. Soc.* **1996,** *143*, 2703.

163. Brown, F. O.; Finnerty, N. J.; Lowry, J. P., *Analyst* **2009,** *134*, 2012.

164. Yusof, N. A.; Daud, N.; Saat, S. Z. M.; Tee, T. W.; Abdullah, A. H., *Int. J. Electrochem. Sci.* **2012,** *7*, 10358.

165. Kumar, S.; Vicente-Beckett, V., *Beilstein J. Nanotechnol* **2012,** *3*, 388.

166. Park, S. J.; Cho, M. S.; Lim, S. T.; Choi, H. J.; Jhon, M. S., *Macromol. Rapid Comm.* **2003,** *24*, 1070.

167. Choucair, M.; Thordarson, P.; Stride, J. A., *Nat Nano* **2009,** *4*, 30.

168. Santos, H. M.; Lodeiro, C.; Capelo-Martínez, J.-L., The Power of Ultrasound. In *Ultrasound in Chemistry*, Wiley-VCH Verlag GmbH & Co. KGaA: 2009; pp 1.

169. Wibetoe, G., Takuwa, D.T., Lund, W.D. and Sawula, G., *Fresnius Journal of Analytical Chemistry* **1999,** *363*.

170. Maja Cvetkovska, T. G., *B. Chem. Tech. Macedonia* **1994,** *13*, 31.

171. Chandrasekhar, P., *Conducting Polymers, Fundamentals and Applications: A Practical Approach*. Kluwer Academic: 1999.

172. Corporation,M. http://www.metokote.com/coatingTechnologies/electrocoat.asp.

173. Fisher, A. C., *Electrode Dynamics*. Oxford University Press: 1996.

174. Bard, A. J.; Faulkner, L. R., *Electrochemical Methods: Fundamentals and Applications*. Wiley: 2000.

175. Iwasita, T.; Schmickler, W.; Herrmann, J.; Vogel, U., *J. Electrochem. Soc.* **1983,** *130*, 2026.

176. Steed, J. W.; Atwood, J. L., *Supramolecular Chemistry*. Wiley: 2009.

177. Keeley, G. P.; Lyons, M. E. G., *Int. J. Electrochem. Sci.* **2009,** *4*, 794.

178. Streeter, I.; Wildgoose, G. G.; Shao, L.; Compton, R. G., *Sensor. Actuat. B-Chem.* **2008,** *133*, 462.

179. Nicholson, R., *Anal. Chem.* **1965,** *37*, 1351

180. Klingler, R. J.; Kochi, J. K., *J. Phys. Chem.* **1981,** *85*, 1731.

181. Bauer, H. H., *J. Electroanal. Chem. Interfac.* **1968,** *16*, 419.

182. Sakata, T.; Nakamura, H., *B. Chem. Soc. Jpn.* **2001,** *74*, 2285.

183. Okajima, T.; Ohsaka, T.; Oyama, N., *B. Chem. Soc. Jpn.* **1991,** *64*, 1305.

184. Alcock, B. National University of Ireland Maynooth, 2005.

185. Greef, R.; Peat, R.; Peter, L. M.; Pletcher, D.; Robinson, J., *Instrumental methods in electrochemistry*. Ellis Horwood Ltd, 1985

186. Fan, F. R. F.; Bard, A. J., *Journal of the Electrochemical Society* **1986,** *133*, 301.

187. Griffiths, P.; De Haseth, J. A., *Fourier Transform Infrared Spectrometry*. Wiley: 2007.

188. Banwell, C. N., *Fundamentals of Moleculr Spectroscopy*. 2nd ed.; 1972.

189. Novoselov, K. S.; Geim, A. K.; Morozov, S. V.; Jiang, D.; Katsnelson, M. I.; Grigorieva, I. V.; Dubonos, S. V.; Firsov, A. A., *Nature* **2005,** *438*, 197.

190. Hiraoka, T.; Izadi-Najafabadi, A.; Yamada, T.; Futaba, D. N.; Yasuda, S.; Tanaike, O.; Hatori, H.; Yumura, M.; Iijima, S.; Hata, K., *Adv. Funct. Mater.* **2010,** *20*, 422.

191. Britto, P. J.; Santhanam, K. S. V.; Rubio, A.; Alonso, J. A.; Ajayan, P. M., *Adv. Mater.* **1999,** *11*, 154.

192. Zhu, Y.; Murali, S.; Cai, W.; Li, X.; Suk, J. W.; Potts, J. R.; Ruoff, R. S., *Adv. Mater.* **2010,** *22*, 3906.

193. Crevillen, A. G.; Pumera, M.; Gonzalez, M. C.; Escarpa, A., *Analyst* **2009,** *134*, 657.

194. Kyrylyuk, A. V.; Hermant, M. C.; Schilling, T.; Klumperman, B.; Koning, C. E.; van der Schoot, P., *Nat. Nanotechnol.* **2011,** *6*, 364.

195. Brownson, D. A. C.; Kampouris, D. K.; Banks, C. E., *Chem. Soc. Rev.* **2012,** *41*, 6944.

196. Agui, L.; Yanez-Sedeno, P.; Pingarron, J. M., *Anal. Chim. Acta.* **2008,** *622*, 11.

197. McCreery, R. L., *Chem. Rev.* **2008,** *108*, 2646.

198. Ohta, T.; Bostwick, A.; McChesney, J. L.; Seyller, T.; Horn, K.; Rotenberg, E., *Phys. Rev. Lett.* **2007,** *98*, 206802.

199. Garry, L. M.; Alcock, B. E.; Breslin, C. B., *ECS Trans.* **2012,** *41*, 1.

200. Goriletsky, V. I., Mitichkin, A. I., Belenko, L. E., Rebrova, T. P., *Semicond. Phys., Quantum Electron. Optoelectron.* **2001,** *4*, 139.

201. Dischler, B.; Bubenzer, A.; Koidl, P., *Solid State Commun.* **1983,** *48*, 105.

202. Kim, H.-S.; Lee, H.; Han, K.-S.; Kim, J.-H.; Song, M.-S.; Park, M.-S.; Lee, J.-Y.; Kang, J.-K., *J. Phys. Chem. B* **2005,** *109*, 8983.

203. Silva, W. M.; Ribeiro, H.; Seara, L. M.; Calado, H. D. R.; Ferlauto, A. S.; Paniago, R. M.; Leite, C. F.; Silva, G. G., *J. Brazil. Chem. Soc.* **2012,** *23*, 1078.

204. Ago, H.; Kugler, T.; Cacialli, F.; Salaneck, W. R.; Shaffer, M. S. P.; Windle, A. H.; Friend, R. H., *J. Phys. Chem. B* **1999,** *103*, 8116.

205. Giri, S.; Das, C. K.; Kalra, S. S., *J. Mater. Sci. Res.* **2012,** *1*.

206. Li, J.; Cassell, A.; Delzeit, L.; Han, J.; Meyyappan, M., *J. Phys. Chem. B* **2002,** *106*, 9299.

207. Liu, C. y.; Bard, A. J.; Wudl, F.; Weitz, I.; Heath, J. R., *Electrochem. Solid St.* **1999,** *2*, 577.

208. Barisci, J. N.; Wallace, G. G.; Baughman, R. H., *J. Electrochem. Soc.* **2000,** *147*, 4580.

209. Stoller, M. D.; Magnuson, C. W.; Zhu, Y.; Murali, S.; Suk, J. W.; Piner, R.; Ruoff, R. S., *Energ. Environ. Sci.* **2011,** *4*, 4685.

210. Ohta, T.; Kim, I.-T.; Egashira, M.; Yoshimoto, N.; Morita, M., *J. Power Sources* **2012,** *198*, 408.

211. Wang, D.-W.; Li, F.; Wu, Z.-S.; Ren, W.; Cheng, H.-M., *Electrochem. Commun.* **2009,** *11*, 1729.

212. Nishiguchi, I.; Peters, D.; Yoshida, J., *Organic and Biological Electrochemistry Symposium in Honor of Yoshihiro Matsumura*. The Electrochemical Society: 2008; Vol. 13.

213. Lee, C.-Y.; Bond, A. M., *Anal. Chem.* **2008,** *81*, 584.

214. Jones, C. P.; Jurkschat, K.; Crossley, A.; Compton, R. G.; Riehl, B. L.; Banks, C. E., *Langmuir* **2007,** *23*, 9501.

215. Dong, X.; Fu, D.; Fang, W.; Shi, Y.; Chen, P.; Li, L.-J., *Small* **2009,** *5*, 1422.

216. Ni, Z. H.; Wang, Y. Y.; Yu, T.; You, Y. M.; Shen, Z. X., *Physical Review B* **2008,** *77*.

217. Hallam, P. M.; Banks, C. E., *Electrochem. Commun.* **2011,** *13*, 8.

218. Ji, X.; Banks, C. E.; Crossley, A.; Compton, R. G., *ChemPhysChem* **2006,** *7*, 1337.

219. Harris , P. J. F., *Philos. Mag.* **2004,** *84*, 3159.

220. Greef, R.; R. Peat; Peter, L. M.; Pletcher, D.; Robinson, J., *Instrumental methods in electrochemistry*. Ellis Horwood Ltd.: 1985.
221. Ramesham, R., *Thin Solid Films* **1999,** *339*, 82.
222. Nalwa, H. S., *Handbook of Surfaces and Interfaces of Materials, Five-Volume Set*. Elsevier Science: 2001.
223. Ambrosi, A.; Pumera, M., *Chemistry* **2010,** *16*, 10946.
224. Ambrosi, A.; Bonanni, A.; Pumera, M., *Nanoscale* **2011,** *3*, 2256.
225. McCreery, R. L.; McDermott, M. T., *Anal. Chem.* **2012,** *84*, 2602.
226. Luo, L.; Zhu, L.; Wang, Z., *Bioelectrochemistry* **2012,** *88*, 156.
227. Ping Xiao, W. W., Jingjing Yu, Faqiong Zhao, *Int. J. Electrochem. Sc.* **2007,** *2*, 149.
228. Hegde, R. N.; Shetti, N. P.; Nandibewoor, S. T., *Talanta* **2009,** *79*, 361.
229. Haas, M. K.; Zielinski, J. M.; Dantsin, G.; Coe, C. G.; Pez, G. P.; Cooper, A. C., *J. Mater. Res.* **2005,** *20*, 3214.
230. Kotaś, J., Stasicka, Z., *Environ. Pollut.* **2000,** *107*, 263.
231. Fanjul-Bolado, P.; Queipo, P.; Lamas-Ardisana, P. J.; Costa-Garcia, A., *Talanta* **2007,** *74*, 427.
232. Wang, G.; Xu, J. J.; Chen, H. Y., *Electrochem. Commun.* **2002,** *4*, 506.
233. Guo, M.; Chen, J.; Li, J.; Tao, B.; Yao, S., *Anal. Chim. Acta* **2005,** *532*, 71.
234. Li, Y.; Wang, P.; Wang, L.; Lin, X., *Biosens. Bioelectron.* **2007,** *22*, 3120.
235. Welch, C. M.; Nekrassova, O.; Compton, R. G., *Talanta* **2005,** *65*, 74.
236. Gu, H.; Rapole, S. B.; Huang, Y.; Cao, D.; Luo, Z.; Wei, S.; Guo, Z., *J. Mater. Chem. A* **2013,** *1*, 2011.
237. Zheng, H.; Lin, L.; Okezaki, Y.; Kawakami, R.; Sakuraba, H.; Ohshima, T.; Takagi, K.; Suye, S.-i., *Beilstein J. Nanotechnol* **2010,** *1*, 135.
238. Pillay, K.; Cukrowska, E. M.; Coville, N. J., *J. Hazard. Mater.* **2009,** *166*, 1067.
239. Goeringer, S.; de Tacconi, N. R.; Chenthamarakshan, C. R.; Rajeshwar, K., *J. Appl. Electrochem.* **2000,** *30*, 891.
240. Wang, G. M.; Ling, Y. C.; Qian, F.; Yang, X. Y.; Liu, X. X.; Li, Y., *J. Power Sources* **2011,** *196*, 5209.
241. Salimi, A.; Hallaj, R.; Khayatian, G.-R., *Electroanalysis* **2005,** *17*, 873.

242. Abbas, A., *Carbon* **2003,** *41*, 3.

243. Prakash, S.; Rajesh, S.; Singh, S. K.; Bhargava, K.; Ilavazhagan, G.; Vasu, V.; Karunakaran, C., *Talanta* **2011,** *85*, 964.

244. Balasubramanian, K.; Burghard, M., *Anal. Bioanal. Chem.* **2006,** *385*, 452.

245. Arami, H.; Mazloumi, M.; Khalifehzadeh, R.; Emami, S. H.; Sadrnezhaad, S. K., *Mater. Lett.* **2007,** *61*, 4412.

246. Tamm, J.; Hallik, A.; Alumaa, A.; Sammelselg, V., *Electrochim. Acta* **1997,** *42*, 2929.

247. Hu, D.; Peng, C.; Chen, G. Z., *ACS Nano* **2010,** *4*, 4274.

248. Puech, P.; Hu, T.; Sapelkin, A.; Gerber, I.; Tishkova, V.; Pavlenko, E.; Levine, B.; Flahaut, E.; Bacsa, W., *Phys. Rev. B* **2012,** *85*, 205.

249. Khajeamiri, A., *Iran. J. Pharm. Res.* **2012,** *11*, 369.

250. Mangold, K. M.; Weidlich, C.; Schuster, J.; Juettner, K., *J. Appl. Electrochem.* **2005,** *35*, 1293.

251. Arrieta Almario, Á. A.; Vieira, R. L., *J. Chil. Chem. Soc.* **2006,** *51*, 971.

252. Ansari, R.; Delavar, A.; Mohammad-khah, A., *Microchim. Acta* **2012,** *178*, 71.

253. Ge, H.; Zhang, J.; Wallace, G. G., *Anal. Lett.* **1992,** *25*, 429.

254. Earley, S.; Alcock, B.; Lowry, J.; Breslin, C., *J. Appl. Electrochem.* **2009,** *39*, 1251.

255. Yu, H.; Wang, Y.; Lian, Y.-Y.; Song, S.-W.; Liu, Z.-Y.; Qi, G.-C., *Electrochim. Acta* **2012,** *85*, 650.

256. Park, D. S.; Shim, Y. B.; Park, S. M., *J. Electrochem. Soc.* **1993,** *140*, 609.

257. Bond, G., *Gold Bull* **2001,** *34*, 117.

258. Sharma, M. K.; Rao, V. K.; Agarwal, G. S.; Rai, G. P.; Gopalan, N.; Prakash, S.; Sharma, S. K.; Vijayaraghavan, R., *J. Clin. Microbiol.* **2008,** *46*, 3759.

259. Qi, Z.-m.; Wei, M.; Honma, I.; Zhou, H., *ChemPhysChem* **2007,** *8*, 264.

260. Liu, G.; Lin, Y.-Y.; Wu, H.; Lin, Y., *Environ. Sci. Technol.* **2007,** *41*, 8129.

261. Zakharova, E. A.; Elesova, E. E.; Skorokhodova, A. A.; Noskova, G. N., *Inorg. Mater.* **2012,** *48*, 1279.

262. Alexeyeva, N.; Laaksonen, T.; Kontturi, K.; Mirkhalaf, F.; Schiffrin, D. J.; Tammeveski, K., *Electrochem. Commun.* **2006,** *8*, 1475.
263. Branagan, D., Unpublished Work. 2013.
264. Alexeyeva, N.; Tammeveski, K., *Anal. Chim. Acta.* **2008,** *618*, 140.
265. Tian, Y.; Yang, F.; Yang, W., *Synthetic Met.* **2006,** *156*, 1052.
266. Inzelt, G.; Pineri, M.; Schultze, J. W.; Vorotyntsev, M. A., *Electrochim. Acta* **2000,** *45*, 2403.
267. Bhaumik, M.; Maity, A.; Srinivasu, V. V.; Onyango, M. S., *J. Hazard. Mater.* **2011,** *190*, 381.
268. Wei, C.; German, S.; Basak, S.; Rajeshwar, K., *J. Electrochem. Soc.* **1993,** *140*, 60.
269. Lin, Y.; Timchalk, C. A.; Matson, D. W.; Wu, H.; Thrall, K. D., *Biomed. Microdevices* **2001,** *3*, 331.
270. Santos, J. H.; Bond, A. M.; Mocak, J.; Cardwell, T. J., *Anal. Chem.* **1994,** *66*, 1925.
271. Kamata, S.; Murata, H.; Kubo, Y.; Bhale, A., *Analyst* **1989,** *114*, 1029.
272. Gismera, M. J.; Hueso, D.; Procopio, J. R.; Sevilla, M. T., *Anal. Chim. Acta.* **2004,** *524*, 347.
273. Singh, L. P.; Bhatnagar, J. M., *Talanta* **2004,** *64*, 313.
274. Yang, W.; Chow, E.; Willett, G. D.; Hibbert, D. B.; Gooding, J. J., *Analyst* **2003,** *128*, 712.
275. Chow, E.; Ebrahimi, D.; Gooding, J. J.; Hibbert, D. B., *Analyst* **2006,** *131*, 1051.
276. Wawrzyniak, U. E.; Ciosek, P.; Zaborowski, M.; Liu, G.; Gooding, J. J., *Electroanalysis* **2013,** *25*, 1461.
277. Janssen, M. J., *J. Inorg. Nucl. Chem.* **1958,** *8*, 340.
278. Villa, J. F.; Hatfield, W. E., *Inorg. Chem.* **1971,** *10*.
279. Cardwell, T. J., Santos, J. H., Bond, A. M., *Anal. Chim. Acta.* **1997,** *340*, 169.
280. O'Riordan, D. M. T.; Wallace, G. G., *Anal. Chem.* **1986,** *58*, 128.
281. Xu, H.; Zeng, L.; Xing, S.; Xian, Y.; Shi, G.; Jin, L., *Electroanalysis* **2008,** *20*, 2655.

282. Yang, W.; Gooding, J. J.; Hibbert, D. B., *Analyst* **2001,** *126*, 1573.

283. Cen, D.; Brayton, D.; Shahandeh, B.; Meyskens, F. L.; Farmer, P. J., *J. Med. Chem.* **2004,** *47*, 6914.

284. Lieder, M., Schläpfer, C. W., *J. Appl. Electrochem.* **2001,** *31*, 1321.

285. Lieder, M., *J. New Mat. Elect. Syst.* **2008,** *11*, 213.

286. Asavapiriyanont, S.; Chandler, G. K.; Gunawardena, G. A.; Pletcher, D., *J. Electroanal. Chem. Interfac.* **1984,** *177*, 229.

287. Heinze, J.; Rasche, A.; Pagels, M.; Geschke, B., *J. Phys. Chem. B* **2007,** *111*, 989.

288. Smie, A.; Synowczyk, A.; Heinze, J.; Alle, R.; Tschuncky, P.; Götz, G.; Bäuerle, P., *Journal of Electroanalytical Chemistry* **1998,** *452*, 87.

289. Sanmatías, A.; Bastos, J. A.; Benito, D.; García-Jareño, J. J.; Vicente, F., *Int. J. Inorg. Mater.* **1999,** *1*, 371.

290. Zawodzinski, T. A.; Derouin, C.; Radzinski, S.; Sherman, R. J.; Smith, V. T.; Springer, T. E.; Gottesfeld, S., *J. Electrochem. Soc.* **1993,** *140*, 1041.

291. Hashemi, P.; Dankoski, E. C.; Petrovic, J.; Keithley, R. B.; Wightman, R. M., *Anal. Chem.* **2009,** *81*, 9462.

292. Ainscough, E. W.; Brodie, A. M., *J.C.S. Dalton* **1977**.

293. Tonkin, E. G.; Valentine, H. L.; Milatovic, D. M.; Valentine, W. M., *Toxicol. Sci.* **2004,** *81*, 160.

294. Victoriano, L. I., *Coordin. Chem. Rev.* **2000,** *196*, 383.

295. Jeliazkova, B. G.; Doicheva, M. A., *Polyhedron* **1996,** *15*, 1277.

296. Dunbar, A.; Omiatek, D. M.; Thai, S. D.; Kendrex, C. E.; Grotzinger, L. L.; Boyko, W. J.; Weinstein, R. D.; Skaf, D. W.; Bessel, C. A.; Denison, G. M.; DeSimone, J. M., *Ind. Eng. Chem. Res.* **2006,** *45*, 8779.

297. Inam, F.; Yan, H.; Reece, M. J.; Peijs, T., *Nanotechnol.* **2008,** *19*, 195710.

298. Pumera, M.; Merkoci, A.; Alegret, S., *Sensor. Actuat. B-Chem.* **2006,** *113*, 617.

299. Tsai, Y. C.; Chen, J. M.; Marken, F., *Microchim. Acta* **2005,** *150*, 269.

300. Mauritz, K. A.; Moore, R. B., *Chem. Rev.* **2004,** *104*, 4535.